LOSSES IN THE INLET SECTION OF COUNTERFLOW WET-COOLING TOWERS

by

Eugene de Villiers

Thesis presented in partial fulfilment of the requirements for the degree M.Sc. Engineering at the University of Stellenbosch

Supervisor: Prof. D.G. Kröger

Department of Mechanical Engineering
University of Stellenbosch
December 1998

DECLARATION

I, the undersigned, hereby declare that the work contained in this thesis is my own original work and I have not previously in its entirety or in part submitted it at any university for a degree.

ABSTRACT

The flow resistances in the inlet sections of counterflow wet-cooling towers are investigated and correlations are derived for inclusion in a one-dimensional tower performance model.

The rain zone loss is modelled using analytical-numerical methods. Experimental verification of the model produces satisfactory confirmation of the method's general validity. Semi-empirical correlations are produced to predict the loss coefficient as a function of six dimensionless variables for both rectangular and circular cooling towers. In addition, a study is made of the heat and mass transfer in the rain zone and its influence on tower performance.

The inlet loss coefficients for dry, isotropically packed, circular and rectangular counterflow cooling towers are determined experimentally and empirical correlations are formulated to fit this data. The inlet losses for isotropic-resistance-fill towers are found to be higher than those for orthotropic-resistance-fill towers.

Computational fluid dynamics is used to investigate the dependence of the inlet loss coefficient on the rain zone characteristics. The rain zone loss generally dampens the inlet loss, but this coupling is indirect and necessitates a large amount of dependent variables. The numerical model is validated by means of experimental data for dry towers and it is found that the degree of accuracy achieved for circular towers exceeds that for rectangular towers. Consequently, the correlation derived to predict this occurrence for circular towers, can be applied more confidently than its rectangular counterpart. An example is presented wherein the improved accuracy in tower performance prediction, when applying this correlation, is shown. Additional measures for tower performance enhancement are also explored.

Keywords: Cooling tower, rain zone, inlet loss

SAMEVATTING

`n Studie is gemaak van vloeiweerstande in die inlaat seksie van nat teenvloei koeltorings met die oog op die afleiding van korrelasies om die verskynsels, vir gebruik in puntmodel koeltoring simulasies, te voorspel.

Die reënsone verlies is gemodelleer met behulp van `n analities-numeriese metode. Die model is geverifieer met behulp van eksperimentele toetse. Semi-empiriese korrelasies word afgelei wat die verlies, as `n funksie van ses dimensielose veranderlikes, vir beide ronde en reghoekige koeltorings, voorspel. Daar word ook `n studie gemaak van die hitte en massa oordrag in die reënsone en hoe dit koeltorings se termiese oordrags vermoë beïnvloed.

Die inlaat verlies vir droë, isotropies gepakte, ronde en reghoekige koeltorings is eksperimenteel bepaal en empiriese korrelasies is geformuleer om die data te pas. Daar is gevind dat die inlaat verlies vir isotropies gepakte torings hoër is as die vir ortotropies gepakte torings.

Numeriese vloei dinamika is gebruik om die afhanklikheid van die inlaat verlies se grootte op die reënsone se eienskappe te ondersoek. Die algemene tendens is vir die reënsone om die inlaat verlies te demp, maar die afhanklikheid is indirek sodat `n groot aantal veranderlikes benodig word om die demping te karakteriseer. Die numeriese model word geverifieer deur middel van eksperimentele data vir droë koeltorings en daar word tot die gevolgtrekking gekom dat ronde torings heelwat meer akuraat gemodelleer word as reghoekige torings. Dit veroorsaak dat die korrelasie wat afgelei is om die demping te voorspel vir ronde torings, met baie meer vertroue toegepas kan word as sy reghoekige eweknie. `n Voorbeeld word gedoen om die verbeterde akuraatheid in koeltoring modellering, wat verkry kan word met behulp van die vergelyking, te wys. Bykomende matriëels, om torings se verkoelings vermoë te verbeter, word ook ondersoek.

Sleutelwoorde: Koeltoring, reënsone, inlaat verlies

ACKNOWLEDGEMENTS

The author would like to thank the following persons for their assistance and contributions to the completion of this thesis:

- My supervisor Prof. D.G. Kröger for his guidance, faith and patient support.
- Kobus Zietsman for his valuable technical advice and assistance.
- Andrea Botha for much needed editing and causing me to start this endeavour in the first place.
- My family and friends for their support.

TABLE OF CONTENTS

NOMENCLATURE

Symbols

A	Area	m^2
a	Acceleration	m/s^2
	Droplet horizontal axis length	m
	Dimensional coefficient	
	Surface area per unit volume	m^2/m^3
b	Droplet vertical axis length	m
C	Coefficient	
C_D	Drag coefficient	
c_p	Specific heat	J/kg K
D	Diffusivity	m^2/s
d	Diameter	m
E	Droplet deformation ratio	
	Mechanical Energy	J
F	Force	N
	Mass flux	kg/m^2s
f	Geometric form factor	
G	Mass flux	kg/m^2s
g	Gravitational acceleration	m/s^2
H	Height	m
i	Enthalpy	J/kg
h	Heat transfer coefficient	W/ m^2K
h_d	Mass transfer coefficient	kg/m^2s
K	Energy loss coefficient	
k	Turbulent energy	m^2/s^2
L	Length	m

M	Mass	kg
m	Mass flow rate	kg/s
n	Number	
p	Pressure	Pa
Q	Heat transfer rate	W
R	Gas constant	J/kg K
Ry	Flow parameter	m^{-1}
r	Radius	m
S	Surface area	m^2
s	Momentum source	N/m^3
T	Temperature	K, °C
t	Time	s
	Thickness	m
u	Velocity	m/s
V	Volume	m^3
	Mean velocity	m/s
v	Velocity	m/s
W	Width	m
w	Work per unit mass	J/kg
	Humidity ratio	kg/kg
X	Mole fraction	
x, y, z	Cartesian co-ordinate	m

Greek symbols

α_e	Kinetic energy coefficient	
β	Mass transfer coefficient	m/s
ε	Turbulence dissipation	m^2/s^3
ϕ	Potential function	m^2/s
μ	Dynamic viscosity	kg/ms

π	Pi	
θ	Angle	
ρ	Density	kg/m^3
σ	Surface tension	N/m
τ	Shear stress	N/m^2
ξ	Adiabatic lapse rate	K/m
ψ	Stream function	m^2/s

Subscripts

a	Air, ambient
ad	Air relative to the droplet
av	Air vapour mixture
amb	Ambient conditions
ct	Cooling tower
ctc	Contraction
cte	Expansion
cv	Control volume
D	Drag
d	Droplet
de	Drift eliminator
e	Energy
eff	Effective
fi	Fill
fr	Frontal
fs	Fill support
G	Gravity
g	Gas
he	Heat exchanger
hes	Heat exchanger support

i	Inlet
i, j, k	Direction indices
il	Inlet louvers
ir	Inlet rounding
L	Length
l	Liquid
	Leakage
m	Mean
n	Nozzle
nds	Number of droplet time steps
o	Outlet, out
r	Radial
rz	Rain zone
s	Saturated
sp	Spray zone
sph	Sphere
T	Condition at terminal velocity
t	Terminal velocity
	Turbulent
	Total
ts	Tower supports
v	Vapour, velocity
w	Water
wb	Wetbulb
wd	Water distribution
x, y	Co-ordinate directions
z	Vertical, Axial
zi	Vertical inlet

μ	Dynamic viscosity
ρ	Density

Superscripts

*	Static
k	Iteration number
n	New
o	Old

Dimensionless Groups

Eo	Eotvos number	$gd^2\left(\rho_l - \rho_g\right)/\sigma_l$
Fr_D	Desimetric Froude number	$\rho v^2 / \left[\Delta\rho g d\right]$
Le_f	Lewis factor	$h/\left(c_p h_d\right)$
Re	Reynolds number	$\rho v d / \mu$
Sc	Schmidt number	$\mu / \rho D$
Sh	Sherwood number	$\beta d / D$

CHAPTER

ONE

INTRODUCTION

The thermodynamic efficiency of the Rankine cycle, which is characteristic of the processes involved in modern fossil fuelled power plants, is such that little more than a third of the available thermal energy can be extracted as electricity. The remaining two thirds have to be removed from the cycle as waste heat by means of a heat sink. The large amounts of waste heat produced in the power generation industry, necessitates large capacity cooling systems.

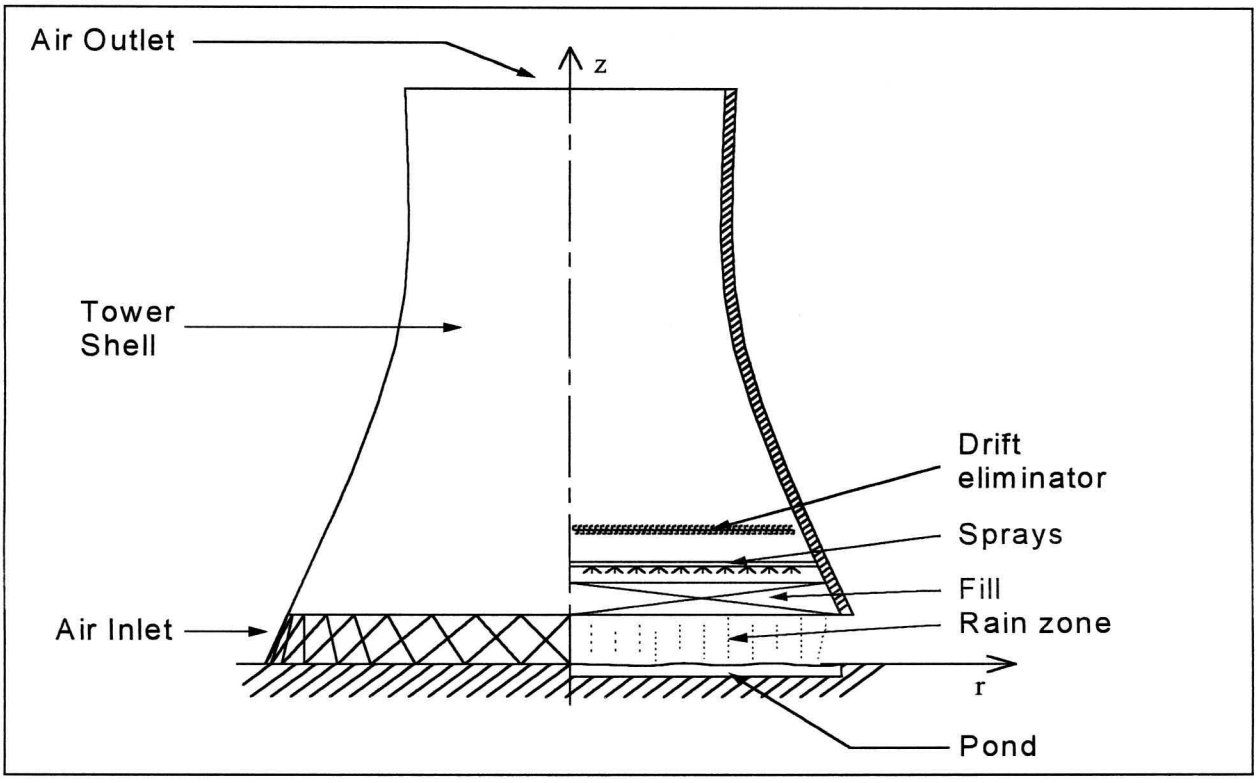

Figure 1.1: *Natural Draft Counterflow Wet-cooling Tower.*

The simplest method to remove this excess heat is by pumping it into the hydrosphere. Most of the earliest power plants utilised this method, in the form of once through cooling systems, where heated water is pumped directly into rivers, lakes and the sea. Ecological awareness and regulations instituted in the early 1970s, along with the decreasing availability of water as heavy

industry expands, have greatly curtailed this method of waste heat disposal. The search for an alternative led to the development of wet-cooling towers, examples of which can be seen in figures. 1.1 and 1.2. The constant circulation of water through these towers enables them to operate with 3-4% of the water supply necessary for the once-through systems. In recent years dry-cooling and hybrid towers have reduced water usage to negligible levels, but their high construction and maintenance cost have ensured that wet-cooling towers remain widely in use.

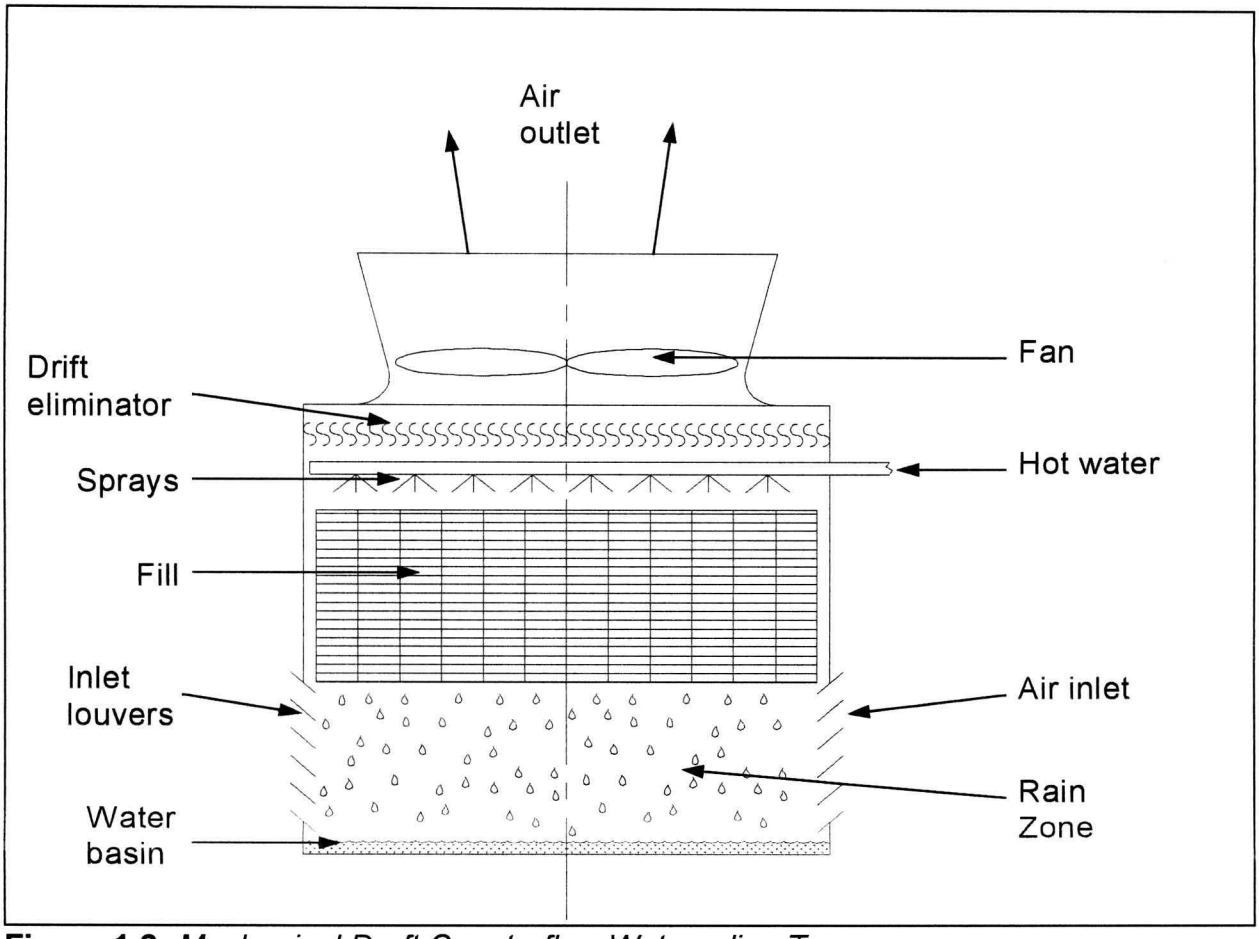

Figure 1.2: *Mechanical Draft Counterflow Wet-cooling Tower.*

The function of a wet-cooling tower is to cool water by bringing it into direct contact with colder, dry air. The cooling occurs as a combination of sensible heat transfer and the evaporation of 1-3% of the water flux. The two key factors in this transfer are interfacial area and contact time between the water and the air, both of which are increased by spraying water over a fill (splash bars or film plates), and passing air through the fill. Tower design mirrors these factors by facilitating optimum airflow patterns and fill arrangement with minimum resistance to airflow. The flow arrangements most commonly used are counterflow and crossflow, where the direction of the

airflow relative to the waterflow, distinguishes the tower type. The counterflow tower will be the focus of this thesis. In the case of a natural draft tower, the airflow through the fill is maintained by the buoyancy effect of warm, moist air flowing through a tall chimney (figure 1.1). In a mechanical draft tower the airflow is provided by a fan (figure 1.2). Natural and mechanical draft towers are both in common use today.

1.1 Modelling Cooling Tower Performance

The thermal efficiency of a power plant is directly dependent on the performance of the plant's heat sink. In the case of an under performing cooling tower, inefficient heat disposal will lead to increased back pressure on the turbines and continuous loss of power generation capability. Even a comparatively small loss of a few megawatts in cooling capacity may amount to millions of rands in lost revenue per year. Surveys conducted by Burroughs [83BO1] and EPRI and TVA [88EP1] showed that a majority of the plants surveyed were operating cooling towers significantly below specification capability. Consequently industry has invested in extensive research and development to improve the accuracy of cooling tower performance prediction.

One of the first attempts at modelling wet-cooling tower processes was made by Merkel [26ME1] in 1926. Since then, many researchers have adapted, modified and improved Merkel's methods for use with a range of cooling tower configurations [52CH1, 76KE1, 77NA1, 83MA1, 84PO1]. In order to successfully model the thermal performance of a given tower design, a mathematical model, that provides an accurate solution to conservation equations for mass, momentum and heat, is needed. In addition, physical models that express resistance to airflow and two-phase heat and mass transfer must be available, usually as empirical correlations of experimental data. Current practice is to use either a one-dimensional point average method or a multi-dimensional finite difference approach to solve the conservation equations.

Several multi-dimensional CFD packages have been developed to predict the performance characteristics of wet-cooling towers. These include two- (VERA 2D [83MA1] , STAR [87CA1]) and three-dimensional (TACT [88RA1]) models. Although these programs vary in sophistication, it is currently impractical to simulate small-scale geometries (e.g. fills, drift eliminators, etc.) and their effects on tower performance. Consequently, even the most powerful

of simulation packages must rely on external input, in the form of experimental correlations, to quantify the transfer characteristics within complex structures. These codes are therefore not necessarily more accurate in their predictions than the point models. In addition, high resolution CFD programs tend to be time consuming and therefore, preclude comprehensive optimisation of tower designs.

The point model relies on control volumes to solve the conservation equations, with average transfer characteristics obtained from empirical or analytical sources. The primary drawback of the point model is that it requires horizontal homogeneity in the fill transfer characteristics, but under the specified conditions it delivers a high degree of accuracy. The point method draft equation has been extensively modified since its inception to include the effects of pressure gradients, dimensional variation and other variables. Kröger [98KR1] presents a highly detailed variation of such a model.

For natural draft towers, a buoyancy driven draft equation couples fluid flow and heat transfer to satisfy the momentum integral. This equation is based on the postulate that the hydrostatic pressure difference, caused by the difference in density of the warm moist air inside the tower and the cooler dry air outside, is equal to the pressure loss experienced by the air as it flows through the tower. In its simplest form it can be expressed as,

$$(\rho_{amb} - \rho_{tower})gH = K_t\left(\frac{1}{2}\rho\, v_{fill}^2\right) \tag{1.1}$$

The left hand side represents the driving force due to buoyancy, while the right hand side of equation (1.1) relates the pressure drop in the airflow due to obstructions such as the fill and entrance effects. For a mechanical wet-cooling tower a similar draft equation is used,

$$\Delta p_{fan} = K_t\left(\frac{1}{2}\rho\, v_{fill}^2\right) \tag{1.2}$$

but the airflow is induced by the pressure difference across the fan, thus the fluid flow is not highly dependent on the heat transfer.

In both cases, K_t, represents the total pressure drop coefficient based on conditions in the fill. Neglecting minor losses, K_t in a wet-cooling tower is the sum of inlet losses, rain zone pressure drop and drag caused by the fill and support structures in its vicinity. Of the three, only the fill associated losses constitute a purely one dimensional axial pressure drop and are consequently geometry independent and simple to configure.

In this study analytical, experimental and numerical methods will be used to investigate the rain zone pressure drop (denoted by K_{rz}), the inlet pressure loss (K_{ct}), and the interdependence between these pressure drop coefficients. The aim is to derive correlations that will accurately predict the magnitude of K_{rz} and K_{ct} under the diverse circumstances found in wet-cooling towers. It will be shown that previous researchers unduly simplified or wrongly modelled these phenomena by neglecting the interdependence between the coefficients, erroneously applying dry-cooling models to wet systems and making mathematical errors in the rain zone analysis. Alternative prediction methods will be presented throughout this thesis. In addition, the heat and mass transfer in the rain zone will be investigated and correlations derived to predict the transfer coefficient, as an extension to the pressure drop analysis (Appendix A).

1.2 Flow Resistances in Wet-cooling Towers

Designing a cooling tower entails the accurate prediction of the cooling capacity of the tower. The enthalpy transfer coefficient (and thus the cooling capacity) for an evaporative heat exchanger is strongly influenced by the mass flux of the cooling medium. The mass flux is in turn dependent on the driving force (buoyancy for a natural draft tower or fan pressure for a mechanical draft tower) and the flow resistances. The flow resistances for a wet-cooling tower can be categorised as follows:

- Flow obstructions in the vicinity of the inlet (tower supports, inlet louvers)
- Inlet losses
- Falling droplets (rain zone, spray zone)
- Flow obstructions in the vicinity of the fill (fill support, fill, water distribution system, drift eliminators)
- Dynamic losses (fill contraction and expansion losses, outlet losses)

Each of these individual losses have been extensively studied, e.g. [61LO1, 82CA1, 86BE1, 88DU1, 92ZH1, 94TE2] and correlations exist to express loss coefficients as a function of the relevant variables. What has been less intensively investigated is the interdependence of these flow resistances. Most of the tower losses are one dimensional in nature and mutually independent. The notable exceptions being the inlet loss and the rain zone pressure drop, both of which include horizontal and vertical components in their loss coefficient. While the rain zone pressure drop is dependent on the inlet flow field, the mean flow below the fill is largely independent of the other flow resistances and K_{rz} can therefore be approximated as an independent resistance. The inlet loss, on the other hand, has been shown to be strongly coupled to vertical resistances in the tower cross-sectional inlet [86GE1].

In dry-cooling towers the inlet losses have been found to be a function of (among other variables) the pressure drop across the heat exchanger assembly. Correlations produced by Terblanche [94TE2] are an example of equations that illustrate this dependency. Terblanche's or similar equations are currently used to find the inlet losses in wet-cooling towers, with the assumption that all losses in the vicinity of the fill are summed to find the equivalent heat exchanger pressure drop. None of these equations can or do, however, take the rain zone pressure drop's effect into account when calculating the inlet loss. Considering that a large part of the rain zone pressure drop occurs near the fill, where droplets are still accelerating rapidly, this omission becomes significant. The primary focus of this thesis will be to correct this discrepancy and to increase the accuracy of tower simulation by providing tools to predict the phenomenon.

1.3 The Rain Zone Pressure Drop

The rain zone pressure drop is caused by the transfer of momentum from falling droplets below the fill to the air stream and *vice versa*. Water, having passed through the fill, forms droplets at the bottom of the packing that fall toward the pond. The interaction of falling droplets and the airflow traversing the rain zone (fig. 1.3) causes the droplets to be retarded in their fall and be displaced toward the tower axis. The mechanical energy expended by the air to accomplish this is registered as a drop in pressure across the rain zone. Accordingly, the rain zone loss coefficient is defined as,

$$K_{rz} = \frac{\Delta p_{rz}}{1/2 \rho_a v_i^2} \tag{1.3}$$

where Δp_{rz} is the pressure drop mentioned above and v_i is the vertical velocity of the cooling medium through the horizontal cross-sectional inlet area of the tower (inlet to the fill).

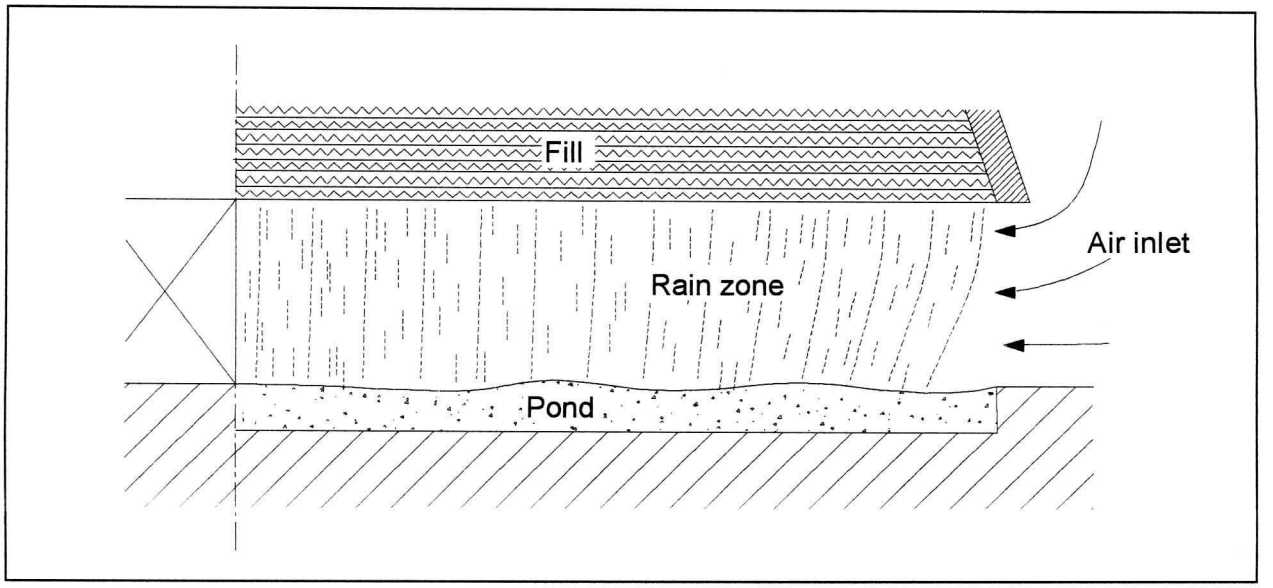

Figure 1.3: *The Rain Zone of a Circular Counterflow Wet-cooling Tower.*

As mentioned previously, the rain zone pressure drop is a major contributing factor to the total tower resistance. It is also inextricably linked to the inlet loss as both these pressure drops coincide in the tower inlet section. As will be explained later in this chapter, the capability to predict the rain zone pressure drop is essential to the analysis of wet-cooling tower inlet losses. For these reasons, it is necessary to acquire correlations that accurately describe the rain zone loss coefficients.

Many researchers have studied the rain zone through the years [61RI1, 61LO1, 86BE1, 86BE01, 92ŠE1, 92ZH1, 90HO1, 94TE1] with approximations of the magnitude of its associated loss becoming successively more accurate. A study of the literature reveals that most of the earlier researchers oversimplified the problem though, while more recent investigations are fraught with conceptual errors and/or inadequate correlations. Chapter 2 of this thesis will be devoted to correcting this deficiency, by repeating the work of previous researchers while attempting to avoid their errors.

Since experimental investigation of the rain zone loss in counterflow towers is made impossible by the coincidence and interdependence of the inlet and rain zone losses, a numerical approach, based on Lagrangian tracking of the drops and a potential flow solution for the airflow, will be utilised to model this phenomenon. A solution for both circular and rectangular geometries will be sought.

1.4 Tower Inlet Losses

Inlet losses are the pressure drops traditionally associated with entrance effects to duct flows. The sudden contraction of flow as it enters the duct (figure 1.4) and high shear stresses in the molecules adjacent to the wall just inside the entrance causes the separation of the accelerating fluid downstream of the entrance. The recirculating fluid produces a pinch in the flow, causing the main stream to contract through a minimum diameter, called the *vena contracta*. Frictional head losses occur mainly at the leading edge of the entrance, where high shear stresses arise, and in the recirculating region bounding the vena contracta. The current theory on recirculating flows and the *vena contracta* is not well developed, consequently the pressure loss for sudden contraction must be found experimentally, such is also the case with cooling towers.

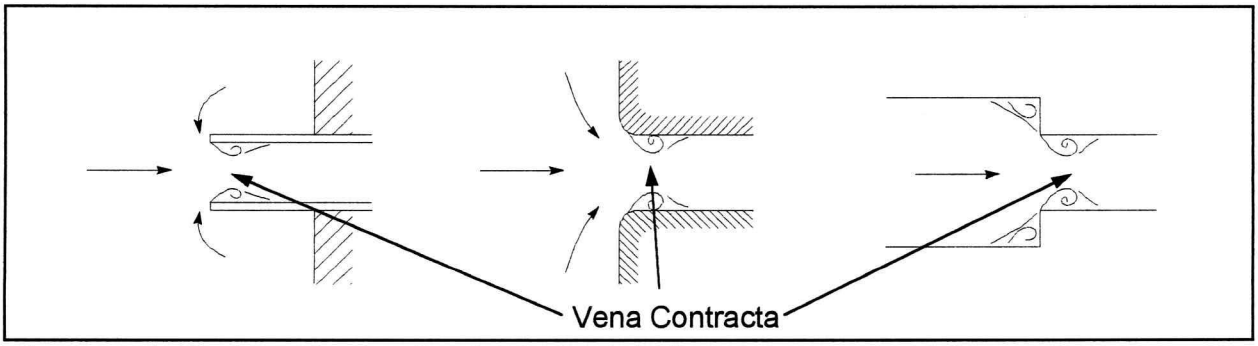

Figure 1.4: *Sudden Contraction in Duct Inlet Flows.*

Tower inlet losses are ascribed not only to conventional entrance effects, but to a complex combination of flow perturbations. To fully illustrate the various effects, consider the path of the air as it enters a cooling tower (fig. 1.5).

Initially the stagnant atmospheric air accelerates toward the tower inlet. Already minor losses occur due to drag over the surface. At the tower inlet the flow contracts and exhibits the characteristics of duct inlet flows. Flow separation will occur at the leading edge of the tower shell unless it is well rounded, in which case contraction losses will be reduced. Additionally,

steep velocity gradients perpendicular to the shell promote turbulence formation and local viscous losses. At the trailing edge of the shell the flow separates commensurate with suddenly expanding duct flows. A volume of fill or heat exchanger will be subject to saturated recirculating flow caused by this separation. The magnitude of the recirculating region is a function of the ratio of the inlet area to the horizontal cross-section area of the tower, where larger entrances tend to suppress recirculation. Higher flow resistances, encountered after the trailing edge in the region of the fill/heat exchanger, cause the velocity distribution through the fill to become more uniform, which equates to a smaller recirculating volume and a corresponding reduction in the inlet loss.

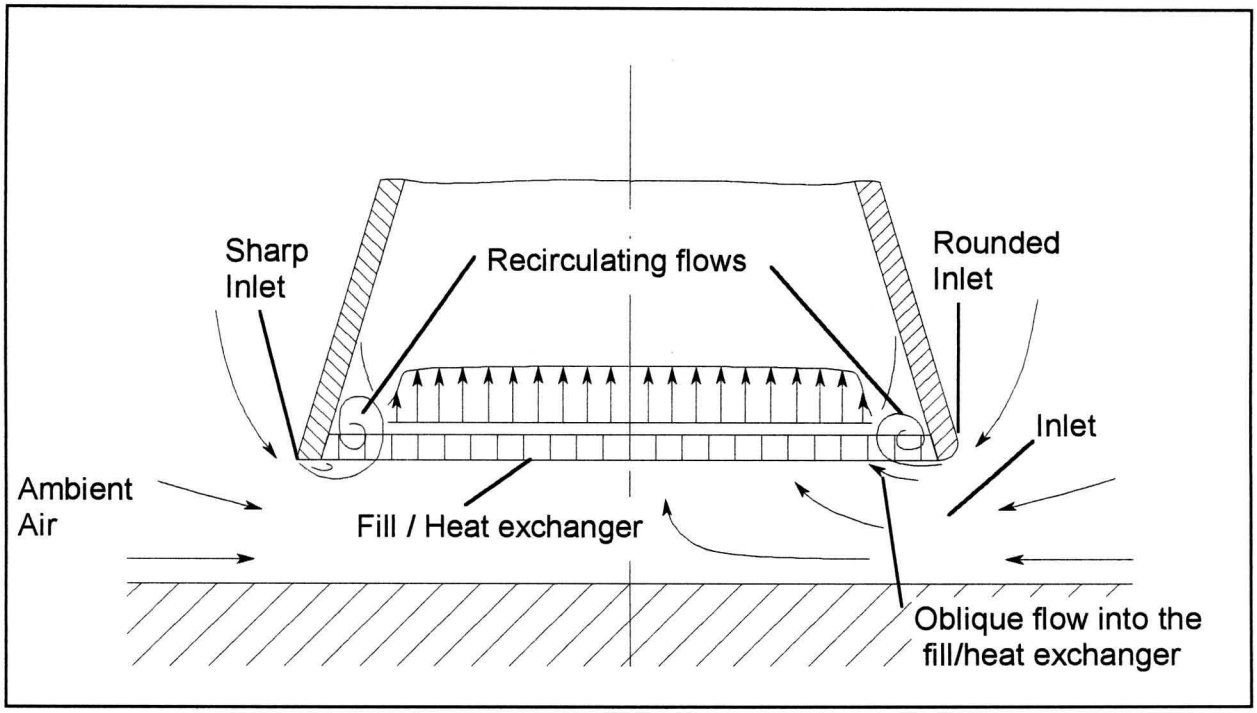

Figure 1.5: *Schematic representation of Tower Inlet Flow Patterns.*

The final effect that amplifies the inlet loss occurs when the coolant enters the fill or heat exchanger. Flow resistances in fills and heat exchangers are established under normal flow conditions, but in cooling towers air commonly enters the assembly at an oblique angle, especially near the entrance. Additional losses accrue, depending on the fill type. In isotropic-splash-type fills, air entering at an oblique angle follows a longer path through the fill resulting in higher pressure difference across the resistance. Orthotropic resistances, such as film-type packing and finned heat exchangers, force oblique flows to undergo separation at the leading edge of the plate/fin as the flow changes direction (fig. 1.6). Head losses similar to suddenly expanding flows are observed. These losses cannot be included in the fill or heat exchanger loss coefficient since

they vary horizontally and are contingent upon the flow field generated by a particular tower geometry.

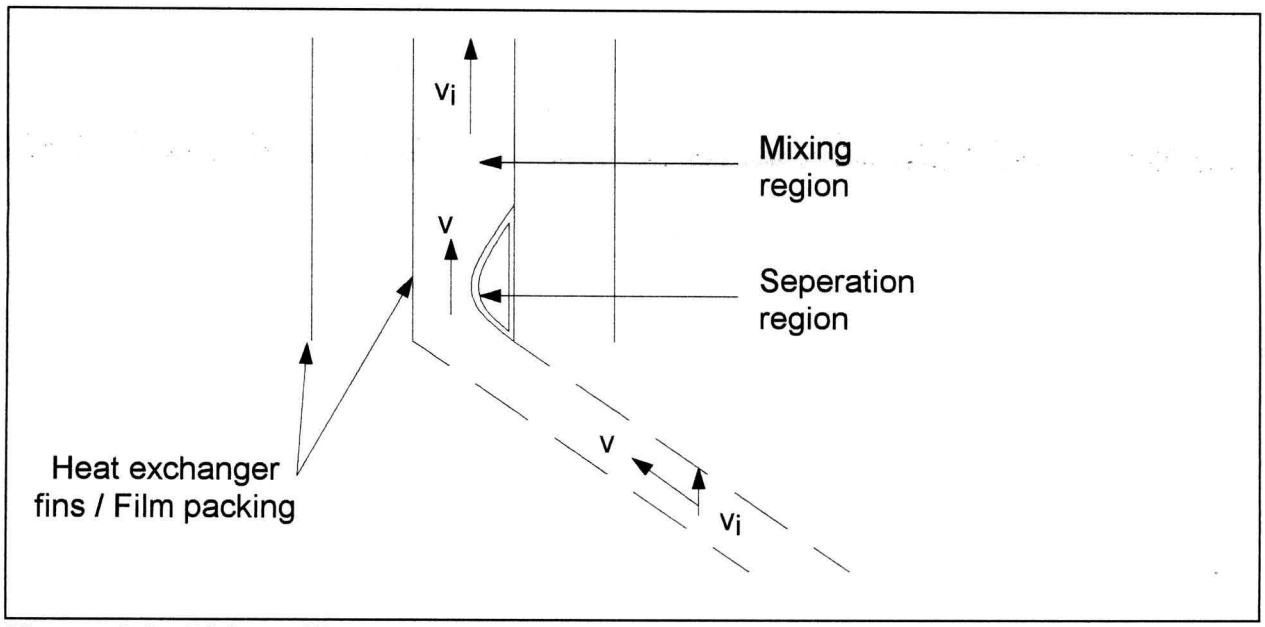

Figure 1.6: *Oblique Flow entering an Orthotropic Resistance.* [98KR1]

Although the total inlet loss can be ascribed to these various effects, their interdependence is such that it is impossible to differentiate their individual contributions to the whole. A sharp inlet, for instance, will not only attenuate the separation regions caused by sudden contraction and expansion, but will significantly affect the obliquity of the flow entering the fill, with corresponding changes in the inlet loss. The oblique flow losses will in turn affect the recirculating flow, etc. In addition, the geometries of cooling towers differ significantly from that of duct flows, with the implication that all derivations and experiments for the standard flow perturbations have to be repeated for each resistance effect. The obvious alternative is to group these losses together and experimentally find the total inlet loss as a function of all the relevant variables.

In staying with the point model approach to tower modelling, a loss coefficient representing the pressure drop associated with the entrance flows to the tower has to be defined. Unfortunately, it becomes clear upon investigation that inlet losses are intrinsic to the flow field in a particular tower arrangement. In other words, inlet losses cannot be determined separate from the tower, as can, for instance, heat exchanger or other static resistance losses. In general terms, inlet losses are the losses in a cooling tower inlet section not accounted for by the known flow resistances.

The inlet loss coefficient for a counterflow cooling tower can be expressed in terms of the change in total pressure between stagnant ambient air, p_a, far from the tower and the air after the drift eliminator (or heat exchanger), p_o. (The drift eliminator is the last flow resistance in the vicinity of the fill, while for a dry-cooling tower there is no nearby resistance above the heat exchanger.) For a uniform velocity distribution after the drift eliminator (heat exchanger) the inlet loss coefficient can be defined as,

$$K_{ct} = \frac{p_a - \left(p_o + \rho_o v_o^2 / 2\right) - \int_0^{Ho} \rho g \, dz}{\rho_a v_i^2 / 2} - K_{sum}\left(\frac{\rho_a}{\rho_{fi}}\right)\left(\frac{A_i}{A_{fr}}\right)^2 \tag{1.4}$$

where A_i is the inlet cross-sectional area of the tower, A_{fr} is the frontal area of the fill and ρ_{fi} is the harmonic mean density of the air flowing through the fill (heat exchanger). The subscript 'i' refers to conditions at the cross-sectional inlet, 'o' to conditions above the drift eliminator (or heat exchanger) and 'a' represents ambient conditions. Furthermore, z is the direction perpendicular to the surface, so that the integral represents the pressure drop caused by the change in elevation of the air flow. For a wet-cooling tower the resistance term, K_{sum}, can be found from,

$$K_{sum} = \left[K_{ts} + K_{il} + K_{rz} + K_{fs} + K_{ctc} + K_{fi} + K_{cte} + K_{sp} + K_{wd} + K_{de}\right]_{fi} \tag{1.5}$$

where all the summed coefficients are referred to average fill conditions. Similarly, K_{sum}, for a counterflow dry-cooling tower with horizontal heat exchangers is given by,

$$K_{sum} = \left[K_{ts} + K_{hes} + K_{ctc} + K_{he} + K_{cte}\right]_{he} \tag{1.6}$$

where summed pressure loss coefficients are referred to conditions through the heat exchanger.

The definition provided by equation (1.4) will only produce reliable data on the inlet losses if applied to full scale cooling towers. This negates any benefit that might be derived from the optimisation of tower design. By making some assumptions, however, a modelling strategy that predicts K_{ct} for full scale wet-cooling towers, can be devised.

1.5 Modelling of Inlet Losses in Wet-cooling Towers

One of the first attempts at modelling cooling tower inlet losses was made by Lowe and Christie [61LO1]. They use an ingenious mathematical model coupled with scale model experiments to find the inlet losses for both empty and packed towers. The experimental data is correlated with full scale measurements and they conclude that empty tower resistance can simply be added to the total flow resistance through the packing. This correspondence seems to be largely fortuitous, as recent investigations [86GE1,88DU1] have shown a strong correlation between the magnitude of the inlet loss and that of the heat exchanger pressure drop.

Since Lowe and Christie, many other researchers [68VO1, 71ZE1, 81GA1, 81MO1, 86GE1, 88DU1, 92ZH1, 94TE1] have used experimental and theoretical techniques in an attempt to study these losses. These focused largely on scale model tests of inlet sections, with or without a fill or heat exchanger, but never include an attempt to account for the rain zone's influence on K_{ct}.

1.5.1 Modelling Options

There are several possible approaches to simulating cooling tower inlet losses,

- Theoretical analytical model
- Experimental evaluation
- Numerical simulation i.e. Computational Fluid Dynamics

or a combination of the above. Each of these methods have their own advantages and disadvantages when used to simulate cooling tower inlet losses. These are detailed briefly below.

Theoretical analysis

Analytically modelling the inlet losses for a tower with an empty shell has been shown to be practical, if somewhat involved [61LO1]. By representing the flow as a two-dimensional system and then mapping it onto the complex plane using the Schwartz-Christoffel theorem an implicit solution for the contraction losses in a hollow tower may be obtained. As soon as flow resistances (fill, rain zone) are added to the model, however, the analysis breaks down. The complex flows

caused by the tower geometry are further disrupted by adding resistances, making the flow field impervious to solution by analytical techniques. Therefore, analytical methods are unsuited to the problem at hand.

Experimental evaluation

Experimental approaches have had great success in predicting the inlet losses in dry-cooling towers [94TE1], provided tower conditions and structure were closely simulated. This is accomplished by use of large test sections, where Reynolds numbers comparable to full scale towers can be achieved, and heat exchanger material similar in structure to actual heat exchanger finned tubes.

When modelling wet towers, the added complexity of the rain zone has to be taken into account. Currently, the calculated pressure drop for the rain zone is simply added to the tower's total resistance. As will be shown later in this thesis, this is a gross simplification of conditions existing in the inlet sections of cooling towers.

To accurately predict the inlet loss for a wet-cooling tower, the effect of the rain zone's resistance on K_{ct} has to be determined. For experimental investigations, this entails adding an additional resistance to the inlet of the test section. This resistance must mirror the effect of falling droplets below the fill. Using normal droplets in a scale model has proven impractical, since the range of droplet Reynolds' numbers and droplet density present in a full sized tower cannot be duplicated on scales other than one to one. Static resistances mimicking the effect of the rain zone, have also proven difficult to implement, because of the large number of variables that characterise the rain zone and the non-homogeneity of the actual rain zone resistance.

When experimentally modelling the inlet loss for wet-cooling towers, a correction term has to be applied to dry-tower data to account for the rain zone resistance. This correction term is difficult to find experimentally. To overcome this problem a numerical approach is suggested.

Numerical simulation

With the advent of high powered computers, the discretized solution of the Navier-Stokes equations for the flow in complex geometries, have become possible. Many researchers have used

computational fluid dynamics modelling (CFD) to simulate the flow in and around cooling towers [83MA1, 88RA1, 97EL1].

Benocci et al. [86BE01] in particular, focuses on the air-droplet interaction in the inlet section of a natural draft tower. The droplet phase, modelled using a Lagrangian approach, is coupled to the gas phase equations via momentum source terms. Droplets are modelled as non-interacting spheres and the effects of turbulence on the gas flow are represented as a fluctuating body force. Although Benocci et al. validate their model using small scale experiments and full scale measurements of the velocity distribution above the fill, they present no correlation that quantifies the momentum transfer characteristics of the inlet section.

Computational fluid dynamics presents a useful tool for the prediction of wet-cooling tower inlet losses. Unfortunately, the turbulence models currently available for use with CFD simulations are impractical for solving the small scale eddies present within large unbounded recirculating regions. The complexity of turbulent flows requires a large number of computations to resolve and is difficult to implement in the large flows present within cooling towers. A classical example is the backward facing step (fig. 1.7), where sudden expansion forms a recirculating region that is currently impervious to accurate numerical solution.

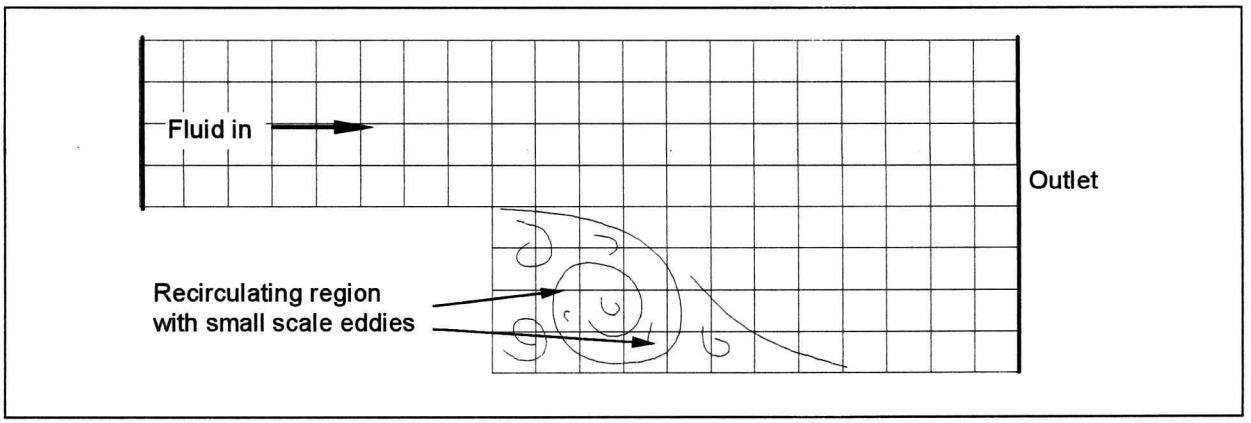

Figure 1.7: *Flow Separation across a Backward Facing Step.*

As noted previously, recirculating flows are a major contributing factor to tower inlet losses. This phenomena does not cause a problem in dry-cooling towers, since the recirculating flow is largely bounded by the heat exchanger fins. In wet-cooling towers with splash type packing or film type fills, where the air enters parallel to the fill sheets, this bounding effect is not present. Numerical

results for such inlets consistently predict lower than expected inlet losses. CFD does, however, satisfy all other criteria when used to model cooling tower flows. Complex geometries, the rain zone, the fill and other static resistances can all be accurately simulated.

The formulation of a turbulent theory to account for the losses experienced in recirculating flows is beyond the scope of this work. Instead, a compromise between numerical and experimental investigations that incorporates certain aspects of both, will be sought.

1.5.2 Modelling Strategy

The chief aim of this thesis is to derive a correlation that predicts the inlet loss coefficient for counterflow wet-cooling towers. Since direct numerical or experimental investigations are impractical, an approximation based on the correction of experimental correlations using CFD will be investigated.

The model, represented by figure 1.8, includes the following:

- Accurate empirical correlations for the inlet loss coefficient in dry-cooling towers. These correlations are found by using scale model experiments and must account for both film type (orthotropic resistance) and splash type (isotropic resistance) fills.
- CFD simulation of dry-cooling tower inlet losses, reflecting the experimental model, for use as datum values for the wet simulation.
- Computational Fluid Dynamic simulation of wet-cooling tower inlet region. The results of this simulation is a pressure loss coefficient that includes the rain zone and inlet pressure loss.
- A correlation that returns the pressure drop for the rain zone caused by momentum transfer to the droplets.

First, experimental correlations for the inlet loss coefficient in dry towers with isotropic and orthotropic packing (fill) must be available. Equations for both rectangular and circular tower geometry are needed, which can either be found in the literature or be derived from scale model tests. Chapter 3 elaborates on the acquisition of these equations.

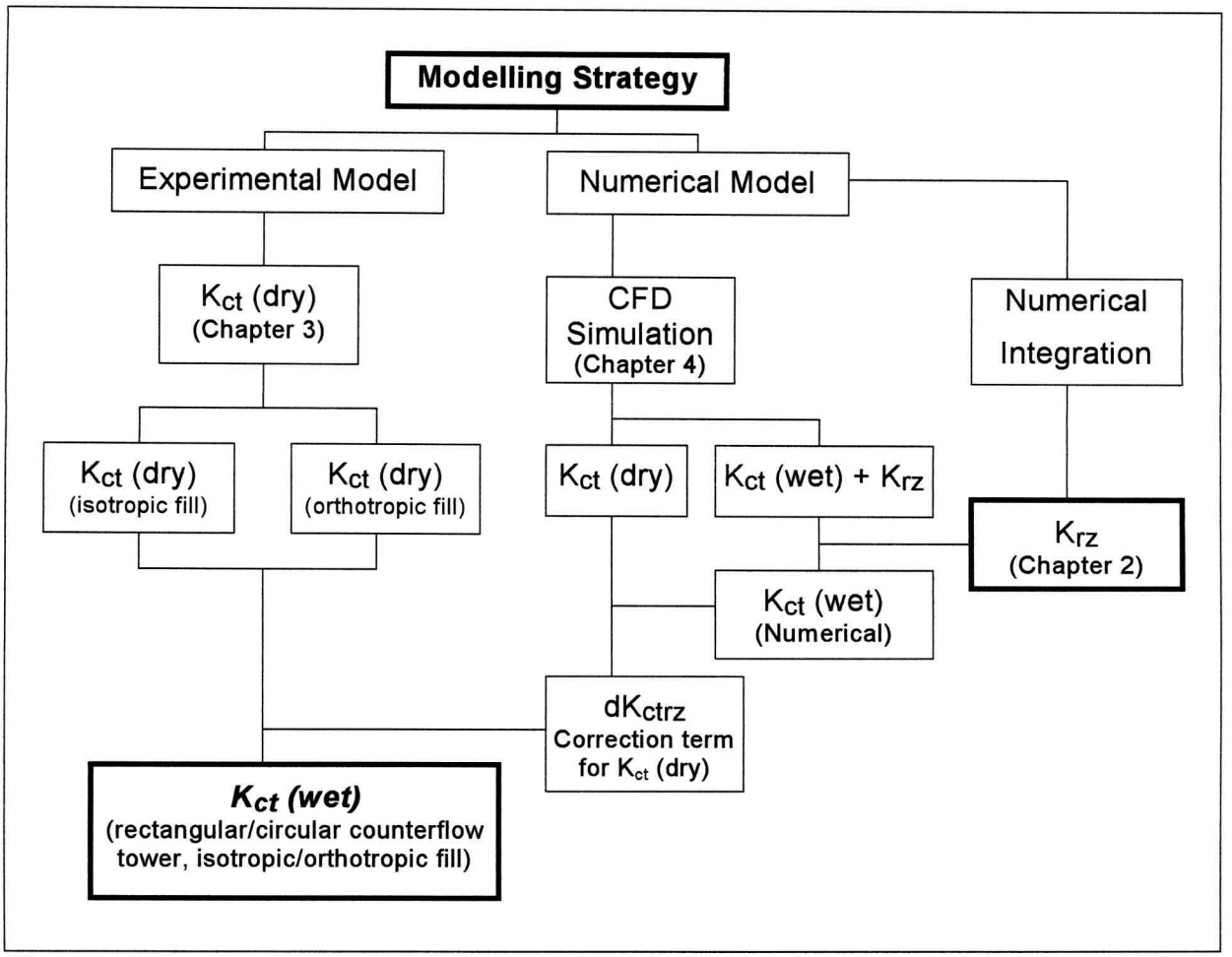

Figure 1.8: *Inlet Loss Coefficient Modelling Strategy.*

The CFD package, Star-CD v3.00 [96CO1], is used to simulate simplified wet-cooling towers. The pressure drop between ambient conditions and the top of the fill is found by using an array of sensor cells above the fill. K_{ct} is extracted from this pressure drop by subtracting the fill and rain zone loss coefficients. (The derivation of the rain zone loss coefficient, K_{rz}, is undertaken in Chapter 2.) Next, the inlet loss correction factor, dK_{ctrz}, is found by simulating dry tower inlet losses and comparing them to the numerical results for wet inlet losses. Applying this correction term to the experimental correlations for dry K_{ct}, yields the inlet loss coefficient for a geometrically similar wet-cooling tower. The methodology of the numerical analysis is discussed in Chapter 4. The influence of the inlet loss correction factor and heat transfer results (Appendix A) on the performance evaluation of a circular wet-cooling tower, is shown in Appendix B. Additional measures to enhance tower performance are also investigated by means of a point-model cooling tower simulation (Appendix B).

CHAPTER

TWO

ANALYSIS OF MOMENTUM TRANSFER IN THE RAIN ZONE OF COUNTERFLOW COOLING TOWERS

In this chapter the rate of momentum transfer in the rain zone of two counterflow cooling tower geometries (circular and rectangular) is analysed using a simplified flow field and numerical integration. Momentum transfer is calculated from the air flows mechanical energy loss caused by air-droplet interaction. The objective of the analysis is to generate equations for use in one-dimensional mathematical cooling tower performance evaluations and inclusion in the inlet loss modelling strategy proposed in Chapter 1.

2.1 Literature Survey of Rain Zone Losses

Rish [61RI1] was one of the first researchers who studied the effect of the rain zone on cooling tower performance. He uses experimental data, from full scale tests on two counterflow towers with film type packing, to derive the following expression for the rain zone loss coefficient,

$$K_{rz} = 0.5249\, L_{rz} \left(\frac{G_w}{G_a} \right)^{1.32} \tag{2.1}$$

The rain zone pressure drop cannot be accurately determined from experimental investigations, since its effect cannot be differentiated from the inlet loss. (Conversely, the inlet loss cannot be determined separately from the rain zone, because of its dependence on the rain zone loss.) Moreover, Rish's equation is limited to a very narrow range of tower geometries (inlet ratios) and a single droplet size, which nullifies its general applicability.

Lowe and Christie [61LO1] also investigate pressure drop in counterflow rain zones, but admit that their results are inconclusive and do not attempt to derive a relation to predict this

phenomenon. They also assume that droplet velocity approaches terminal velocity for most of the rain zone volume, which is not usually the case. Numerical investigations have shown that, for modern tower geometries, droplets mostly reach terminal velocity just before entering the pond.

Benton and Rehberg [86BE1] investigate the rain zone pressure drop for pure counterflow and crossflow scenarios using a Lagrangian approach to droplet modelling. Missimer and Bracket [86MI1] use experimental methods to calculate the pressure drop in crossflow rain zones. Neither approach is applicable to the two-dimensional flows present within operational counterflow wet-cooling tower inlet sections.

Benocci et al. [86BE01] use computational fluid dynamics to model the air-droplet interaction in the inlet section of a natural draft counterflow wet-cooling tower. No method is presented for predicting the rain zone pressure drop, separate from the inlet loss, however.

Šedina [92ŠE1] uses various methods [61LO1, 86BE1] to determine the rain zone loss and then validates the calculations using full scale measurements. It must be emphasised again that an experimental evaluation of two-dimensional rain zones will always include aspects of the inlet loss and will therefore produce erroneous results regarding the rain zone.

Hoffmann and Kröger [90HO1] and Terblanche [94TE1] assume a potential flow solution to the inlet airflow field which acts on droplets that are modelled using a Lagrangian approach. They also assume, erroneously, that the component forces of the air acting on the droplets may be summed and the resulting pressures added in vector form to find the pressure drop relative to the inlet and outlet sections of the rain zone. In mathematical form,

$$\Delta p_{rz} = \left[\left(\frac{\sum_1^n F_x}{A_{zi}} \right)^2 + \left(\frac{\sum_1^n F_z}{A_i} \right)^2 \right]^{0.5} \tag{2.2}$$

where $A_{zi} = \pi d_i H_i$ is the vertical inlet area below the shell and $\sum_1^n F_x$ and $\sum_1^n F_z$ are the sums of all the drag forces acting on the droplets in the horizontal and vertical directions respectively. If

one investigates the mechanics of the problem it becomes clear that droplet drag forces applied in such a manner will result in a non-physical pressure value and not a pressure drop across the rain zone. The more correct approach would be to consider the rain zone pressure drop to originate from work done by the air stream on the falling drops i.e.

$$\Delta p_{rz} = \sum_{1}^{n} \left[\frac{F_x v_{ax}}{A_i v_i} + \frac{F_z v_{az}}{A_i v_i} \right] \tag{2.3}$$

where v_{ax} and v_{az} are the components of the local air velocity and v_i is the average velocity of the air leaving the rain zone, i.e. $v_i \approx m_a / (\rho_a \pi r_i^2)$. Zhenguo et al. [92ZH1] employ this approach, but renege to fit an adequate equation to numerical data, with the result that the relation is only valid for a very narrow range of some of the primary variables. Most inquiries into rain zone characteristics also fail to incorporate the effects of droplet deformation. In this thesis an approach that follows from the work of Terblanche and Zhenguo et al. will be used in an attempt to arrive at a more accurate simulation.

Before analysing the momentum transfer in the rain zone of a counterflow wet-cooling tower, certain simplifying approximations must be made:

- No droplet agglomeration, collision or coalescence occurs. (This is not strictly true; these phenomena do seem to have a variable effect on rain zone characteristics, but formulation of such a model is beyond the scope of this work.)
- The water mass flow through the fill is evenly distributed and all droplet diameters are equal. (In practice, an effective droplet diameter must be used.)
- Droplets enter the rain zone with zero absolute velocity. (Numerical tests have shown that variable droplet inlet velocities have a relatively small influence on overall performance if they (the drops) enter the rain zone at below 10 percent of the drop's terminal velocity.)
- Falling droplets have little effect on the velocity distribution of the air, so that a potential flow solution to the air flow, neglecting droplet effects, is a good approximation [92ZH1].
- There is no mutual interaction between droplets with regards to mass transfer and viscous drag.

- Both droplet and air physical properties change negligibly while traversing the rain zone. (A study by Conradie [93CO1] indicates less than one percent overall variation of the mass transfer coefficient.)

2.2 The Rain Zone Air Velocity Field

The volume of inviscid free stream flow in operational cooling towers is large compared to viscous boundary layer flow, especially in the rain zone. Therefore, potential flow theory can be used to find a good approximate solution to the airflow field in the inlet section of a counterflow cooling towers. The following analysis of the airflow in a circular tower is based on work done by Hoffmann and Kröger [90HO1].

2.2.1 Circular Cooling Towers

Consider the airflow patterns in the inlet section of a circular counterflow cooling tower (Fig. 2.1). The flow is axi-symmetrical and if frictional effects can be neglected a solution must be obtained for a two-dimensional cylindrical co-ordinate potential flow problem. Hoffmann obtains a simple solution to the problem by assuming the air velocity through the fill to be uniform. Under such circumstances the following boundary conditions are applicable:

$v_{az}(r,0)=0$;	impervious surface
$v_{ar}(0,z)=0$;	symmetry axis (tower axis)
$v_{az}(r,H_i)=v_i$, constant;	uniform flow through fill

By defining a potential function $\phi(r,z)$, the radial and axial components of the air velocity vector are given respectively by

$$v_{ar} = -\partial\phi / \partial r \tag{2.4}$$

and

$$v_{az} = -\partial\phi / \partial z \tag{2.5}$$

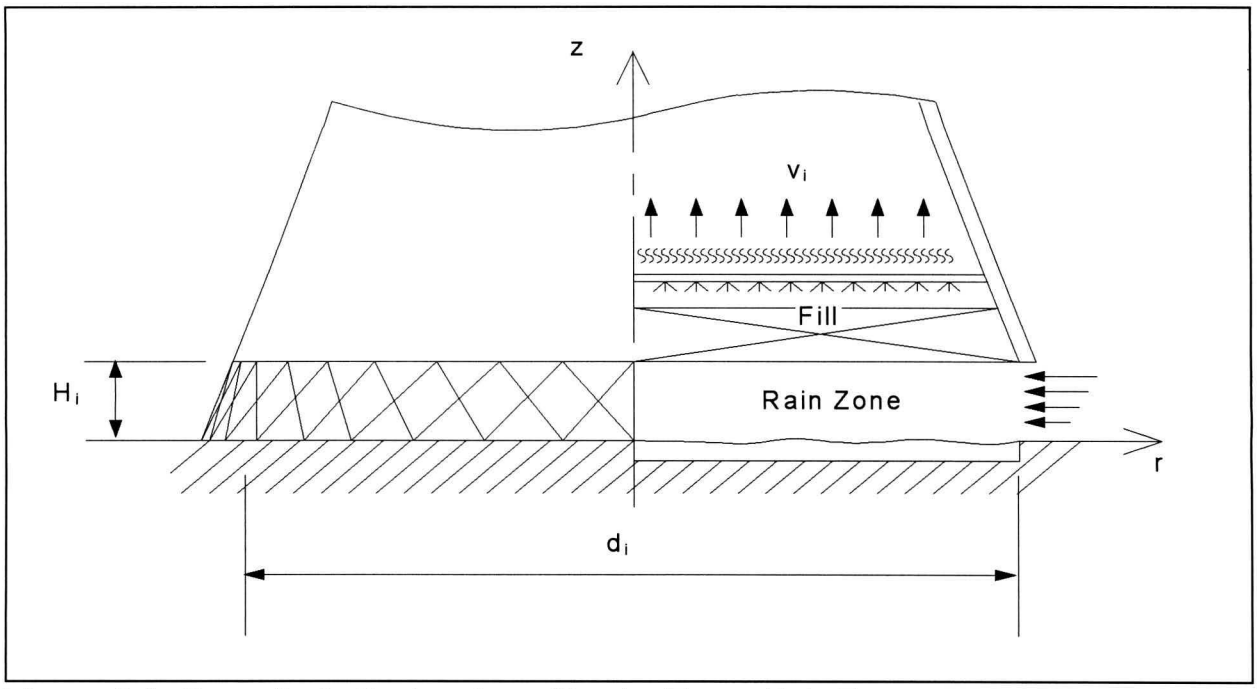

Figure 2.1: *Co-ordinate System for a Circular Tower Rain Zone.*

It can be shown that if ϕ is mathematically smooth enough, the criterion for irrotational flow is satisfied. The continuity equation for steady, axi-symmetrical , incompressible flow becomes,

$$\frac{\partial v_{ar}}{\partial r}+\frac{v_{ar}}{r}+\frac{\partial v_{az}}{\partial z}=0 \tag{2.6}$$

By substituting equations. (2.4) and (2.5) with their partial derivatives into equation (2.6) the equation of continuity written in terms of the potential function, ϕ, may be found.

$$\frac{\partial^2 \phi}{\partial r^2}+\frac{1}{r}\frac{\partial \phi}{\partial r}+\frac{\partial^2 \phi}{\partial z^2}=0 \tag{2.7}$$

The boundary conditions for the continuity equation now become

$$\partial\phi / \partial z(r,0)=0$$

$$\partial\phi / \partial r(0,z)=0$$

$$\partial\phi / \partial z(r,H_i)=v_i$$

A fourth boundary condition is needed to complete the solution of equation (2.7). If the influx of ambient air at the tower inlet is considered purely radial the last boundary condition is obtained.

$$v_{az}(r_i, z) = -\partial\phi / \partial z(r_i, z) = 0$$

In practice such a flow field can only be achieved with a well rounded inlet in the absence of inclined inlet louvers and support struts, but the above boundary condition serves as an adequate approximation. The solution of Eq. (2.7) is found by separation of variables, with λ_n denoting the roots of $J_0(\lambda r_i) = 0$.

$$\phi(r,z) = \sum_{n=1}^{\infty} \frac{-2v_i}{\lambda_n^2 r_i} \frac{J_0(\lambda_n r)}{J_1(\lambda_n r_i)} \frac{\cosh(\lambda_n z)}{\sinh(\lambda_n H_i)} \tag{2.8}$$

with $r_i = d_i / 2$. The infinite series of equation (2.8) may be reduced to a finite number of terms, provided that the converged solution is approached. Consider an example of a tower with the following dimensions: $H_i = 8\,\text{m}$, $d_i = 104\,\text{m}$ and $v_{az}(r, H_i) = v_i = 1\,\text{m/s}$. For a point $(r,z) = (36.575, 5.0)$ a convergence test is done to determine the two partial derivatives of equation (2.8). The results are presented in table 1. Adequate convergence is reached after 50 terms. The resultant velocity vector diagram is shown in figure 2.2.

Table 2.1: Convergence check for partial derivatives of equation. (2.8)

Number of terms	Radial velocity component [m/s]	Axial velocity component [m/s]
25	2.28533	0.62327
40	2.28567	0.62326
50	**2.28591**	**0.62326**
60	2.28567	0.62326

Except for a small discontinuity at the upper edge of the tower inlet caused by merging boundary conditions, the flow may be described by simple linear representations of it's vector components (axial and radial), as shown in figure 2.3. The only deviation that the Bessel function solution shows from the simplified form, is near the tower's inlet. This region and the deviation are small enough, compared to the average flow field, to be ignored.

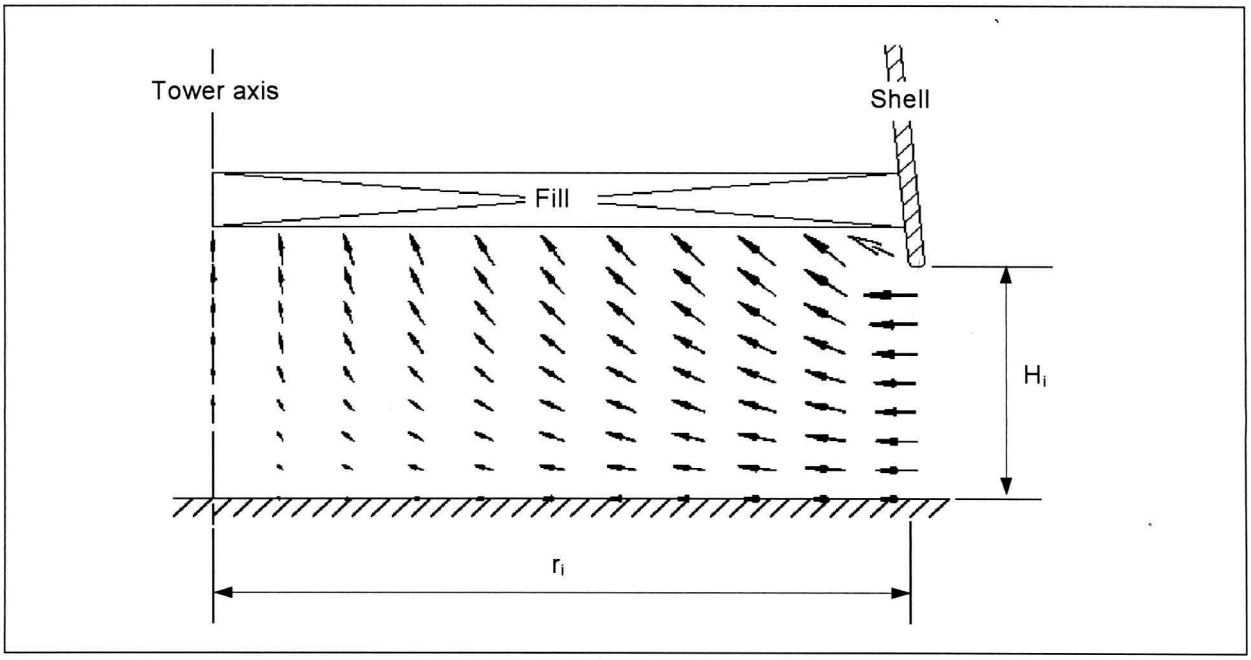

Figure 2.2: *Air Flow Patterns in the Inlet Section of a Natural Draft Cooling Tower.*

The linear model that satisfies equation (2.6) gives the radial air velocity as

$$v_{ar} = -\frac{v_i}{2H_i} r \tag{2.9}$$

and the axial velocity as

$$v_{az} = \frac{v_i}{H_i} z \tag{2.10}$$

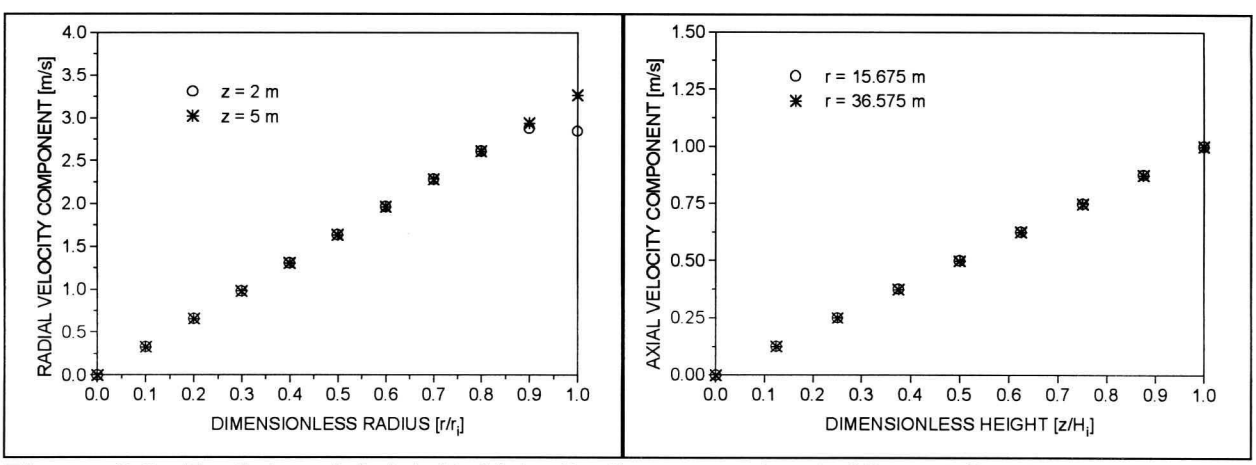

Figure 2.3: *Radial and Axial Air Velocity Components at different Sections in the Rain Zone.*

2.2.2 Rectangular Cooling Towers

In the absence of cross-winds, the flow field in the inlet section of a rectangular tower (fig. 2.4) is essentially symmetrical around the tower centreline. A uniform velocity distribution above the fill may be assumed for high flow resistance towers and if the inlet flow is considered to be purely horizontal, analogous to circular towers, a closed solution to the flow field may be obtained. For the two-dimensional Cartesian co-ordinates, associated with rectangular towers, it is simpler and more convenient to define the flow in terms of a Stokes stream function, $\psi(x,z)$, instead of the potential function employed in the previous section. For a stream function the velocity components are given by,

$$v_x = \frac{\partial \psi}{\partial z} \tag{2.11}$$

and

$$v_z = -\frac{\partial \psi}{\partial x} \tag{2.12}$$

so that continuity is implicitly satisfied.

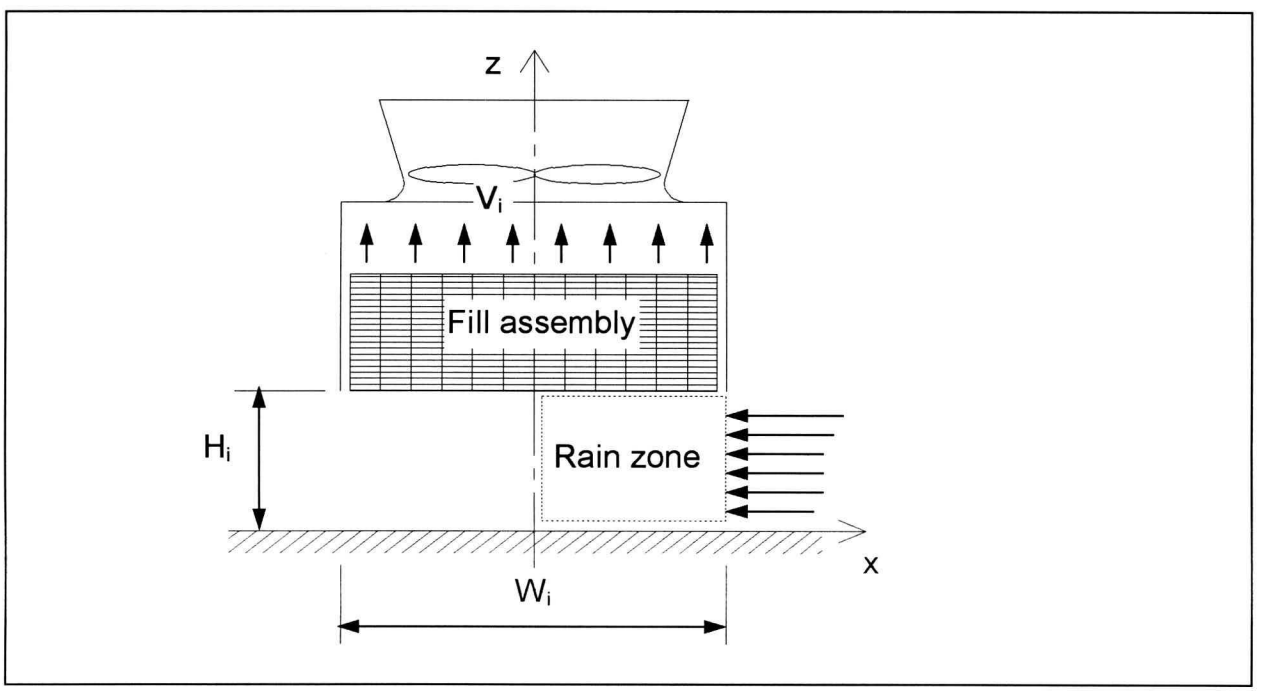

Figure 2.4: *Co-ordinate System for Rectangular Tower Rain Zone.*

For irrotational inviscid plane flow the following relation must be true,

$$\frac{\partial^2 \psi}{\partial x^2} + \frac{\partial^2 \psi}{\partial z^2} = 0 \tag{2.13}$$

which is Laplace's equation. Equation (2.13) can now be solved using separation of variables and the following boundary conditions,

$$v_z(x, H_i) = -\frac{\partial \psi}{\partial x}(x, H_i) = v_i \ ; \qquad \text{uniform vertical flow through fill} \tag{2.14a}$$

$$v_x(0, z) = \frac{\partial \psi}{\partial z}(0, z) = 0 \ ; \qquad \text{symmetry plane} \tag{2.14b}$$

$$v_z(x, 0) = -\frac{\partial \psi}{\partial x}(x, 0) = 0 \ ; \qquad \text{solid surface} \tag{2.14c}$$

$$v_z(W_i / 2, z) = -\frac{\partial \psi}{\partial x}(W_i / 2, z) = 0 \ ; \qquad \text{purely horizontal inflow} \tag{2.14d}$$

The general solution to equation (2.13) is given by,

$$\psi = (A + Bx)(E + Fz) + (C\cosh \kappa x + D\sinh \kappa x)(G\cos \kappa z + H\sin \kappa z) \tag{2.15}$$

where $A,\ldots,H$ are arbitrary constants and κ is a arbitrary non-zero constant. Since only the velocities $-\frac{\partial \psi}{\partial x}$ and $\frac{\partial \psi}{\partial z}$ are of interest, the value of the stream function ψ at the point $(x, z) = (0, 0)$, can be arbitrarily chosen equal to zero, thus

$$\psi(0,0) = 0 \tag{2.16}$$

By using this as a starting point, boundary conditions (2.14b) and (2.14c) can be integrated along the z and x-axis respectively to give,

$$\psi(0, z) = 0 \tag{2.17a}$$

and

$$\psi(x,0) = 0 \tag{2.17b}$$

Now apply these boundary conditions to equation (2.15) to find,

$$\psi(0,z) = 0 = A(E + Fz) + C(G\cos\kappa z + H\sin\kappa z) \tag{2.18}$$

so $A = 0$ and $C = 0$. Update equation (2.15) to incorporate this result,

$$\psi = x(I + Jz) + (\sinh\kappa x)(K\cos\kappa z + L\sin\kappa z) \tag{2.19}$$

where *BE* is written as *I*, *BF* as *J*, *DG* as *K* and *DH* as *L*. Continuing, set

$$\psi(x,0) = 0 = xI + (\sinh\kappa x)(K\cos\kappa z) \tag{2.20}$$

For equation (2.20) to equal zero for all *x*, requires that $I = 0$ and $K = 0$. Apply to equation (2.19),

$$\psi = Jzx + L\sinh\kappa x.\sin\kappa z \tag{2.21}$$

Recall that $\psi(0,z) = 0$, which means that $\psi(0,H_i) = 0$. Integrating boundary condition (2.14a) from $(0,H_i)$ to (x,H_i) results in,

$$\psi(x,H_i) = -v_i x \tag{2.22}$$

Applying this condition to equation (2.21) produces,

$$\psi(x,H_i) = -v_i x = JH_i x + L\sinh\kappa x.\sin\kappa H_i \tag{2.23}$$

Rearrange

$$\psi(x,H_i)=0=(JH_i+v_i)x+L\sinh\kappa x.\sin\kappa H_i \tag{2.24}$$

so that

$$(JH_i+v_i)=0 \tag{2.25}$$

and

$$L\sinh\kappa x.\sin\kappa H_i=0, \tag{2.26}$$

thus $J=-\frac{v_i}{H_i}$ and $\sin\kappa H_i=0$, which is true for $\kappa=\frac{n\pi}{H_i};-\frac{n\pi}{H_i}\ (n=1,2,3.....)$. With the aid of superposition, equation (2.21) now becomes,

$$\psi=-\frac{v_i}{H_i}zx+2\sum_{n=1}^{\infty}L_n\sinh\left(\frac{n\pi}{H_i}x\right).\sin\left(\frac{n\pi}{H_i}z\right) \tag{2.27}$$

The x-derivative of equation (2.27) is

$$\frac{\partial\psi}{\partial x}=-\frac{v_i}{H_i}z+2\sum_{n=1}^{\infty}L_n\frac{n\pi}{H_i}\cosh\left(\frac{n\pi}{H_i}x\right).\sin\left(\frac{n\pi}{H_i}z\right) \tag{2.28}$$

Now invoke the final boundary condition for purely horizontal inlet flow (2.14d),

$$\frac{\partial\psi}{\partial x}(W_i/2,z)=0=-\frac{v_i}{H_i}z+2\sum_{n=1}^{\infty}L_n\frac{n\pi}{H_i}\cosh\left(\frac{n\pi W_i}{2H_i}\right).\sin\left(\frac{n\pi}{H_i}z\right)\qquad(0<z<H_i) \tag{2.29}$$

Observing that equation (2.29) is of precisely the same form as the *half-range sine expansion* [88GR1] with 'α'$= H_i$, 'β_n'$= 2L_n \frac{n\pi}{H_i}\cosh\left(\frac{n\pi W_i}{2H_i}\right)$ and $f(z) = \frac{v_i}{H_i}z$, it follows directly that,

$$2L_n \frac{n\pi}{H_i}\cosh\left(\frac{n\pi W_i}{2H_i}\right) = \frac{2}{H_i}\int_0^{H_i} \frac{v_i}{H_i} z.\sin\left(\frac{n\pi z}{H_i}\right)dz \tag{2.30}$$

Rearrange to find L_n,

$$L_n = \frac{1}{n\pi\cosh\left(\frac{n\pi W_i}{2H_i}\right)}\int_0^{H_i} \frac{v_i}{H_i} z.\sin\left(\frac{n\pi z}{H_i}\right)dz \tag{2.31}$$

Recalling that $\int y\sin y dy = -y\cos y + \sin y + C$, equation (2.31) now becomes,

$$L_n = \frac{v_i H_i}{(n\pi)^3\cosh\left(\frac{n\pi W_i}{2H_i}\right)}\int_0^{H_i} \frac{n\pi z}{H_i}.\sin\left(\frac{n\pi z}{H_i}\right)\frac{n\pi dz}{H_i} = \frac{v_i H_i}{(n\pi)^3\cosh\left(\frac{n\pi W_i}{2H_i}\right)}\left(-\frac{n\pi z}{H_i}\cos\frac{n\pi z}{H_i} + \sin\frac{n\pi z}{H_i}\right)_0^{H_i}$$

$$= \frac{v_i H_i}{(n\pi)^3\cosh\left(\frac{n\pi W_i}{2H_i}\right)}\left(-\frac{n\pi z}{H_i}\cos\frac{n\pi z}{H_i} + \sin\frac{n\pi z}{H_i}\right)_0^{H_i} = \frac{-v_i H_i}{(n\pi)^2\cosh\left(\frac{n\pi W_i}{2H_i}\right)} \tag{2.32}$$

Substitute the relation for L_n into equation (2.27) to find the solution,

$$\psi = -\frac{v_i}{H_i}zx - 2v_i H_i \sum_{n=1}^{\infty} \frac{\sinh\left(\frac{n\pi}{H_i}x\right)}{\cosh\left(\frac{n\pi W_i}{2H_i}\right)}.\frac{\sin\left(\frac{n\pi}{H_i}z\right)}{(n\pi)^2} \tag{2.33}$$

It is useful to recall at this stage that $\sin(\theta_1 + \theta_2) = \sin\theta_1\cos\theta_2 + \cos\theta_1\sin\theta_2$, the *sine law*. From which can be deduced that,

$$\sin(\frac{n\pi}{H_i}H_i - \frac{n\pi}{H_i}z) = \sin\left(\frac{n\pi}{H_i}H_i\right)\cos\left(-\frac{n\pi}{H_i}z\right) + \cos\left(\frac{n\pi}{H_i}H_i\right)\sin\left(-\frac{n\pi}{H_i}z\right) = -\sin\left(\frac{n\pi}{H_i}z\right) \qquad (2.34)$$

Modifying equation (2.33) accordingly, produces,

$$\psi = -\frac{v_i}{H_i}zx + 2v_iH_i\sum_{n=1}^{\infty}\frac{\sinh\left(\frac{n\pi}{H_i}x\right)}{\cosh\left(\frac{n\pi W_i}{2H_i}\right)}.\frac{\sin\left(\frac{n\pi}{H_i}(H_i - z)\right)}{(n\pi)^2} \qquad (2.35)$$

The reason for this substitution is not immediately apparent, but as will be seen later, it is necessary to make the solution applicable to the physical problem. Differentiation of equation (2.35) gives the velocity components of the rain zone air velocity field, so that the horizontal component is

$$v_x = \frac{\partial\psi}{\partial z} = -\frac{v_i}{H_i}x - 2v_i\sum_{n=1}^{\infty}\frac{\sinh\left(\frac{n\pi}{H_i}x\right)}{\cosh\left(\frac{n\pi W_i}{2H_i}\right)}.\frac{\cos\left(\frac{n\pi}{H_i}(H_i - z)\right)}{(n\pi)} \qquad (2.36)$$

and the vertical component

$$v_z = -\frac{\partial\psi}{\partial x} = \frac{v_i}{H_i}z - 2v_i\sum_{n=1}^{\infty}\frac{\cosh\left(\frac{n\pi}{H_i}x\right)}{\cosh\left(\frac{n\pi W_i}{2H_i}\right)}.\frac{\sin\left(\frac{n\pi}{H_i}(H_i - z)\right)}{(n\pi)} \qquad (2.37)$$

A comparison of the horizontal inlet velocity [eq. (2.36)] with values generated by a numerical (CFD) simulation of the tower inlet (Chapter 4) shows the validity of the analytical flow field solution (figure 2.5). The deviation of the compared velocities at the tower shell $(z = 6 = H_i)$ is caused by a viscous boundary layer, which is not incorporated into the stream function solution, but otherwise the agreement is excellent. Inspection of equation (2.36) and figure 2.5 reveals the necessity for the substitution made in equation (2.35): the normal solution would give an inverted

account of the summation term. This effect stems from the contradiction of boundary conditions at the top of the inlet i.e. $v_z(W_i/2, H_i) = 0$ and $v_z(W_i/2, H_i) = v_i$.

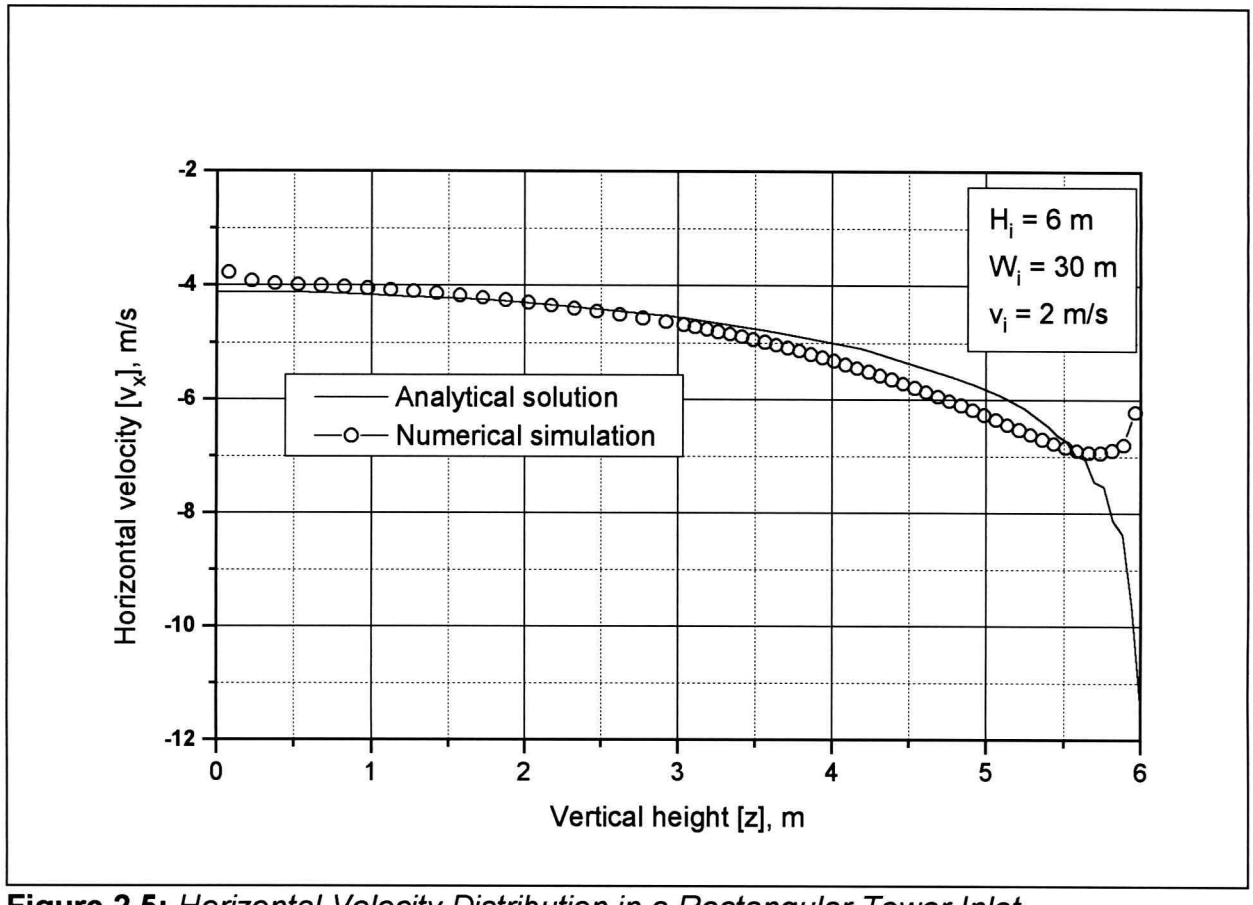

Figure 2.5: *Horizontal Velocity Distribution in a Rectangular Tower Inlet.*

Although equations (2.36) and (2.37) give a accurate description of the rain zone velocity field, they are to cumbersome to employ in a extended rain zone loss coefficient prediction scheme. The time needed to generate the volume of data required to fit an accurate correlation for the rain zone loss, would increase by many orders of magnitude if the summation terms of the velocity components were included in the simulation. Therefore, the summation terms are assumed to have a relatively small influence on the eventual pressure drop and removed from velocity equations. The validity of this simplification is shown in figure (2.6), where the results produced by the different flow fields are compared under unfavourable conditions (with a small inlet width to height ratio $(W_i / H_i = 3)$). The results are found to be sufficiently similar to justify the exclusion. The relatively small change in the calculated rain zone loss is because of the dominant effect of the droplet velocity on the pressure drop.

The effect of the droplets on the air flow field must also be taken into account. This interaction tends to dampen the air velocity distribution, so that it becomes more uniform, with the result that the rain zone loss increases somewhat in magnitude [92ZH1]. Neglecting the summation terms from the velocity equations has a similar effect, so that this assumption becomes not only acceptable but applicable.

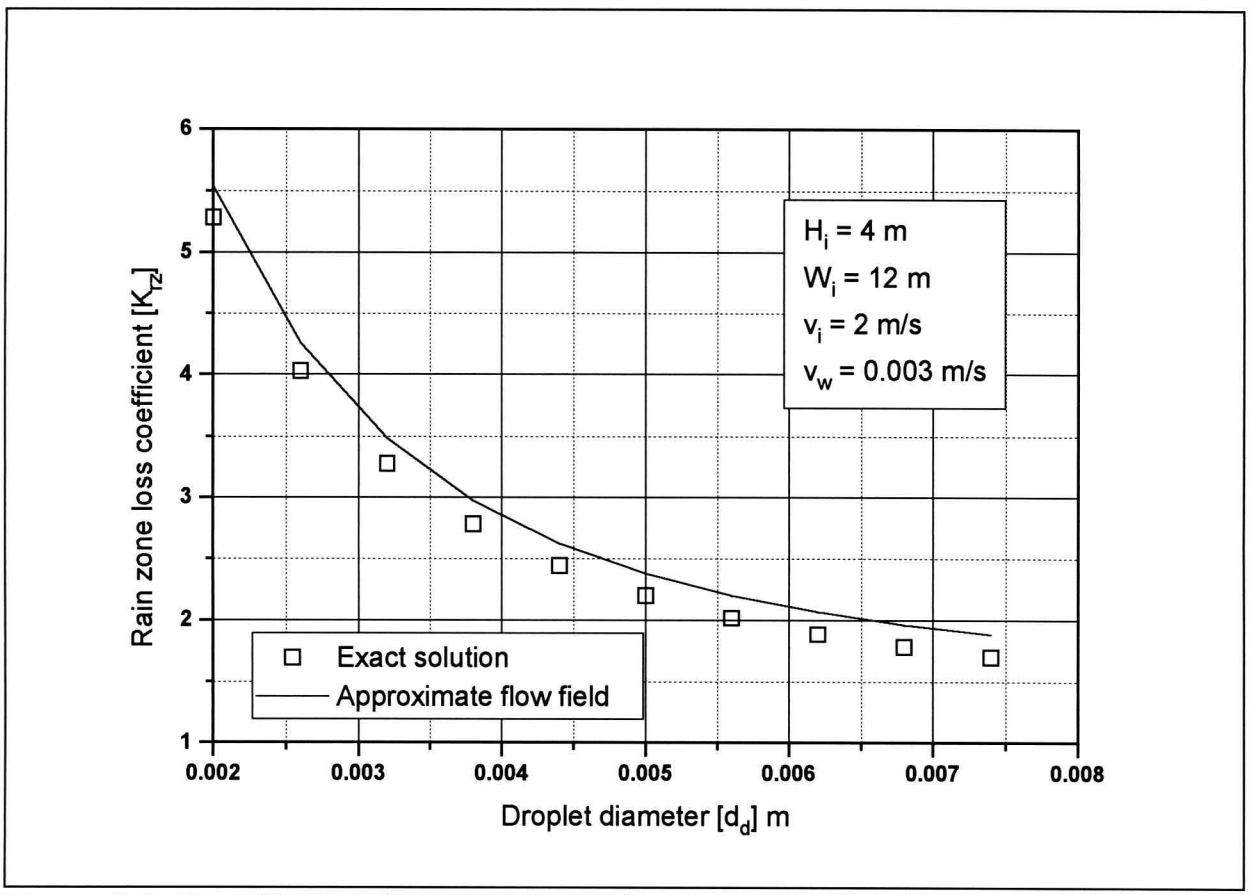

Figure 2.6: *The effect of Flow Field Approximation on the Rain Zone Loss.*

The air velocity components are now,

$$v_x = -\frac{v_i}{H_i}x \tag{2.38}$$

and

$$v_z = \frac{v_i}{H_i}z \tag{2.39}$$

for the horizontal and vertical components respectively (fig. 2.7).

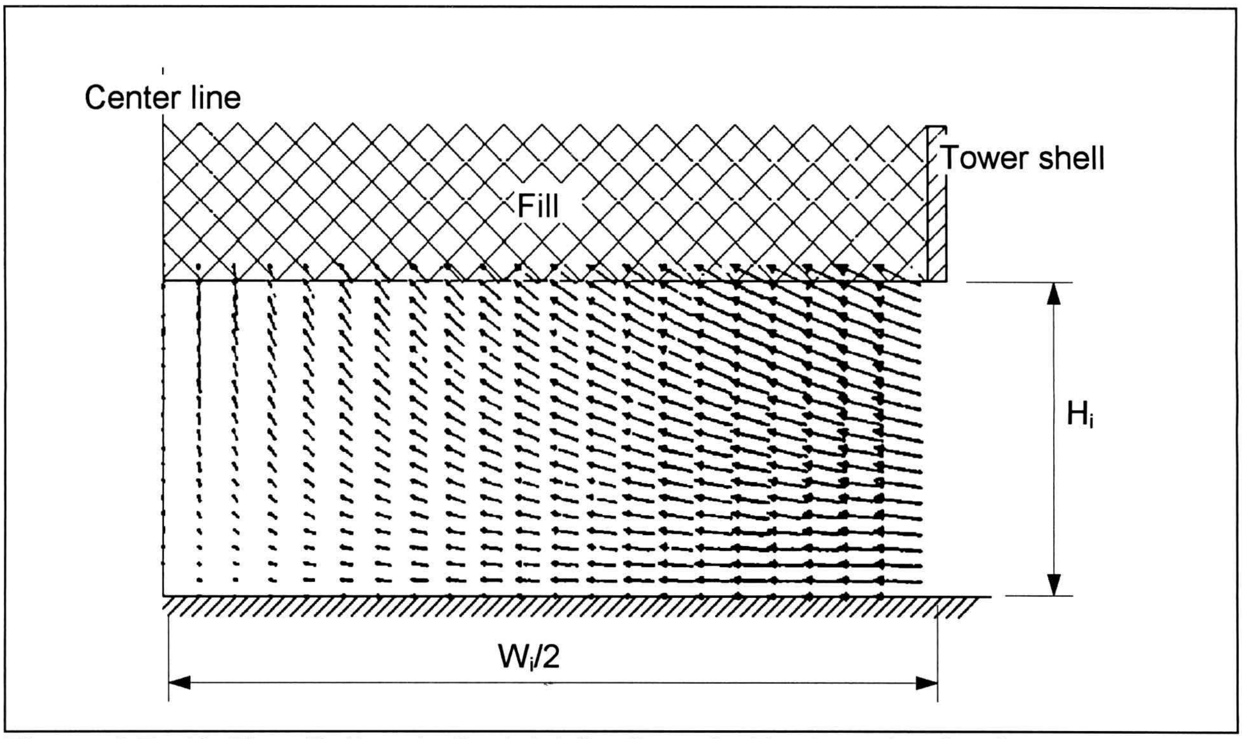

Figure 2.7: *Air Flow Pattern in the Inlet Section of a Rectangular Cooling Tower.*

2.3 Aerodynamic Drag on Droplets

The total drag force acting on a droplet may be found from,

$$\overline{\mathbf{F}}_D = C_D A_d \rho_a \overline{\mathbf{v}}_{ad}^2 / 2 \tag{2.40}$$

where $\overline{\mathbf{v}}_{ad}$ is the velocity of the air flow relative to the drop, C_D is the drag coefficient and A_d it's cross-sectional area. To accurately simulate the drag force, it is therefore, essential that the drag coefficient and cross-sectional area of the falling droplets are correctly modelled.

Many researchers have investigated the effect of deformation on the terminal velocity of free falling droplets [49GU1, 70PR1, 71PR1, 75GR1, 77BE1, 77PR1]. Beard and Chuang [87BE1] assert that droplet deformation is dependent on four factors, namely: surface tension, hydrostatic pressure, aerodynamic pressure and internal circulation. Researchers [72LE1, 87BE1] have found, however, that the effect of internal circulation for small droplets $(d_d \leq 9\,\text{mm})$ is negligible and Beard and Chuang ignore this effect in their model. Although droplets have been found to

oscillate during the first few meters of their fall [41LA1], this phenomenon does not seem to visibly effect droplet terminal velocity [77BE1, 87BE1].

Photographic analysis by Muira et al. [77MU1] and others, have shown that falling droplets are not spherical, as previously supposed, but assume a flattened elliptical shape as they approach terminal velocity. This deformation has to be taken into account in the computation of the droplet's drag coefficient, C_D and cross-sectional area, A_d. For purposes of analysis the deformation is described as the ratio of the droplet's axial height to radial diameter, as shown in figure 2.8.

$$E = b/a \leq 0 \qquad (2.41)$$

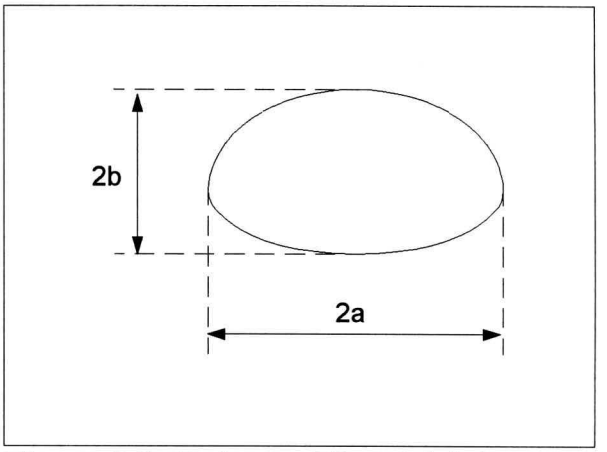

Figure 2.8: *Deformed Droplet Axi*

Beard and Chuang [87BE1] developed a numerical model which predicts this deformation at droplet terminal velocity (v_t) in stagnant air and that correlates well with experimental data. By numerically solving the resulting Laplace equation the deformation caused by aerodynamic drag can be observed. An empirical equation by Dreyer [94DR1] fits their data,

$$E_T = \frac{1}{1+0.148Eo^{0.85}} \qquad (2.42)$$

where, Eo, the Eotvos number, is defined by,

$$Eo = \frac{gd_d^2(\rho_w - \rho_a)}{\sigma_w} \qquad (2.43)$$

During droplet acceleration an equation by Dreyer [94DR1] gives the deformation as a function of velocity, terminal velocity (v_t) and terminal velocity deformation,

$$E = 1 - \left[\frac{v_{ad}}{v_t}\right]^2 (1 - E_T) \tag{2.44}$$

Droplet terminal velocity in stationary air, v_t, is found by equating the drag force, $\left(\overline{\mathbf{F}}_D\right)$,to the gravity force, $\left(M_d \times g\right)$, on the droplet,

$$v_t = \sqrt{\frac{2M_d g}{\rho_a A_d C_D}} \tag{2.45}$$

where the mass of the droplet is $M_d = \rho_w \pi d_d^3 / 6$. This equation must be solved iteratively since the drag coefficient, C_D, is dependent on the droplet's velocity. Once the drag coefficient has been found, the deformation ratio, E, can be used to calculate the ratio of the drag coefficient of a deformed drop to that of a solid sphere [94DR1].

$$\frac{C_D}{C_{Dsph}} = 1 - 0.17185(1-E) + 6.692(1-E)^2 - 6.605(1-E)^3 \tag{2.46}$$

The equation for the drag coefficient, C_{Dsph}, for solid spheres is given by Turton and Levenspiel [86TU1] as,

$$C_{Dsph} = \frac{24}{\mathrm{Re}}(1 + 0.173\,\mathrm{Re}^{0.657}) + \frac{0.413}{1 + 16300\,\mathrm{Re}^{-1.09}} \tag{2.47}$$

which is valid for $\mathrm{Re} = \rho_a v_{ad} d_d / \mu_a \leq 200{,}000$. The enlarged cross-sectional area, A_d, of a deformed drop is given by

$$A_d = \frac{\pi(d_d E^{-0.333})^2}{4} \tag{2.48}$$

The modified drag coefficient and droplet cross-sectional area may now be used in concert with the flow fields derived in section 2.2 to find the pressure drop in the rain zone.

2.4 Pressure Drop in the Rain Zone.

Recall that the drag force on a droplet is given by,

$$\bar{\mathbf{F}}_D = A_d C_D \rho_a \bar{\mathbf{v}}_{ad}^2 / 2 \tag{2.40}$$

The relative velocity of the air, $\bar{\mathbf{v}}_{ad}^2$, is a function of the droplet and air velocity vectors. Since the air velocity is known as a function of position in the rain zone, it is necessary to find the droplet velocity as a function of the same. Once this has been achieved the work done by the air on the droplets can be integrated across the rain zone to arrive at the rain zone pressure drop.

2.4.1 Circular Cooling Towers

In the polar co-ordinates of a circular cooling tower the velocity of the air relative to the droplet is given by,

$$\left|\bar{\mathbf{v}}ad\right| = \sqrt{(v_{az} - v_{dz})^2 + (v_{ar} - v_{dr})^2} \tag{2.49}$$

with an angle of $\theta_{ad} = \arctan\left[(v_{az} - v_{dz})/(v_{ar} - v_{dr})\right]$, where v_{dz} and v_{dr} are the droplet's axial and radial velocity components.

Consider now an accelerating droplet in the rain zone. If the buoyancy force on the drop is neglected, the forces acting on the drop are gravity and drag. The resulting force is found from,

$$\left|\bar{\mathbf{F}}d\right| = \sqrt{(\sin\theta_{ad}\left|\bar{\mathbf{F}}_D\right| - M_d g)^2 + (\cos\theta_{ad}\left|\bar{\mathbf{F}}_D\right|)^2} \tag{2.50}$$

that acts in the direction $\theta_F = \arctan\left[\left(\sin\theta_{ad}\left|\bar{\mathbf{F}}_D\right| - M_d g\right)^2\right) \Big/ \cos\theta_{ad}\left|\bar{\mathbf{F}}_D\right|\Big]$, (fig. 2.9).

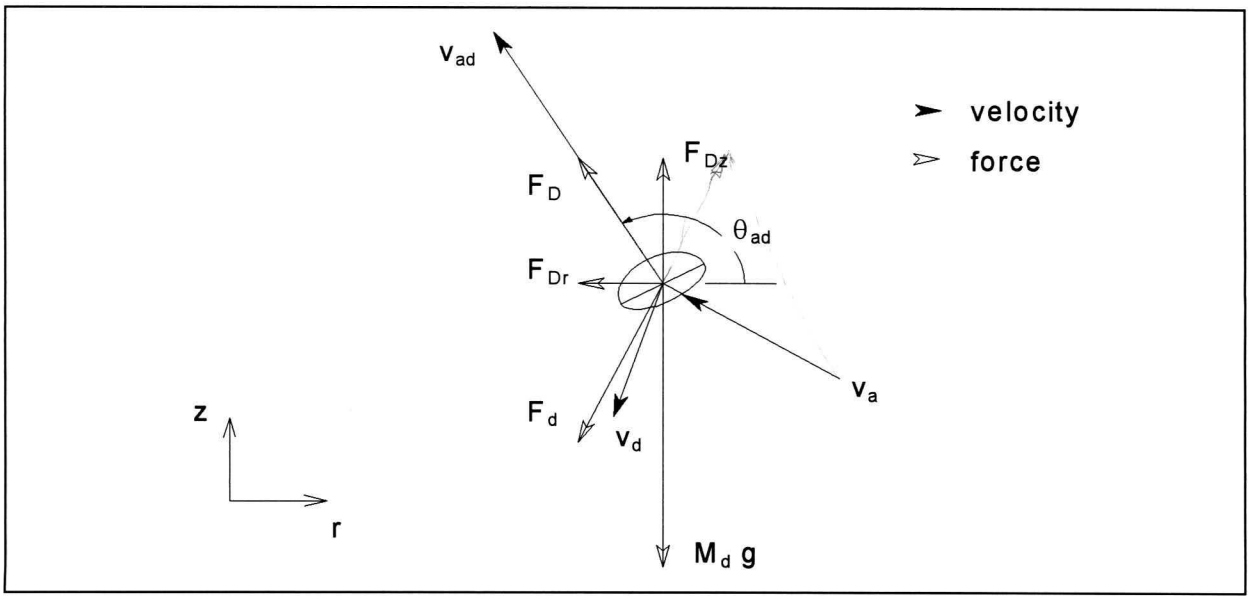

Figure 2.9: *Distribution of Forces and Velocities for a Droplet in the Rain Zone.*

Thus, the axial acceleration of the drop is given by

$$a_{dz} = \left(\sin\theta_{ad}\left|\overline{\mathbf{F}}_D\right| - M_d g\right)/M_d$$
$$= \tfrac{1}{2}C_D A_d \rho_a (v_{az} - v_{dz}) \times \left[(v_{az} - v_{dz})^2 + (v_{ar} - v_{dr})^2\right]^{0.5} / M_d - g \qquad (2.51)$$

while the radial acceleration, due only to drag, can be found from

$$a_{dr} = \cos\theta_{ad}\left|\overline{\mathbf{F}}_D\right| / M_d$$
$$= \tfrac{1}{2}C_D A_d \rho_a (v_{ar} - v_{dr}) \times \left[(v_{az} - v_{dz})^2 + (v_{ar} - v_{dr})^2\right]^{0.5} / M_d \qquad (2.52)$$

Equations (2.51) and (2.52) may be written in differential form,

$$\frac{dv_{dz}}{dt} = \frac{F_{Dz}}{M_d} - g \qquad (2.53)$$

$$\frac{dv_{dr}}{dt} = \frac{F_{Dr}}{M_d} \qquad (2.54)$$

with starting values: $v_{dz} = v_{dr} = 0$ at $t = 0$. Drop velocity and displacement are found by integration of equations. (2.53) and (2.54) with respect to time using a numerical method, in this case a 4th order Runge-Kutta equation. By employing these discrete values, droplet velocity can then be found as a function of its position in the rain zone.

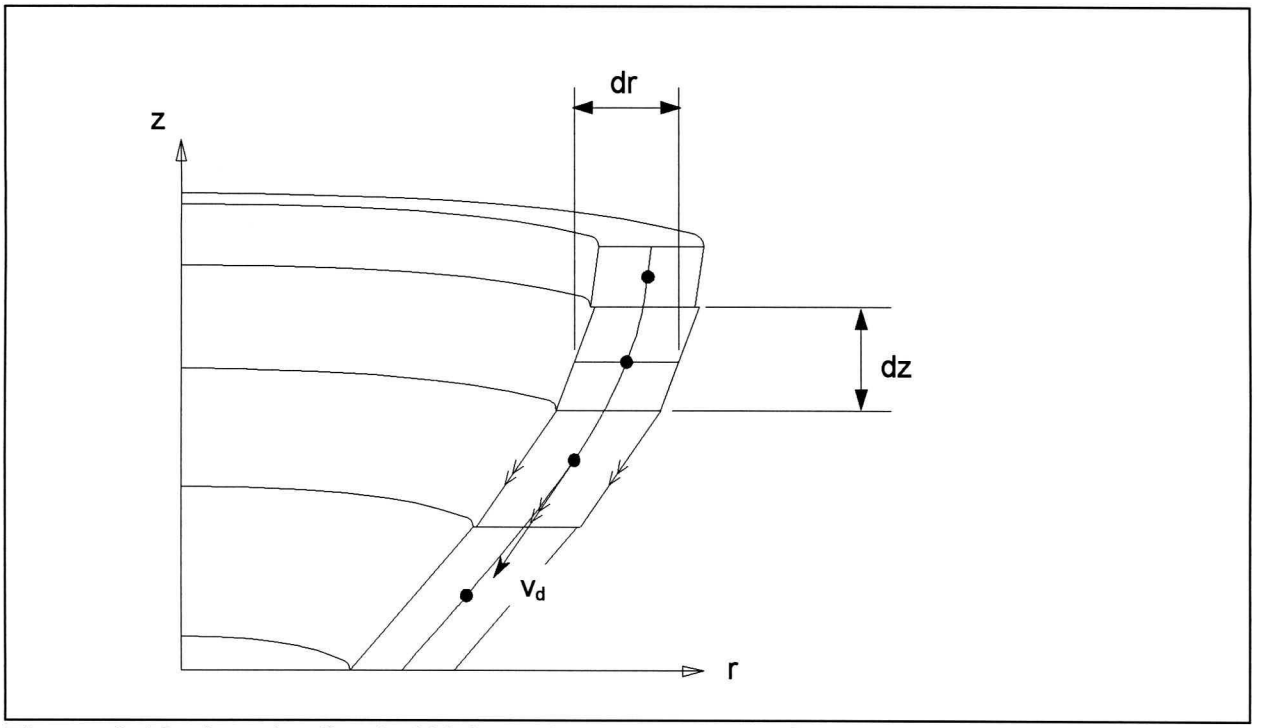

Figure 2.10: *Annular Control Volume for Droplets in a Circular Cooling Tower.*

Consider an annular control volume (CV) in the rain zone (fig. 2.10), it's centre at a point where the droplet velocity has been previously calculated. Let the sides of the annulus be parallel to the velocity vector of the droplet. Make the height, *dz*, and the width, *dr*, of the control volume small enough so that the change in droplet velocity through the control volume becomes negligible. The annulus now describes a stream tube for the droplets entering the control volume. Since the water flow rate through the fill is uniform, the water flow rate through subsequent vertical control volumes must also be uniform. Therefore, the number of drops passing through the control surface, $dA=2\pi rdr$, per second can be found from,

$$n = 2\pi rdr\left[\frac{6G_w}{\rho_w \pi d_d^3}\right] \tag{2.55}$$

where G_w is the water mass flow rate per unit area. It is assumed that the depth of the control volume, *dz*, is small enough, so that the vertical velocity of the droplet, v_{dz}, in the control volume can be considered constant. Now the number of drops in a control volume at a given position is

$$n_{cv} = \left[\frac{6G_w}{\rho_w \pi d_d^3}\right]\frac{2\pi r dr dz}{v_{dz}} \tag{2.56}$$

Work is done upon a droplet, by the air stream, as it falls through a control volume, *dz* by $2\pi rdr$. This work can be translated into a total pressure drop across the rain zone, by using the energy equation for steady flow through a stream tube with shaft work and/or friction.

First, consider energy transfer in the radial direction. The air moves through a radial distance of *dr* as it traverses the control volume. The change in energy of the air caused by the radial component of the drag force on a single droplet can be found from,

$$dE_{ar} = F_{Dr}dr \tag{2.57}$$

where $F_{Dr} = |\overline{\mathbf{F}}_D|\sin\theta_{ad}$ and θ_{ad} is the direction of the air velocity relative to the droplet. Assume that the work done on the droplet is constant across the control volume and that air velocities are constant inside the control volume. Then the time it takes the air to traverse the control volume is,

$$t_{ar} = \frac{v_{ar}}{dr} \tag{2.58}$$

The mean energy transfer rate caused by radial forces on the droplet in the control volume is found by dividing equation (2.57) by equation (2.58),

$$\frac{dE_{ar}}{dt} = \frac{F_{dr}dr}{t_{ar}} = F_{Dr}v_{ar} \tag{2.59}$$

To find the same for an entire CV, simply multiply equation (2.59) by the number of droplets in the control volume.

$$\frac{dE_{arcv}}{dt} = n_{cv} F_{Dr} v_{ar} \tag{2.60}$$

Similarly, the transfer rate caused by forces in the axial direction is found to be,

$$\frac{dE_{azcv}}{dt} = n_{cv} F_{Dz} v_{az} \tag{2.61}$$

where $F_{Dz} = \left|\overline{\mathbf{F}}_D\right| \cos\theta_{ad}$ .To find the work done in the control volume per unit mass of air flowing through the rain zone, w_{cv}, add the axial and radial energy transfer rates and divide by the total air mass flux.

$$w_{cv} = \left[\frac{dE_{azcv}}{dt} + \frac{dE_{arcv}}{dt}\right] / m_a \tag{2.62}$$

The pressure drop in the rain zone, caused by the falling drops, is found by summing the work done in all the control volumes and substituting it into the energy equation for a stream tube.

$$\Delta p_{rz} = \rho_a \int_0^{H_i} \int_0^{r_i} w_{cv} \tag{2.63}$$

The dimensionless loss coefficient, based on the fill frontal area, is defined as,

$$K_{rz} = \frac{\Delta p_{rz}}{\frac{1}{2}\rho_a v_i^2} \tag{1.3}$$

or in an expanded simplified form,

$$K_{rz} = 3\left(\frac{v_w}{v_i}\right)\left(\frac{H_i}{d_d}\right)\int_0^{H_i}\int_0^{r_i}\frac{C_D}{E^{0.666}}\frac{\left[v_{ad}^2\right]^{0.5}}{v_{dz}v_i^2}\times\left(v_{ar}(v_{ar}-v_{dr})+v_{az}(v_{az}-v_{dz})\right)\frac{rdrdz}{r_i^2 H_i} \tag{2.64}$$

where $v_w = m_w / \left(\rho_w \pi r_i^2\right)$. It is obvious that only the integral need be solved numerically. Inspection of the source equations reveals, that the integral in the rain zone loss coefficient equation is dependent on the following variables, $(d_d, r_i, H_i, v_i, \rho_a, \rho_w, \mu_a, \sigma_w, g)$. By utilising dimensional analysis, these variables may be arranged to form dimensionless groups, thereby decreasing the active variables to six. The integral function is reduced to the following relation:

$$I = f(a_L d_d, a_L r_i, a_L H_i, a_v v_i, a_\rho \rho_a, a_\mu \mu_a) \tag{2.65}$$

where the "*a*-" coefficients represent combinations of g, ρ_w, σ_w and constants that make up each particular dimensionless group.

$$a_\mu = 3.061\times10^{-6}\left[\frac{\rho_w^4 g^9}{\sigma_w}\right]^{0.25} \tag{2.66a}$$

$$a_\rho = \frac{998.0}{\rho_w} \tag{2.66b}$$

$$a_v = 73.298\left[\frac{g^5\sigma_w^3}{\rho_w^3}\right]^{0.25} \tag{2.66c}$$

and

$$a_L = 6.122\left[\frac{g\sigma_w}{\rho_w}\right]^{0.25} \tag{2.66d}$$

All these coefficients are equal to unity for $g = 9.8\text{m/s}^2$ and $T_w = 22.72°C$. Since g, ρ_w, and σ_w never vary substantially, this particular arrangement allows greater freedom when fitting curves to the numerical data, by removing the usual interdependence of the dimensionless groups. The results of numerical integration produced the following correlation for the rain zone loss coefficient,

$$K_{rz} = 3a_v v_w \left(\frac{H_i}{d_d}\right)\left[0.22460 - 0.31467 a_\rho \rho_a + 5263.04 a_\mu \mu_a \right.$$
$$+ 0.775526 \times \left[1.4824163 \exp(71.52 a_L d_d) - 0.91\right] \times \left[0.39064 \exp(2.1824 \times 10^{-2} a_L \frac{d_i}{2}) - 0.17\right]$$
$$\times \left[2.0892(a_v v_i)^{-1.3944} + 0.14\right] \times \exp\left[(0.8449 \ln(a_L \frac{d_i}{2}) - 2.312) \times (0.3724 \ln(a_v v_i) + 0.7263)\right.$$
$$\left.\left.\times \ln\left[206.757(a_L H_i)^{-2.8344} + 0.43\right]\right]\right] \qquad (2.67)$$

which fits the numerical data with an average error of less than 3 percent and is valid for,

$0 \leq T_a \leq 40°C$;
$10 \leq T_w \leq 40°C$;
$0.927 \leq \rho_a \leq 1.289 kg/m^3$;
$992.3 \leq \rho_w \leq 1000 kg/m^3$;
$1.717 \leq \mu_a \leq 1.92 \times 10^{-5} kg/ms$;
$0.0696 \leq \sigma_w \leq 0.0742 N/m$;
$0.002 \leq d_d \leq 0.008 m$;
$9.7 \leq g \leq 10 m/s^2$;
$60 \leq d_i \leq 140 m (or 30 \leq r_i \leq 70 m)$;
$4 \leq H_i \leq 12 m$;
$0.00075 \leq v_w \leq 0.003 m/s$
and $1 \leq v_i \leq 3 m/s$.

Plotted results of the numerical integration are shown for selected variables in figures 2.11 - 2.14. The data is generally smooth and continuously increasing or decreasing. Divergence of the data is taken into account by the '$\exp^{[\ln]}$' term in equation (2.67), giving the equation greater accuracy as multiple variables approach restriction values. Since it is impossible to directly measure the rain zone pressure drop in a circular counterflow cooling tower, no comparison with experimental data could be made. There will, however, be an attempt later in this chapter to corroborate the numerical analysis using a different experimental approach. In brief, equation (2.67) satisfies the requirement for an accurate correlation to predict the rain zone loss coefficient in terms of the standard variables.

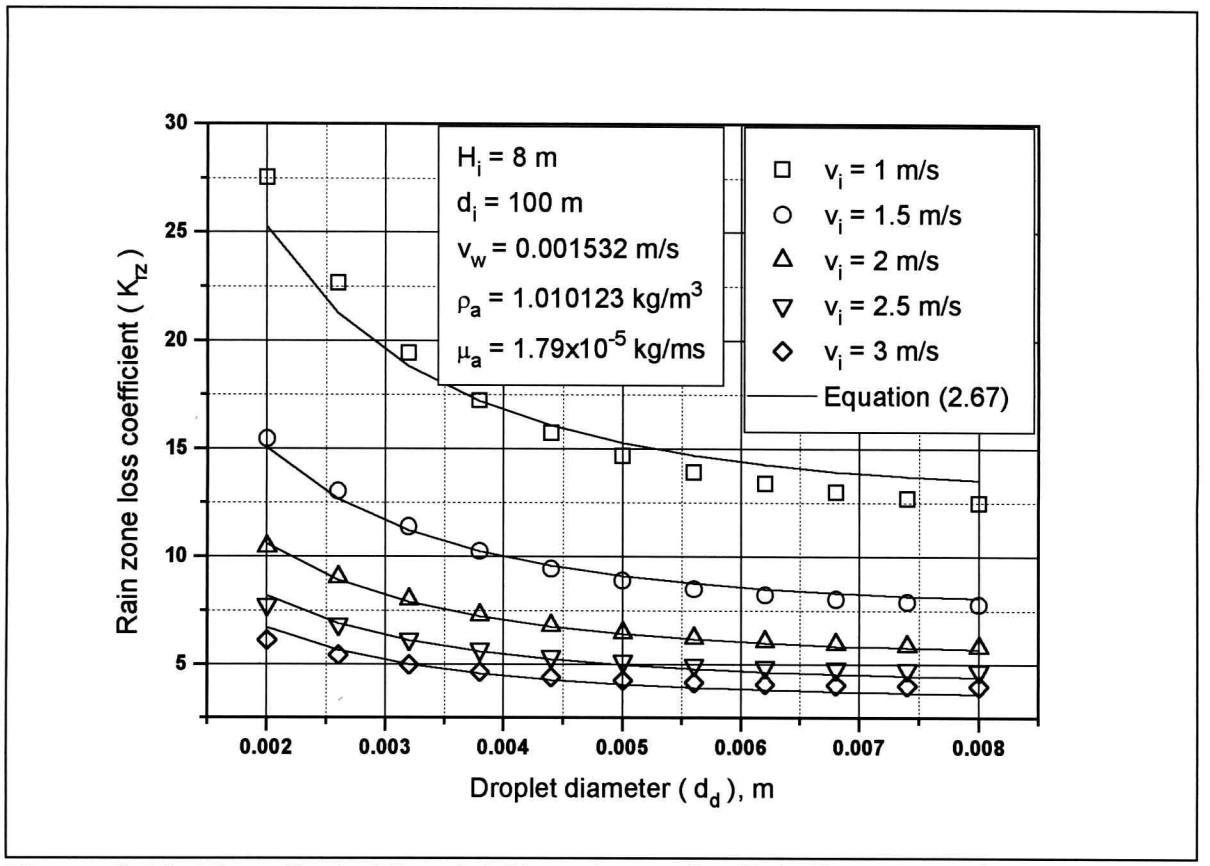

Figure 2.11: *The effect of Droplet Diameter on the Rain Zone Loss Coefficient.*

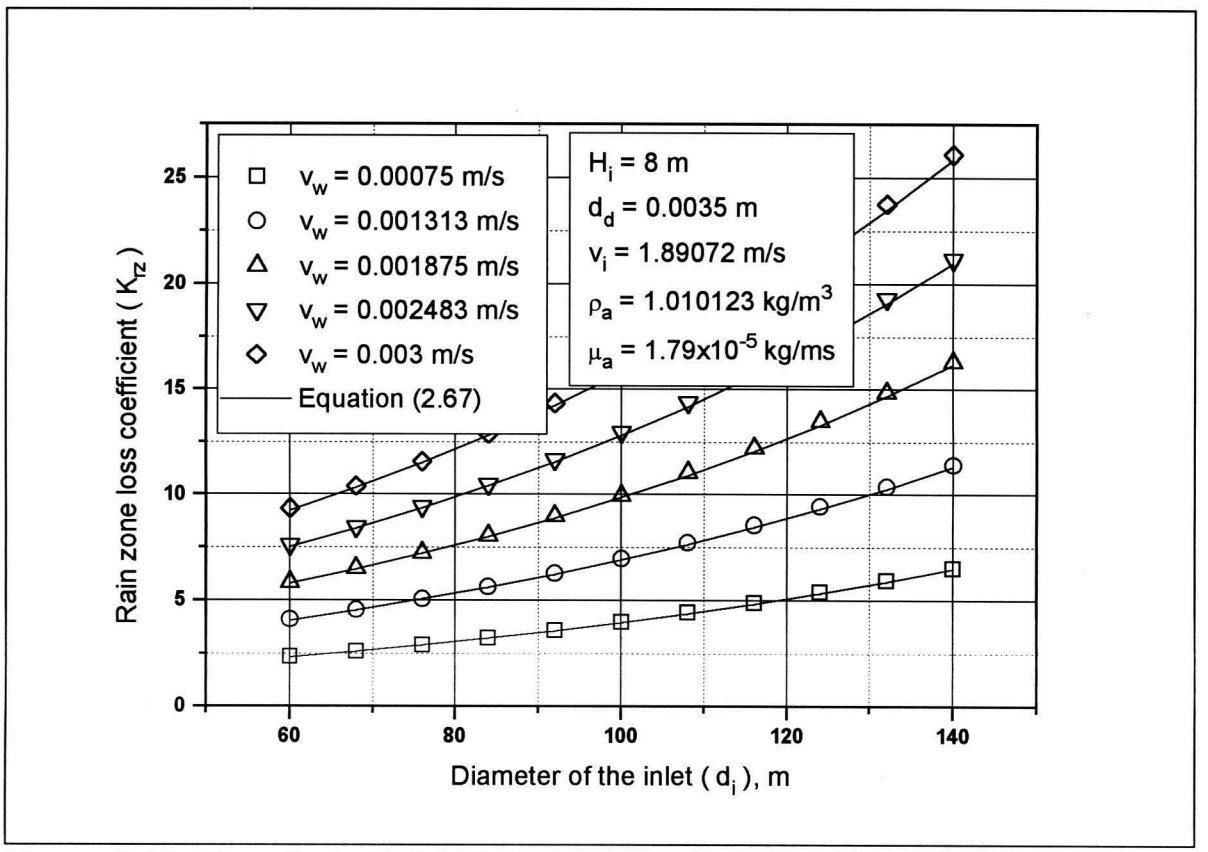

Figure 2.12: *The effect of Inlet Diameter on the Rain Zone Loss Coefficient.*

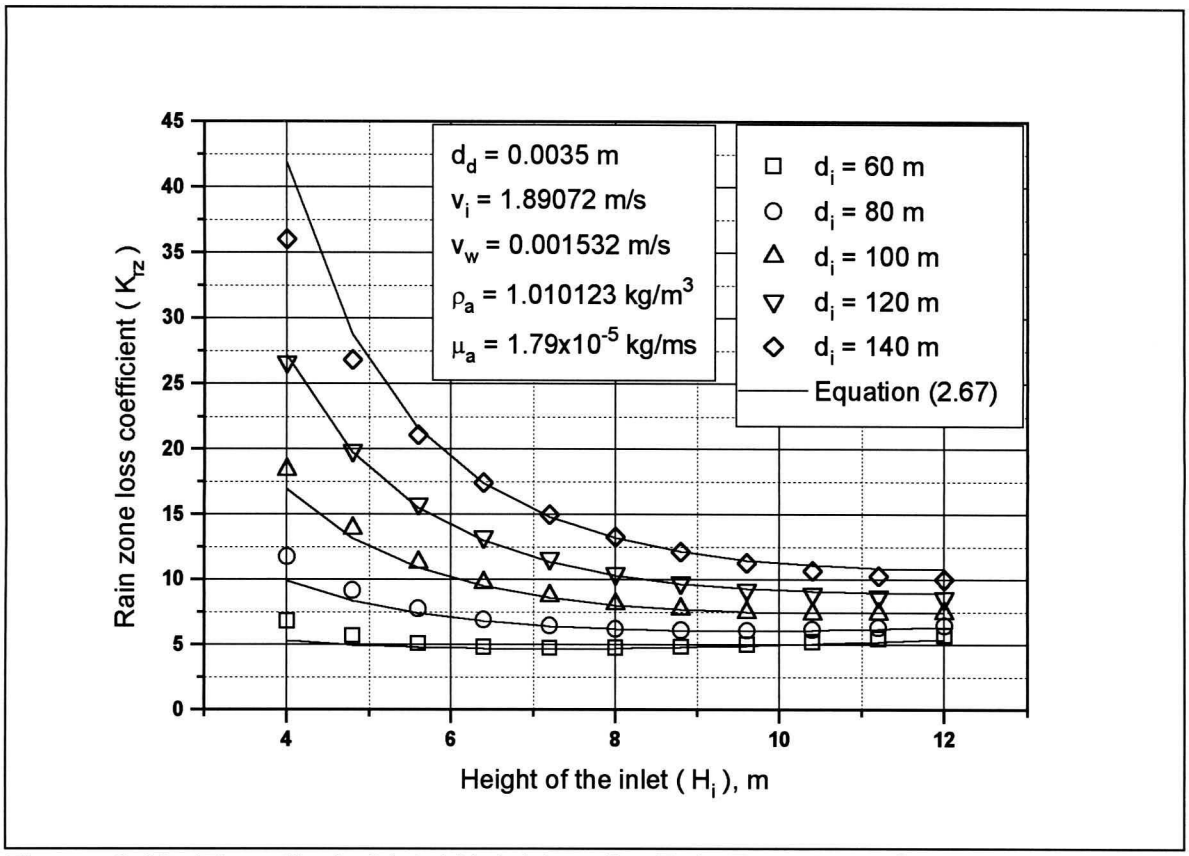

Figure 2.13: *The effect of Inlet Height on the Rain Zone Loss Coefficient.*

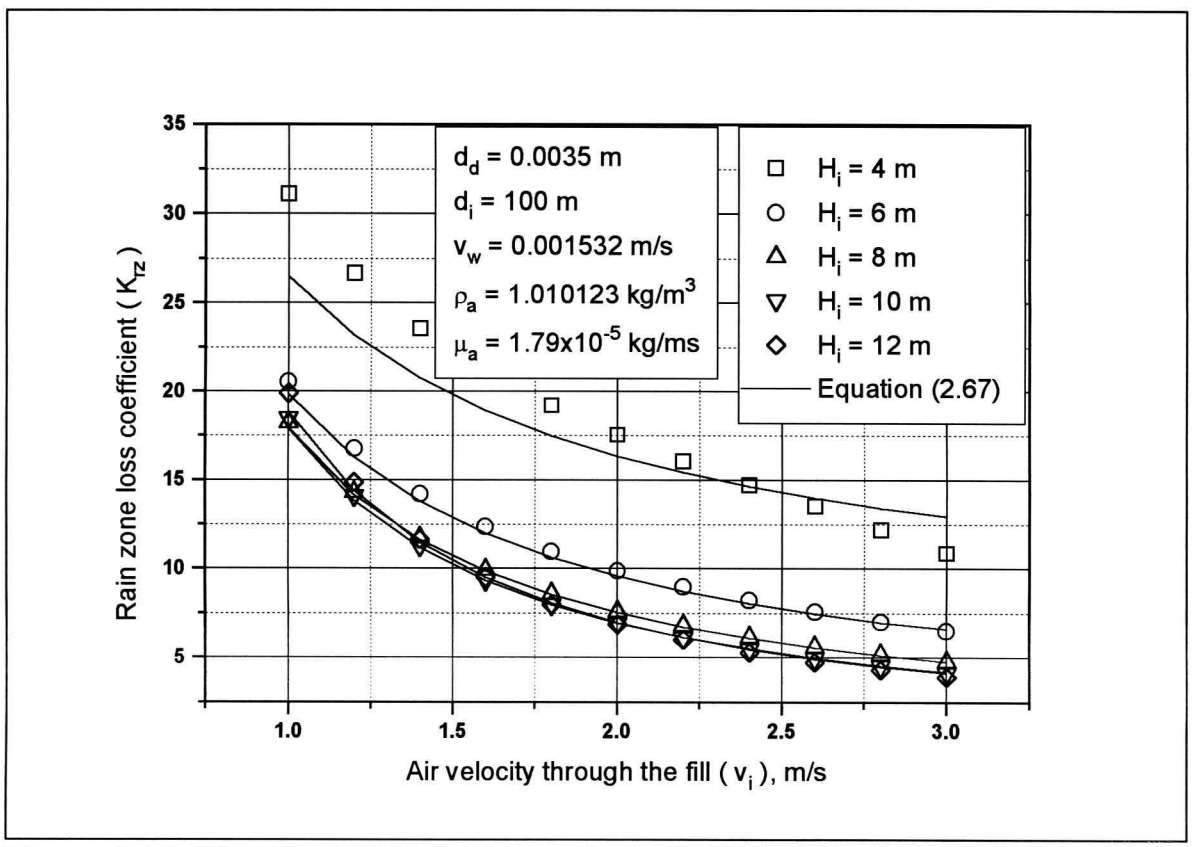

Figure 2.14: *The effect of Air Inlet Velocity on the Rain Zone Loss Coefficient.*

2.4.2 Rectangular Cooling Towers

The derivation of the rain zone pressure drop for rectangular cooling towers is similar to that for circular towers. In the Cartesian co-ordinate system associated with rectangular towers (fig. 2.4) the droplet vertical acceleration due to drag and gravity is given by,

$$\begin{aligned} a_{dz} &= \left(\sin\theta_{ad}\left|\overline{\mathbf{F}}_D\right| - M_d g\right)/M_d \\ &= \tfrac{1}{2}C_D A_d \rho_a (v_{az} - v_{dz}) \times \left[(v_{az} - v_{dz})^2 + (v_{ay} - v_{dy})^2\right]^{0.5}/M_d - g \end{aligned} \tag{2.68}$$

while the horizontal acceleration, due only to drag, can be found from

$$\begin{aligned} a_{dr} &= \cos\theta_{ad}\left|\overline{\mathbf{F}}_D\right|/M_d \\ &= \tfrac{1}{2}C_D A_d \rho_a (v_{ay} - v_{dy}) \times \left[(v_{az} - v_{dz})^2 + (v_{ay} - v_{dy})^2\right]^{0.5}/M_d \end{aligned} \tag{2.69}$$

where the air local velocities are found from equations (2.38) and (2.39). Numerical integration of the droplet acceleration returns the droplet velocity as a function of its position in a rectangular tower.

To find the pressure drop in the rain zone, the mechanical energy expended, on the droplets by the air stream, must be summed for each control volume in the inlet section. In a rectangular tower, these control volumes are prism shaped, with their vertical sides parallel to the calculated droplet velocity vector (fig. 2.15). The droplet stream tube described by the CV ensures that the water flux, G_w, in consecutive control volumes remains constant. With the assumption of constant droplet diameter and vertical velocity the number of droplets in a control volume of one meter thickness can be found from,

$$n_{cv} = \left[\frac{6G_w}{\rho_w \pi d_d^3}\right]\frac{dxdz}{v_{dz}} \tag{2.70}$$

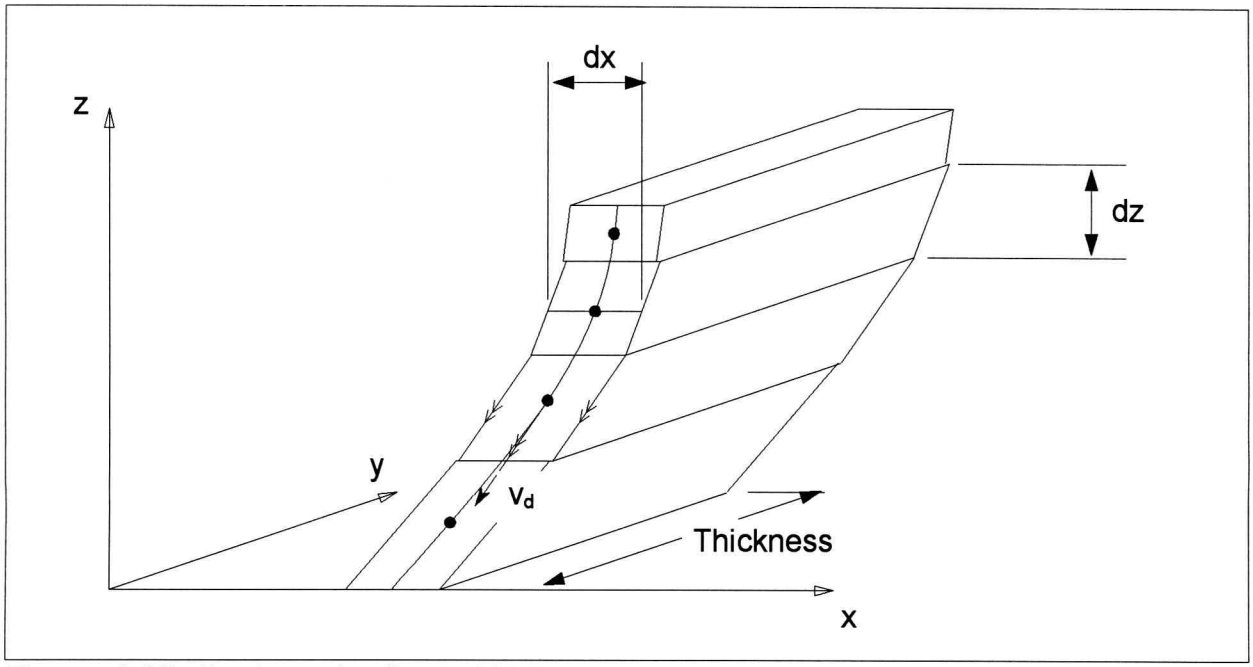

Figure 2.15: *Rectangular Control Volume for Droplets in a Rectangular Tower.*

Using the same approach as in section 2.4.1, the work done in the control volume per unit mass of air is represented by,

$$w_{cv} = \frac{n_{cv}}{m_a}\left[F_{Dz}v_{az} + F_{Dx}v_{ax}\right] \tag{2.71}$$

and the rain zone pressure drop for a rectangular tower can therefore be found from,

$$\Delta p_{rz} = \rho_a \int_0^{H_i} \int_0^{W_i/2} w_{cv} \tag{2.72}$$

After moving the constants of integration and applying dimensional analysis, the integral in equation (2.72) is found to have the following functional dependency,

$$I = f(a_L d_d, a_L W_i, a_L H_i, a_v v_i, a_\rho \rho_a, a_\mu \mu_a) \tag{2.73}$$

where the 'a-' coefficients are identical to those employed in the circular tower scenario. A curve fit of the resulting numerical data, produced the following semi-empirical correlation for the loss coefficient in induced draft rectangular cooling towers,

$$K_{rz} = a_v v_w \frac{3}{2}\frac{H_i}{d_d}\left\{0.219164 + 8278.7 a_\mu \mu_a - 0.30487 a_\rho \rho_a \right.$$
$$+ 0.954153 \times \left[0.328467 \exp(135.7638 a_L d_d) + 0.47\right] \times \left[26.28482 (a_L H_i)^{-2.95729} + 0.56\right]$$
$$\times \left[2.177546 (a_v v_i)^{-1.46541} + 0.21\right] \times \exp\left[\ln\left[0.204814 \exp(0.133036 a_L \frac{W_i}{2}) + 0.21\right]\right.$$
$$\left.\left. \times \left[3.9186 \exp(-0.3 a_L H_i)\right] \times \left[0.31095 \ln(a_L d_d) + 2.63745\right]\right]\right\} \qquad (2.74)$$

where the restrictions that differ from the circular tower are: $1 \le v_i \le 5\,\text{m/s}; 2 \le H_i \le 8\,\text{m}$; and $4 \le W_i \le 40\,\text{m}$. A graphic representation of the results is shown in figure 2.16.

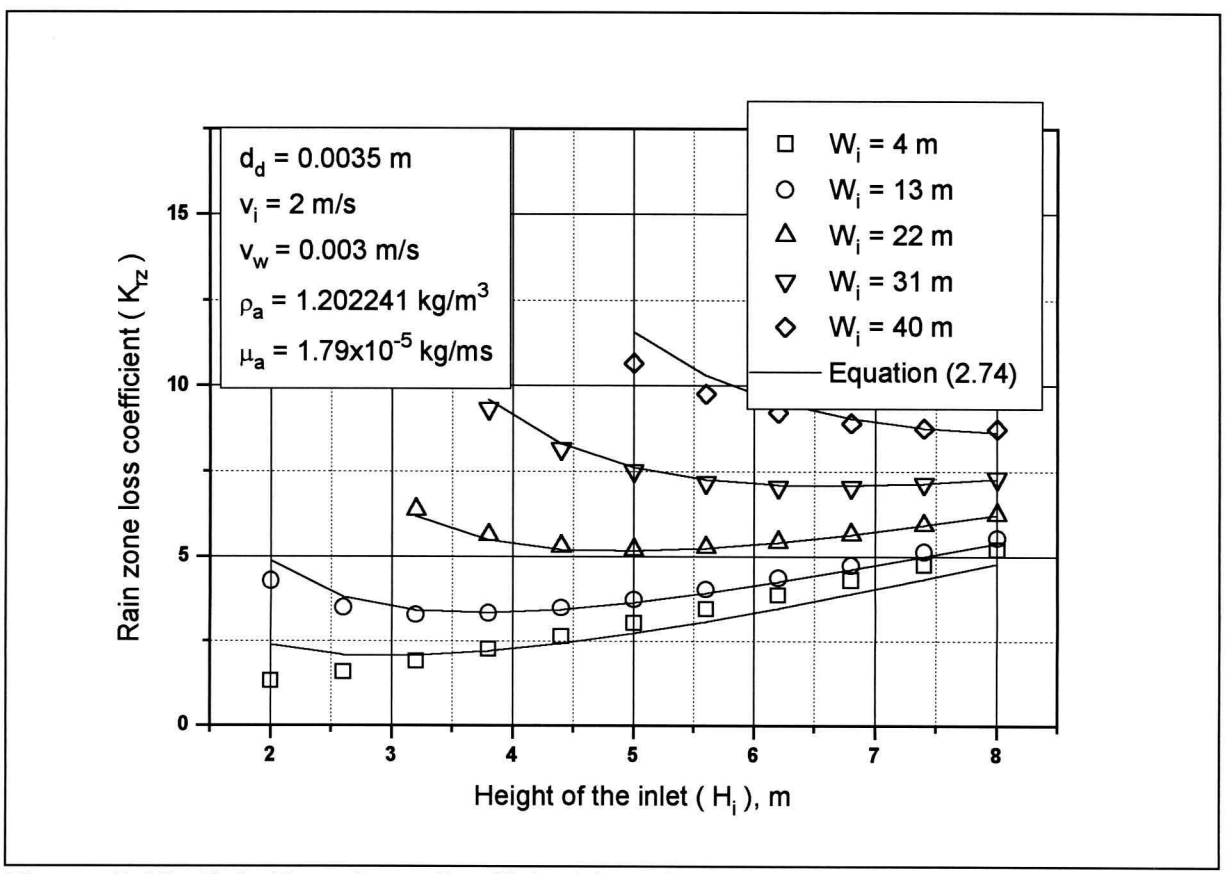

Figure 2.16: *Rain Zone Loss Coefficient for a Rectangular Cooling Tower.*

In a rectangular induced draught tower, care must be taken to ensure that water droplets are not entrained into the fill. This is done by obeying the following relation,

$$v_i \times \left[1 + \left(\frac{1}{2} W_i / H_i\right)^2\right]^{0.5} \le v_t \qquad (2.75)$$

where, v_t, the droplet terminal velocity, can be found from equation (2.45).

2.5 Experimental Comparison.

Although the pressure drop caused by falling droplets in a cooling tower inlet section cannot be measured with certainty, the pressure drop in a purely one-dimensional flow field can. To this end, a purely counterflow test arrangement was used to measure the pressure drop caused by downward falling droplets in an upward moving air stream. Since no inlet losses occur in such a rain zone, the data can be compared to a numerical solution of the problem to find the effective droplet diameter associated with a certain fill or water distribution system.

The one-dimensional nature of the experiment greatly simplifies the numerical solution. An approach similar to that used in the circular and rectangular tower analysis is employed to find the rain zone loss coefficient. A fit of the resulting data produces the following correlation,

$$\begin{aligned} K_{rz} = a_v v_w \{ & 10645988 a_\mu \mu_a - 130.7774 a_\rho \rho_a - 32.6634 \\ & + 888.6645 \times \left[2.45287 (a_v v_i)^{-1.93315} + 0.34 \right] \times \left[4.03861 \exp(-574.542 a_L d_d) + 0.493 \right] \\ & \times \exp\left[(65.26215 a_L d_d + 0.74827) \times \ln\left[6.09836 \exp(0.0767 a_L H_i) - 6.1 \right] \right] \} \end{aligned} \qquad (2.76)$$

with altered restrictions being: $1 \le v_i \le 5 \text{m/s}; 0.5 \le H_i \le 5.5 \text{m}$ and the 'a-' coefficients remaining unchanged.

The experiments were conducted in a test section 1.84 m high, with a 1.5×1.5 m cross-sectional area. Two sets of tests were conducted to investigate the effects of different fill material on the droplet size distribution. The first experiment included expanded metal sieves of decreasing density at the top of the rain zone (to break up the water stream in a manner similar to splash type packing). For comparison, a droplet diameter of 3.5 mm was used in the equation, the results of which can be seen in figure 2.15. For the second experiment, asbestos sheets simulating film type packing were installed at the top of the rain zone. A comparison with equation (2.58) can be seen in figure 2.18 for a 5 mm droplet.

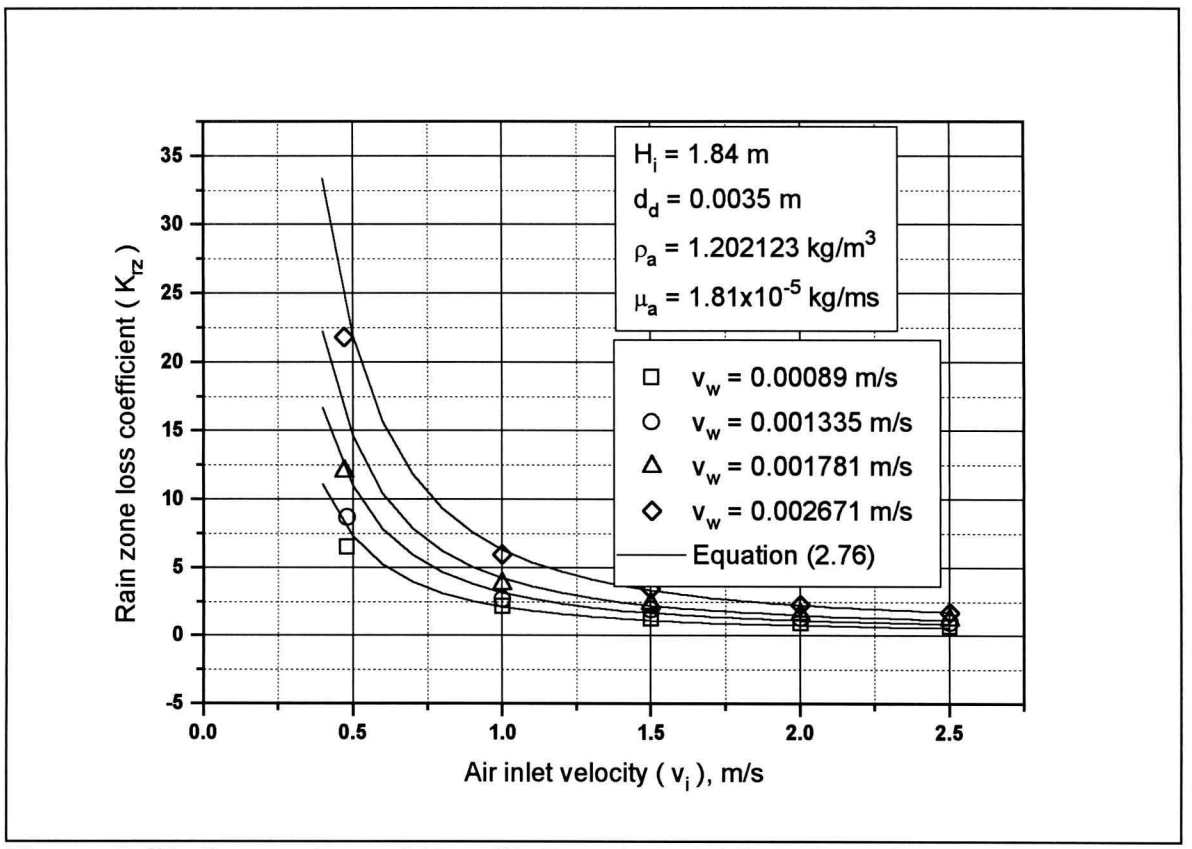

Figure 2.17: *Comparison of K_{rz} with Experimental Data for a Counterflow Tower.*

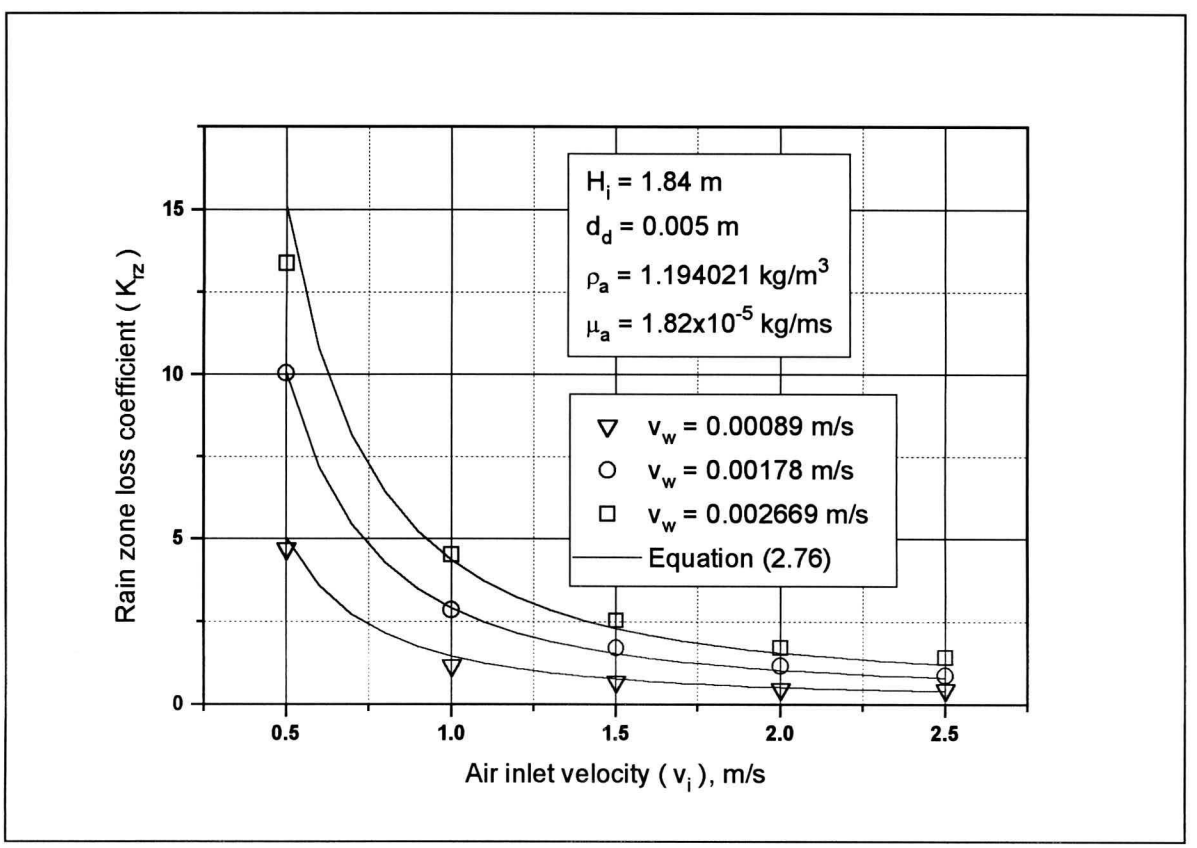

Figure 2.18: *Comparison of K_{rz} with Experimental Data for a Counterflow Tower.*

Experimentally obtained loss coefficients for a purely counterflow scenario agree well with the numerical results for droplet diameters of 3.5 and 5 mm. Since identical methods were used to derive the rain zone loss coefficients for the circular and rectangular geometries, it is not unrealistic to assume that these equations will produce accurate results under similar fill conditions.

It must be noted that the expressions are curve fits of numerically generated data and that they will reflect any deficiency in the numerical analysis. In this regard, the effective drop diameter, d_d, poses some questions. Although the counterflow experiment gives tentative evidence for 3.5 and 5 mm droplets, this is only true for a specific fill type and water distribution system. An attempt must be made to accurately predict droplet size for a range of applications. Despite possible deficiencies, the new equations overcome many of the defects inherent in previous methods of rain zone pressure drop prediction and comply with the model requirements set in Chapter 1.

CHAPTER

THREE

EXPERIMENTAL EVALUATION OF COOLING TOWER INLET LOSSES

The purpose of this chapter is to find correlations for the inlet losses of counterflow wet-cooling towers that exclude the effects of the rain zone. As stated previously, these losses have to be determined experimentally and correlations for both circular and rectangular tower geometries must be formulated. In addition, the consequences of employing either splash (isotropic) or film (orthotropic) type packing as fill material must be considered.

3.1 Literature Survey of Experimental Inlet Losses

A scale model experiment that simulates the inlet conditions of a cooling tower, must adhere to certain dictums to ensure its validity. In addition to the fact that all dimensions must be accurately scaled, the Reynolds' numbers of the test section and actual tower must be of the same order of magnitude to ensure similar turbulent characteristics. Also, the fill structure must be geometrically equivalent, especially near the entrance, where oblique flows are common.

A study of the literature reveals, that most experimental investigations of the inlet loss do not satisfy the aforementioned criteria [61LO1, 71ZE1, 81BU1, 81GA1, 81MO1]. Some of the researchers neglect the influence of the fill entirely, while others simulate the fill erroneously by using perforated plates or wire meshes. These deficiencies were overcome by Geldenhuys and Kröger [86GE1]. They use small pitch, finned-tube radiator material to simulate the fill, which closely models operational conditions in orthotropic packing (film type fill), and a large wedge shaped cooling tower model, where high Reynolds numbers ($+10^6$) are obtainable. Their results are applicable to large circular, natural draft, counterflow dry-cooling towers, with a uniform horizontal distribution of the heat exchangers, that completely covers the inlet section.

Further studies, using the same experimental arrangement, were conducted by Du Preez and Kröger [88DU1]. They determined the influence of unpacked areas (caused by gaps between rectangular heat exchangers fitted in a circular tower) on the inlet loss. Du Preez and Kröger's results are applicable only to circular, natural draft dry-cooling towers.

More recently, Terblanche and Kröger [94TE2] investigated the effects of the axial velocity distribution above the fill on the inlet loss coefficient. The same wedge section model used by Geldenhuys and Kröger was employed, but additional tests were done to determine the losses for rectangular cooling towers. The velocity distribution above the heat exchanger was found to be non-uniform, and a corresponding correction term was included to account for this effect. Terblanche's data, for the inlet loss coefficient of circular counterflow dry-cooling towers, is correlated by,

$$K_{ct} = \left[100 - 18\left(\frac{d_i}{H_i}\right) + 0.94\left(\frac{d_i}{H_i}\right)^2 \right] \times K_{he}^{\left[-1.28 + 0.183\left(\frac{d_i}{H_i}\right) - 7.769E-3\left(\frac{d_i}{H_i}\right)^2 \right]} \tag{3.1}$$

and is valid for $10 \leq d_i / H_i \leq 15$ and $5 \leq K_{he} \leq 25$. Terblanche also derived an equation to predict the inlet losses for rectangular towers,

$$K_{ct} = \left[1.1 + 1.1\left(\frac{W_i}{2H_i}\right)^3 - 0.05\left(\frac{W_i}{2H_i}\right)\exp\left(\frac{W_i}{2H_i}\right) \right] \times K_{he}^{\left[-0.29 + 0.079\cos\left(\frac{180}{\pi}\frac{W_i}{2H_i}\right) + 0.102\sin\left(\frac{180}{\pi}\frac{W_i}{2H_i}\right) \right]} \tag{3.2}$$

for $0 \leq W_i / H_i \leq 10$ and $4 \leq K_{he} \leq 80$, where W_i is the total width of the tower. Equations (3.1) and (3.2) are applicable to cooling towers with sharp inlets. For circular towers with well rounded inlets ($r_{ir} / d_i \approx 0.01$), Terblanche proposes the following correlation,

$$K_{ct} = 1.5\exp\left[0.2\frac{d_i}{H_i} \right] \times K_{he}^{\left[-0.4645 + 0.02303\left(\frac{d_i}{H_i}\right) - 0.00095\left(\frac{d_i}{H_i}\right)^2 \right]} \tag{3.3}$$

which must obey the same restrictions as equation (3.1). Although tests were done to determine the effect of inlet rounding on rectangular towers, no correlation was produced. Figure 3.1 depicts the consequences of rounding the inlet to a rectangular counterflow cooling tower.

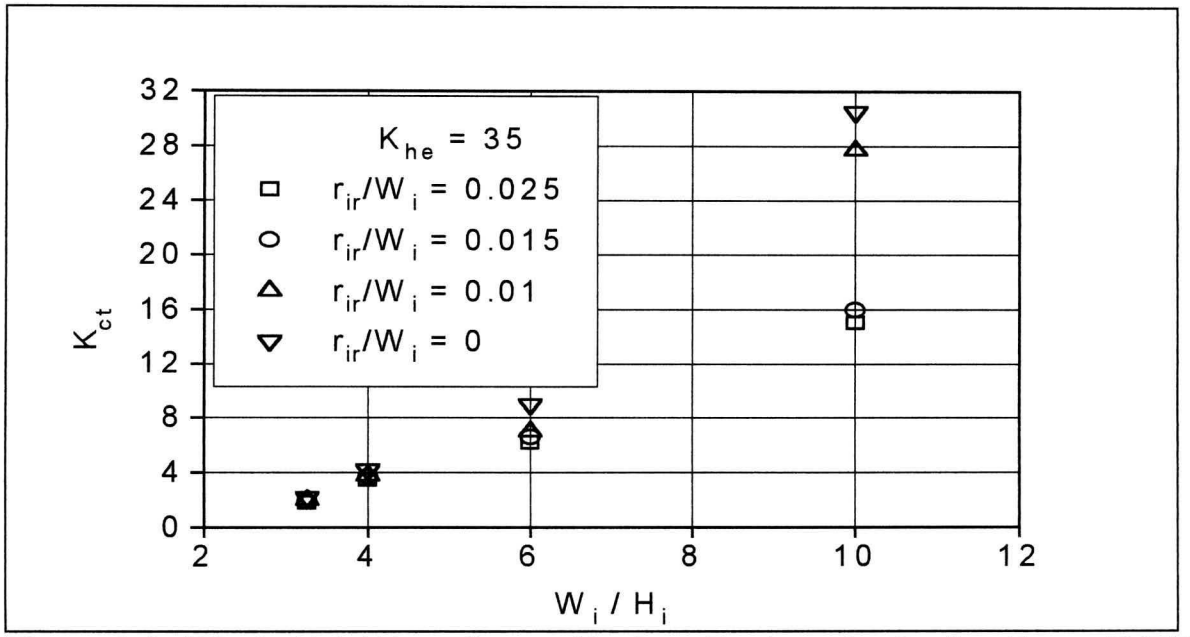

Figure 3.1: *Effect of Inlet Rounding on K_{ct} for a Rectangular Cooling Tower* [94TE1].

All of Terblanche's experiments were done with dry-cooling towers in mind, but since the heat exchanger material, used in these experiments, is geometrically similar to film type (orthotropic) packing, the results are also valid for wet towers similar fills.

Terblanche's equations are adequate for inclusion in the modelling strategy proposed in Chapter 1 and satisfy the requirement for experimental correlations of the inlet loss coefficient in orthotropically packed counterflow wet-cooling towers. No correlations for the inlet loss coefficient in isotropically packed (splash type fill) cooling towers were found in the literature.

3.2 Experimental Model

The same scale model used by Terblanche and Kröger was employed to experimentally find the inlet losses for isotropically packed towers. The notable exception being the fill material, which was replaced by a more isotropic resistance, resembling operational splash type packing (fig. 3.2).

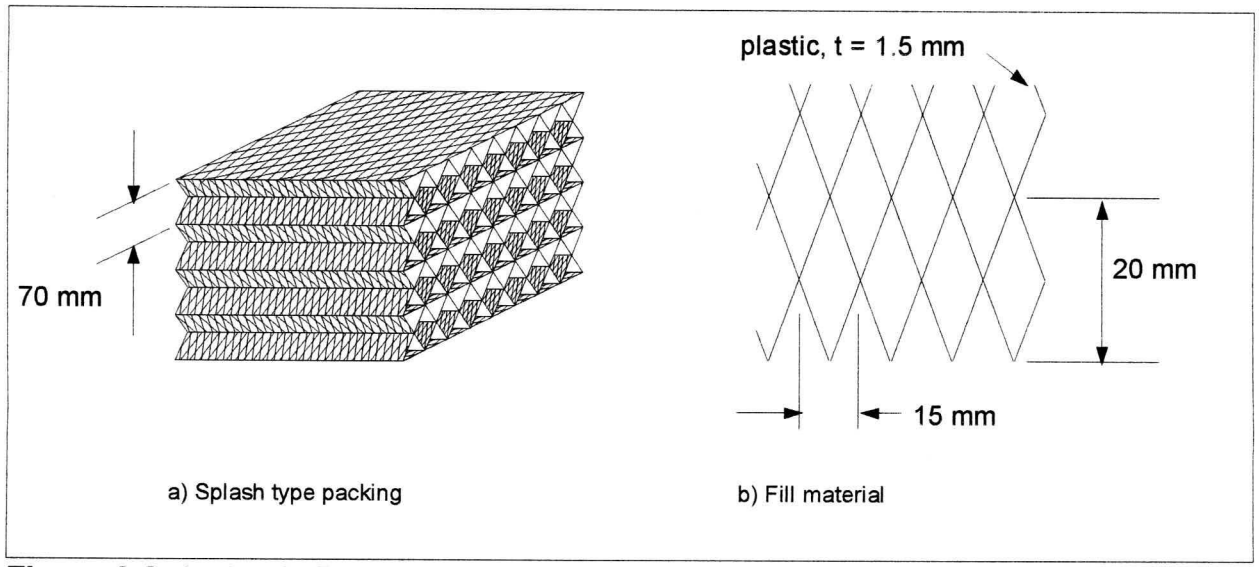

Figure 3.2: *Isotropic Resistance Fill Material (Trickle Grid).*

To obtain experimental values for the inlet loss coefficient in accordance with equation (1.4), certain simplifications and approximations have to be made. In addition to the fact that rain zone effects are ignored for the time being, the following assumptions were made concerning the experimental arrangement:

- The effects of gravity can be ignored. By using a horizontal test section, the integral term that represents the buoyancy force in equation (1.4) becomes redundant, thus $\int_0^{Ho} \rho g\, dz = 0$.
- The flow is adiabatic and incompressible. Since there is no heat or mass transfer in the scale model and pressure differences are relatively small, this assumption is valid. The assumption implies that the air density throughout the model is constant, thus $\rho = \rho_a$.
- The fill material is homogeneously distributed across the inlet section. There is no flow contraction and therefore, $A_{fr} = A_i$.
- The velocity distribution above the fill is uniform. Although Terblanche [94TE1] shows that this is not the case, the effect is small compared to experimental error and will be ignored.
- The fill is the only flow obstruction in the tower. It is assumed that all the axial resistances in the vicinity of the fill are summed to arrive at the total resistance. Also, static flow obstructions before the fill (tower supports, inlet louvers) are not present in the model. Terblanche reveals [94TE2] that the inlet losses are independent of these obstructions in any case. Therefore, $K_{sum} = K_{fi}$.

Employing these assumptions reduces equation (1.4) to,

$$K_{ct} = \frac{p_a - p_o}{\rho_a v_i^2 / 2} - 1 - K_{fi} \tag{3.4}$$

where $v_i = A_i / (\rho_a m_{av})$ and p_o is the static pressure after the fill. Equation (3.4) can now be applied to an experimental scale model.

3.3 Circular Cooling Towers

The inlet losses for a circular cooling tower are dependent on the inlet diameter, d_i, the inlet height, H_i, and the radius of the inlet rounding, r_{ir} (fig. 3.3). The magnitude of the fill loss coefficient and other obstacles in its immediate vicinity, referred to as K_{fi}, also has a strong influence on the inlet loss. The geometry of the fill has a small, but measurable effect, therefore isotropic distributed resistances will be used consistently as fill material (fig. 3.2) throughout the experimental procedure.

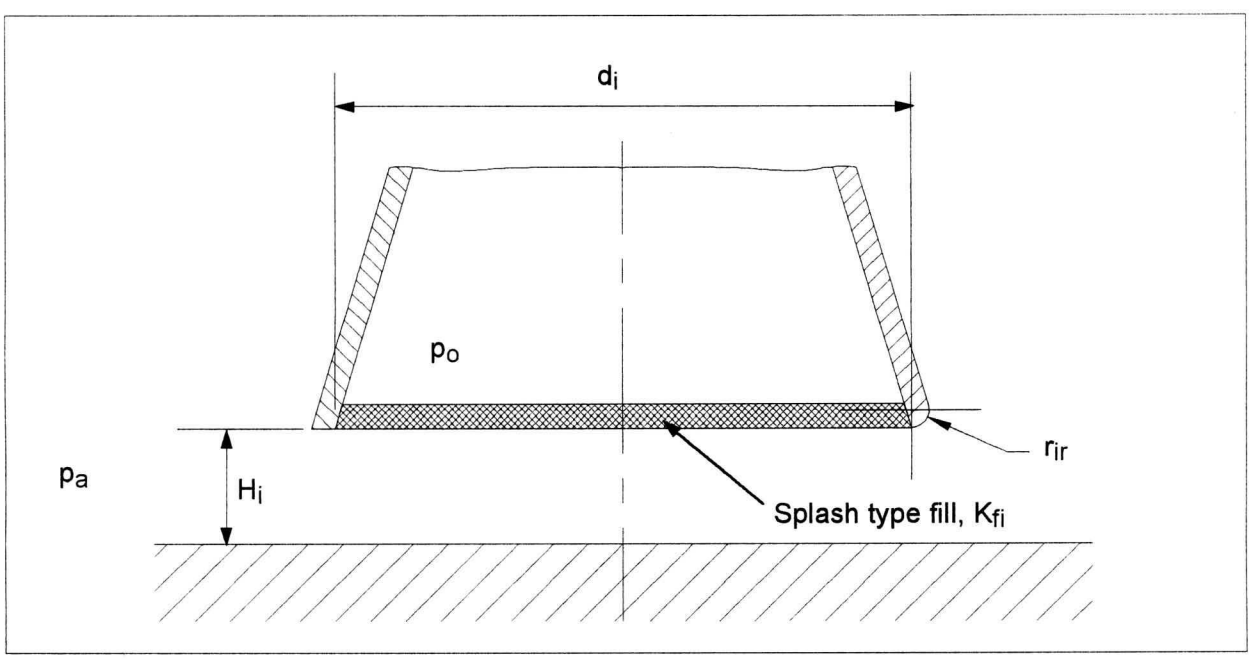

Figure 3.3: *Schematic representation of Experimental Model for a Circular Tower.*

Applying dimensional analysis to the variables governing the inlet loss, reduces the functional dependency of the inlet loss coefficient to,

$$K_{ct} = f\left(\frac{d_i}{H_i}, \frac{r_{ir}}{d_i}, K_{fi}\right) \tag{3.5}$$

By utilising the description of dependencies provided above, a scale model, that can vary each of the dimensionless groups independently (and thereby facilitate the formulation of empirical correlations), can be constructed.

3.3.1 Experimental Apparatus

The test facility, as shown in figure 3.4, represents a wedge shaped section of a horizontally arranged, circular cooling tower. Equivalent Reynolds numbers far in excess of a comparable size cylindrical model can be achieved, because of the model's section nature. Reynolds numbers, based on the frontal area, of up to 2×10^6 have been observed, which compare well with operational wet-cooling towers, where Reynolds numbers of around 10^7 are common.

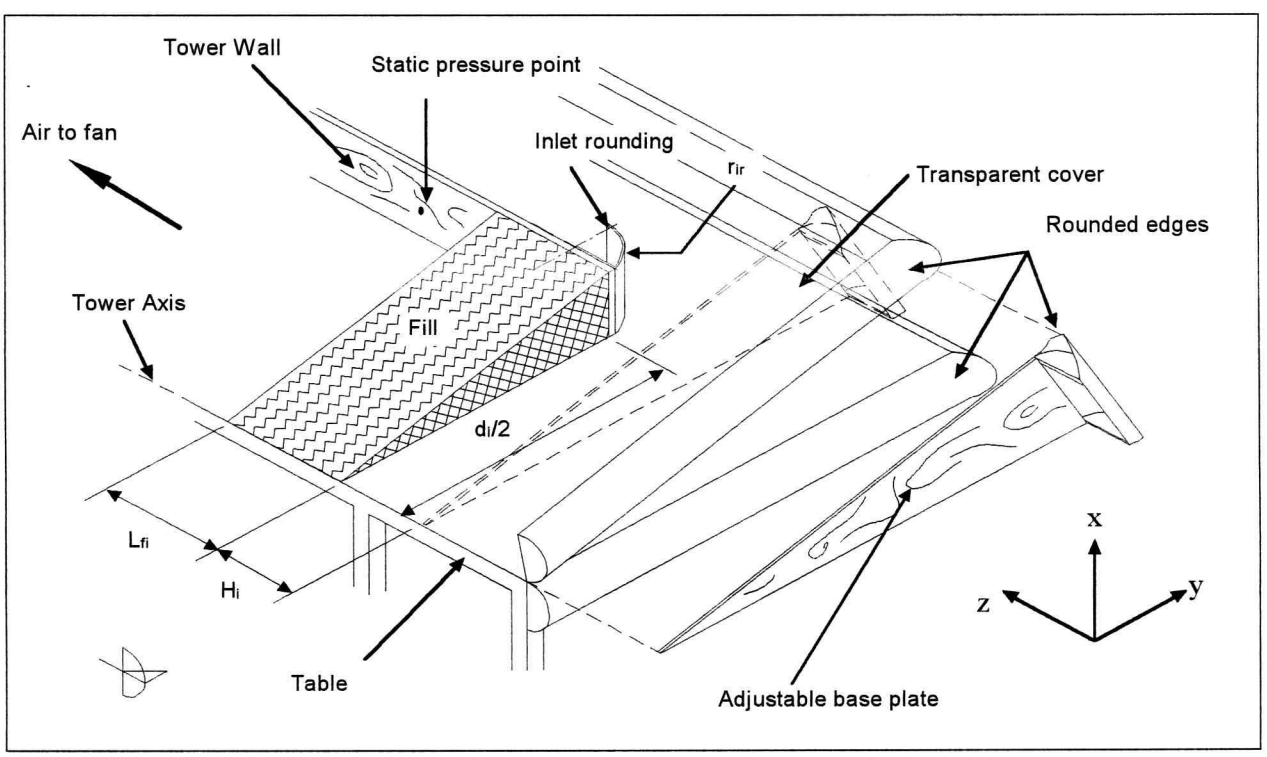

Figure 3.4: *Section Model of a Cylindrical Cooling Tower.*

The scale model consists of a smooth horizontal table covered with transparent perspex plates. The plates are supported by a rectangular wall on the one side, which represents the cooling

tower shell, while the other side rests on the table, emulating the tower's centre line. Since the air flow in cooling towers, in the absence of cross-winds, is essentially axi-symmetrical, the triangular section created by this arrangement, accurately represents a small arc of a complete cooling tower. A computational fluid dynamic simulation of the experimental setup was used to investigate the influence of the perspex side plates on the inlet loss results. The effects were found to be negligible, allowing the wedge shaped experimental setup to be used with confidence. The ground beneath the cooling tower is represented by a triangular base plate, which can be adjusted to change the inlet height, H_i, of the model tower. This allows testing at variable d_i / H_i ratios. The model is also equipped with several removable inlet roundings, of different radii, to obtain a range of r_{ir} / d_i values. The inlet roundings consist of shaped aluminium plates that attach to the bottom of the tower shell with a 90° angle. The fill is modelled using plastic splash type packing (trickle grid) (fig. 3.2), where the magnitude of the fill resistance, K_{fi}, is controlled by varying the packing thickness. In addition, the edges of the table, lid and base plate are well rounded to prevent local flow separation from corrupting the test data. A wind tunnel, equipped with a variable speed fan, is connected to the outlet of the tower section and is used to draw air through the model. The mass flow rate of air in the wind tunnel is measured by sized elliptical nozzles, situated in a special chamber inside the tunnel.

3.3.2 Testing Procedure

Wet and dry bulb temperature measurements were made using glass bulb thermometers and atmospheric pressure was measured with a mercury column manometer. Static pressure differences in the test section and wind tunnel were measured with *Endress+Hauser Deltabar* pressure transducers coupled to a data logging program, *Log_cf*, via a *Schlumberger SI 35951C* IMP.

As mentioned previously, air is drawn through the test section by the wind tunnel fan. This action produces a negative gauge pressure in the scale model and wind tunnel. Since the experimental arrangement is not entirely air tight, a small amount of air leaks into the assembly during normal testing. Therefore, the air mass flux measured by the nozzles is slightly greater than that passing through the inlet section.

To compensate for this error the model has to be calibrated to take this additional air flux into account. This is accomplished by sealing the entrance to the test section and then measuring the leakage flow, m_l, for a range of static pressures, p_o, above the fill.

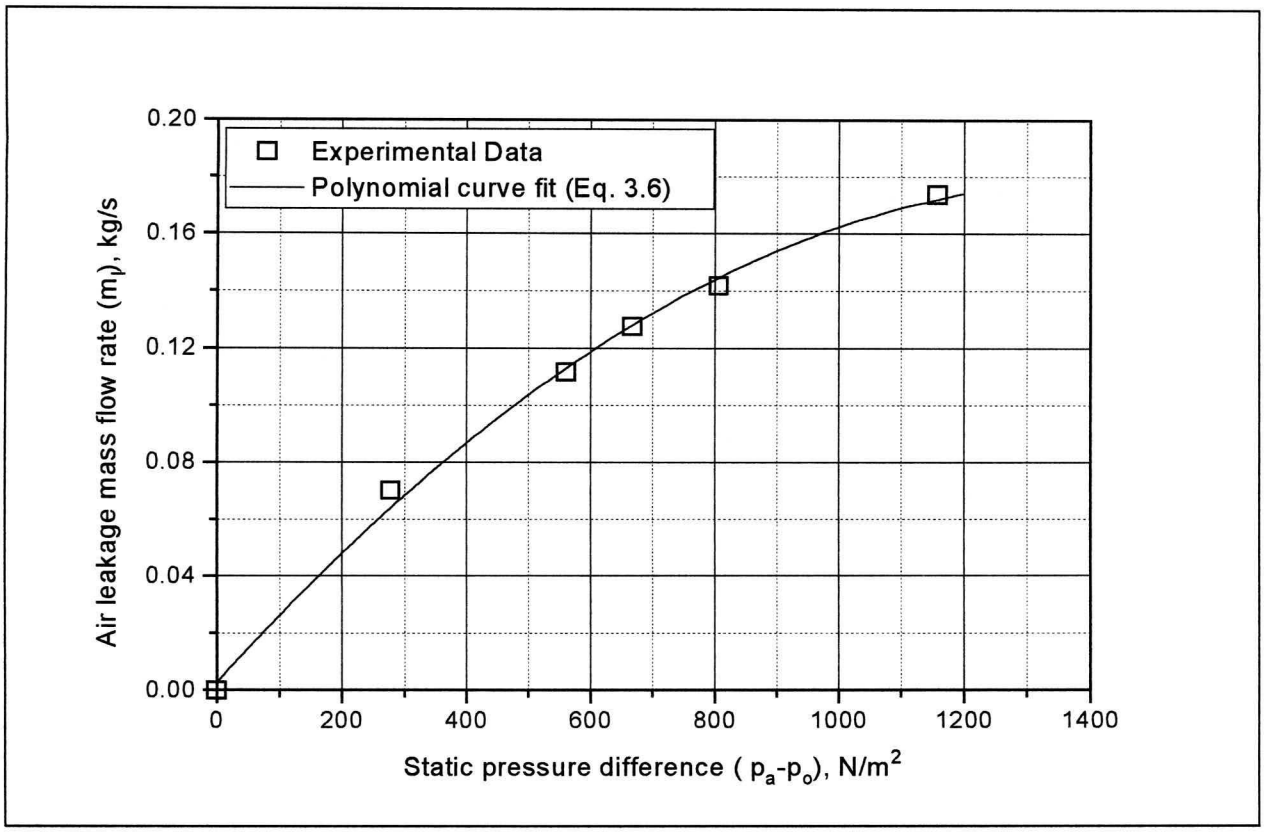

Figure 3.5: *Correlation for Air Leakage Mass Flow Rate of Circular Tower Model.*

From this data (fig. 3.5) a correlation between the static pressure difference and leakage air mass flow rate for the cylindrical model was obtained. The correlation is given by,

$$m_l = (p_a - p_o)\left[2.52 \times 10^{-4} - 8.943 \times 10^{-8}(p_a - p_o)\right] \tag{3.6}$$

For each experimental run the static pressure difference, $(p_a - p_o)$, was measured and used in conjunction with equation (3.6) to determine the leakage air mass flow rate. The correct mass flow rate, used in further calculation, is then the air mass flow rate through the elliptical nozzles minus the leakage flow:

$$m_{av} = m_n - m_l \tag{3.7}$$

where m_{av} is the mass flow rate of the air-vapour mixture through the fill.

The fill loss coefficient was determined under normal flow conditions, using the experimental arrangement shown in figure 3.6. The base plate is removed from the original model, while the tower shell plate is extended to the base of the table. Static pressure drop across the fill is measured by two pressure tap points, inserted in the model shell at equal distances before and after the fill. The fill loss coefficient is defined by,

$$K_{fi} = \frac{\Delta p_{fi}}{\rho_a v_i^2 / 2} \tag{3.8}$$

where Δp_{fi} is the static pressure drop across the fill and v_i is defined for equation (3.4).

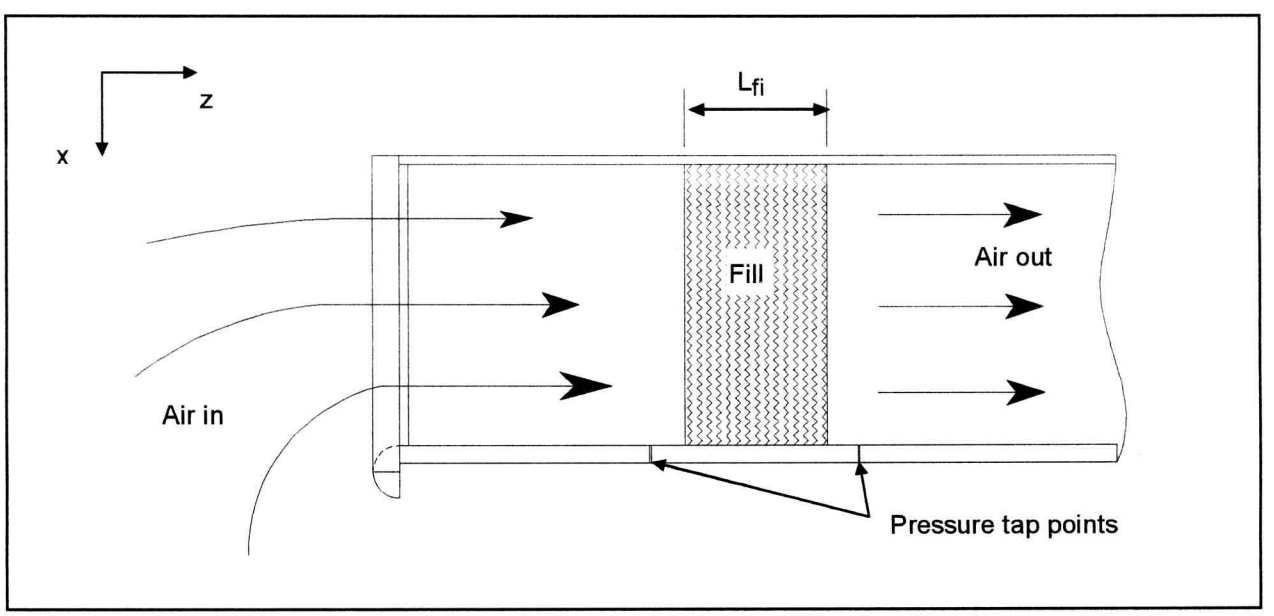

Figure 3.6: *Normal Flow arrangement for Fill Pressure Drop calibration.*

By varying the mass flow rate, the fill pressure loss coefficient, K_{fi}, can be determined for different values of the flow parameter, defined as, $Ry = \rho_a v_i / \mu_a$. These values are then used to derive a correlation that predicts the fill loss coefficient.

Figure 3.7 shows the data and curve fit for such a procedure for a fill length, L_{fi}, of 0.32 m. The correlation is given by,

$$K_{fi} = 5 \times 10^{-7} Ry + 15.548 \qquad (3.9)$$

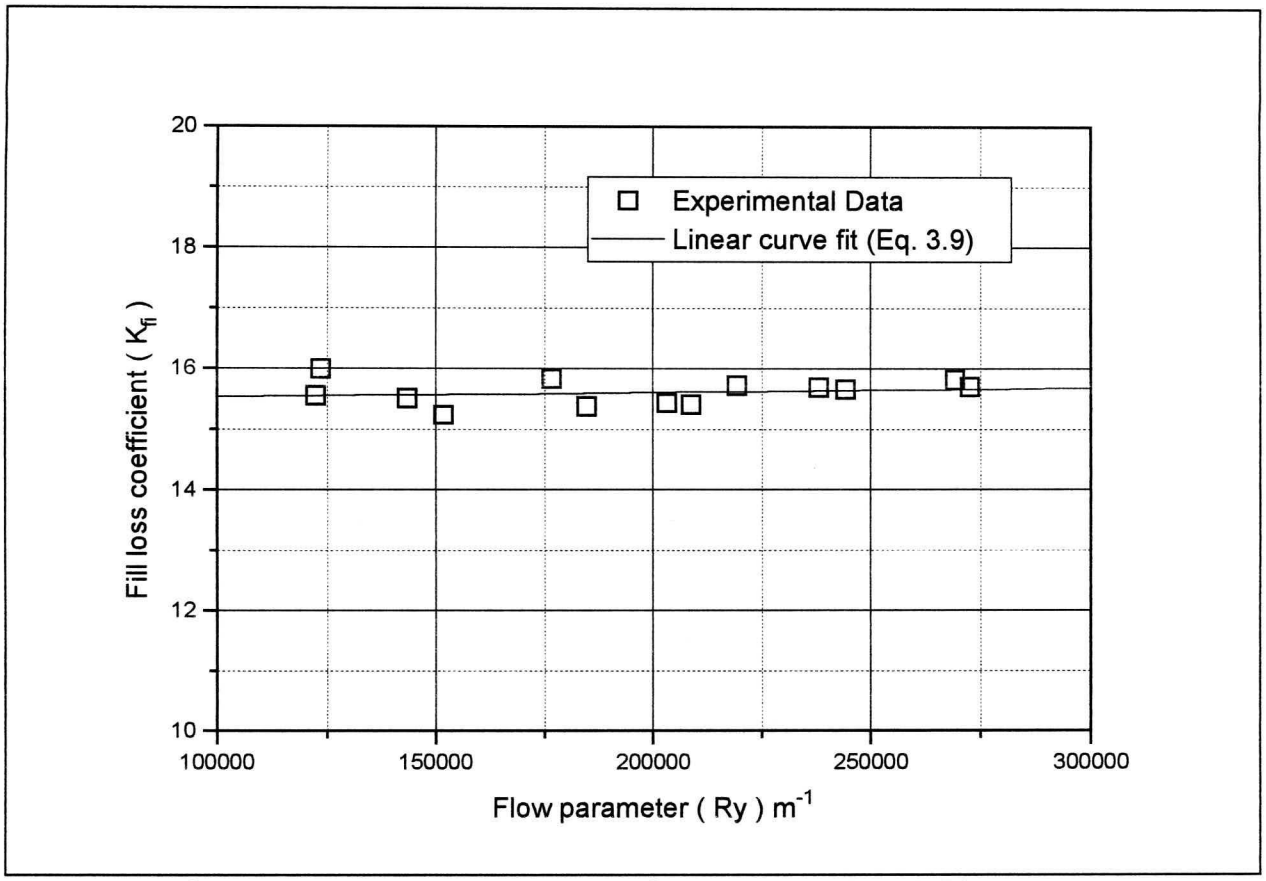

Figure 3.7: *Calibration of Fill Pressure Loss Coefficient for L_{fi} = 0.32 m.*

The near constant value of the fill pressure loss coefficient is ascribed to the lack of boundary layer growth, as encountered in film type packing at similar Reynolds numbers. The fine lattice structure of splash type packing does not provide the continuous surfaces necessary for the development of boundary layers, with the consequence that free stream Reynolds numbers through the fill are uniformly high. Turbulent, high Reynolds number flows around blunt objects usually approach constant values for their loss coefficients (e.g. sphere drag coefficient) and such is the case in the fill normal flow calibrations.

The normal flow experiment was repeated for a range of fill lengths to obtain correlations for fill loss coefficients in the vicinity of $K_{fi} \approx 5, 10, 15, 20$ and 25. The results of these procedures are shown in figure 3.8.

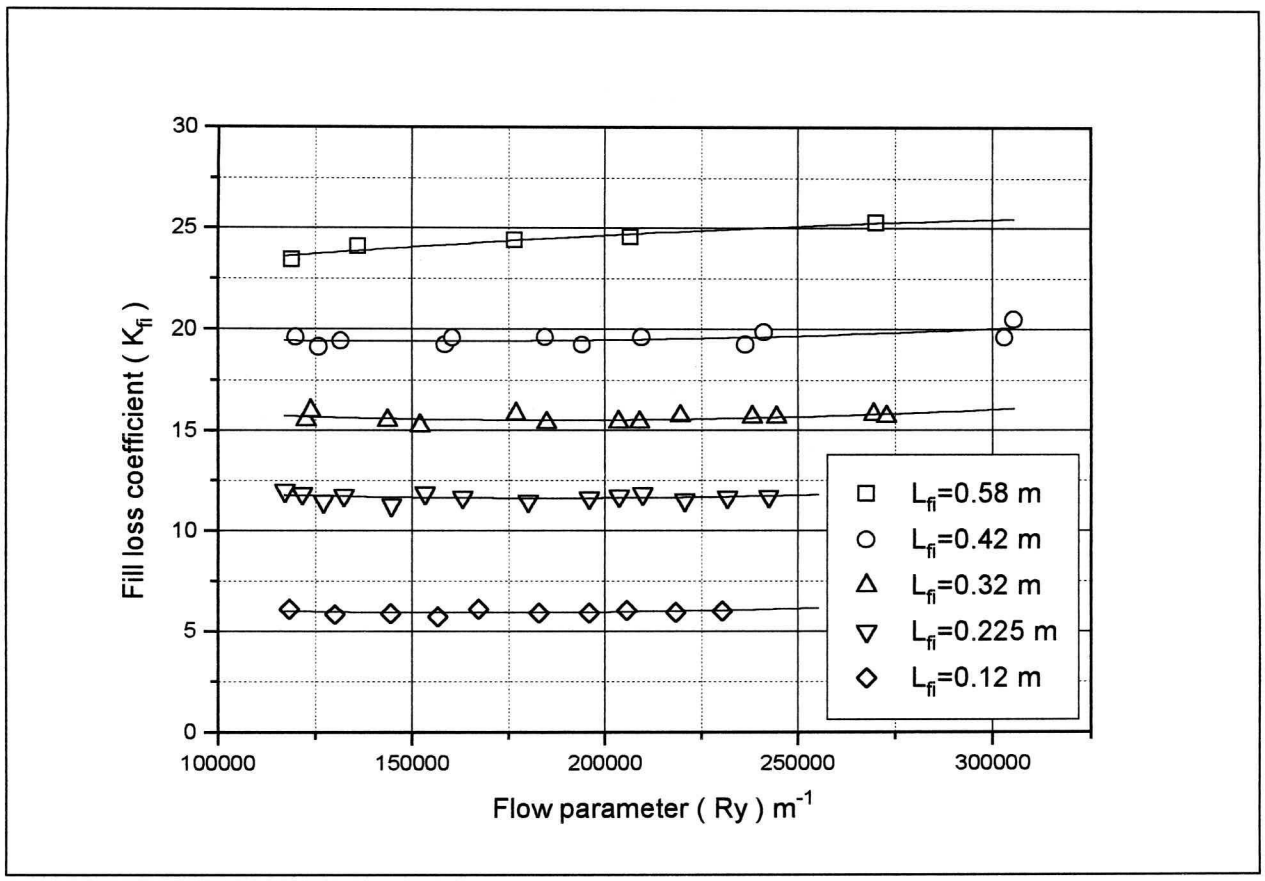

Figure 3.8: *Fill Pressure Loss Calibration for Circular Cooling Tower Model.*

The inlet loss coefficient is determined by measuring the difference between atmospheric pressure and the pressure after the fill and then subtracting the calculated fill pressure drop from the result, according to equation 3.4. Tests were done at the five values for K_{fi} mentioned previously. For each of the fill configurations, the base plate was moved to represent five different values for the inlet diameter to inlet height ratio, d_i / H_i. For each of these settings, roundings were affixed to the inlet, so that the inlet loss coefficient was measured for sharp inlets as well as for four different inlet rounding radii.

3.3.3 Experimental Results

The data generated by the experimental procedure is highly non-linear for two of the three dimensionless groups. This fact is illustrated in figures 3.9 and 3.10 for r_{ir}/d_i and K_{fi} as the respective primary variables. This non-linearity severely impedes the generation of accurate correlations to describe the inlet loss coefficient and adds much to the complexity of such correlations. To simplify the curve fitting procedure, the data set associated with $d_i/H_i = 5$ was dropped from the analysis, enabling a more accurate fit of the remaining data. Since existing natural draft counterflow wet-cooling towers usually have inlet diameter to height ratios of between ten and fifteen, this simplification does not negatively affect the validity of the relation.

For a circular counterflow cooling tower with an isotropic resistance fill the correlation for the inlet loss coefficient is given by,

$$K_{ct} = \left(0.011266\mathrm{e}^{\left(0.093\frac{d_i}{H_i}\right)} K_{fi}^2 - 0.3105\mathrm{e}^{\left(0.1085\frac{d_i}{H_i}\right)} K_{fi} + 4.5614\mathrm{e}^{\left(0.131\frac{d_i}{H_i}\right)} - 1.7522 \right)$$
$$+ \sinh^{-1}\left[\left(\frac{10970.19\mathrm{e}^{\left(-0.2442K_{fi}\right)} + 1391.27}{d_i/H_i - 15.7258} + 1205.54\mathrm{e}^{\left(-0.23K_{fi}\right)} + 109.314 \right) \times \left(\frac{2r_{ir}}{d_i} - \frac{0.01942}{d_i/H_i - 27.929} - 0.016866 \right) \right] \qquad (3.10)$$

which is valid for $7.5 \le d_i/H_i \le 15$, $5 \le K_{fi} \le 25$ and $0 \le r_{ir}/d_i \le 0.02$. The maximum error encountered when fitting equation (3.10) to the experimental data occurs at $d_i/H_i = 7.5$ and is approximately 10 percent of the inlet loss coefficient, while the average error is only 2.5 percent. The agreement is adequate for the purposes of this investigation, since experimental uncertainty can account for a deviation of up to 3 percent of the measured value.

As mentioned previously, the complexity of equation (3.10) is caused largely by the non-linearity of the experimental data. The inverse hyperbolic sine function in the second term of equation (3.10) accounts for the inflection point in the r_{ir}/d_i dependent data shown in figure 3.9. Previous researchers neglected this dependency in favour of simplicity or used two different

equations to predict the loss coefficient before and after the inflection point [94TE2]. The error in this approach seems to be significant, since the inlet loss coefficient continues to decrease, albeit slowly, with increased inlet rounding radius after the inflection point (fig. 3.9).

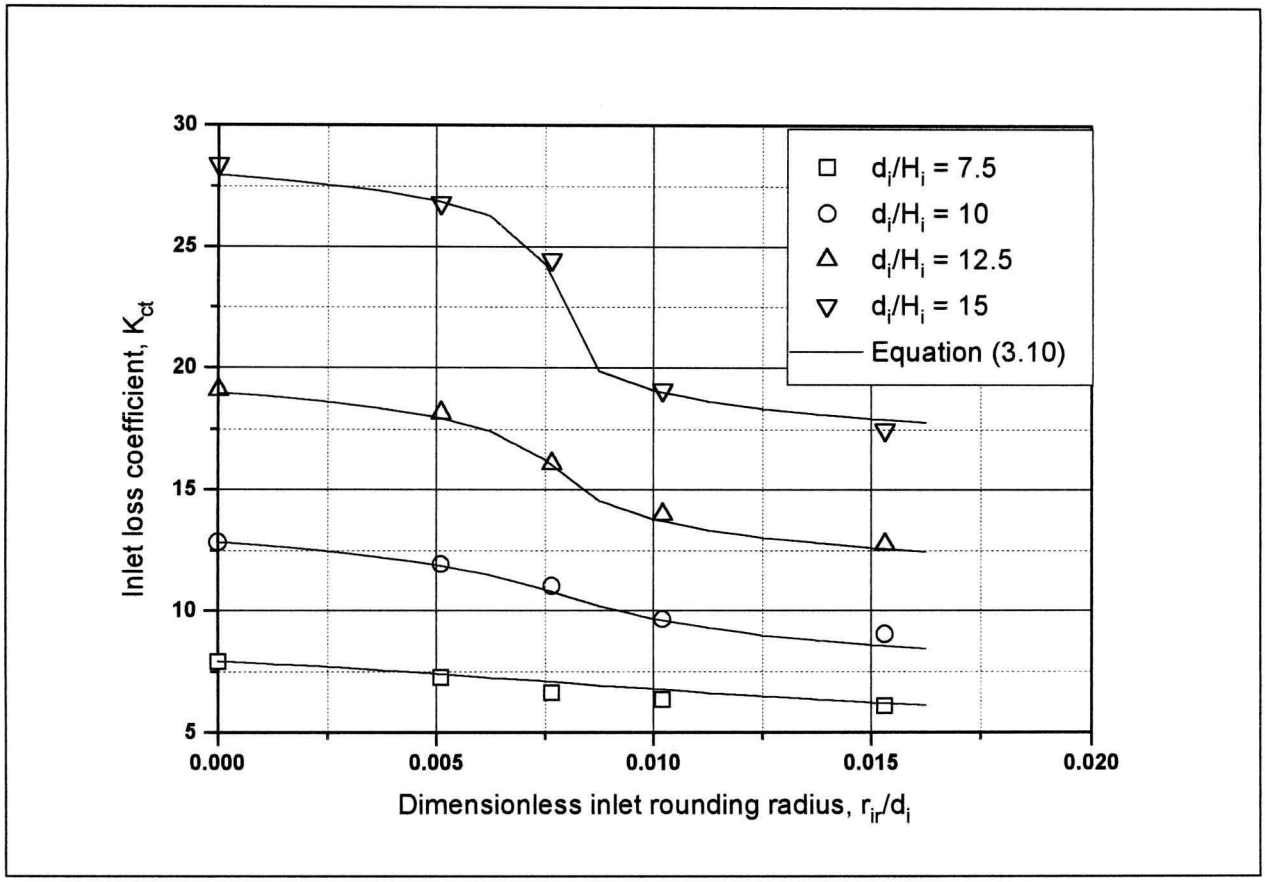

Figure 3.9: *Inlet Loss Coefficient for a Circular Tower with Splash Type Fill,* $K_{fi} = 5.975$.

The necessity for the parabolic function in the first term of equation (3.10) can be seen clearly in figure 3.10. This trend in fill resistance dependent data is unique to isotropic fills and the explanation probably lies in the recirculating flows next to the inlet. The local minimum created by this distribution, implies an optimum value for the inlet loss coefficient in isotropically packed towers for a fill loss coefficient of magnitude ~15. Figure 3.11 shows the dependency of K_{ct} on the inlet diameter to height ratio. The data is smooth and continuously increasing and is approximated well by the exponential functions used in equation (3.10).

In summary, equation (3.10) accurately represents the data generated by scale model experiments of isotropically packed circular counterflow cooling towers and is adequate for inclusion in the modelling strategy proposed in Chapter 1.

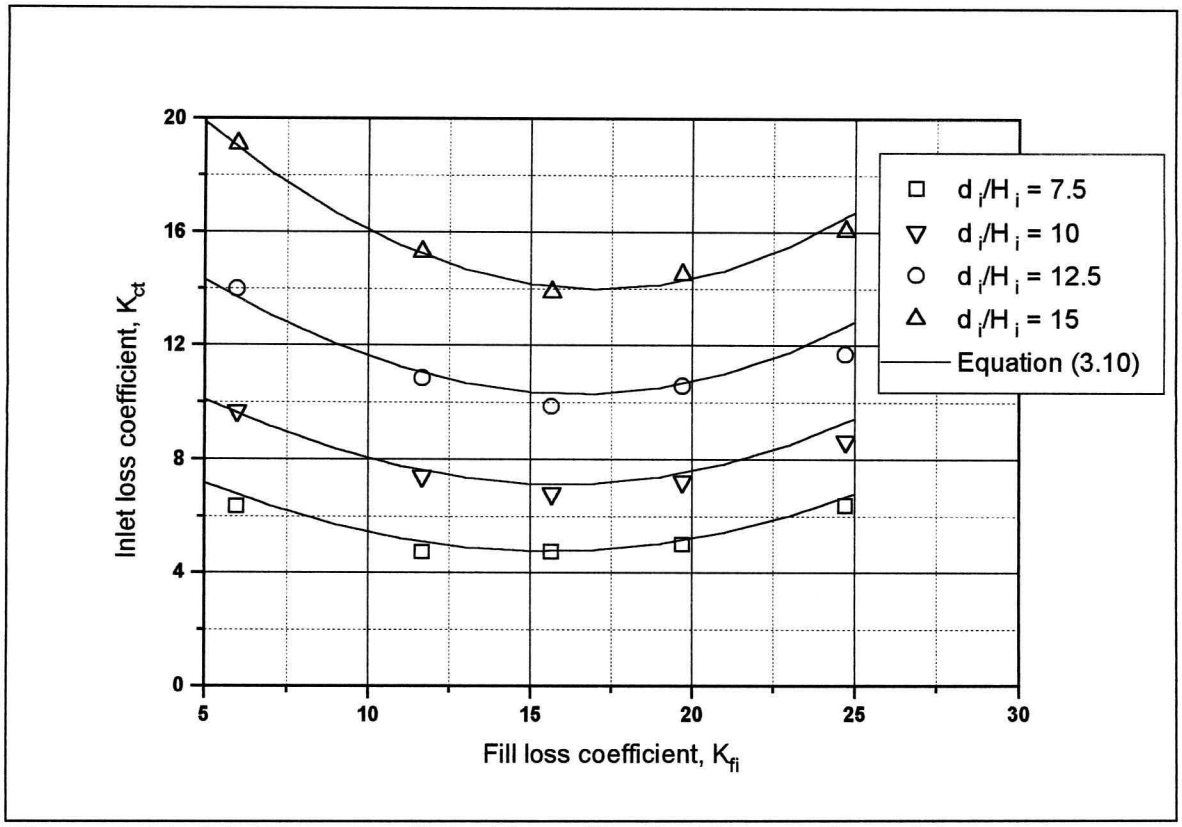

Figure 3.10: *Inlet Loss Coefficient for a Circular Tower with* $r_{ir} / d_i = 0.0102$.

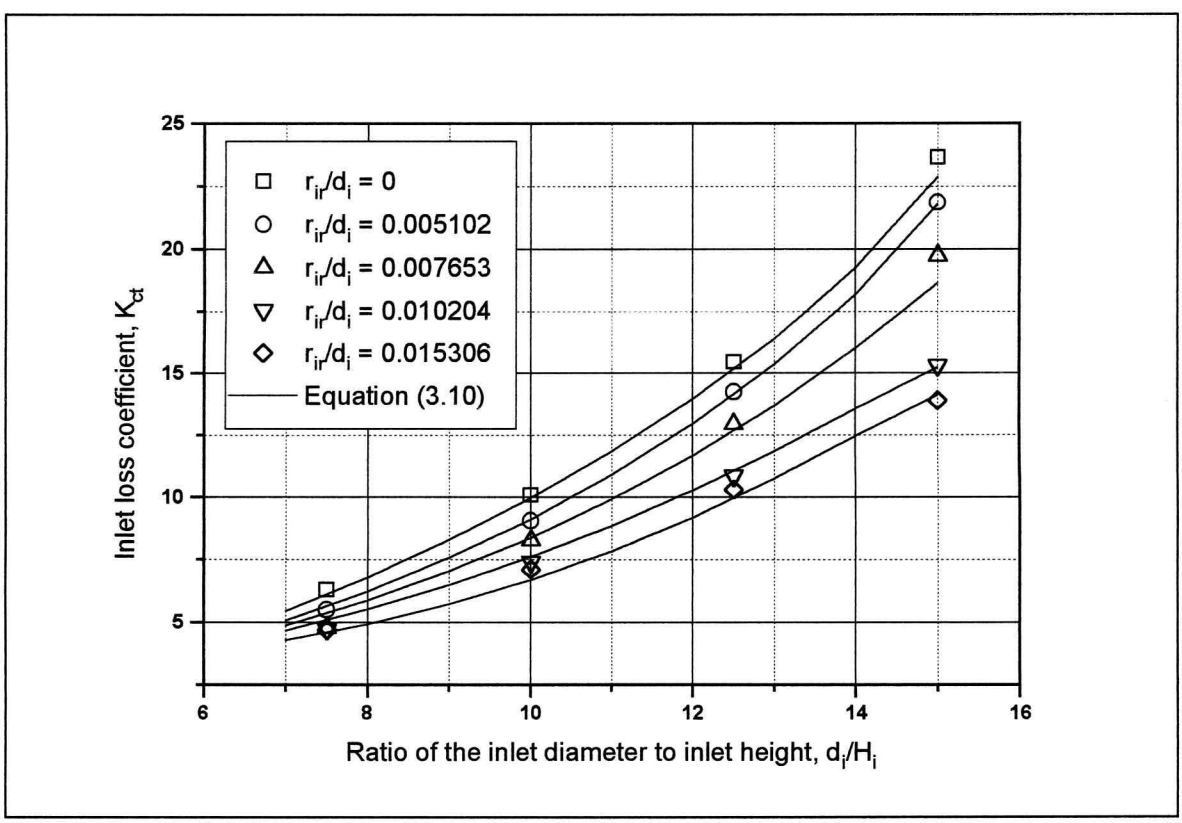

Figure 3.11: *Inlet Loss Coefficient for a Circular Tower with Splash Pack,* $K_{fi} = 11.66$.

3.4 Rectangular Cooling Towers

The inlet losses for rectangular cooling towers are dependent on the same variables as the circular tower, except for the inlet diameter which is replaced by the inlet width, W_i (fig 3.12). The other strong variables are the inlet height, H_i, the radius of the inlet rounding, r_{ir} and the fill loss coefficient (and other obstacles in its immediate vicinity), K_{fi}. The same splash type packing used in the circular tower experiments (fig. 3.2) was used as fill material in the rectangular tower experiments.

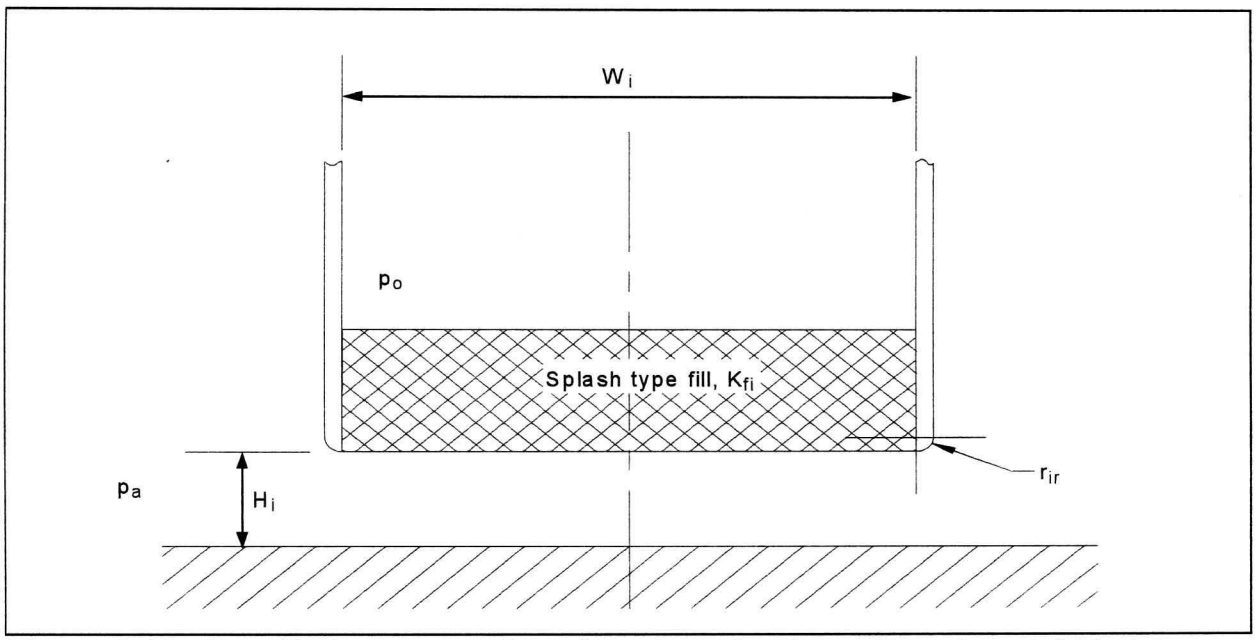

Figure 3.12: *Simplified representation of Rectangular Tower Experimental Model.*

After dimensional analysis the inlet loss coefficient for rectangular towers has the following functional relationship,

$$K_{ct} = f\left(\frac{W_i}{H_i}, \frac{r_{ir}}{W_i}, K_{fi}\right) \tag{3.11}$$

Again a scale model, based on dependencies provided by equation (3.11), can be constructed.

3.4.1 Experimental Apparatus

The test facility, for the rectangular tower, differs from the circular model in the important respect that the one side of the perspex lid rests not on the table, but on another rectangular wall (fig

3.13). The resultant configuration represents a horizontally arranged, nearly two-dimensional section of a rectangular cooling tower. Although Reynolds numbers in the rectangular section are lower than in the circular section, they still compare favourably to operational conditions, being less than ten times smaller than the Reynolds numbers (6×10^6) associated with full scale towers.

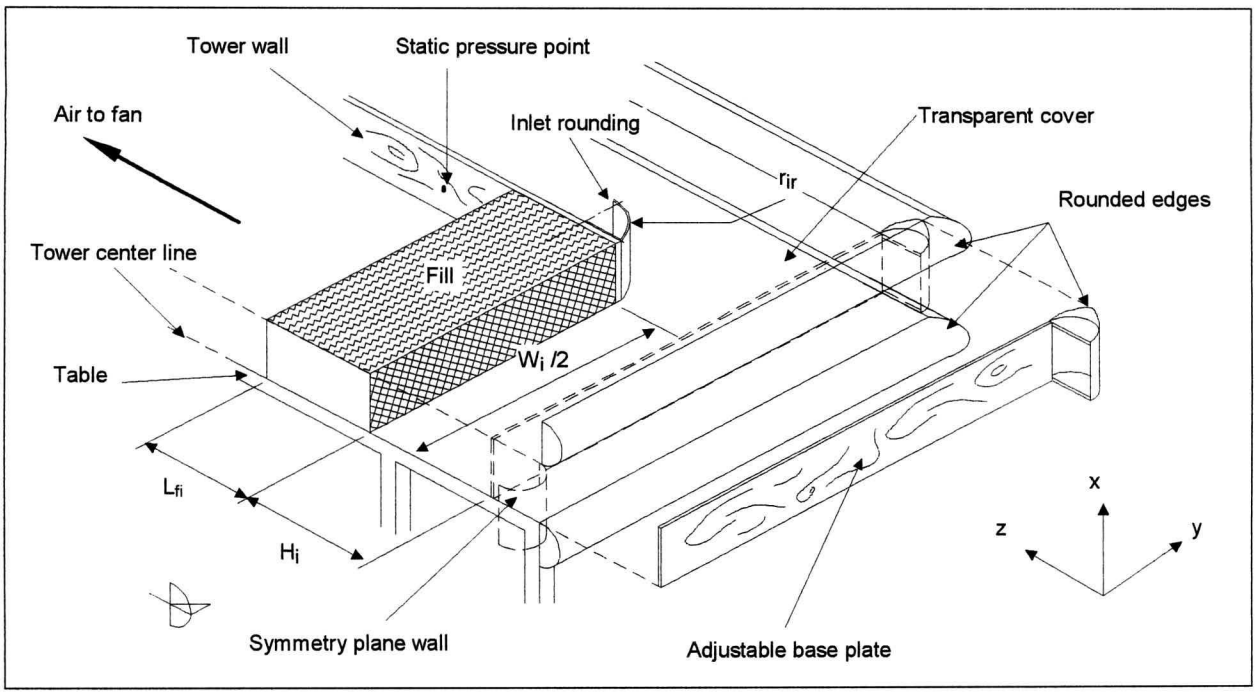

Figure 3.13: *Section Model of a Rectangular Tower.*

The rectangular scale model also consists of a smooth horizontal table covered with transparent perspex plates, but the plates are supported by a rectangular wall on both sides. These walls represent the cooling tower shell and centre line respectively. The axi-symmetric flow present within this rectangular section, therefore represents a small slice of a bank of rectangular cooling towers. The base plate for the rectangular model is obviously rectangular, but all other fittings and adjustments are identical to those for a circular tower, except for the variables specified in equation (3.11).

3.4.2 Testing Procedure

Measurements for the rectangular model were likewise done in a similar manner to the circular tower experiment. The leakage air mass flow rate was determined separately for the rectangular model, but the procedure was the same. The correlation for the leakage air mass flow rate data in figure 3.14 is given by,

$$m_l = 1.5317 \times 10^{-4}(p_a - p_o) \tag{3.12}$$

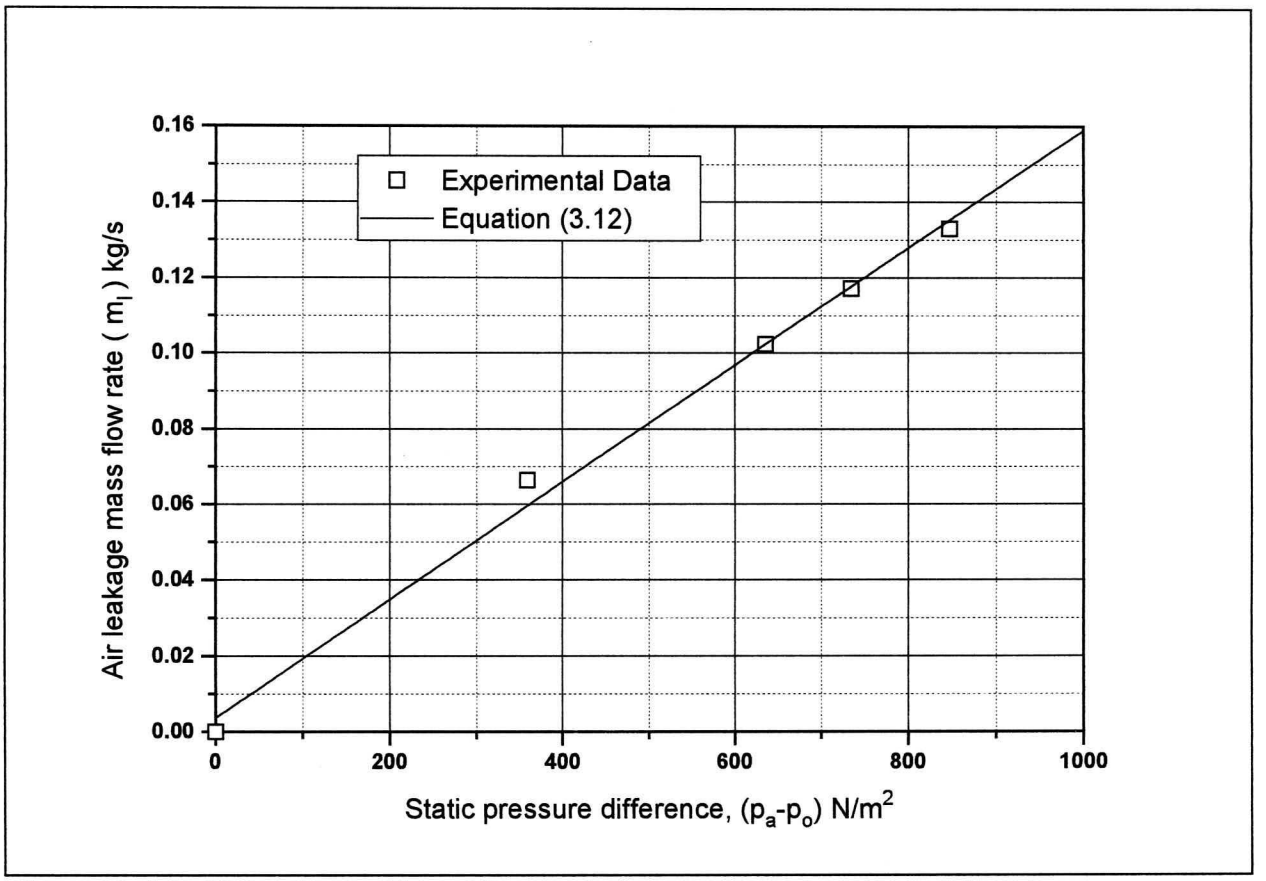

Figure 3.14: *Air Leakage Mass Flow Rate for Rectangular Tower Model.*

The fill loss coefficient for the rectangular model was determined under normal flow conditions similar to the experimental arrangement shown in figure 3.6. The base plate is removed and the tower wall plate is extended to the base of the table. Static pressure drop across the fill is measured at the same pressure tap points as in the circular model and the rectangular fill loss coefficient is also defined by equation (3.8).

Again, the mass flow rate was varied and the fill loss coefficient, K_{fi}, determined for different values of the same flow parameter, Ry. The correlations that predict the fill loss coefficient and the data for different fill lengths are shown in figure 3.15. It is noteworthy that the fill lengths for the rectangular tower are somewhat longer than those for the circular model with comparable loss coefficients. This was caused by denser packing of the fill material in the circular configuration enforced by the triangular shape of the section.

For the rectangular tower model the fill loss coefficient was calibrated for four different values in the vicinity of $K_{fi} \approx 5,10,15$ and 25. By moving the base plate the inlet width to height ratio, W_i / H_i, was varied between 1 and 10 for five discrete values. Three different inlet rounding radii and a sharp inlet were employed for each inlet width to height ratio during rectangular tower testing.

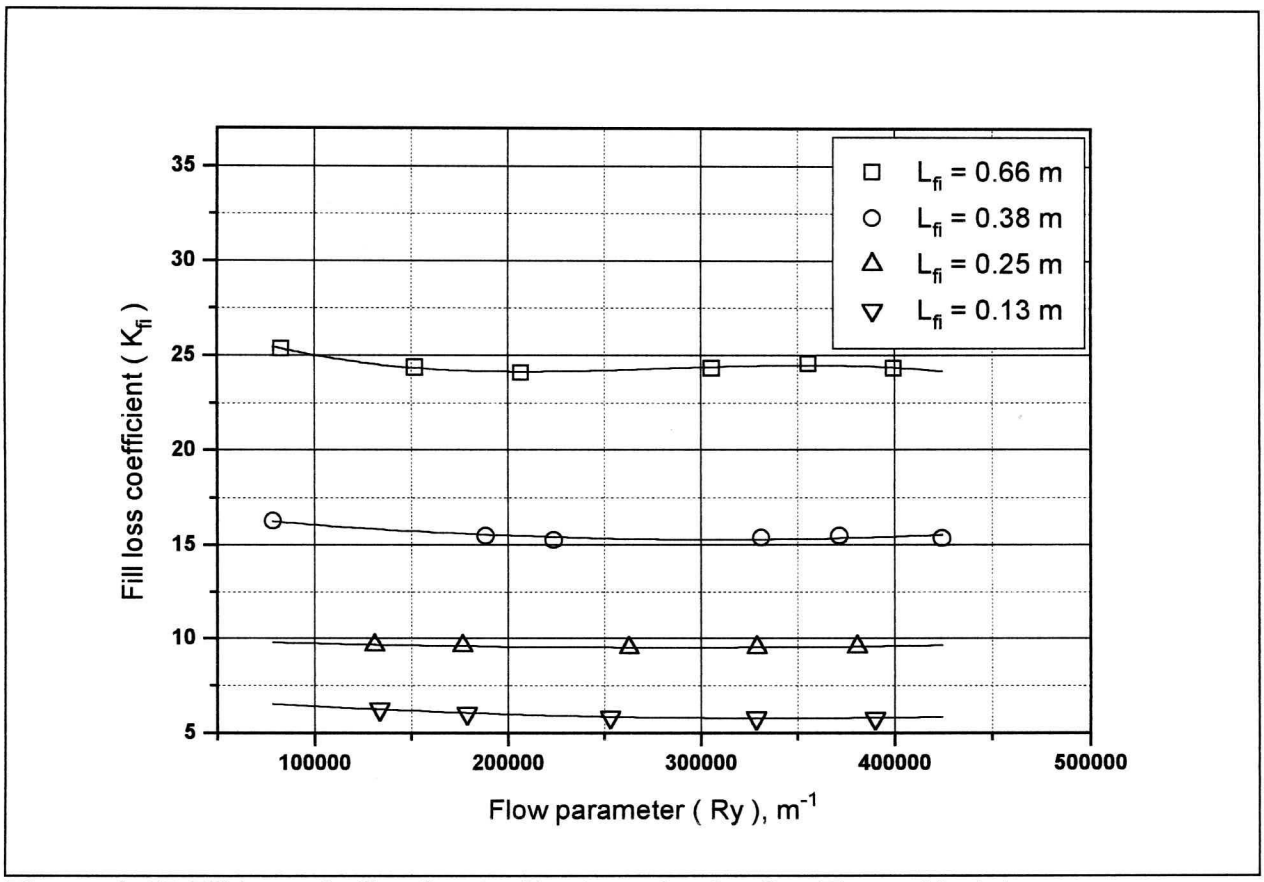

Figure 3.15 *Fill Loss Calibration for Rectangular Cooling Tower Model.*

3.4.3 Experimental Results

The experimental inlet loss coefficient data for rectangular towers is also highly non-linear. Fortunately, the loss coefficient converges to a relatively constant value for the low values of the inlet width to height ratio (commonly encountered in rectangular tower assemblies (fig. 3.18)), greatly simplifying the curve fitting procedure. For the rectangular tower analysis the data associated with $W_i / H_i = 10$, was not incorporated in the fitted correlation. The inlet loss coefficient for rectangular towers is considerably higher than its circular counterpart for

comparable inlet width to height ratios. This effect is caused by the larger inlet cross-sectional area to inlet vertical area encountered in rectangular towers. Consequently, rectangular towers are built with inlet width to height ratios smaller than circular towers to avoid these high inlet losses. Values of W_i / H_i well below 5 are the rule, justifying the aforementioned exclusion.

The correlation for the inlet loss coefficient for rectangular counterflow cooling towers fitted with isotropic flow resistance fills is given by,

$$K_{ct} = 0.2339 + \left(3.919\times10^{-3}K_{fi}^{2} - 6.840\times10^{-2}K_{fi} + 2.5267\right)\times e^{\frac{W_i}{H_i}\left(0.5143-0.1803e^{\left(0.0163K_{fi}\right)}\right)} - \sinh^{-1}\left(2.7704e^{\left(0.9581\frac{W_i}{H_i}\right)}\times e^{\left(K_{fi}\left(2.457-1.015\frac{W_i}{H_i}\right)\times10^{-2}\right)}\times\left(\frac{r_{ir}}{W_i}-0.013028\right)\right) \quad (3.13)$$

Equation (3.13) is valid for $5\le K_{fi}\le 25$, $0\le r_{ir}/W_i\le 0.025$ and $1\le W_i/H_i\le 7.5$, but will give fairly accurate results for inlet ratios below one. The average error of equation (3.13) is about 2.4 percent of the experimental data.

The same inflection point encountered in the r_{ir} dependant data of the circular tower experiment can be seen in figure 3.16. The magnitude of the sudden change in inlet loss coefficient across the inflection, decreases with the inlet width to height ratio. This trend is encountered throughout the data, as the inlet loss coefficient approaches a constant value for very low values of the inlet ratio (Fig. 3.18). It is interesting to note, that the same inflection phenomenon is apparent in the rectangular tower data of Terblanche (fig. 3.1) [94TE2], giving credence to this observation. The inflection is caused by the cessation of sudden contraction losses as the inlet rounding becomes more pronounced [88WH1]. The parabolic shape of the fill loss coefficient dependant data is still present in the rectangular tower inlet loss (Fig. 3.17), but the shape of the parabola is less pronounced and changes with the inlet ratio. The effect is not shown in any of the figures, but the parabolic curve seems to rotate clockwise with increased inlet width to height ratio, until it resembles the negative exponential trend found in orthotropic resistance towers. No explanation for this phenomenon is known.

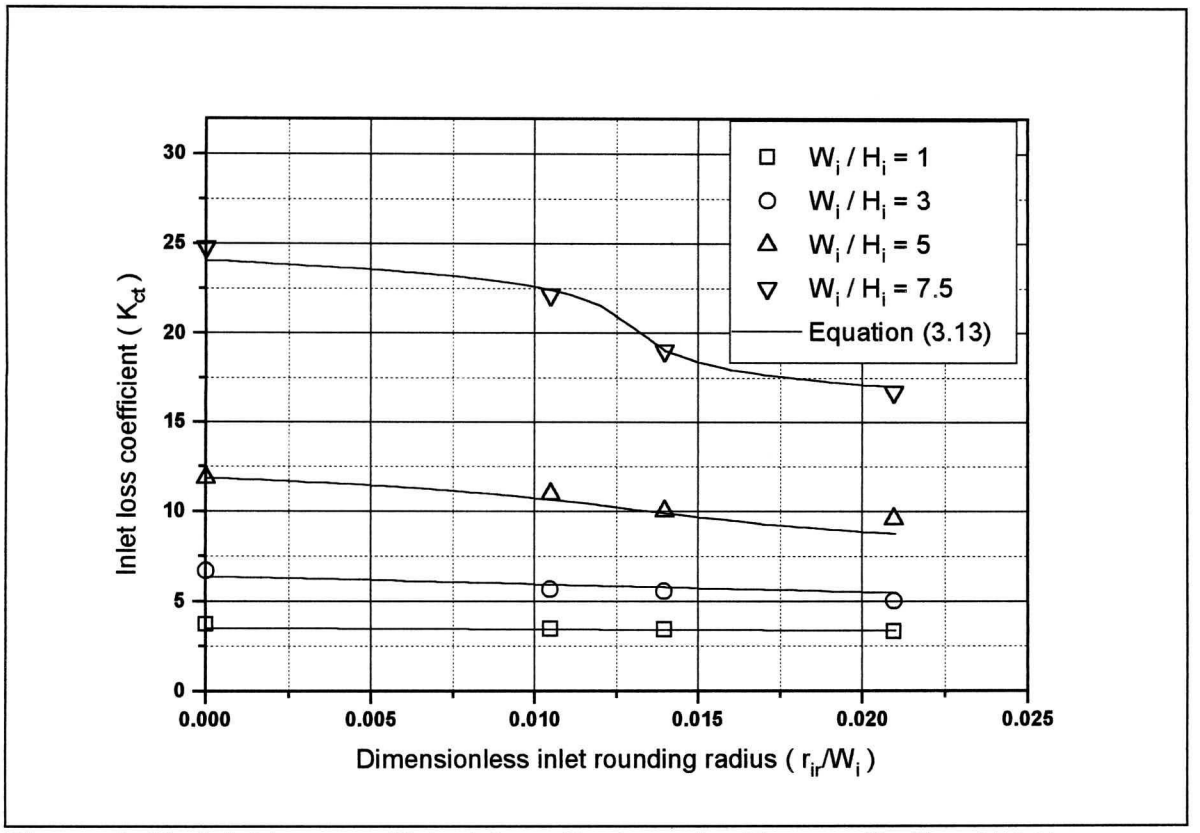

Figure 3.16: *Inlet loss coefficient for a Rectangular Tower with* $K_{fi} = 15.261$.

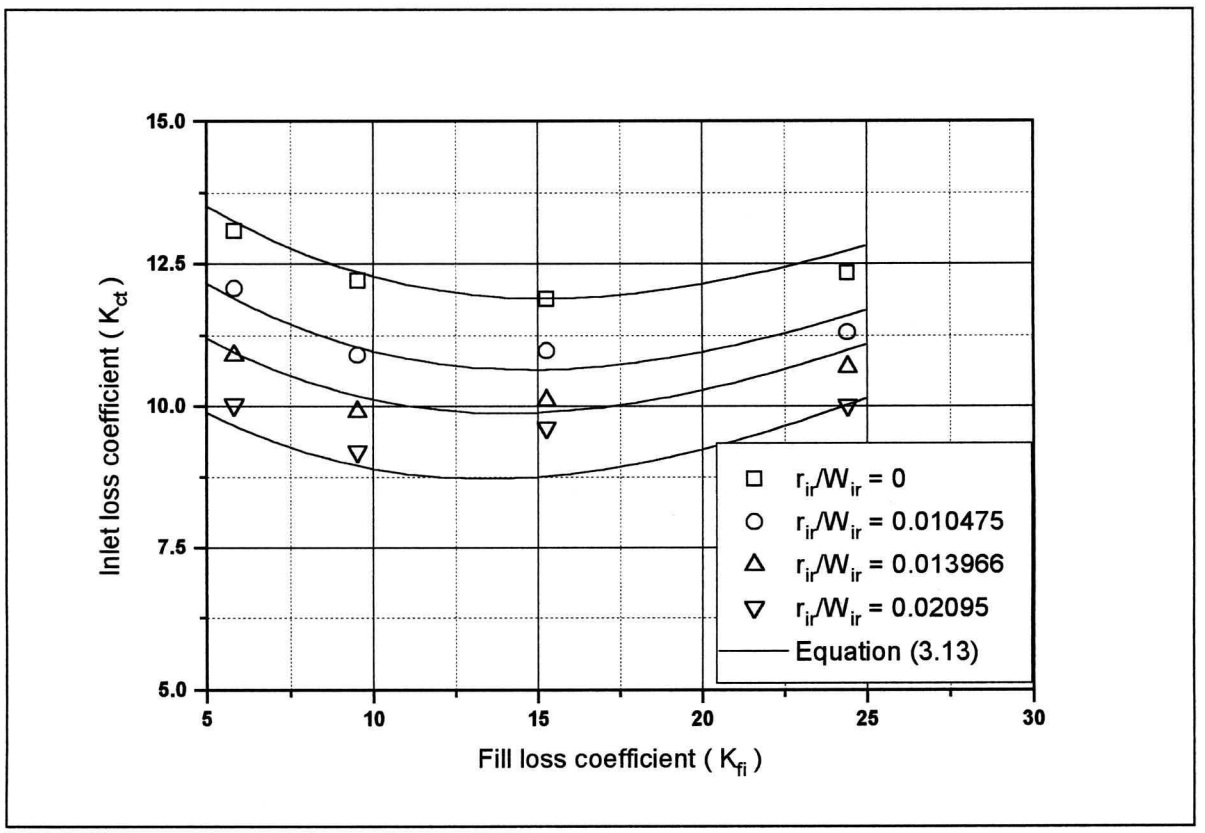

Figure 3.17: *Inlet Loss Coefficient for a Rectangular Tower with* $W_i / H_i = 5$.

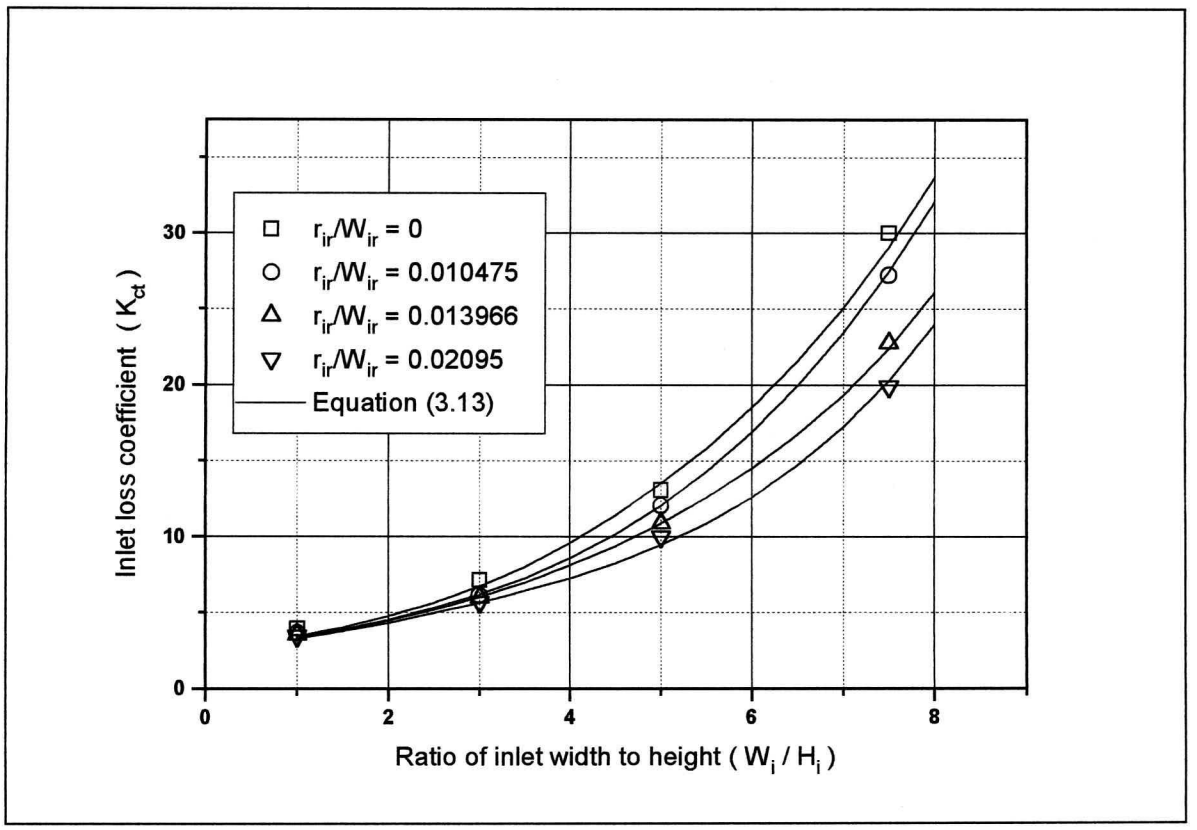

Figure 3.18: *Inlet Loss Coefficient for a Rectangular Tower with* $K_{fi} = 5.81$.

Equation (3.13) is a good approximation of the divergent data generated by the rectangular tower experiments and can be included in Chapter 1's modelling strategy.

CHAPTER

FOUR

NUMERICAL SIMULATION OF THE INLET LOSSES IN COUNTERFLOW WET-COOLING TOWERS

This chapter will explore the dependence of the tower inlet losses on the rain zone flow resistance and in doing so will derive a correction factor to account for this interaction. The primary investigation will make use of the CFD package STAR-CD v.3.0 [96CO1] to find the losses in the inlet section of various dry and wet counterflow towers. The results of the wet-cooling tower simulation will be modified using the equations for the rain zone loss coefficient derived in Chapter 2. These modified results, divided by the numerical dry tower data, generate a correction term. Applying this term to dry-cooling tower inlet losses (Chapter 3), yields the true inlet loss for an equivalent counterflow wet-cooling tower. This procedure must be repeated for rectangular and circular cooling towers with either isotropic or orthotropic resistance packing.

4.1 Mathematical Model

The mathematical modelling practices employed in the STAR-CD thermofluids analysis system and the numerical techniques used to solve them, are discussed briefly in this section. Although the code has the capability to comprehensively simulate a complete cooling tower, this is not the aim of this thesis. For wet-cooling tower simulation a gas-droplet model is employed that consists of two distinct sets of equations; one set governing the gas phase and another governing the droplet phase. To save computing time, each of these equation sets has to be extensively simplified, so that only components crucial to inlet loss prediction are active. For the gas phase the following assumptions were made:

- The mean flow field is steady and therefore, time independent, which implies that all time derivatives are equal to zero.

- The air flow is isothermal. No heat is transferred to or from the air. Since only the change in momentum of the air is of interest in this analysis, this becomes a valid assumption. The change in temperature dependent properties is ignored.
- The flow is incompressible. Changes in pressure within an operational tower inlet section are relatively small (typically in the order of 10^2 Pa), as are changes in temperature (about 15 to 20 K). Correspondingly, the variation in gas density between the inlet and fill outlet is 'small'. The influence of this change in density on the mechanisms that cause pressure drops in the inlet section is 'small' as well, substantiating this assumption.
- The flow is Newtonian and turbulent. For a typical natural draft cooling tower, Reynolds numbers in the inlet section are of the order $+10^7$, which is in the turbulent flow regime.
- The flow field in the tower inlet section is essentially two-dimensional. This implies axi-symmetrical flow for a circular tower and planar flow for rectangular towers.

The dispersed (droplet) phase governing equation must be identical to the equations employed to find the rain zone loss in Chapter 2 to ensure similarity between the two models. The assumptions applicable to the CFD analysis will therefore be the same as those made in Chapter 2 with one exception. The falling droplets do affect the velocity distribution of the air and not just the mechanical energy expended by the air stream. A numerical study by Zhenguo et al. [92ZH1] asserts that the increase in rain zone resistance encountered using this method is only about 3 percent. This change is small enough not to invalidate the equations for the rain zone loss coefficient and will be ignored henceforth. The assumptions now applicable to the governing equations of the CFD droplet model are,

- No droplet agglomeration, collision, coalescence or break-up occurs, i.e. droplet diameters stay constant throughout the rain zone.
- There is no heat or mass transfer to or from the droplets. All droplet temperature dependent properties therefore remain constant. This assumption is substantiated by the negligible effect of droplet thermal characteristics on momentum transfer.
- Turbulence does not affect the droplet momentum transfer characteristics, nor do the droplets influence the continuous phase turbulence conservation equations. This assumption is made because of the considerable uncertainty as to how to account for the effects of the droplet phase on the gas phase turbulence. For this analysis, therefore, these effects are ignored.

- The only forces acting on the droplet are aerodynamic drag and gravitational force. The only other forces that might be considered are the buoyancy force and added mass force. Since the pressure gradient in the rain zone is 'small' and the density of air is three orders of magnitude smaller than that of water, these forces can be safely ignored.

The linking of the simplified gas phase and droplet phase equations accounts for the following model of gas-droplet interaction. The viscous nature of the gas causes droplets moving relative to the gas to experience aerodynamic drag. The law of conservation of momentum dictates that this aerodynamic drag, acting to change the momentum of the droplets, also changes the momentum of the air in a signwise opposite manner. This interaction results in a perturbation of the local gas velocity by the motion and displacement of the droplets and *vice versa*, which is accounted for by appropriate inter-phase momentum source terms in the gas phase momentum equations.

4.1.1 The Gas Phase Model

The gas phase, occupying most of the calculation domain, is considered a continuum. With the assumptions of the previous section the Navier Stokes equations are, in Cartesian tensor notation for a stationary reference frame:

$$\frac{\partial}{\partial x_j} u_j = 0 \tag{4.1}$$

$$\frac{\partial}{\partial x_j}\left(\rho u_j u_i - \tau_{ij}\right) = -\frac{\partial p}{\partial x_i} + s_i \tag{4.2}$$

where x_i — Cartesian co-ordinate (i = 1, 2)

u_i — absolute fluid velocity in the direction x_i

p — piezometric pressure = $p_s - \rho_0 g_m x_m$ where p_s is static pressure, ρ_0 is reference density, the g_m are gravitational field components and the x_m co-ordinates from a datum where ρ_0 is defined

ρ — density

τ_{ij} — stress tensor components

s_i — momentum source components

and repeated subscripts denote summation.

For the simplified tower simulation the momentum source components, s_i, will include the resistance and entrance effects of the fill and any interaction of the air with the dispersed (droplet) phase. Since the gas phase density is considered constant, buoyancy forces can be ignored.

For turbulent flows, u_i, p, τ_{ij} and other dependent variables assume their time average values. The constitutive relation connecting τ_{ij} to the velocity gradients is, for Newtonian fluids,

$$\tau_{ij} = 2\mu\, s_{ij} - \frac{2}{3}\mu\frac{\partial u_k}{\partial x_k}\delta_{ij} - \rho\overline{u_i' u_j'} \tag{4.3}$$

where μ is the molecular dynamic viscosity and δ_{ij}, the 'Kronecker delta', is unity for $i = j$ and zero otherwise. The u' terms are turbulent fluctuations of the air velocity around the time averaged velocity and the over bar denotes the time averaging process. s_{ij}, the rate of strain tensor, is given by,

$$s_{ij} = \frac{1}{2}\left(\frac{\partial u_i}{\partial x_j} + \frac{\partial u_j}{\partial x_i}\right) \tag{4.4}$$

The $-\rho\overline{u_i' u_j'}$ term in equation (4.3) represents the additional Reynolds stresses due to turbulent fluctuations and is linked to the time averaged velocity field via a turbulence model.

For the purposes of this simulation the standard $k-\varepsilon$ turbulence model, comprising of differential transport equations for the turbulent kinetic energy, k and its dissipation rate, ε, is employed. The model combines turbulent Reynolds number forms of the k and ε equations for the free stream with algebraic 'law of the wall' representations of the flow within boundary layers. It is assumed that the turbulent Reynolds stresses and scalar fluxes are linked to the time averaged flow properties in a fashion similar to the laminar stresses [eq. (4.3)], i.e.

$$-\rho\overline{u_i' u_j'} = 2\mu_t s_{ij} - \frac{2}{3}\left(\mu_t \frac{\partial u_k}{\partial x_k} + \rho k\right)\delta_{ij} \tag{4.5}$$

where

$$k \equiv \frac{\overline{u_i' u'}_i}{2} \tag{4.6}$$

defines the turbulent kinetic energy and μ_t the turbulent viscosity. The turbulent viscosity is linked to k and ε by,

$$\mu_t = \frac{C_\mu \rho k^2}{\varepsilon} \tag{4.7}$$

where $C_\mu = 0.09$ is an empirical coefficient, usually taken as a constant equal to the specified value. Subject to the original assumptions (steady, incompressible, two-dimensional flow), the simplified transport equation for turbulent energy becomes,

$$\frac{\partial}{\partial x_j}\left(\rho u_j k - \frac{\mu_{eff}}{\sigma_k}\frac{\partial k}{\partial x_j}\right) = 2\mu_t s_{ij}\frac{\partial u_i}{\partial x_j} - \rho\varepsilon \tag{4.8}$$

where $\mu_{eff} = \mu + \mu_t$ and σ_k is an empirical coefficient equal to unity for the $k-\varepsilon$ model. The first term on the right hand side of the equation represents turbulent generation by shear and normal stresses and the second viscous dissipation of turbulent energy. For closure another relation, in this case the rate of change of dissipation, is required. For the same assumptions as above,

$$\frac{\partial}{\partial x_j}\left(\rho u_j \varepsilon - \frac{\mu_{eff}}{\sigma_\varepsilon}\frac{\partial \varepsilon}{\partial x_j}\right) = 2C_{\varepsilon 1}\frac{\varepsilon}{k}\mu_t s_{ij}\frac{\partial u_i}{\partial x_j} - C_{\varepsilon 2}\rho\frac{\varepsilon^2}{k} \tag{4.9}$$

where $\sigma_\varepsilon = 1.22, C_{\varepsilon 1} = 1.44$ and $C_{\varepsilon 2} = 1.92$ are empirical coefficients taken from references [74LA1, 79RO1, 83EL1]. The right-hand side terms represent effects analogous to those found in the turbulent energy transport equation [eq. (4.8)].

The high Reynolds number $k-\varepsilon$ model is not valid in boundary layers that form adjacent to no-slip walls, where molecular and turbulence effects are of comparable magnitude. Therefore, special algebraic formulae, called 'wall functions', are required to represent the velocity and turbulence distribution within these regions. The wall functions currently employed are inexact, being based on the following assumptions,

- The flow is predominantly one-dimensional, with velocity variation being perpendicular to the wall.
- The effects of pressure gradients are negligible ensuring a uniform shear stress in the layer.
- Turbulence production and dissipation are balanced.
- The turbulence length scale varies linearly.

If these assumptions are valid for a given domain a relatively accurate solution can be obtained for the boundary layer from the following formulae for cross stream profiles,

$$u^+ = \begin{cases} y^+ & ,y^+ \le y_m^+ \\ \frac{1}{\kappa}\ln\left(Ey^+\right) & ,y^+ > y_m^+ \end{cases} \tag{4.10}$$

where u^+ — u/u_τ

u — tangential fluid velocity

u_τ — $\left(\tau_w/\rho\right)^{\frac{1}{2}}$

τ_w — wall shear stress

y^+ — $\rho C_\mu^{\frac{1}{4}} k^{\frac{1}{2}} y/\mu$

κ, E — empirical constants, where

$\kappa = 0.42$

$E = 9.0$ (for hydrodynamically smooth walls)

and y_m^+ must satisfy the equation,

$$y_m^+ - \frac{1}{\kappa}\ln\left(Ey_m^+\right) = 0 \tag{4.11}$$

The turbulence parameters in boundary layers are found from,

$$k = C_\mu^{\frac{1}{2}} \frac{\tau_w}{\rho} \tag{4.12}$$

and

$$\varepsilon = C_\mu^{\frac{3}{4}} \frac{k^{3/2}}{\kappa y} \tag{4.13}$$

The equilibrium distribution of k [eq. (4.12)] is only invoked if the normal k transport equation (with modified production and dissipation terms to account for the steep near-wall variations in u and ε) predicts equilibrium flow at the edge of the boundary layer.

It must be emphasised that existing turbulence models, including the k-ε model, are inexact representations of the physical phenomena involved. The degree of inexactness of a given model depends largely on the nature of the flow to which it is being applied and the circumstances that give rise to 'good' or 'bad' results are based mainly on experience. Recirculating flow, a flow pattern that is central to this investigation, is one of the conditions that defies accurate numerical solution and therefore, dictates that the CFD solution be complemented by experimental work. Otherwise, equations (4.1-13) adequately describe the continuum phase of the simulation subject to assumptions made at the beginning of the chapter and have to be solved using an iterative numerical technique.

4.1.2 Dispersed (droplet) Phase Model

The droplet phase is modelled using a Lagrangian/Eulerian approach in which the conservation of momentum equation is written in a co-ordinate system that moves with each individually modelled element. The gas phase equations are still expressed in their Eulerian continuum form, but are suitably modified to take account of the presence of the dispersed phase.

The large number of droplets present in the rain zone preclude individual modelling, therefore, only a sample of the total droplet population is analysed. Each of the samples is followed from injection until hitting the ground and an appropriate portion of the total quantity of water injected per unit time is then assigned to each of the trajectories. By determining the drag force along each trajectory, the droplet-gas momentum exchange can be calculated.

The Lagrangian conservation equation is written in instantaneous vector form with the subscript d denoting droplet properties and unsubscripted quantities referring to the continuous phase. The momentum equation for a droplet of mass M_d is

$$M_d \frac{d\bar{\mathbf{u}}_d}{dt} = \bar{\mathbf{F}}_D + \bar{\mathbf{F}}_G \tag{4.14}$$

here $\bar{\mathbf{F}}_D$ is the drag force (fig. 4.1), given by

$$\bar{\mathbf{F}}_D = \tfrac{1}{2} C_D \rho A_d \left|\bar{\mathbf{u}} - \bar{\mathbf{u}}_d\right| \left(\bar{\mathbf{u}} - \bar{\mathbf{u}}_d\right) \tag{4.15}$$

where C_D, the drag coefficient and A_d the droplet cross-sectional area for deformed droplets can be found from equations (2.23-30) in section 2.3 (the deformation properties were added to the analysis in the form of a user subroutine and are not inherent to STAR-CD). The gravitational force, $\bar{\mathbf{F}}_G$, is simply

$$\bar{\mathbf{F}}_G = M_d \bar{\mathbf{g}} \tag{4.16}$$

where $\bar{\mathbf{g}}$ is the gravitational acceleration vector.

Knowledge of the droplet velocity allows its instantaneous position vector, $\bar{\mathbf{x}}_d$, to be calculated by integrating:

$$\frac{d\bar{\mathbf{x}}_d}{dt} = \bar{\mathbf{u}}_d \tag{4.17}$$

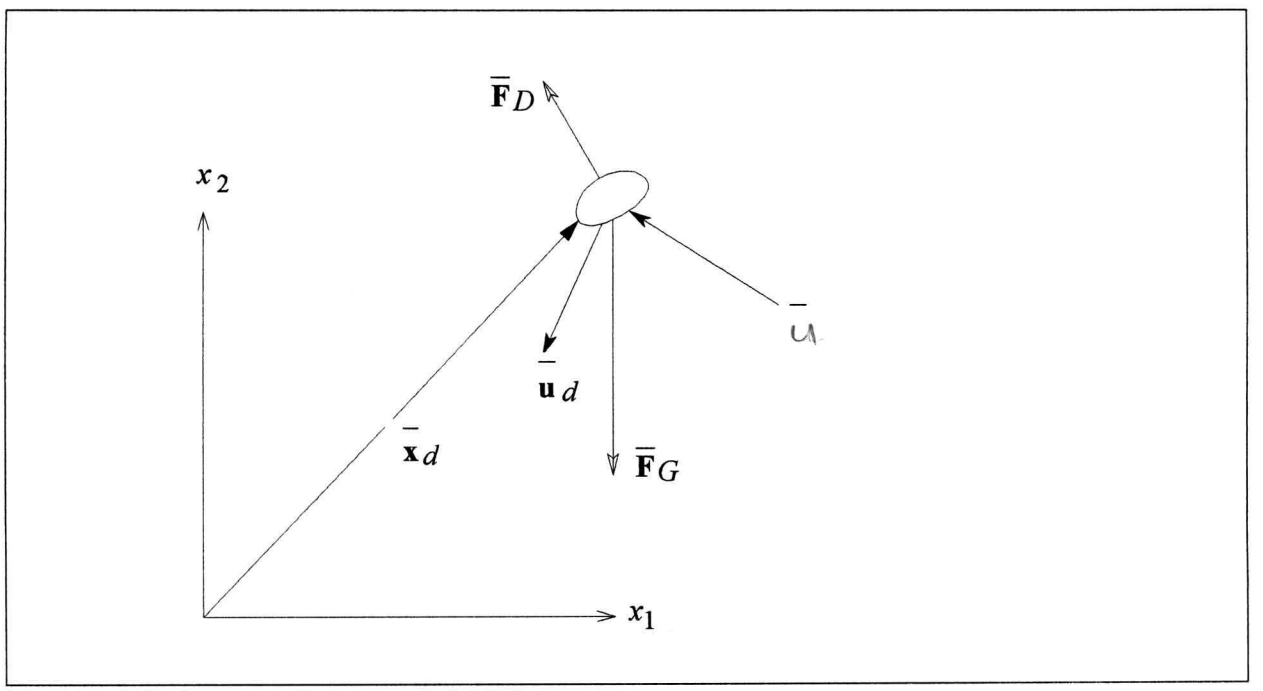

Figure 4.1: *Lagrangian Droplet Motion.*

Displacement of the carrier fluid (air) by the dispersed phase (droplets) is taken into account by a fractional volume, α, occupied by the continuous phase. The effect on the gas equations is to replace the density ρ and the effective viscosity μ_{eff} in the transport terms on the left-hand sides with the products $\alpha\rho$ and $\alpha\mu_{eff}$, respectively. Additionally, all right-hand terms, representing sources and other effects, must be multiplied by α.

The Lagrangian equations, when integrated over an arbitrary volume, yield the changes in momentum of each discrete element (droplet) between its entry and exit. The sum of these changes for all element crossing the volume provides, with a change in sign, the net momentum extracted from the carrier fluid, which is the source term for the continuous phase momentum equation.

4.1.3 Discretisation Practices

The differential equations governing the conservation of mass, momentum, turbulence etc. within the fluid (section 4.1.1), are discretised by means of the finite volume (FV) method [80PA1]. Accordingly, they are integrated across the individual computational cells and then approximated in terms of the cell-centred nodal values of the dependent variables, ensuring that the discretised forms retain the conservation properties of the parent equations. For the purposes of discretisation, STAR-CD presents the steady state conservation equations in the following general co-ordinate free form,

$$\overline{\nabla}\cdot\left(\rho\overline{\mathbf{u}}\phi-\Gamma_\phi\overline{\nabla}\phi\right)=s_\phi \tag{4.18}$$

where $\overline{\mathbf{u}}$ is the local fluid velocity vector, ϕ represents any of the dependent variables i.e. u_i, k and ε, and Γ_ϕ and s_ϕ are the associated diffusion and source coefficients, deduced from the parent conservation equations. An exact form of equation (4.18), valid for an arbitrary volume, V, bounded by a closed surface, S, can be written as [81WA1],

$$\int_S\left(\rho\overline{\mathbf{u}}\phi-\Gamma_\phi\overline{\nabla}\phi\right)\cdot d\overline{\mathbf{S}}=\int_V s_\phi dV \tag{4.19}$$

where $\overline{\mathbf{S}}$ is the surface vector. If V and S are taken to be the volume V_p and discrete faces S_j (j = 1, N [number of faces]) of a computational cell respectively (fig. 4.2), equation (4.19) becomes,

$$\underbrace{\sum_j\int_{S_j}\left(\rho\overline{\mathbf{u}}\phi-\Gamma_\phi\overline{\nabla}\phi\right)\cdot d\overline{\mathbf{S}}}_{T_1}=\underbrace{\int_{V_p}s_\phi\,dV}_{T_2} \tag{4.20}$$

From here onwards, approximations are introduced. The first term, T_1, of the above is split into separate contributions C_j and D_j due to convection and diffusion, respectively. Each

contribution is expressed in terms of average values over the cell faces, denoted by $(\ )_j$, thus T_1 becomes

$$T_1 \approx \sum_j \left(\rho \bar{\mathbf{u}} \phi \cdot \bar{\mathbf{S}}\right)_j - \sum_j \left(\Gamma_\phi \bar{\nabla} \phi \cdot \bar{\mathbf{S}}\right)_j \equiv \sum_j C_j - \sum_j D_j \tag{4.21}$$

The diffusion terms are approximated by a cell face-centred expression,

$$D_j \approx \Gamma_{\phi,j} \left[f_j^l (\phi_N - \phi_P) + \left(\bar{\nabla} \phi \cdot \bar{\mathbf{S}} - f_j^l \bar{\nabla} \phi \cdot \bar{\mathbf{x}}_{PN} \right)_j \right] \tag{4.22}$$

The first term in the brackets represents the normal diffusion between P and the neighbouring cell-centred node, N (fig. 4.2), while the second term is the cross-diffusion. The f_j^l terms represent geometric factors brought about by non-orthogonal cells, $\bar{\mathbf{x}}_{PN}$ the displacement vector between P and N, and $\Gamma_{\phi,j}$ is the interpolated cell face diffusivity.

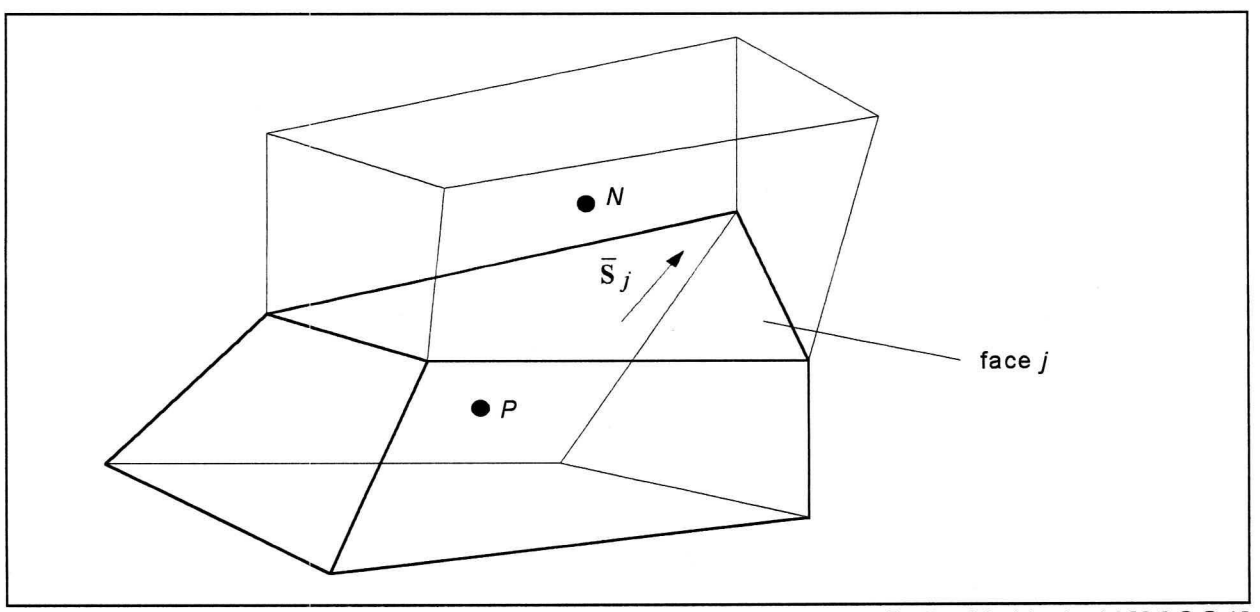

Figure 4.2: *Typical Cell with Centred Node P and Neighbour Cell with Node N* [96CO1].

For the convective terms C_j, STAR-CD provides the user with a range of discretisation options. A sensitivity study, that compared the inlet losses achieved using a higher order central differencing scheme with those produced using a upwind defferencing (UD) scheme, showed that

the lower order UD scheme provides adequate accuracy for the current scenario, coupled with rapid convergence. Implementation of the UD scheme, which selects the nearest upwind neighbour value for ϕ_j (figure 4.3), produces the following discretised relation,

$$C_j^{UD} \equiv F_j \begin{cases} \phi_P & , \quad F_j \geq 0 \\ \phi_{N+} & , \quad F_j < 0 \end{cases} \tag{4.23}$$

where

$$F_j \equiv \left(\rho \bar{\mathbf{u}} \cdot \bar{\mathbf{S}}\right)_j \tag{4.22}$$

is the mass flux through face j and ϕ_j, the average value at the face, is derived from the nodal values in accordance with equation (4.23). The cell face value of the dependent properties, Γ is obtained in a similar fashion.

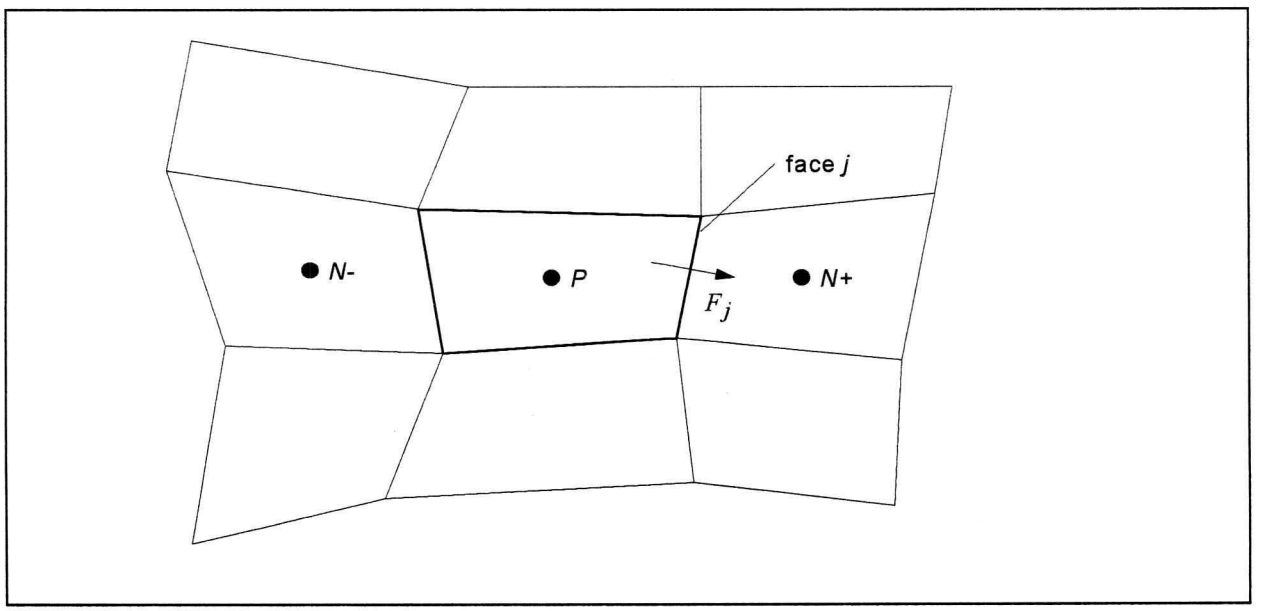

Figure 4.3: *Node Labelling Convention for Flux Discretisation* [96CO1].

The second term of equation (4.20), T_2, contains components representing sources and sinks of the transported property, and/or additional flux terms, depending on the form of the dependent variable. Fluxes and other gradient-containing terms are approximated in a similar fashion to the

T_1 term, while non-gradient quantities are found from cell-centred nodal values. In general, the second term can be represented by the following quasi-linear form,

$$T_2 = s_1 - s_2\phi_P \tag{4.23}$$

The final form of the discretised finite volume equation is obtained by substituting the various approximated terms back into equation (4.20) and then implementing the discretised continuity equation,

$$\sum F_j = 0 \tag{4.24}$$

The result, in compact form, is

$$A_P\phi_P = \sum_m A_m\phi_m + s_1 \tag{4.25}$$

where A_m represents the effects of convection and diffusion, the summation includes all neighbouring nodes involved in the flux discretisation and

$$A_P \equiv \sum_m A_m + s_2 \tag{4.26}$$

An equation such as (4.25) exists for each continuum cell and if the continuity set is included, there are as many such equation sets as there are dependent variables. STAR-CD solves the flow field by iterative solution of these equation sets.

The Lagrangian conservation equations governing the velocity and position of the dispersed droplets in a continuous fluid phase are of ordinary first order differential form. The equations are integrated along the trajectories of the computational droplets (fig. 4.4), each comprising of a sample of the real droplet population.

A discretised first-order Euler-implicit form of the droplet momentum equation is used to determine the droplet trajectories as part of the solution,

$$M_d \frac{\left(\bar{\mathbf{u}}_d^n - \bar{\mathbf{u}}_d^o\right)}{\delta t_d} = \bar{\mathbf{F}}_D^n + \bar{\mathbf{F}}_G^n \tag{4.27}$$

where n and o denote the 'new' and 'old' values spanning the integration time step δt_d, which is some fraction (chosen for accurate resolution) of the total time it takes the droplet to traverse each cell. The local values of the fluid velocity required to resolve droplet drag, $\bar{\mathbf{F}}_D^n$, and deformation properties, are interpolated from nodal values.

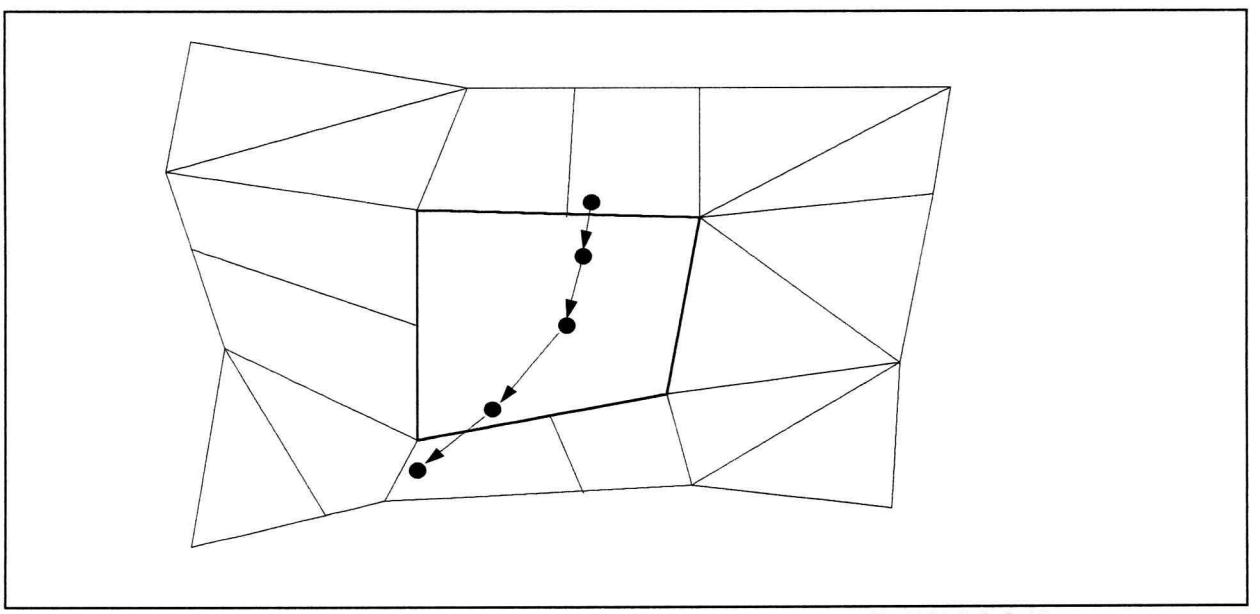

Figure 4.4: *Lagrangian Droplet Traversing a Computational Cell* [96CO1].

Equation (4.27) incorporates the average rate of momentum transfer of a single computational droplet due to drag over a time increment δt_d. Therefore, the total change in momentum (denoted $\overline{\Delta \mathbf{F}}_d$) of a group of droplets traversing a given cell with a residence time of $t = n_{dts}\delta t_d$ (where n_{dts} is the number of droplet time steps) can be found from,

$$\overline{\Delta \mathbf{F}}_d = \frac{1}{n_{dts}} \sum_{\substack{\# \\ drops}} \sum_{n_d} \left(M_d \frac{\left(\bar{\mathbf{u}}_d^n - \bar{\mathbf{u}}_d^o \right)}{\delta t_d} - \bar{\mathbf{F}}_G^n \right) \tag{4.28}$$

This quantity, with an opposite sign, represents the average rate of momentum loss of the fluid for a given cell and is inserted as a sink in the gas phase momentum equation.

4.1.4 Solution Algorithms

To solve the algebraic finite-volume equations, resulting from the discretisation of the continuum phase governing equations, a variant of the implicit SIMPLE method [72PA1] is employed. For the STAR-CD code, the method is adapted to handle the additional complexities of non-orthogonal, unstructured mesh formulations, but in all other respects resembles the widely published format. Consequently, only the most cursory of explanations will be attempted.

The SIMPLE algorithm employs a form of predictor-corrector strategy, enabled by the use of operator splitting, to temporarily decouple the flow equations so that they can be solved sequentially. In other words, the velocity vector set of unknowns is split into a sequence of scalar sets. The solution sequence involves a predictor stage, which produces a provisional velocity field derived from the momentum equations and a provisional pressure distribution. The provisional fields are then refined in the corrector stage by demanding simultaneous satisfaction of the momentum and continuity balances. Continuity is ensured with the aid of an equation set for pressure, derived by combining the finite-volume momentum and mass conservation equations. The above sequence is repeated, with embedded updating of the field-dependent coefficients, until a solution is reached and since each step in the sequence is only an approximation under-relaxation must be employed to stabilise the process.

Convergence of the of the algorithm is checked by means of a normalised absolute residual sum, R_ϕ^k, defined by

$$R_{\phi}^{k} \equiv \frac{\sum \left| r_{\phi}^{k} \right|}{M_{\phi}} \tag{4.29}$$

where r_{ϕ}^{k} is the residual at a particular grid location and iteration k, found from the imbalance in the FV transport equation (4.25) caused by incomplete solution, i.e.

$$r_{\phi}^{k} = A_P \phi_P^{k} - \sum_m A_m \phi_m^{k} - s_1 \tag{4.30}$$

The summation in equation (4.29) is over all cells in the mesh and the normalisation factor, M_{ϕ}, is computed by summing the relevant fluxes over all inflow and outflow boundaries. Calculations are terminated when R_{ϕ}^{k} values for all of the solution variables have fallen below some user specified value. For the current simulation the maximum allowed residual was consistently set equal to 10^{-3}. Satisfaction of this type of criterion and the near constancy of the field values constitute sufficient grounds for convergence.

To solve the droplet phase, the Lagrangian equations are solved for each iteration of the carrier fluid equations, with implicit coupling between the two sets as described in previous sections. The Lagrangian solution at each iteration tracks the computational droplet from its injection point until it hits the ground, where it is removed from the calculation domain. In order to allow for a change in droplet trajectories due to evolution of the gas flow field during the iteration process, the related momentum sources are accumulated and then divided by the iteration counter. This produces averages that gradually reach their steady-state values. The normal convergence criteria apply.

4.2 Numerical Setup and Procedure

A brief overview is given in this section, of the geometries, boundary conditions and other devices used to construct a numerical wet-cooling tower simulation, within the CFD code STAR-CD. Although STAR-CD incorporates an extensive user interface, such a direct approach is time consuming, especially if multiple geometries must be simulated. A program, TWRGEN, was therefore written, to enable the rapid production of variable dimension tower input codes, which were subsequently fed into the CFD package. The program (TWRGEN) allows the user to control all the parameters relevant to a tower simulation and then automatically generates all input files and subroutines necessary to the numerical solution. This enables rapid construction of the large number of tower variations necessary to generate the required correlations for the inlet/rain zone loss dependence. These variations include circular and rectangular towers, with isotropic or orthotropic fills and a range of rain zone characteristics.

4.2.1 Tower Geometry

The cell structure seen in figure 4.5, is an extension of the discretisation practices described in section 4.1. The wedge shaped section represents a ten degree arc of a circular cooling tower. The rationale behind this approach is the same as for the experimental test section described in Chapter 3. Also, modelling the tower as a two-dimensional axi-symmetrical problem significantly reduces computational time and geometrical complexity.

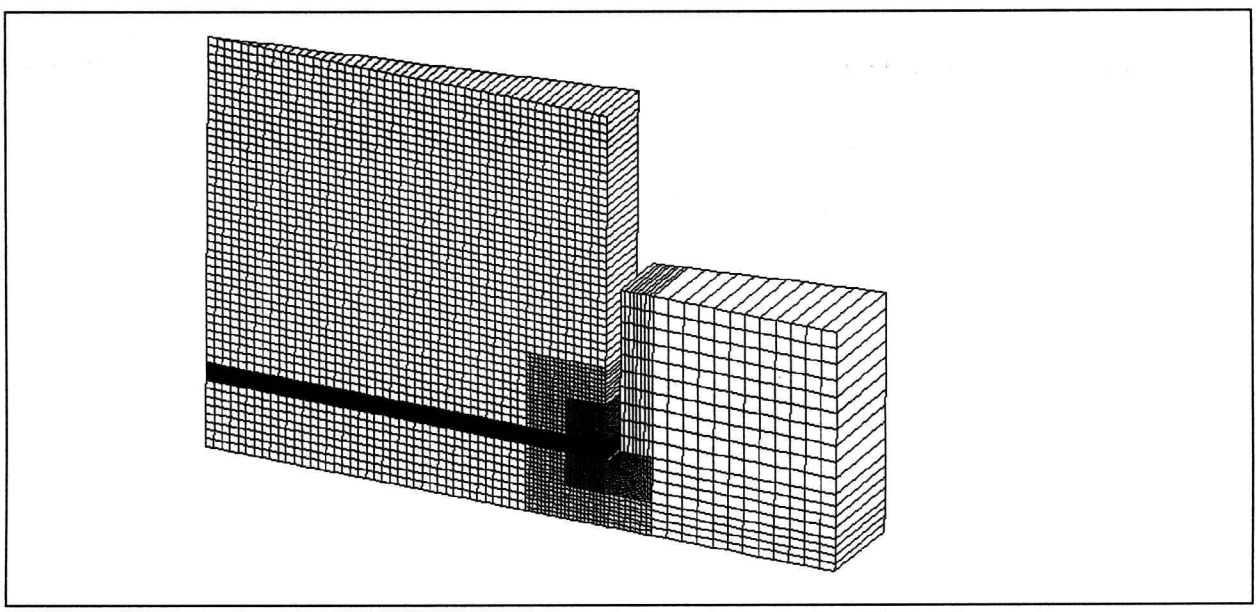

Figure 4.5: *Typical Circular Tower Computational Mesh for CFD Simulation.*

To improve the accuracy of the solution, the flow field was not specified at the tower entrance. Instead, the flow was allowed to develop naturally, by adding an additional volume to the outside of the tower (right-hand side rectangle in figure 4.6). The flow accelerates from ambient conditions, so that when it arrives at the tower inlet, the velocity distribution should be similar to that encountered in an operational tower.

As can be seen in figure 4.6, several refinements were made to the computational mesh, especially in the inlet and recirculation regions. Higher resolution grids are needed in these areas to resolve the high velocity and pressure gradients that are generated as the ambient air accelerates through the pinch created by the tower inlet and then rapidly decelerates as it enters the tower proper. The recirculating flow region is also of great importance, since the viscous action present therein is one of the main contributing factors to the tower inlet loss (even though it cannot be accurately simulated).

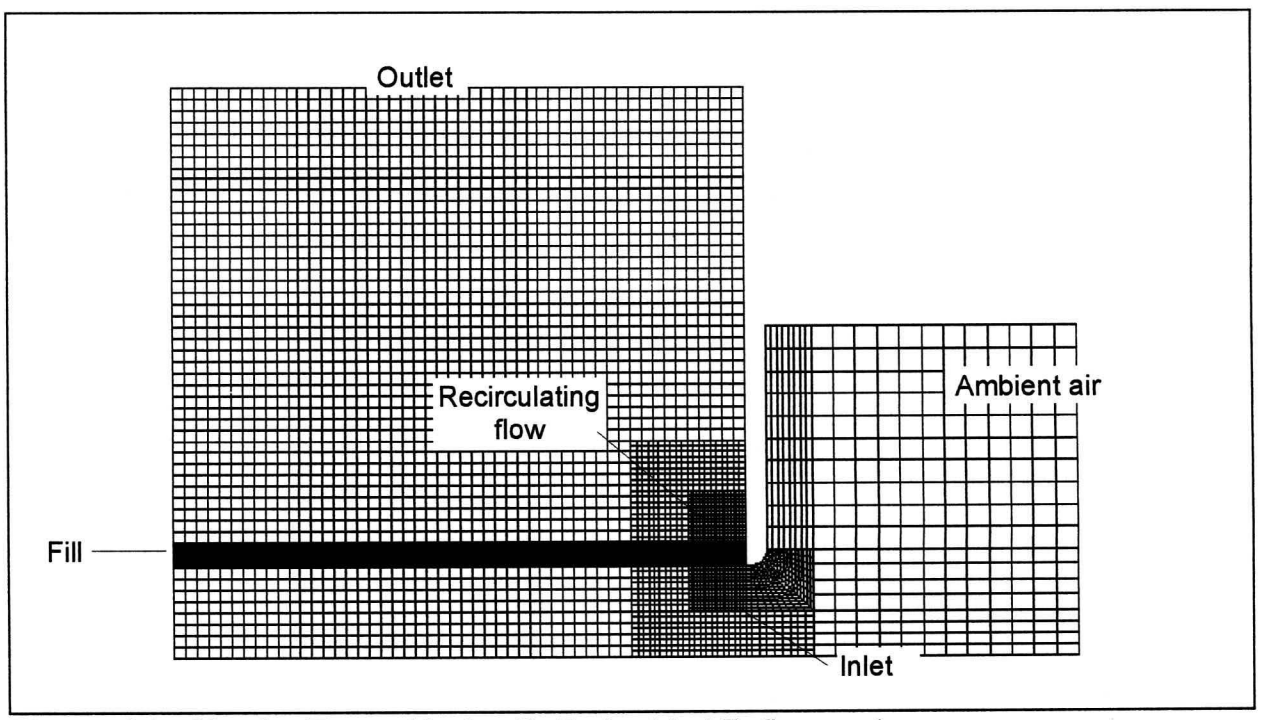

Figure 4.6: *Circular Tower Mesh with Embedded Refinement.*

Except for the near wall cells and the fill cells, the individual cell aspect ratios were kept near to unity to facilitate convergence. The flow within the former (which cannot be seen on any of the figures because of their small size) is essentially one-dimensional and is modelled as such (section 4.1). Also, the effect of boundary layers within large flows, such as cooling towers, is rather small

so that any inaccuracies become negligible. The aspect ratio of the fill cells is about 1:10, which is not excessive. The fine vertical resolution stems from the need to accurately depict the momentum sink embodied by the fill, inasmuch as the inlet loss is strongly dependent on the pressure drop across the fill assembly.

The general structure of the rectangular tower mesh can be seen in figure 4.7. Although the rectangular mesh is more or less planar in nature, the embedded refinements and general geometry are essentially the same as those employed in the circular tower.

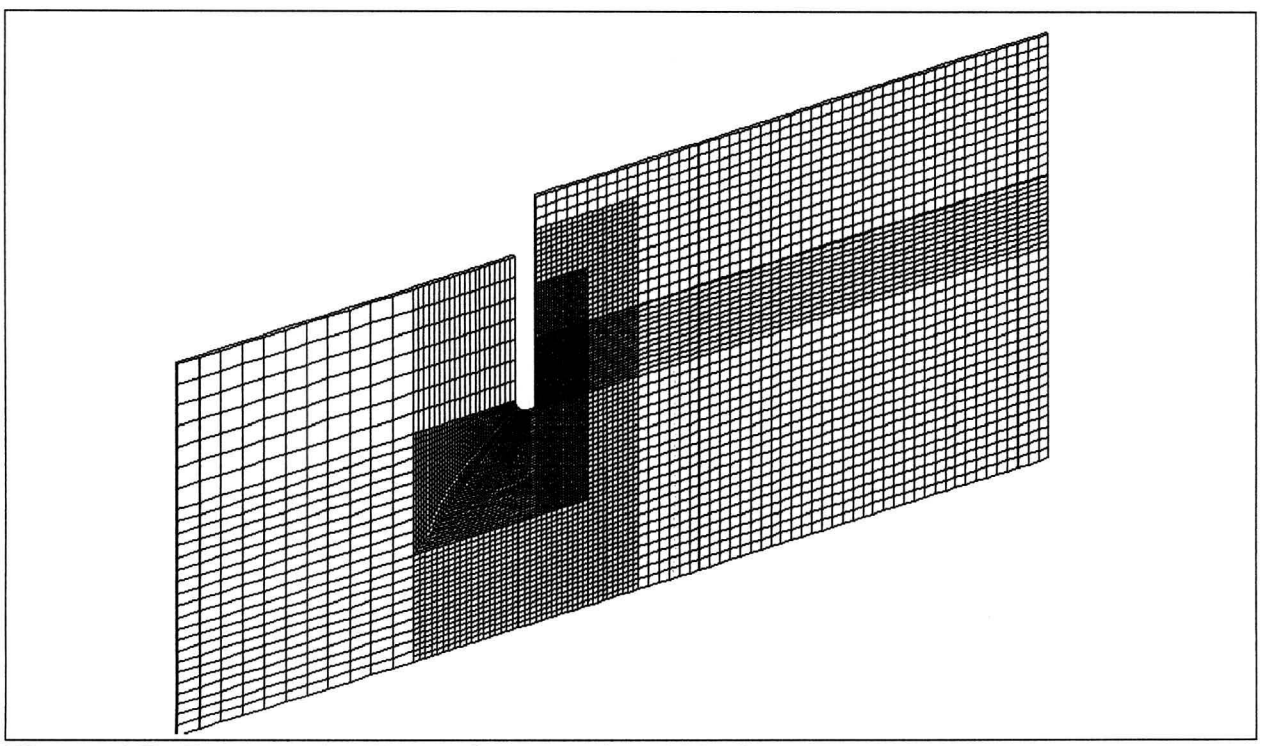

Figure 4.7: *Rectangular Tower Computational Mesh.*

4.2.2 Boundary Conditions

In order to solve a computational domain, a CFD solver needs initial and boundary conditions. For a steady-state problem, only the latter are necessary and for the geometries shown above, these conditions will consist of inlets, outlets, walls and symmetry surfaces. The various applications to the tower geometry can be seen in figure 4.8, although the large symmetry planes on either side of the computational domain are not shown (for obvious reasons).

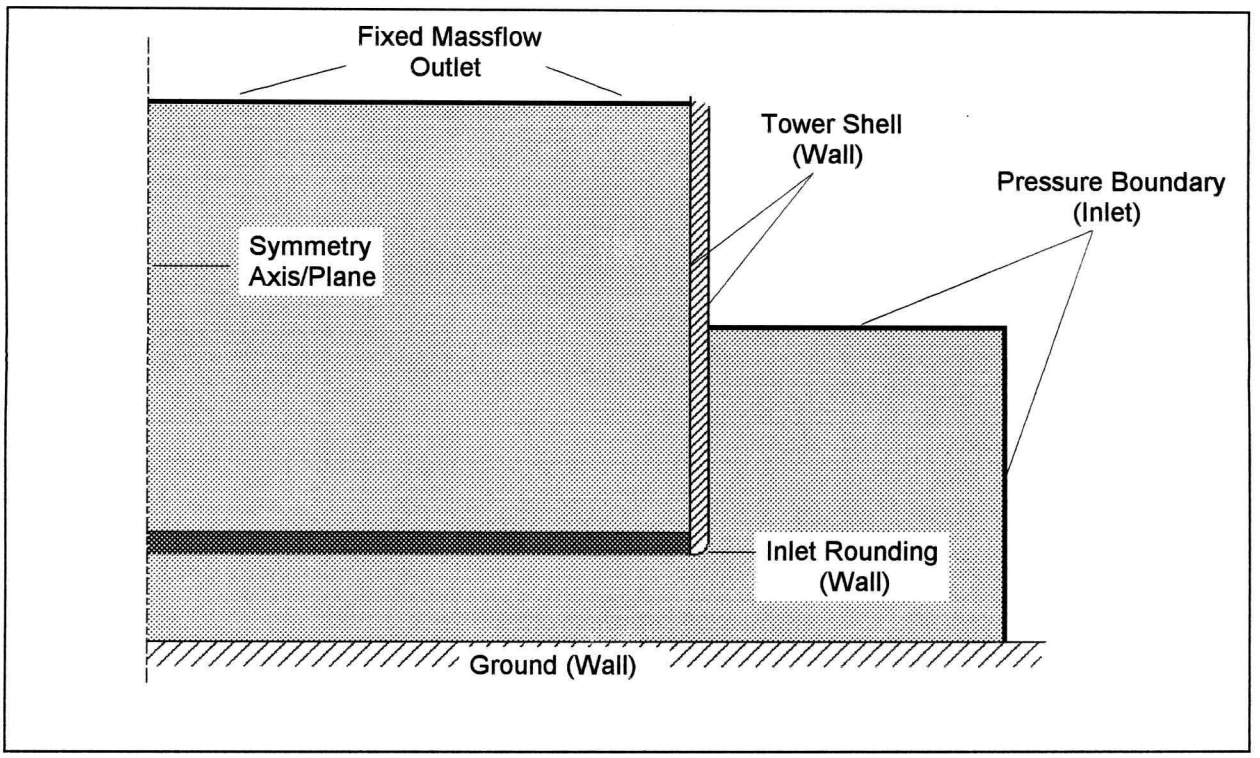

Figure 4.8: *Boundary Conditions for a Counterflow Cooling Tower.*

The implications of each of these boundary conditions and their specific influences on the flow are described by the following,

- Walls - impermeable surfaces, all fluxes perpendicular to a wall are equal to zero. For the 'no-slip' conditions enforced for the tower, all fluxes along the wall's surface (parallel) are also equal to zero. The wall boundaries were generally considered hydrodynamically smooth, partly because no alternative data was available and also because of the small influence of the boundary layer. Near wall cells were adjusted to comply with the turbulent wall function specification that $30 \leq y^+ \leq 100$, where $y^+ = \rho C_\mu^{1/4} k^{1/2} y / \mu$ and y is the perpendicular distance from the wall to the near wall, cell centred, node. Walls include the tower shell (inside and outside surface) the ground and any other solid surface.

- Symmetry Planes - all fluxes and gradients perpendicular to a symmetry plane at the plane are equal to zero. No other special conditions are enforced, so the planes act somewhat like a smooth mirror for the flow. In the tower model they (the symmetry planes) are encountered chiefly along the large surfaces that are used to 'cut' the tower section from its neighbouring volume. For the rectangular tower an additional symmetry plane must be added to the

centreline (see fig. 4.8) to avoid automatic enforcement of wall conditions. The symmetry axis in the circular tower does not have to be explicitly defined in STAR-CD, since it is deduced from the convergence of the outer symmetry planes.

- Pressure Boundaries - environmental piezometric pressure along the selected boundaries is constant i.e. $p = p_S + \frac{1}{2}\rho V^2 - \rho g z$, where p_S is the static pressure. In other words, the stagnation pressure along the pressure boundary shown in figure 4.8 is a constant, modified by gravitational effects to produce a hydrostatic environment. This ensures that the mechanical energy of the air entering the computational domain is equivalent at all points. Since the pressure boundaries are generally inflow boundaries, turbulence quantities have to be specified for the flow. For the $k-\varepsilon$ turbulence model, turbulence intensity, $I = \frac{u'}{U}$, and a turbulence length scale l (generally a length an order of magnitude smaller than the narrowest duct) have to be specified. Throughout the numerical simulations, the value of the inlet turbulence intensity was chosen as five percent and the turbulence length scale as a third of the inlet height. The velocity component at this type of boundary are calculated from the local pressure gradients, which were removed sufficiently far from the tower inlet to ensure natural development of the approach velocity distribution. Throughout the simulation, the value of the pressure boundary was chosen as 100 kPa.

- Outlet Boundaries - a fixed mass outflow rate is prescribed across this boundary. No velocities are specified, so that the velocity distribution at the outlet is purely a function of the internal model domain. In brief, the conditions prevailing at a fixed mass flux boundary must obey the following relation, $m_{out} = constant = \int_{outlet} \rho \mathbf{V} \cdot d\mathbf{S}$.

The combination of pressure and fixed mass outflow boundaries ensure that the velocity distribution inside the computational domain is not biased by externally imposed conditions and removes the dependency on experimentally determined velocity boundaries. Flow in the tower develops according to the stricture of the model geometry and the approximated laws of fluid flow, so that the resulting flow field is a close approximation of reality.

4.2.3 Fill Simulation

The precise extent and location of the fill can be seen in figure 4.6. As noted previously, two types of fill, isotropic and orthotropic resistance, had to be simulated. The former is relatively simple to implement, requiring only that for the selected fill cells, the change in momentum per unit volume be specified. This is done by means of a user subroutine, SORMOM.F, wherein the linearised form of the momentum sources for the different co-ordinate directions are given by,

$$s_i = s1_i - s2_i \times u_i \ , \ [\mathrm{N/m^3}] \tag{4.31}$$

(No summation) For the resistance embodied by the fill, the first source term, $s1_i$, represents a momentum gain and is equal to zero. The coefficient in the second term, $s2_i$, can be found directly from the definition of the fill loss coefficient,

$$\frac{\Delta p}{L_{fi}} = \frac{1}{2}\rho V^2 K_{fi} / L_{fi} \tag{4.32}$$

where L_{fi} is the vertical fill dimension, added to find the volumetric fill momentum loss, so that $s2_i$ becomes,

$$s2_i = \left(\frac{1}{2}\rho K_{fi} / L_{fi}\right) \times |u_i| \tag{4.33}$$

In an isotropic fill, the $s2_i$ coefficient is variable only insofar as the magnitude of the velocity components, $|u_i|$, of the different co-ordinate directions differ. In other words $s2_i / |u_i|$ is constant in all directions. For a film type orthotropic fill, however, at least one of the $s2_i$ coefficients will be very large to simulate the impermeability of the fill in that direction. The 'large' coefficient will force the fluid to flow only perpendicular to its direction of influence, by 'sinking' all the momentum in that direction. This is obviously not what occurs in reality, so an adjustment must be made to the flow to counteract the loss of momentum caused by entry into the orthotropic resistance area. In addition, entrance losses occur when flow enters the film type fill at

an oblique angle (as described in section 1.4) and these must also be accounted for, since they form part of the inlet loss.

The path of air entering an orthotropic resistance fill at an oblique angle can be seen in figure 4.9. The oblique angle of the air velocity vector must be changed to vertical as it enters the body of the fill. This is done by removing all horizontal momentum from the flow and then replacing it with vertical momentum.

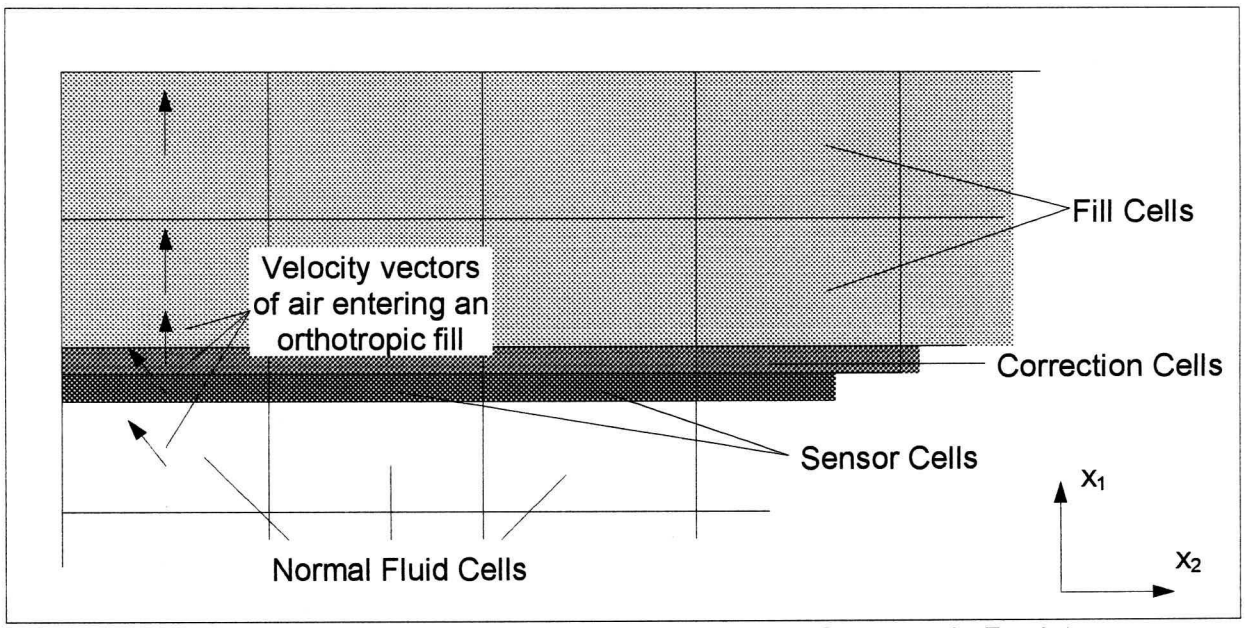

Figure 4.9: *Discretised Representation of the Inlet to an Orthotropic Resistance.*

This exchange of momentum is accomplished by adding two layers of cells to the bottom of the fill (fig. 4.9). These cells are thin enough so that any change in vertical momentum across them will be negligible. The bottom of the two cell layers, labelled the sensor cells, has no resistance to the flow and serves only to record the angle of the air entering the fill. This angle is passed to the top cell layer, the correction cells, where flow modifications are made.

For flow entering a film type resistance, as described above, the resistance in the horizontal direction tends toward infinity, therefore, the $s2_i$ coefficient for the horizontal direction in a correction cell will be given by,

$$s2_2 \rightarrow \infty \tag{4.34}$$

The vertical momentum that has to be added to the flow in the correction cell, because of this sinking of the horizontal momentum, is given by,

$$\Delta mv = \tfrac{1}{2}\rho u_2^2 \tag{4.35}$$

where u_2 is the horizontal air velocity in the sensor cell. Equation (4.35) can be written in loss coefficient form in terms of the vertical velocity in the correction cell,

$$K_{ix} = \frac{u_2^2}{u_1^2} = \frac{1}{\tan^2\theta} = \left(\frac{1}{\sin^2\theta} - 1\right) \tag{4.36}$$

where θ is the angle of attack of the velocity vector in the sensor cell found from $\theta = \tan^{-1}\left(\frac{u_1}{u_2}\right)$ and it is assumed that the vertical velocity, u_1, is constant across the two cell layers. In addition, oblique flow entering the film type fill undergoes expansion losses. These can be expressed, in loss coefficient form, as [98KR1],

$$K_{i\theta} = \left(\frac{1}{\sin\theta} - 1\right)^2 \tag{4.37}$$

where θ is the same as for the horizontal sink losses. Finally, the vertical source term coefficient, $s2_1$, for the correction cell is found by subtracting equation (4.36) from equation (4.37) and adding the result to the normal fill vertical resistance,

$$\begin{aligned} s2_1 &= \tfrac{1}{2}\rho\left[\left(K_{fi}/L_{fi}\right) + \left(K_{i\theta} - K_{ix}\right)/L_{cc}\right] \times |u_1| \\ &= \tfrac{1}{2}\rho\left[\left(K_{fi}/L_{fi}\right) + 2\left(1 - \frac{1}{\sin\theta}\right)/L_{cc}\right] \times |u_1| \end{aligned} \tag{4.38}$$

where L_{cc} is the length of the correction cell.

4.2.4 Droplet Modelling

Since STAR-CD models droplets using a time-derivative Lagrangian tracking scheme, initial conditions must be supplied for each droplet packet. Figure 4.10 shows the typical initial positions and velocity vectors of droplets in a counterflow rain zone.

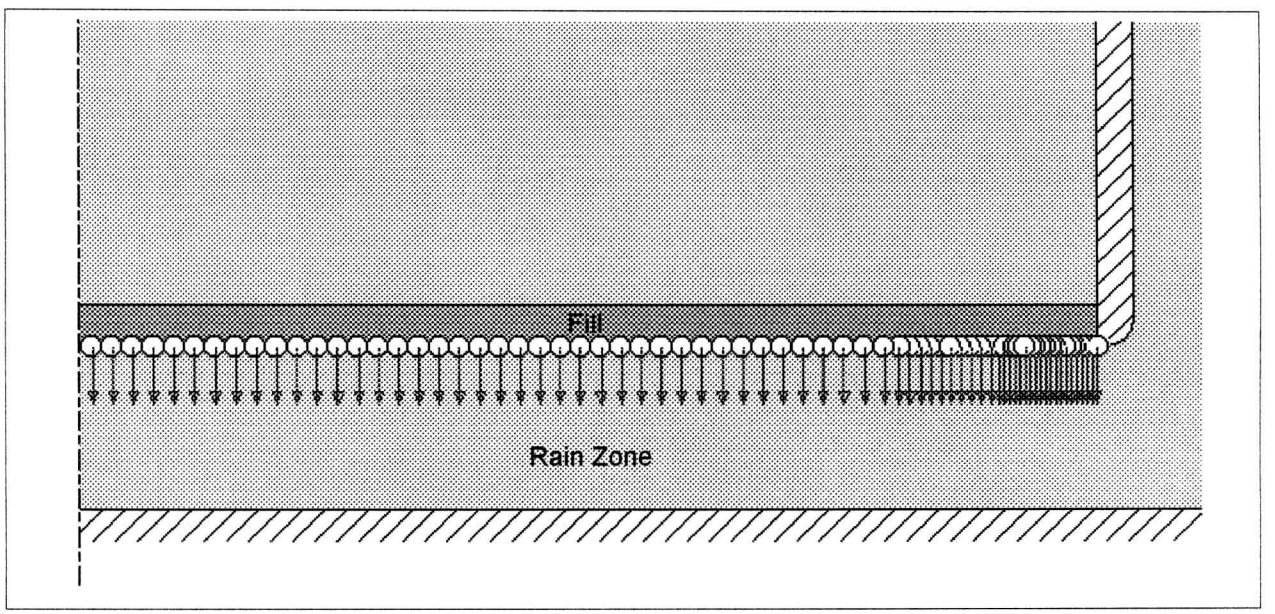

Figure 4.10: *Droplet Initial Conditions*

To avoid infinities during flow initialisation, the initial velocity of the droplet was chosen as 0.1 m/s in the negative vertical direction. Sensitivity studies showed that such a low initial velocity has no significant effect on the inlet or rain zone loss. Other parameters passed to the CFD solver, via the program TWRGEN, include: the droplet diameter, d_d ; the number of droplets associated with a particular computational drop, n_d (calculated to provide a uniform water flux); the droplet's initial position (i.e. the height of the inlet and the droplet's horizontal position) and droplet thermophysical properties. As can be seen in figure 4.10, more droplet packets were introduced near the tower inlet. This is to ensure homogeneous distribution of the momentum loss caused by droplet drag in the fine grid, high velocity inlet area.

Droplets hitting the wall that represents the ground were removed from the computational domain by means of a user subroutine, DROWBC.F. The pond at the bottom of the rain zone was ignored and no heat or mass transfer was included in the droplet simulation.

4.2.5 Data Acquisition and Manipulation

The pressure drop caused by the inlet losses, the rain zone and the fill was measured by a row of specialized cells inserted above the packing (fig. 4.11). The cells return the flow's piezometric pressure and vertical velocity, so that the total mechanical energy loss experienced by the flow, between ambient conditions and the top of the fill, can be calculated. This data is automaticly written to file during the solution process, a sample distribution of which is shown in figure 4.12. The velocity magnitude is fairly uniform across most of the fill (with the recirculating region near r = 50 m causing a deviation), while the pressure distribution varies with less than 3 Pa, about 5 percent of the average pressure drop.

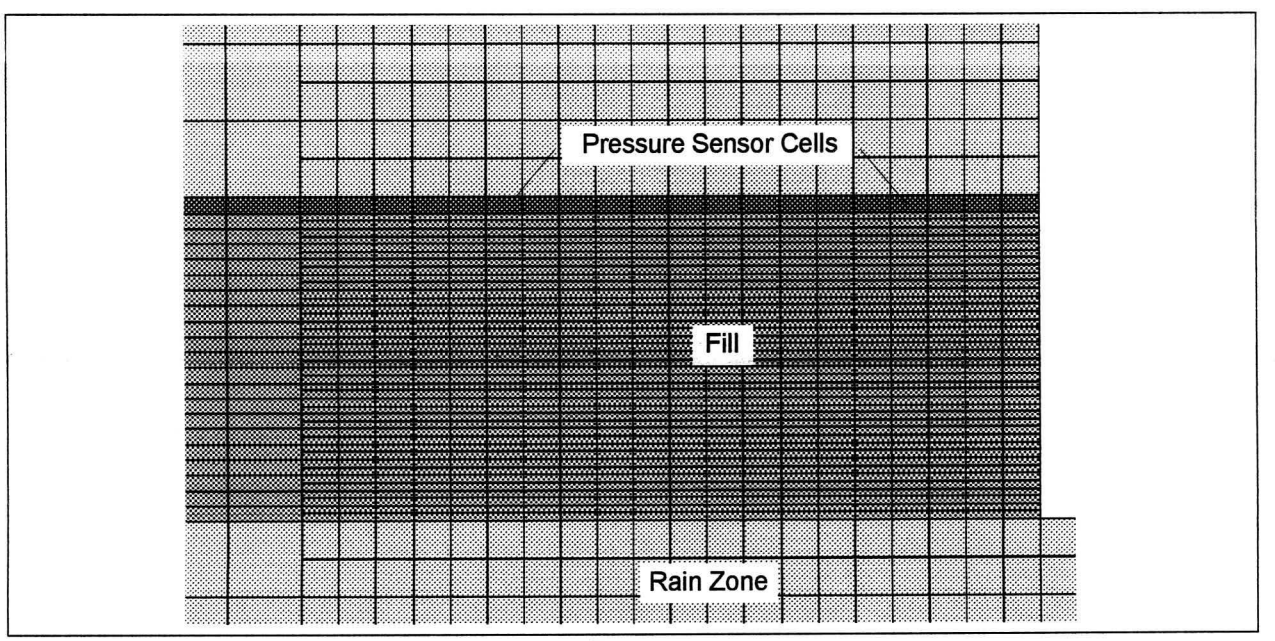

Figure 4.11: *Position of Data Capturing Cells.*

The total loss coefficient, defined in terms of the average fill outlet velocity, is given by,

$$K_t = \left[p_a - \left(\overline{\left(p_s + \tfrac{1}{2}\rho u_1^2 \right)}_{sc} + \rho g\left(H_i + L_{fi} \right) \right) \right] / \left(\tfrac{1}{2}\rho v_i^2 \right) \tag{4.39}$$

where the subscript *sc* denotes conditions in the sensor cells, the overbar a mass flux based averaging process across the fill outlet and p_a is the ambient stagnation pressure at ground level. The inlet loss coefficient for a wet-cooling tower can now be found from,

$$K_{ct} = K_t - \left(K_{fi} + K_{rz}\right) \tag{4.40}$$

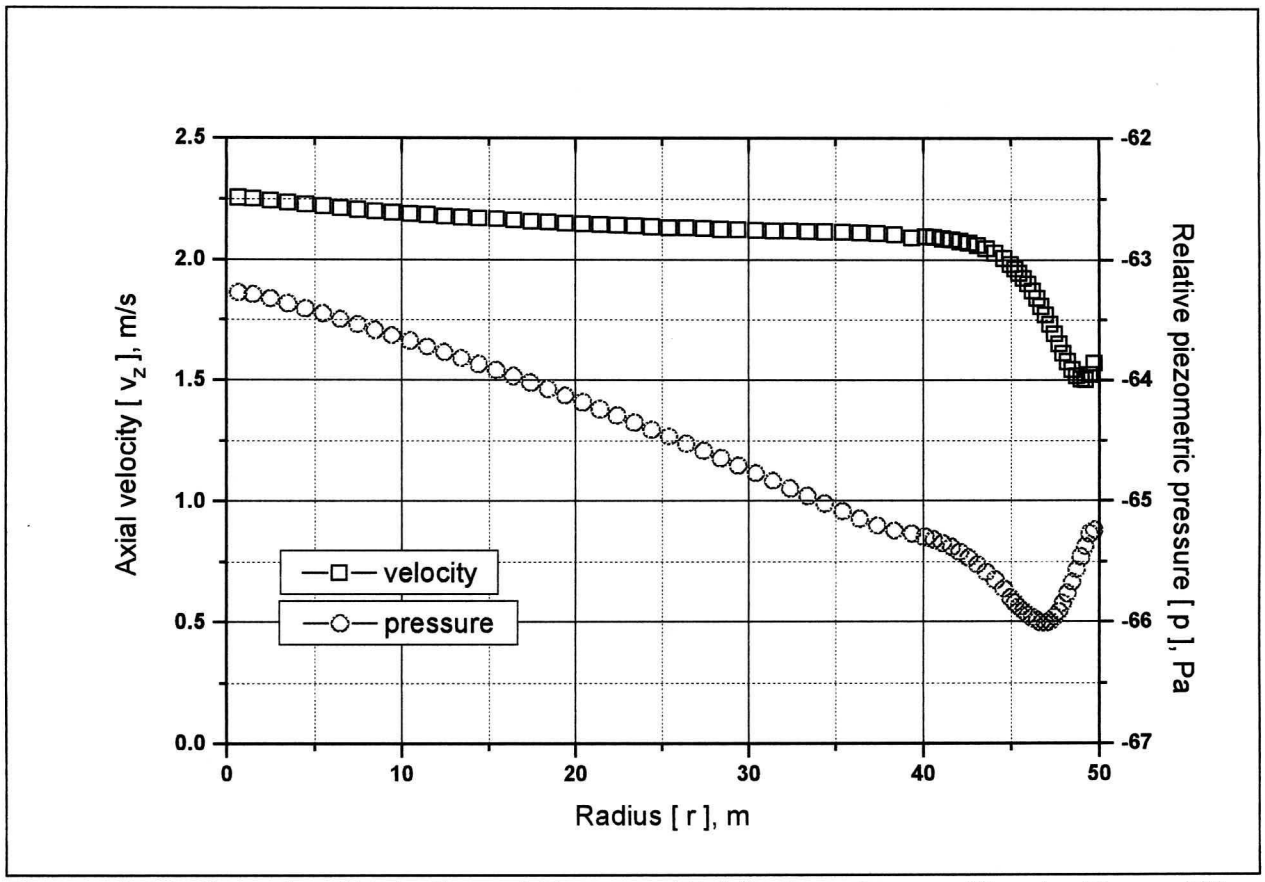

Figure 4.12: *Sample of Velocity and Pressure Distribution above a Circular Tower Fill.*

As stated previously, inaccuracies in the numerical turbulence model will cause a deviation from the actual physical value for the inlet loss coefficient (especially for isotropic fills). To compensate for this error, the experimental inlet loss coefficients for dry-cooling towers is modified in the following manner,

$$K_{ct(wet)} = K_{ct(dry)} \times dK_{ctrz} \tag{4.41}$$

where

$$dK_{ctrz} = \frac{K_{ct(wet,numerical)}}{K_{ct(dry,numerical)}} \tag{4.42}$$

and $K_{ct(dry)}$ can be found from the equations in Chapter 3. This is an approximation of the wet-cooling tower inlet loss, but the size of the error will be bounded by the difference between the numerical and experimental dry-cooling tower values. It also serves to define trends in the interdependency of the inlet and rain zone losses.

4.3 Numerical Results

All CFD calculations were done using an IBM RISC system / 6000 C10. Unfortunately, with an average of 8000 computational cells per model and the inclusion of turbulence modelling, Lagrangian droplet tracking and unspecified boundary velocities, the average time to convergence was about three hours per run. The inlet loss correction factor, dK_{ctrz}, is a function of all eleven variables that characterise the inlet and rain zone losses. The time needed to explore all the dependencies and divergent influences of these variables using CFD is prohibitive. It was therefore decided to exclude any 'weak' variables from the analysis after a thorough screening process. The 'strong' functional dependency for the inlet loss correction factor is given by,

$$dK_{ctrz} = f\left(d_i (or\ W_i), H_i, d_d, G_w, G_a, K_{fi}\right) \tag{4.43}$$

Sample solutions of a circular wet-cooling tower flow field can be seen in figures 4.13 and 4.14. (The rarefied vector field in figure 4.13 is caused by constraints on the size of the plot file employed to generate the image.) The pressure contour plot (fig. 4.14) distinctly shows the effects of the rain zone on the pressure distribution. The effect of the accelerating air in the inlet and especially along the inlet rounding can also be clearly observed.

Figure 4.15 depicts a vector diagram of the recirculating flow encountered next to the bottom of the tower shell. This recirculation is a large contributing factor to the inlet loss, but since it is neither a free stream nor a boundary layer flow, it cannot be accurately simulated by the available turbulence modelling techniques and therefore causes an inaccuracy in the simulated results. The magnitude of the uncertainty is dependent on the size of the recirculating flow, but a quantitative analysis of this effect does not form part of this thesis. The trajectories of the computational (or sample) droplets are shown in figure 4.16 and are nearly identical to the analytical solution.

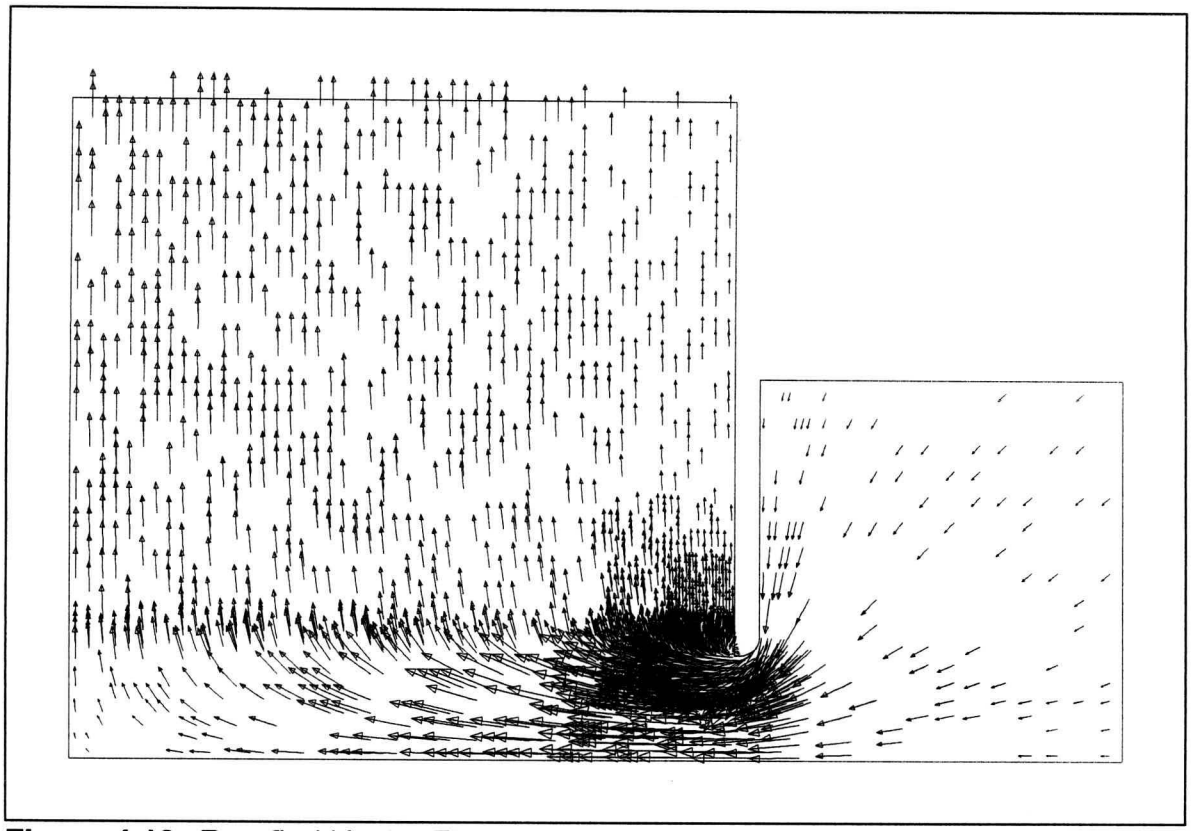

Figure 4.13: *Rarefied Vector Flow Field in the Inlet Section of a Circular Cooling Tower.*

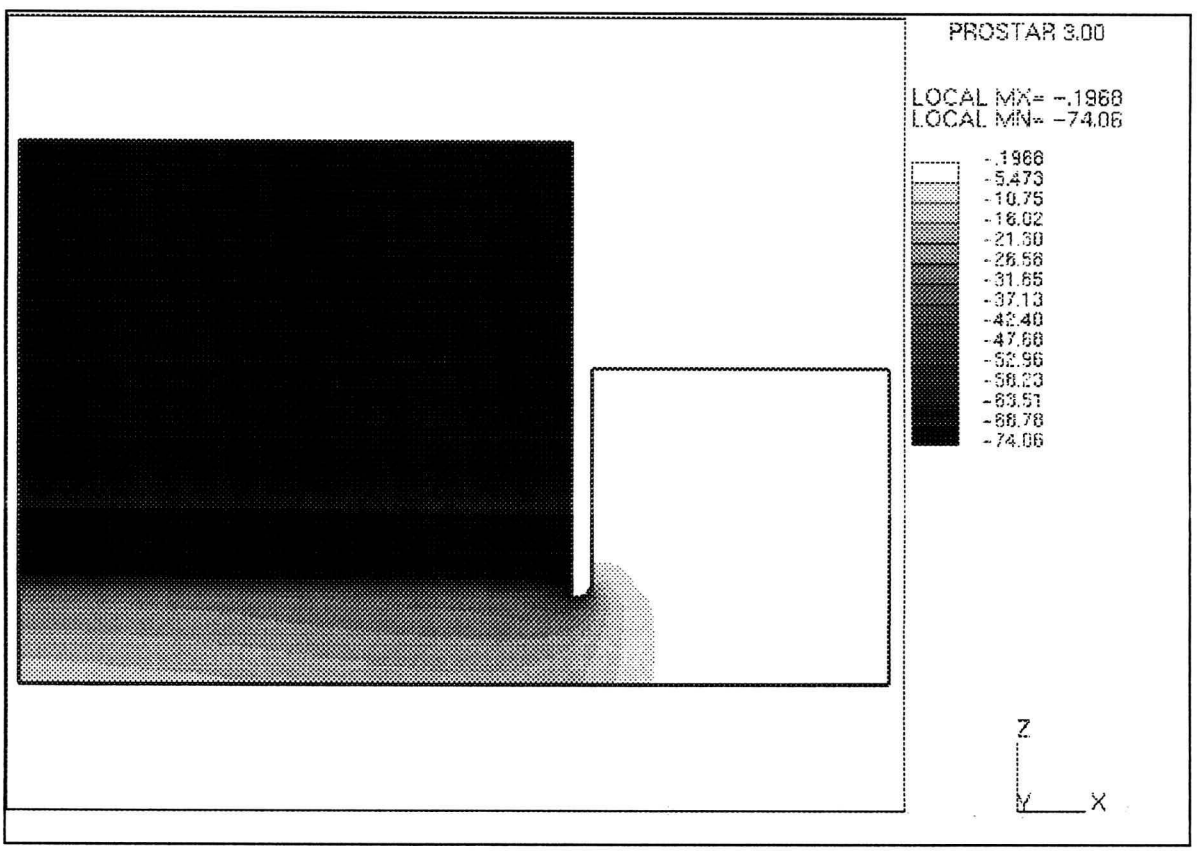

Figure 4.14: *Relative Piezometric Pressure Distribution.*

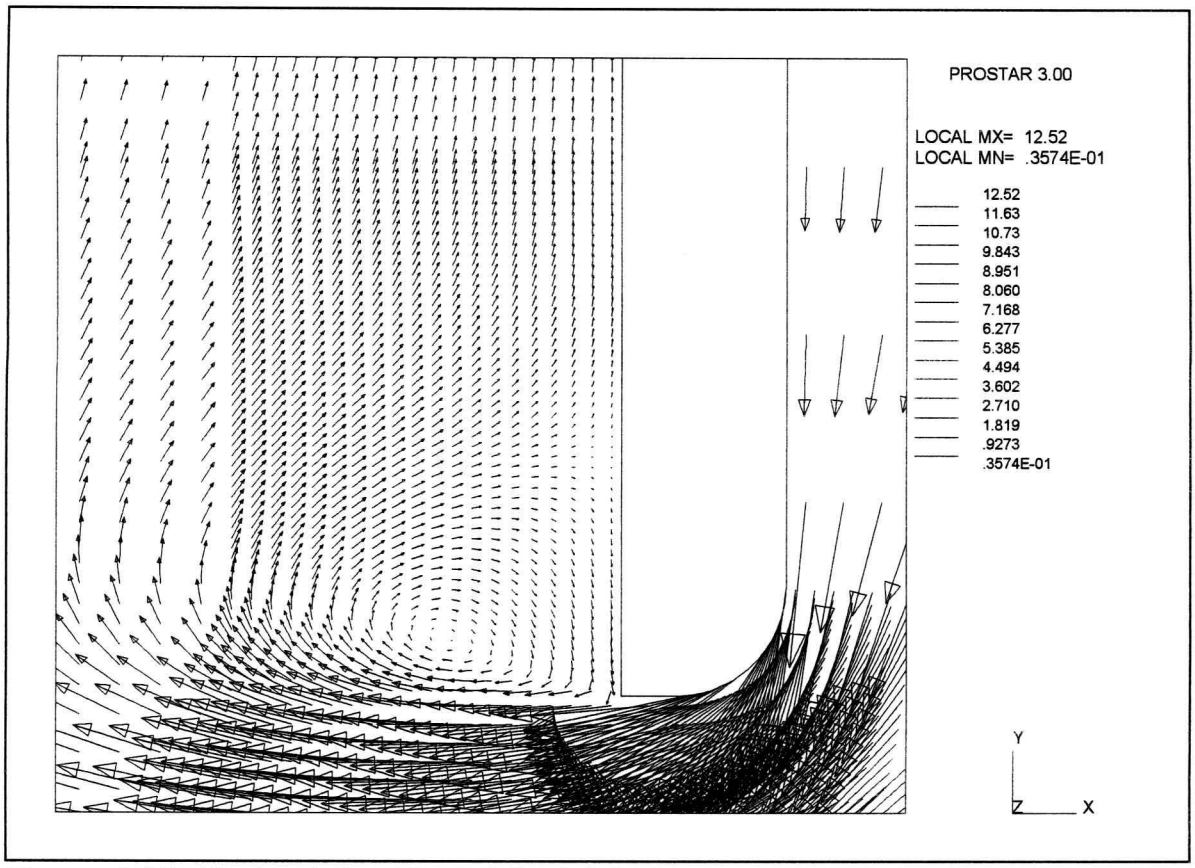

Figure 4.15: *Recirculating Flow at the Inlet.*

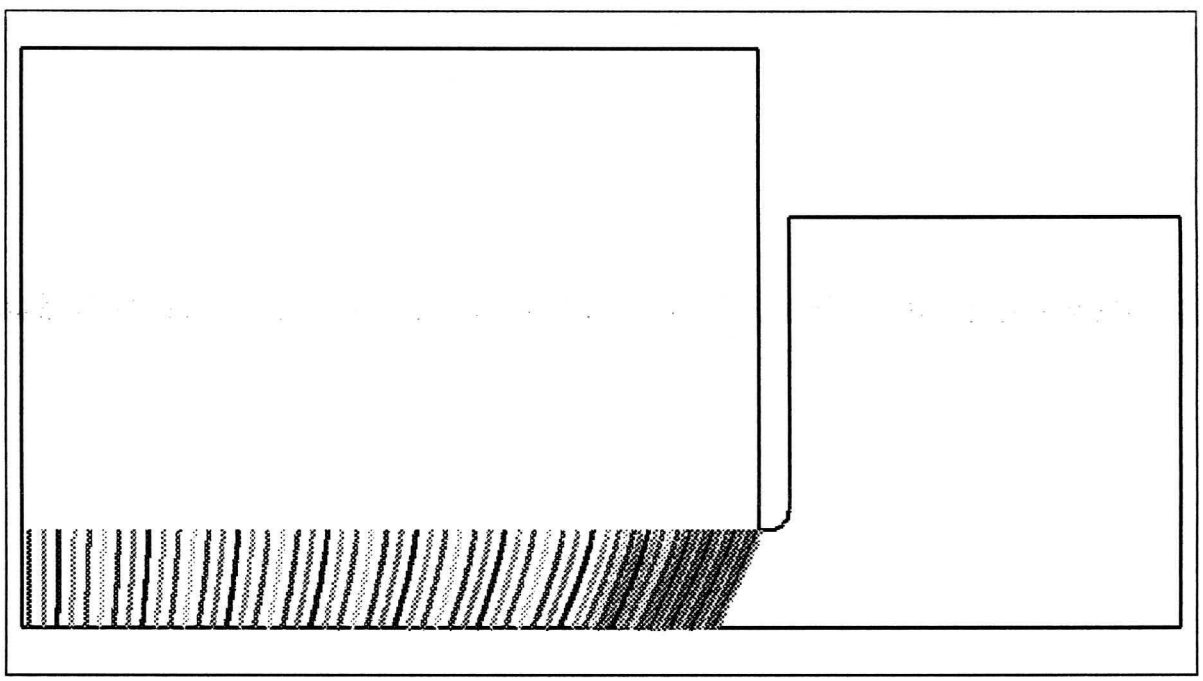

Figure 4.16: *Computational Droplet Trajectories.*

4.3.1 Circular Cooling Towers

The general validity of the current analysis is dependent on the degree of similarity between the experimental and numerical simulations of the dry-cooling tower inlet loss coefficient. For a circular tower with an isotropic splash type fill, the correspondence between the numerical and experimental solutions can be seen in figures 4.17 and 4.18. The numerical solution's values are consistently lower than is the case for the experimental tests. This is in accordance with the predicted deficiency in the modelling of the recirculating flow region. The larger deviation at high values of the fill loss coefficient, seen in figure 4.18, are ascribed to turbulence production in the recirculating and oblique flow fill regions present in the experimental test case. These phenomena could not be duplicated in the CFD simulation since they are dependent on the fine geometric structure of the experimental fill and no theory currently exists whereby such effects could be reproduced.

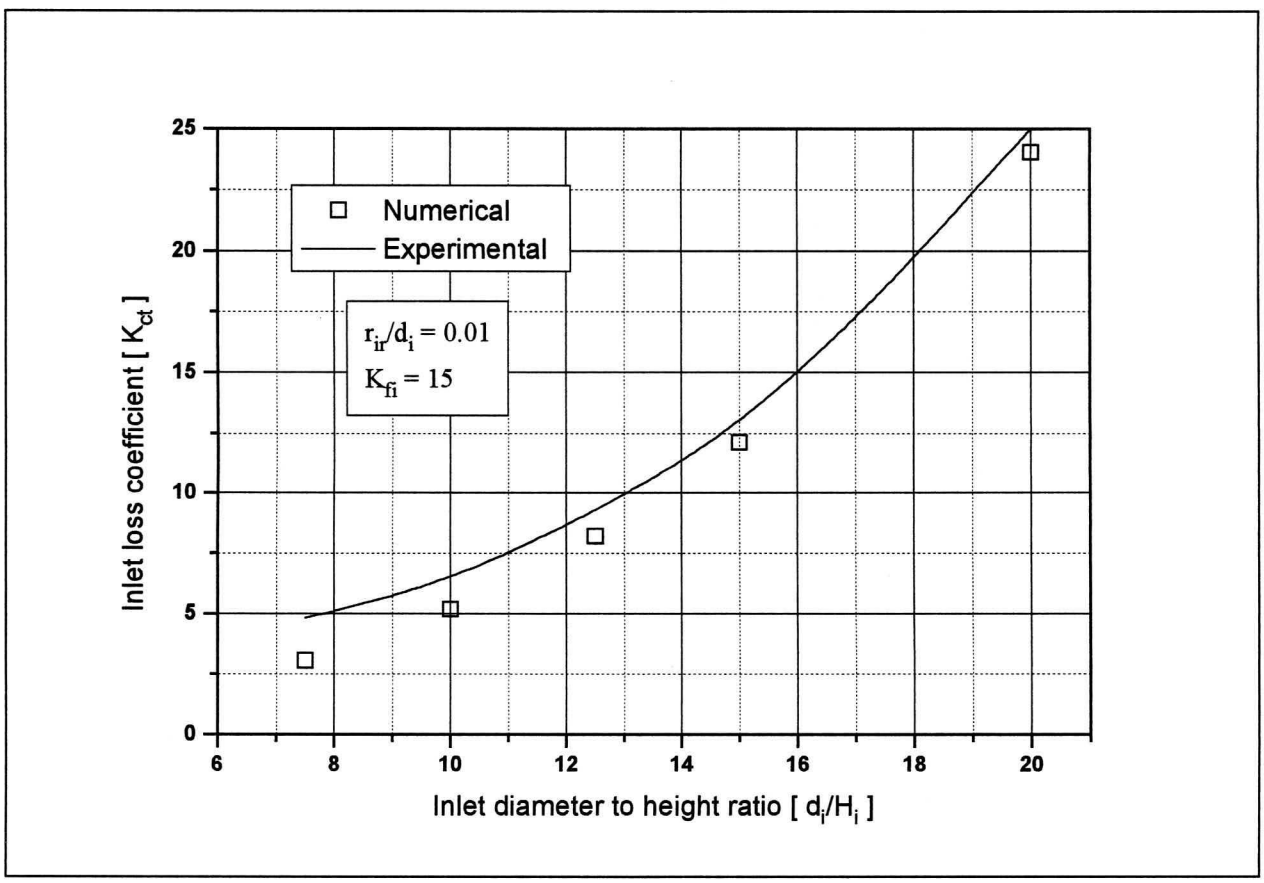

Figure 4.17: *Correspondence between Experimental and Numerical Solutions of the Inlet Loss for Circular Dry-cooling Towers with Isotropic Fill.*

In general, though, the agreement between the two approaches is sufficient to engender a large degree of confidence in further results obtained using the numerical model and the applicability of such results to the experimental results is assured.

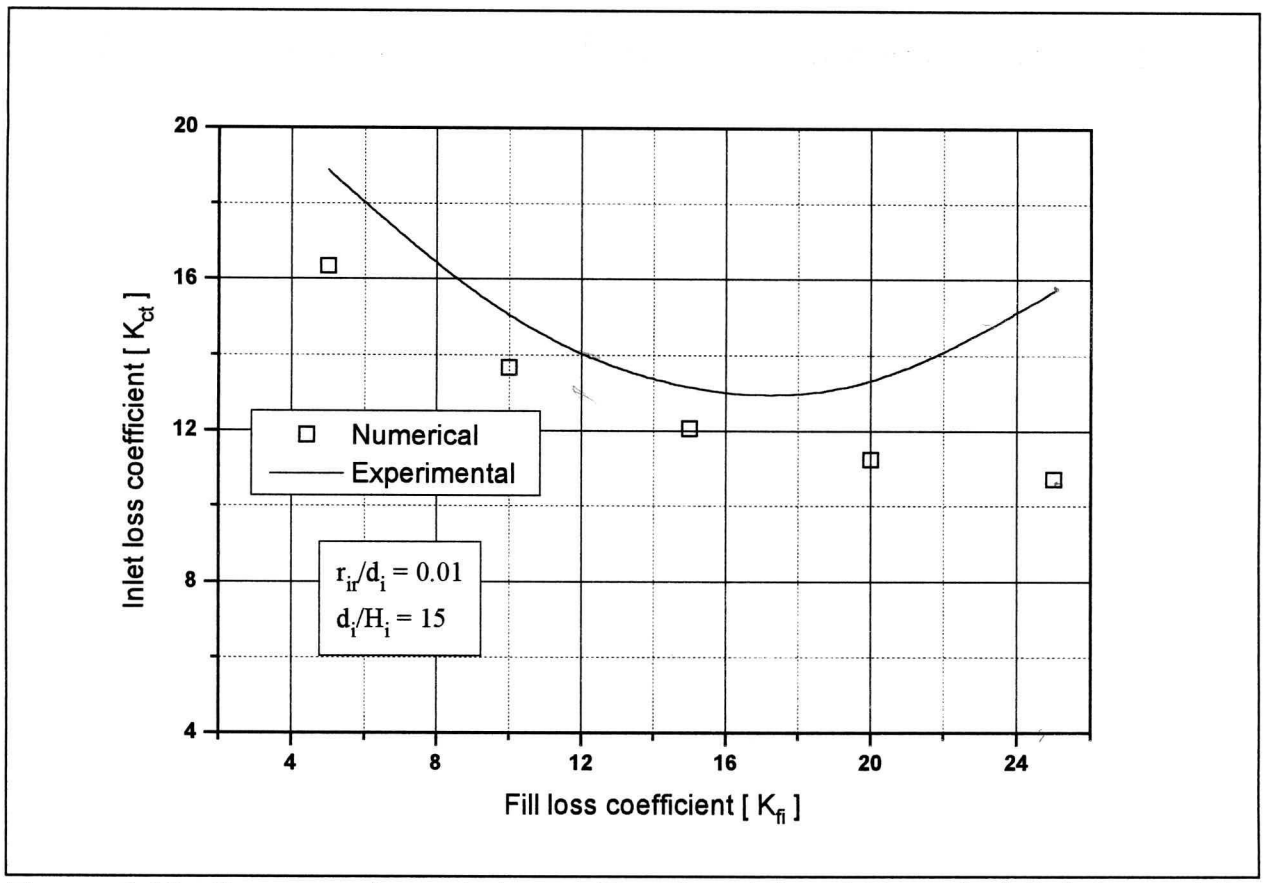

Figure 4.18: *Correspondence between Experimental and Numerical Solutions of the Inlet Loss for Circular Dry-cooling Towers with Isotropic Fill.*

For a circular counterflow wet-cooling tower, with an isotropic flow resistance fill, the correlation for the inlet loss correction factor is given by,

$$dK_{ctrz} = \left[0.2394 + 80.1\left(\frac{0.0954}{d_i / H_i} + d_d\right)e^{\left(0.395\frac{G_w}{G_a}\right)} - 966.0\left(\frac{d_d}{d_i / H_i}\right)e^{\left(0.686\frac{G_w}{G_a}\right)} - 0.3195\left(\frac{G_w}{G_a}\right)\right] \times\left(1 - 0.06825G_w\right)K_{fi}^{0.09667}e^{8.7434(1/d_i - 0.01)} \quad (4.44)$$

which is valid for $7.5 \le d_i / H_i \le 20$, $3 \le d_d \le 6$mm, $1 \le G_w \le 3$ kg/m^{2}s, $1.2 \le G_a \le 3.6$ kg/m^{2}s, $80 \le d_i \le 120$ m and $5 \le K_{fi} \le 25$ (where $G_a = \rho_a v_i$ and $G_w = \rho_w v_w$). The lack of consistent use

of dimensionless groups is caused by the exclusion of the 'weak' variables, so that insufficient dimensional variables are available to complete the Π-groupings. The average error encountered using the fitted correlation, is less than 4 percent, which is adequate considering the inaccuracies of the numerical simulation and the fact that the correction factor is used to modify an existing loss coefficient. Figures 4.19 and 4.20 compare the curve fit with the numerically generated data.

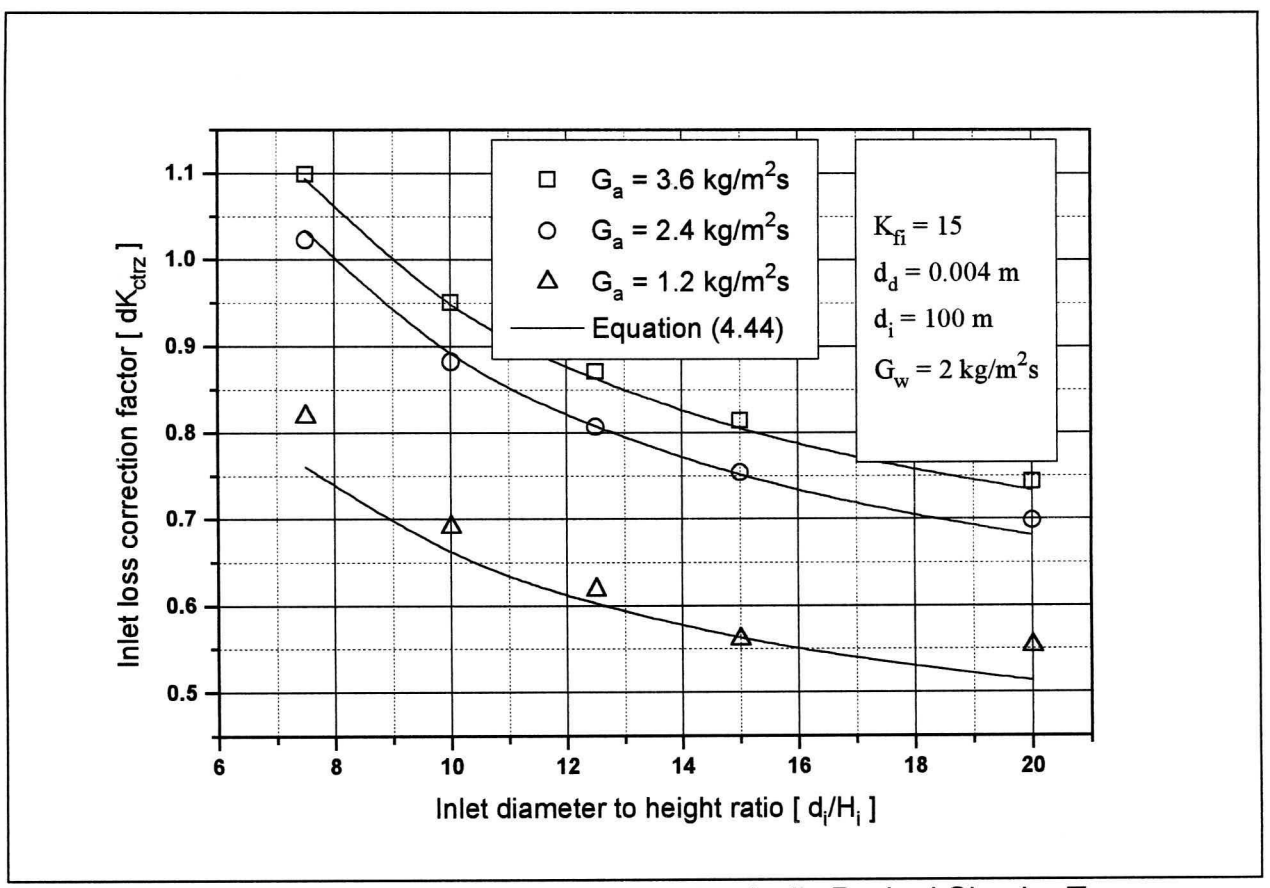

Figure 4.19: *Inlet Loss Correction Factor for Isotropically Packed Circular Towers.*

The general trend is for the added resistance of the rain zone to dampen the inlet loss in an effect similar to that caused by increased fill resistances. This change is not directly coupled to the rain zone loss, though, necessitating the large number of dependent variables.

Values of the inlet loss correction factor in excess of one are found in cases where the magnitude of the rain zone loss overshadows that of the inlet loss. In such cases, it is advisable that the inlet loss correction factor be taken as unity. The discrepancy is caused by deviations of the inlet flow field in low inlet loss towers from the idealised situation assumed in Chapter 2. This causes the rain zone loss encountered in the CFD solution to be slightly larger than the analytically predicted

value. If, however, the inlet loss is a lot smaller than the rain zone loss, this error is amplified causing the above unity values seen in figures 4.19 and 4.20. Mathematically, the error is encountered as

$$dK_{ctrz} = \frac{K_{ct(wet)}}{K_{ct(dry)}} + \frac{\left(K_{rz(numerical)} - K_{rz(analytical)}\right)}{K_{ct(dry)}} \tag{4.45}$$

where the second term on the right-hand side represents the error value. Fortunately, sensitivity studies have shown that the error is usually small and always conservative and that significant effects are limited to low inlet diameter to height ratio towers. In practice circular towers with inlet diameter to height ratios below ten are seldom encountered. Also, the deviation in dK_{ctrz} will tend to correct the error made by using the analytical rain zone loss solution in the first place, so that the validity of equation (4.44) is assured.

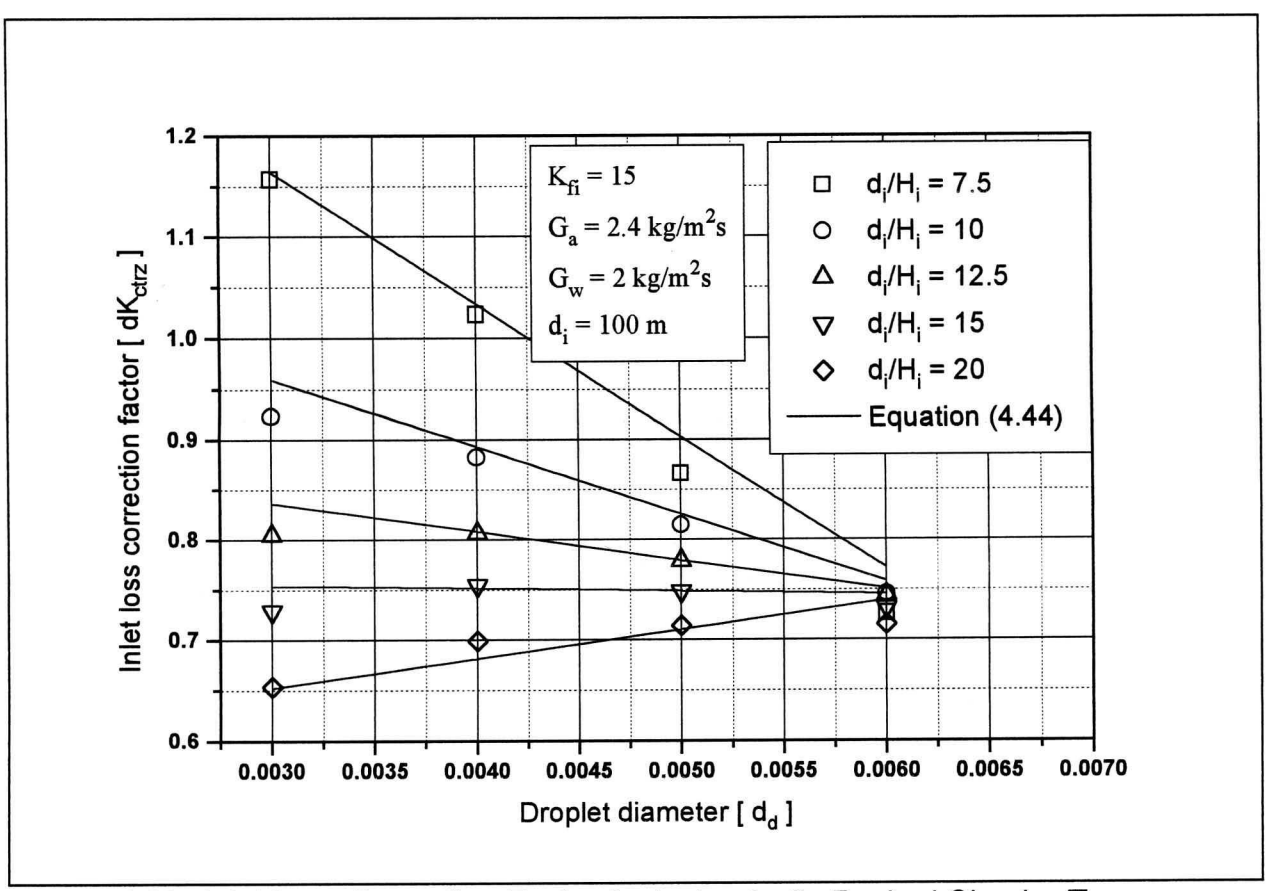

Figure 4.20: *Inlet Loss Correction Factor for Isotropically Packed Circular Towers.*

The agreement between numerically and experimentally determined inlet losses, for orthotropically packed circular dry-cooling towers, is shown in figure 4.21.

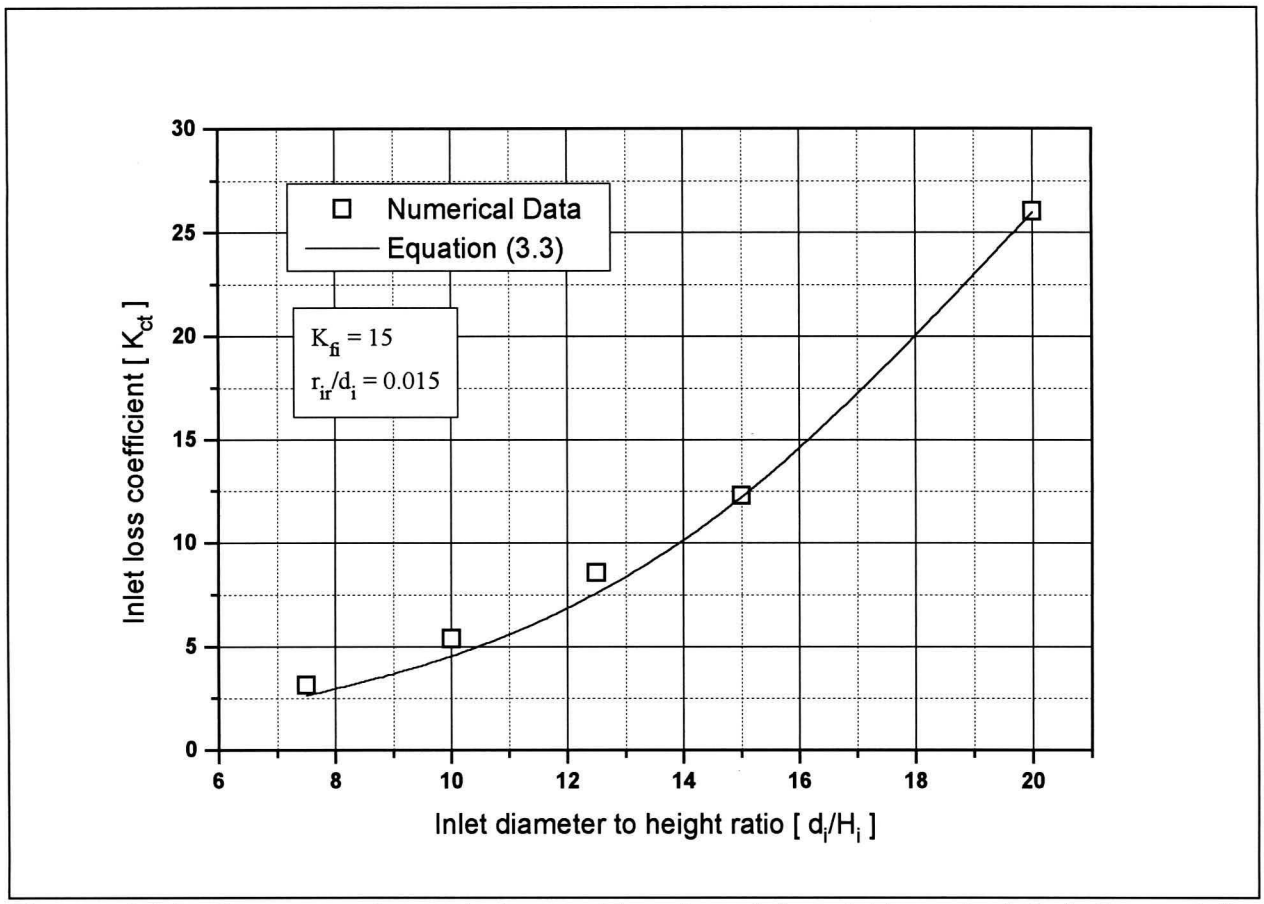

Figure 4.21: *Correspondence between Experimental and Numerical Solutions of the Inlet Loss for Circular Dry-cooling Towers with Orthotropic Fill.*

The accuracy of the numerical solution is ascribed to the lack of large unbounded recirculating flows in the orthotropic film type fill. A computational fluid dynamic simulation of circular orthotropic fill resistance towers can, therefore, be used with confidence to examine the effects of the rain zone on the inlet loss coefficient of such towers.

Upon investigation it was found that the inlet loss correction factor, for circular orthotropically packed towers, closely resembles that associated with isotropically packed towers. So much so that equation (4.44) represents an adequate correlation of the correction factor for the current case. Figure 4.22 shows a sample of this correspondence between the inlet loss correction factor for isotropic and orthotropic fill resistance towers.

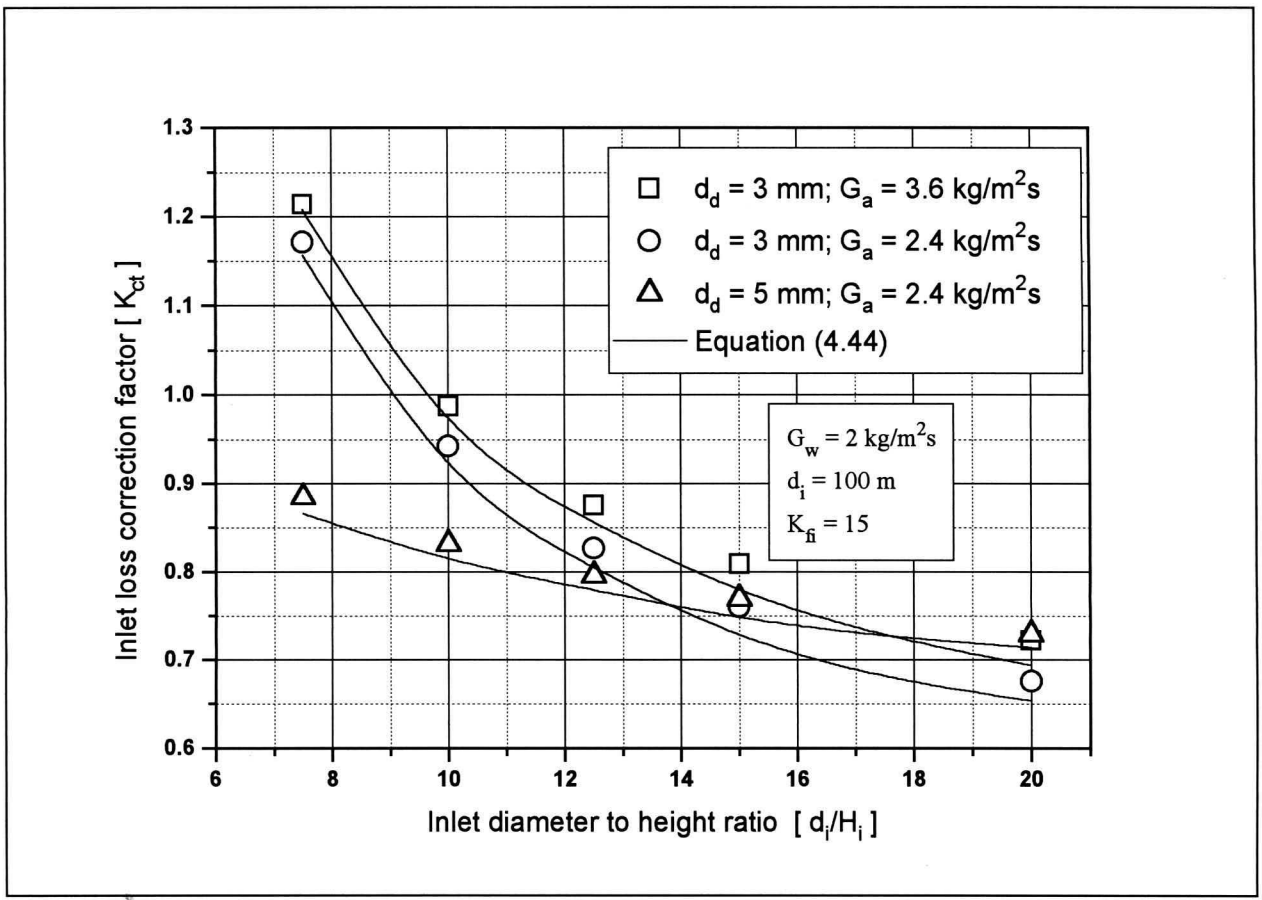

Figure 4.22: *Comparison of Inlet Loss Correction Factors for Orthotropic and Isotropic, Fill Resistances.*

4.3.2 Rectangular Cooling Towers

The correspondence between experimentally and numerically generated inlet loss coefficients for isotropically packed rectangular towers, seen in figure 4.23, is poor compared to that encountered in circular towers. While the difference in inlet loss coefficient between experimental and numerical methods for circular towers never exceeds 30 percent (and that for very low inlet diameter to height ratios), that for rectangular towers is commonly in excess of a hundred percent. This poor agreement is thought to be caused by a larger comparative recirculating region in rectangular towers, so that the error made during numerical modelling becomes correspondingly greater. Any results obtained from the CFD simulation must, therefore, be viewed with caution and lack the degree of confidence that is associated with the circular tower model. This is especially true at the low inlet width to height ratios with which operational rectangular towers are commonly constructed. Fortunately, the magnitude of the inlet loss in such towers is comparatively small and the inlet loss correction factor is close to unity, so that any

expected improvement in tower performance, because of the correction factor, would be marginal. It therefore, becomes acceptable to ignore the inlet loss correction factor in cases where $W_i / H_i \leq 3$

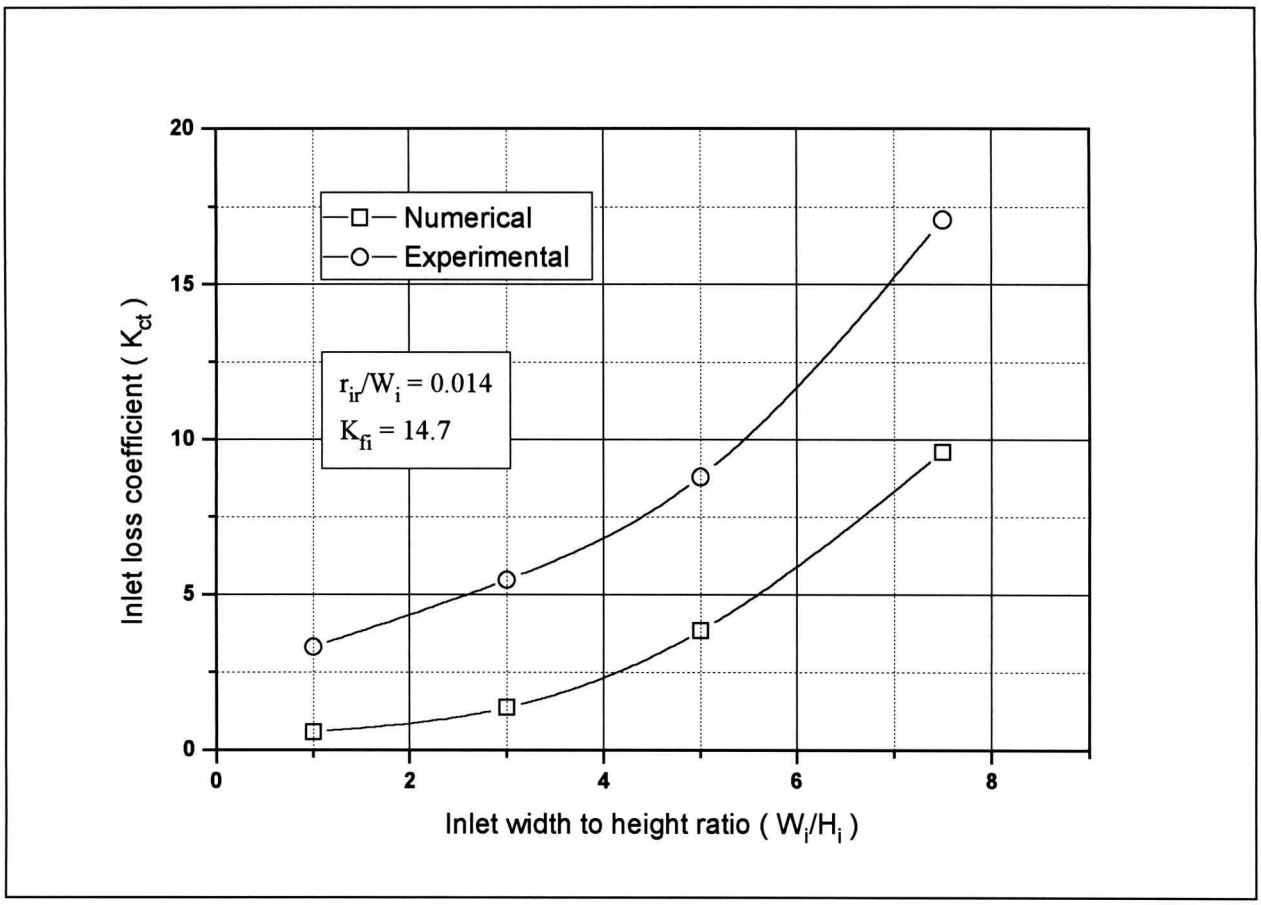

Figure 4.23: *Comparison between Experimental and Numerical Solutions of the Inlet Loss for Rectangular Dry-cooling Towers.*

Where the inlet loss correction factor for a rectangular tower is needed, the following empirical correlation provides the required value,

$$dK_{ctrz} = 1 - G_w \left(0.123 - 12.12 d_d - 272.255 d_d^2 + 5.04 \times 10^{-4} . \mathrm{e}^{0.466 \frac{W_i}{H_i}} \right) \times \left(1 - 1.16 \times 10^{-3} . \mathrm{e}^{G_a} \right) \quad (4.46)$$

and is valid for $3 \leq W_i / H_i \leq 7.5$, $3 \leq d_d \leq 6\,\mathrm{mm}$, $1 \leq G_w \leq 3\ \mathrm{kg/m^2 s}$ and $2 \leq G_a \leq 6\ \mathrm{kg/m^2 s}$. It must be emphasised, that this equation can only be used with any degree of confidence at high

W_i / H_i values and since this is not normally the case, it becomes prudent to take the conservative approach by ignoring the influence of the rain zone loss on the inlet loss. Considering that this influence is small at low inlet height to width ratios, this practice becomes acceptable. The correspondence between equation (4.46) and the numerical data is shown in figure 4.24.

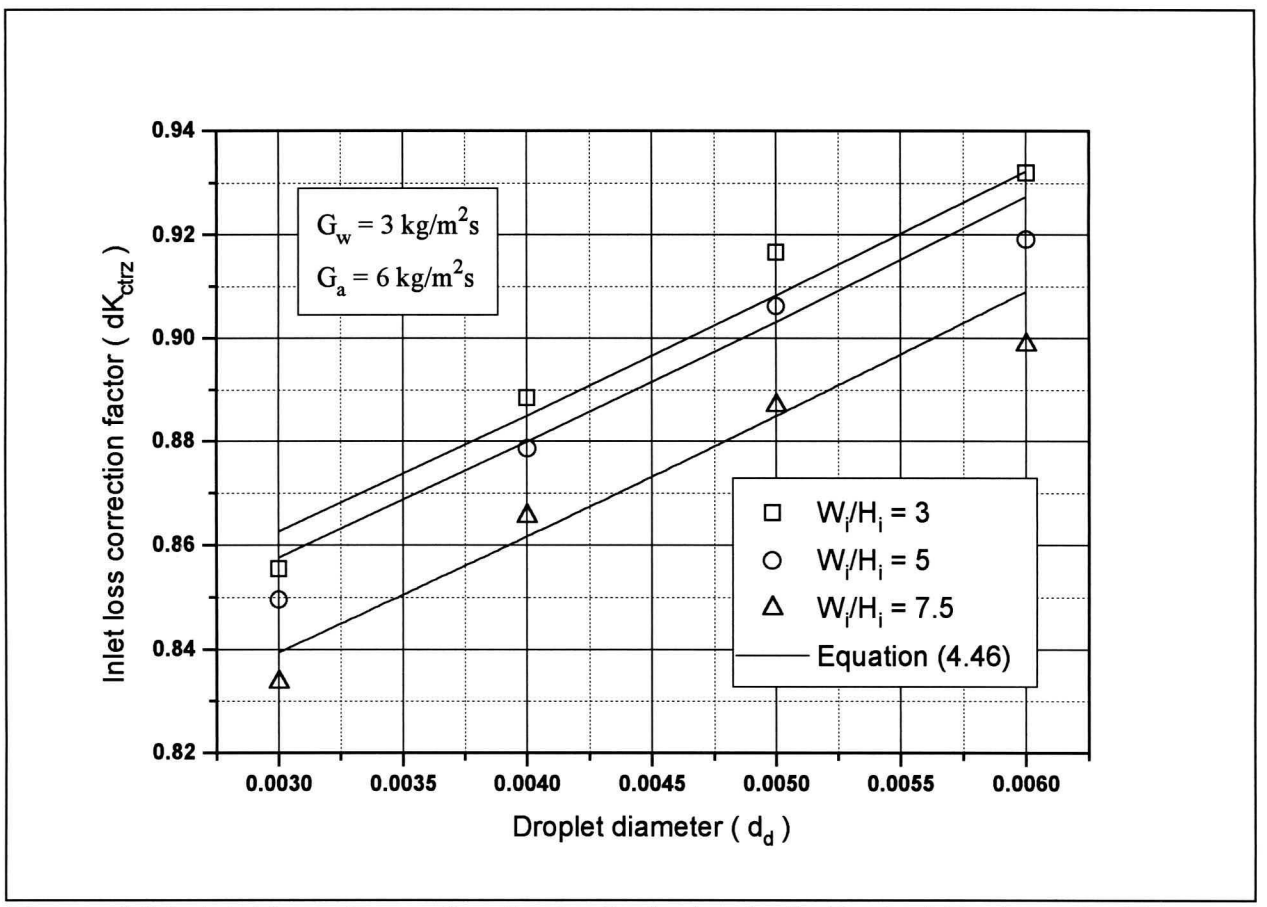

Figure 4.24: *Inlet Loss Correction Factor for Isotropically Packed Rectangular Towers.*

For orthotropic-fill-resistance rectangular towers the effect of the rain zone on the inlet loss coefficient is small and the validity thereof uncertain. The conservative approach of ignoring the rain zone's influence, is therefore suggested, but if a correction factor is required, equation (4.46) will provide an adequate representation of the rain zone's dampening effect.

CHAPTER FIVE

CONCLUSION

This thesis set out to improve the accuracy of cooling tower performance prediction. To this end, a study was made of the flow resistances that influence the performance of counterflow wet-cooling towers. Two of the more complex and less understood flow resistances, namely the inlet loss and the rain zone loss, were investigated. It was shown that, previous researchers assumed, erroneously, that the inlet losses for towers with film type fills could be applied universally (to splash pack towers) and that earlier models of the rain zone contain invalid modelling assumptions. An analysis was also made of the dependence of the inlet loss on the magnitude and characteristics of the rain zone and fill losses. The rain zone was found to have a damping effect on the inlet loss, while towers with isotropic resistance packing exhibited higher inlet losses than comparable orthotropically packed towers. Prediction tools in the form of empirical and semi-empirical correlations (for use in a one-dimensional cooling tower performance evaluation) were derived, to provide the designers of cooling towers with greater accuracy when modelling these phenomena.

An analytical-numerical model was used to simulate the pressure drop in the rain zones of circular and rectangular cooling towers. The rain zone's effect is simulated as mechanical energy expended by the cooling fluid and droplet deformation is included as a function of its (the droplet's) dynamic properties. Calculating the rain zone loss for a wide variety of practical tower applications produced two semi-empirical correlations (for rectangular and circular towers) for the rain zone loss coefficient. These correlations are presented in terms of standard tower dimensions and flow variables and are formulated to incorporate the non-linearity of the rain zone data. Although uncertainty exists as to the effect of droplets on the rain zone flow field and the effective size of these droplets when encountered in operational towers, the model was partially validated by means of experimental and numerical methods. A one-dimensional counterflow simulation and experiment was used to substantiate the model in terms of operational applicability

and effective droplet size, while numerical simulations of tower rain zones provide tentative approval of the original modelling assumptions. In conjunction with the pressure drop analysis, a study was made of the heat and mass transfer in the rain zone, from which equations that provide the corresponding Merkel number for rectangular and circular towers were formulated. Simulations were conducted that show the positive effect, of decreasing the droplet diameter in the rain zone, on a cooling tower's heat rejection rate.

Although cooling tower inlet losses have been extensively studied in the past, it was found that no correlations existed to predict the inlet loss for towers with isotropic resistance fills and/or rain zones. These deficiencies were addressed by, firstly, conducting experiments to find the inlet loss for dry isotropically packed towers. The data from these experiments was used to formulate correlations for the dry inlet loss coefficient in circular and rectangular towers. The results show that distinctly different inlet losses are encountered when employing isotropic resistance fills (compared to orthotropic resistances). In addition, increasing the inlet rounding's radius was found to continuously decrease the magnitude of the inlet loss, even after the inflection point reported by previous researchers. Secondly, computational fluid dynamic (CFD) was used to investigate the effect of the rain zone's resistance on the inlet loss coefficient in circular and rectangular towers (with isotropic and orthotropic resistance fills). Equations for a correction factor were correlated from the results. Applying this correction factor to a dry inlet loss, produces an inlet loss (that is generally smaller than its dry counterpart) for an equivalent wet-cooling tower. The correction factor is most applicable to circular towers, where good agreement, between experimental and numerical dry tower simulations, validates the modelling strategy. A 'weak' agreement between numerical and experimental results for rectangular towers, caused by large recirculating regions and relatively small inlet losses, casts doubt on the efficacy of the corresponding correction factor. Studies of operational tower configurations show, however, that the influence of the correction factor in rectangular towers is small and may be ignored in favour of a more conservative approach. Whether the fill resistance is orthotropic or isotropic was found to have little effect on the size of the correction factor. A sample solution of an operational circular tower, shows the significant effect of rain zone damping (and thus the inlet loss correction factor) on the cooling tower's performance.

In conjunction, the prediction tools presented in this thesis provide greater accuracy and confidence when calculating the mass flow rate and therefore the heat rejection rate in counterflow wet-cooling towers. It is suggested, however, that an attempt be made to validate the complete set of equations in terms of applicability to operational towers and effective droplet diameters.

A logical extension of this investigation is to characterise recirculating flows in general and their effects on tower performance in particular, so that complete CFD solutions of cooling towers (especially rectangular towers) and related flow structures can be confidently explored. The ability to accurately model cooling towers and therefore recirculating flows using CFD, (without the inclusion of experimental data) would provide prediction and optimisation capability for a range of applications heretofore unknown. The increased confidence and accuracy of results, with associated cost reductions, would be considerable, especially as available computing power increases.

REFERENCES

[26ME1] Merkel, F. :*Verdunstungskühlung*, VDI-Zeitschrift, vol. 70, pp 123 - 128, 1926.

[34GI1] Gilliland, E.R., :*Diffusion Coefficients in Gaseous Systems*, Ind. Eng. Chem., Vol. 26, pp. 681, 1934.

[41LA1] Laws, J.O., *Measurement of the Fall Velocity of Water Drops and Raindrops*, Transactions of the American Geophysical Union, Part III, 22nd Annual Meeting, pp. 709-721, 1941.

[49GU1] Gunn, R. and Kinzer, G.D., *The Terminal Velo0city of Fall for Water Droplets in Stagnant Air*, Journal of Meteorology, Vol. 6, pp. 243-248, 1950.

[52CH1] Chilton, H., *Performance of Natural-draught Water Cooling Towers*, Proceedings of the Institute of Electrical Engineers, Vol. 99, No. 71, pp.440 - 456, 1952.

[52RA1] Ranz, W.E. and Marshall, W.R., *Evaporation from Drops*, Chemical Engineering Progress, Vol. 48, No. 3, pp. 141 - 146, 1952.

[61LO1] Lowe H.J. and Christie, D.G., *Heat Transfer and Pressure Drop Data on Cooling Tower Packing, and Model Studies of the Resistance of Natural Draught Towers to Airflow*, International Development in Heat Transfer, Part V, ASME, New York, 1961.

[61RI1] Rish, R.F., *The Design of a Natural Draught Cooling Tower*, Proceedings of the 2nd International Heat Transfer Conference, Boulder, Colorado, 1961.

[68VO1] Vogelsang, E. and Hackeschmidt, M., *Experimentelle Untersuchungen über die Ungleichförmigkeit der Strömung in Verdunstungskühlern*, Luft- und Kältetechnik, Vol. 7, pp.306 - 318, 1968.

[69GO1] Gosman, A.D., Pun, W.M., Runchal, A.K., Spalding, D.B. and Wolfstein, M., *Heat and Mass Transfer in Recirculating Flows*, Acedemic Press, London, 1969.

[70PR1] Pruppacher, H.R. and Beard, K.V., *A Wind Tunnel investigation of the Internal Circulation and Shape of Water Drops Falling at Terminal Velocity in Air*, Quarterly Journal of the Royal Meteorological Society, Vol. 96, pp. 247-256, 1970.

[71PR1] Pruppacher, H.R. and Pitter, R.L., *A Semi-empirical Determination of the Shape of Cloud and Rain Drops*, Journal of Atmospheric Sciences, Vol. 28, pp. 86-94, 1971.

[71ZE1] Zembaty, W. and Konikowski, T., *Untersuchung über den aerodynamischen Widerstand von Kühlturmen*, Brennst. -Wärme-Kraft, Vol. 23, No. 10, pp. 441-445, 1971.

[72LE1] Le Clair, B.P., Hamielec, A.E., Pruppacher, H.R. and Hall, W.D., *A Theoretical study of the Internal Circulation in Water Drops Falling at Terminal Velocity in Air*, Journal of Atmospheric Sciences, Vol. 29, pp. 728-740, 1972.

[72PA1] Patankar, S.V. and Spalding, D.B., *A Calculation Procedure for Heat, Mass and Momentum in Three-dimensional Parabolic Flows*, International Journal of Heat and Mass Transfer, Vol. 15, 1972.

[74LA1] Launder, B.E. and Spalding, D.B., *The Numerical Computation of Turbulent Flow*, Comp. Meth. in Appl. Mech. & Eng., Vol. 3, pp. 269, 1974.

[75GR1] Green, A.W., *An Approximation for the Shape of Large Raindrops*, Journal of Applied Meteorology, Vol. 14, pp. 1578-1583, December 1975.

[76KE1] Kelly, N.W., *Kelly's Handbook of Crossflow Cooling Tower Performance*, N.W. Kelly and Associates, Kansas City, MO, 1976.

[76YO1] Yao, S. and Schrock, V.E., *Heat and Mass Transfer from Freely Falling Drops*, ASME Journal of Heat Transfer, pp. 120 - 126, February 1976.

[77BE1] Beard, K.V., *On the Acceleration of Large Water Drops to Terminal Velocity*, Journal of Applied Meteorology, Vol. 16, pp. 1068-1071, October 1977.

[77MU1] Muira, K., Muira, T. and Ohtani, S., *Heat and Mass Transfer to and from Droplets*, AIChE Symposium Series, Vol. 73, No. 163, pp. 95 - 102, 1977.

[77NA1] Nahavandi, A.M. and Oellinger, J.J., *An Improved Model for the Analysis of Evaporative Counterflow Cooling Towers*, Nuclear Engineering Design, Vol. 40, North Holland Publishing. Co., 1977.

[77PR1] Pruppacher, H.R. and Klett, J.D., *Microphysics of Clouds and Precipitation*, D. Reidel Publishing. Co., Holland, 1977.

[79RO1] Rodi, W., *Influence of bBuoyancy and Rotation on Equations for Turbulent Length Scale*, Proceedings of the 2nd Symposium on Turbulent Shear Flows, 1979.

[80PA1] Patankar, S.V., *Numerical Heat Transfer and Fluid Flow*, Hemisphere, Washington, D.C., 1980.

[81BU1] Buxmann, J. and Völler, G., *Die Bedeutung des Eintriettsdrucverlustes beim Naturzug-Trocken Kühlturm*, Bernnst-Wärme-Kraft, No. 718, Vol. 33, pp. 313-316, 1981.

[81GA1] Garde, M.A., *Experimental Evaluation of entrance Losses of Flared Natural Draft Cooling Towers*, M.Sc. Thesis, Cornell University, 1981.

[81MO1] Moore, F.K. and Garde, M.A., *Aerodynamic Losses of Highly Flared Natural Draft Cooling Towers*, 3rd Waste Heat Management Conference, Miami, 1981.

[81WA1] Warsi, Z.V.A., *Conservation form of the Navier-Stokes equations in General Nonsteady Co-ordinates*, AIAA Journal, Vol. 19, pp. 240-242, 1981.

[82CA1] Cale, S.A., *Development of Evaporative Cooling Packing*, Commision of European Communities, Report EUR 7709 EN, Luxemburg, 1982.

[83BO1] Boroughs, R.D. and Terrell, J.E., *Survey of Utility Cooling Towers*, TVA Report OP/EDT - 83/13, 1983.

[83EL1] El Tahry, S.H., *k-ε Equations for Compressible Reciprocating Engine Flows*, AIAA J. Energy, Vol. 7, No. 4, pp. 345-353, 1983.

[83MA1] Majumdar, A.K., Singhal, A.K. and Spalding, D.B., *Numerical Modelling of Wet Cooling Towers*, Transactions of the ASME Journal of Heat Transfer, Vol. 105, pp.728 - 743, November 1983

[84PO1] Poppe, M. and Rögener, H., *Berechung von Rückkühlwerken*, VDI-Wärmteatlas, pp. Mh 1 - Mh 15, 1984.

[86BE1] Benton, D.J. and Rehberg, R.L., *Mass Transfer and Pressure Drop in Sprays Falling in a Free Stream at Various Angles*, Proceeding of the 5th IAHR Cooling Tower Workshop, Monterey, California, September 1986.

[86BE01] Benocci, C., Buchlin, J.M. and Weinacht, P. : *Prediction of the Air-droplet Interaction in the Inlet Section of s Natural Draft Cooling Tower*, Proceedings of the 5th IAHR Cooling Tower Workshop, Monterey, California, September 1986.

[86GE1] Geldenhuys, J.D. and Kröger, D.G., *Aerodynamic Inlet Losses in Natural Draft Cooling Towers*, Proceedings of the 5th IAHR Cooling Tower Workshop, Monterey, 1986.

[86GÕ1] Gõsi, P., *Practical conclusions from Cooling Tower Model Studies*, Proceedings of the 5th IAHR Cooling Tower Workshop, Monterey, 1986.

[86MI1] Missimer, J.R. and Brackett, C.A., *Model Tests of the Rain Zone of a Counterflow Natural Draft Cooling Tower*, Proceedings of the 5th IAHR Cooling Tower Workshop, Monterey, 1986.

[86TU1] Turton, R. and Levenspiel, O., *A Short Note on the Drag Correlation for Spheres*, Powder Technology, Vol. 47, pp. 83 - 86, 1986.

[87BE1] Beard, K.V. and Chuang, C. : *A New Model for the Equilibrium Shape of Raindrops*, Journal of Atmospheric Sciences, Vol. 44, No. 11, pp. 1509 - 1524, 1987.

[87CA1] Caytan, Y., *Numerical Simulation of the Operation of Natural Draft Cooling Towers*, 5th International Conference on Numerical Methods in Thermal Problems, Montreal, June 1987.

[88BE1] Benton, D.J. and Waldrop, W.R., *Computer Simulation of Transport Phenomena in Evaporative Cooling Towers*, Journal of Engineering for Gas Turbines and Power, Vol. 110, pp. 190, April 1988.

[88DU1] Du Preez, F. and Kröger D.G., *Experimental Evaluation of Aerodynamic Inlet Losses in Natural Draft Cooling Towers*, Proceedings of the 6th IAHR Cooling Tower Workshop, Pisa, Italy, 1988.

[88EP1] EPRI and TVA report, *Performance Monitoring of Power Plant Operations*, Power Magazine, August 1988.

[88GR1] Greenberg, M.D., *Advanced Engineering Mathematics*, Prentice Hall, Englewood Cliffs, New Jersey, 1988.

[88RA1] Radosavljevic, D. and Spalding, D.B., *Simultaneous Prediction of Internal and External Aerodynamic and Thermal Flow Fields of a Natural Draft Cooling Tower in a Cross-wind*, 6th IAHR Cooling Tower Workshop, Pisa, Italy, 1988.

[88WH1] White, F.M., *Fluid Mechanics*, McGraw-Hill Book Co., Singapore, 1988.

[90HO1] Hoffmann, J.E. and Kröger, D.G., *Analysis of Heat, Mass and Momentum Transfer in the Rain Zone of a Natural Draft Counterflow Cooling Tower*, Proceedings of the 7th IAHR Cooling Tower and Spray Pond Symposium, Leningrad, USSR, 1990.

[92ŠE1] Šedina, M., *Heat and Mass Transfer and Pressure Drop in the Rain Zone of Cooling Towers*, Proceedings of the 8th IAHR Cooling Tower and Spray Pond Symposium, Karlsruhe, Germany, 1992

[92ZH1] Zhenguo, Z., Jingling, S. and Xiansong, C., *Study on Airflow Resistances in Natural Draft Cooling Towers*, Proceedings of the 8th IAHR Cooling Tower and Spray Pond Symposium, Karlsruhe, Germany, 1992.

[93CO1] Conradie, C.F.G., *Die Verkoelingsvermoe van Nat Koeltorings en Droë/Nat Stelsels by Kragstasies*, M. Eng Thesis, University of Stellenbosch, Stellenbosch, 1993.

[94DR1] Dreyer, A.A., *Modelling of Cooling Tower Splash Pack*, Ph.D. Dissertation, University of Stellenbosch, Stellenbosch, 1994.

[94TE1] Terblanche, J.E., *Inlaat verliese by Koeltorings*, M. Eng. Thesis, University of Stellenbosch, Stellenbosch, 1993.

[94TE2] Terblanche, J.E. and Kröger, D.G., *Experimental Evaluation of the Aerodynamic Inlet Losses in Cooling Towers*, South African Institute of Mechanical Engineers R & D Journal, Vol. 10 No. 2, pp. 41 - 44, 1994.

[96CO1] Computational Dynamics Limited, *Star-CD version 3.0 Manual*, Olympic House, London, 1996.

[97CR1] Crous, P.G., *Koeltoringontwerp*, Final year project B. Eng, University of Stellenbosch, Stellenbosch, 1997.

[97EL1] Eldredge, T.V., *Cooling Tower Modelling with Computational Fluid Dynamics*, EPRI TR-108483 2113, Proceedings Cooling Tower Technology Conference, pp. 1.49-1.60, July 1997.

[98KR1] Kröger, D.G., *Air Cooled Heat Exchangers and Cooling Towers*, University of Stellenbosch Press, Stellenbosch, 1998.

[99BA1] Baard, T.W., *Expanded Metal Cooling Tower Fill*, M. Eng Thesis, University of Stellenbosch, Stellenbosch, 1999.

APPENDIX A

HEAT AND MASS TRANSFER IN THE RAIN ZONE

The heat and mass transfer associated with the droplets in the rain zone was calculated, as an extension of the analytical-numerical model used to find the rain zone loss coefficient in Chapter 2. The transfer coefficient is given in terms of a Merkel number, that is used as part of the point model approach to cooling tower performance prediction. In this section the methodology of the process will be described and semi-empirical correlations will be derived to fit the resultant data. All assumptions made about the nature of the rain zone, in Chapter 2, apply to the current analysis.

Since the rain zone mass transfer coefficient is typically used in an analysis similar to that of Merkel [26ME1], it is unnecessary to calculate the heat transfer coefficient. This derives from Merkel's assumption that the Lewis factor, $h/\left(c_{pma}h_d\right)$, is equal to unity for wet-cooling towers.

In the absence of reciprocal droplet interaction, single drop correlations are applicable for heat and mass transfer applications in the rain zone. Ranz and Marshall [52RA1] propose the following semi-empirical correlation for the mass transfer coefficient for a single drop,

$$Sh = \beta d_d / D = 2 + 0.6\,\mathrm{Re}_d^{\,0.5}\, Sc^{0.33} \qquad \text{(A.1)}$$

which is valid for $2 < \mathrm{Re}_d < 800$, where β is the mass transfer coefficient, the Schmidt number is found from, $Sc = \mu_a / (\rho_a D)$ and the droplet Reynolds number is given by, $\mathrm{Re}_d = \rho_a v_{ad} d_d / \mu_a$. The velocity of the air relative to the droplet, v_{ad}, is found from equation (2.49), in the same manner as that employed to find the rain zone loss coefficient.

Muira et al. [77MU1] show that this correlation [Eq. (A.1)] accurately predicts their mass transfer data for Reynolds numbers of up to 2000. It is therefore, accepted that the correlation is accurate

for the entire rain zone, where the mean Reynolds number seldom exceeds 1500. Poppe [84PO1] derived the following relation between the mass transfer coefficients h_d and β for droplets with a diameter larger than 1mm:

$$h_d = (\beta p_a / R_v T_a) \ln\left[\frac{w_s + 0.622}{w + 0.622}\right] / (w_s - w) \tag{A.2}$$

where h_d is the humidity driven mass transfer coefficient. The evaporation loss from a single droplet can now be calculated from

$$m_d = h_d S_d (w_s - w) = h_d \pi d_d^2 (w_s - w) \tag{A.3}$$

where $S_d = \pi d_d^2$ represents the surface area of the droplet. Since air velocities within a control volume are considered constant, the mass transfer coefficient for all droplets within that volume will also be constant (control volumes are defined the same as in Chapter 2). For a circular tower, the number of droplets in a control volume, at any given time, can be found from equation (2.56). Multiplying the result with equation (A.3), produces the evaporation rate for a circular tower control volume,

$$m_{cv} = n_{cv} h_d \pi d_d^2 (w_s - w) \tag{A.4}$$

Integration of equation (A.4) yields the water vapour mass transfer rate for an entire circular tower rain zone.

$$m_{rz} = \int_{rz} n_{cv} dm_d = \int_o^{H_i} \int_0^{d_i/2} n_{cv} h_d S_d (w_s - w) \tag{A.5}$$

Since it has been assumed that the humidity potential is approximately constant throughout the rain zone (Chapter 2), the mean mass transfer coefficient can be found from,

$$h_{drz}a_{rz} = \frac{4}{\left(H_i \pi d_i^2\right)} \int_0^{H_i} \int_0^{d_i/2} n_{cv} h_d S_d \tag{A.6}$$

or in dimensionless form of the Merkel number

$$\frac{h_{drz}a_{rz}H_i}{G_w} = \frac{4}{\left(G_w \pi d_i^2\right)} \int_0^{H_i} \int_0^{d_i/2} n_{cv} h_d S_d \tag{A.7}$$

The complete expanded version of the above equation is found by substituting equations (2.56), (A.1) and (A.2) into equation (A.7). By moving all the constants of integration to the left of the integral, the number of variables used in the empirical curve fitting will be greatly reduced and the accuracy of the equation will benefit from the similarity to the analytical model. After simplification and rendering in non-dimensional form, the relation has the following form.

$$\frac{h_{drz}a_{rz}H_i}{G_w} = 12\left(\frac{D}{v_i d_d}\right) \times \left(\frac{H_i}{d_d}\right) \times \left(\frac{p_a}{R_v T_a} / \rho_w\right) \times \ln\left[\frac{w_s + 0.622}{w + 0.622}\right] / (w_s - w)$$
$$\times \int_0^{H_i} \int_0^{d_i/2} \left(\frac{v_i}{v_{dz}}\right)(2 + 0.6\,\mathrm{Re}_d^{0.5}\, Sc^{0.33})\left(\frac{4rdrdz}{d_i^2 H_i}\right) \tag{A.8}$$

It is clear from equations (A.8) and (A.1) that the integral is dependent upon the variables ($d_d, d_i, H_i, v_i, \rho_a, \rho_w, \mu_a, \sigma_w, g$ and D). The diffusion coefficient, D, evidently has a much smaller presence in the integral (in Sc) than outside and since it is a weak variable, it is dropped from the list of dependants to simplify analysis. The variables may now be arranged in the same dimensionless groups as for the pressure drop coefficient [eq. (2.65)]. The integral is solved numerically and dimensional analysis and curve fitting of the results produce the following semi-empirical relation,

$$\frac{h_{drz}a_{rz}H_i}{G_w} = 12\left(\frac{D}{v_i d_d}\right)\left(\frac{H_i}{d_d}\right)\left(\frac{p_a}{R_v T_a}/\rho_w\right) \times Sc^{0.33} \times \ln\left[\frac{w_s + 0.622}{w + 0.622}\right]/\left[w_s - w\right]$$
$$\times\left[0.90757a_\rho\rho_a - 30341.04a_\mu\mu_a - 0.37564 + 4.04016 \times \left[\left(0.55 + 41.7215(a_L d_d)^{0.80043}\right)\right.\right.$$
$$\times\left(0.713 + 3.741(a_L H_i)^{-1.23456}\right) \times \left(3.11\mathrm{e}^{(0.15a_v v_i)} - 3.13\right)$$
$$\left.\left. \times \mathrm{e}^{\left[\left(5.3759\mathrm{e}^{-0.2092a_L H_i}\right) \times \ln\left(0.3719\mathrm{e}^{0.00191a_L d_i} + 0.55\right)\right]}\right]\right] \qquad \text{(A.9)}$$

where the restrictions and "a-" coefficients are identical to those used for the rain zone loss coefficient equation and $R_v = 461.52$ J/kgK for water vapour. The correlation fits the data with an average error of less than 2,5 percent. Figure A.1 shows the correspondence between equation (A.9) and numerical data. It also shows the strong influence of the droplet diameter on the Merkel number. The implication is, that smaller droplets in the rain zone will significantly increase a tower's heat rejection rate, offering a cost effective way to improve tower performance.

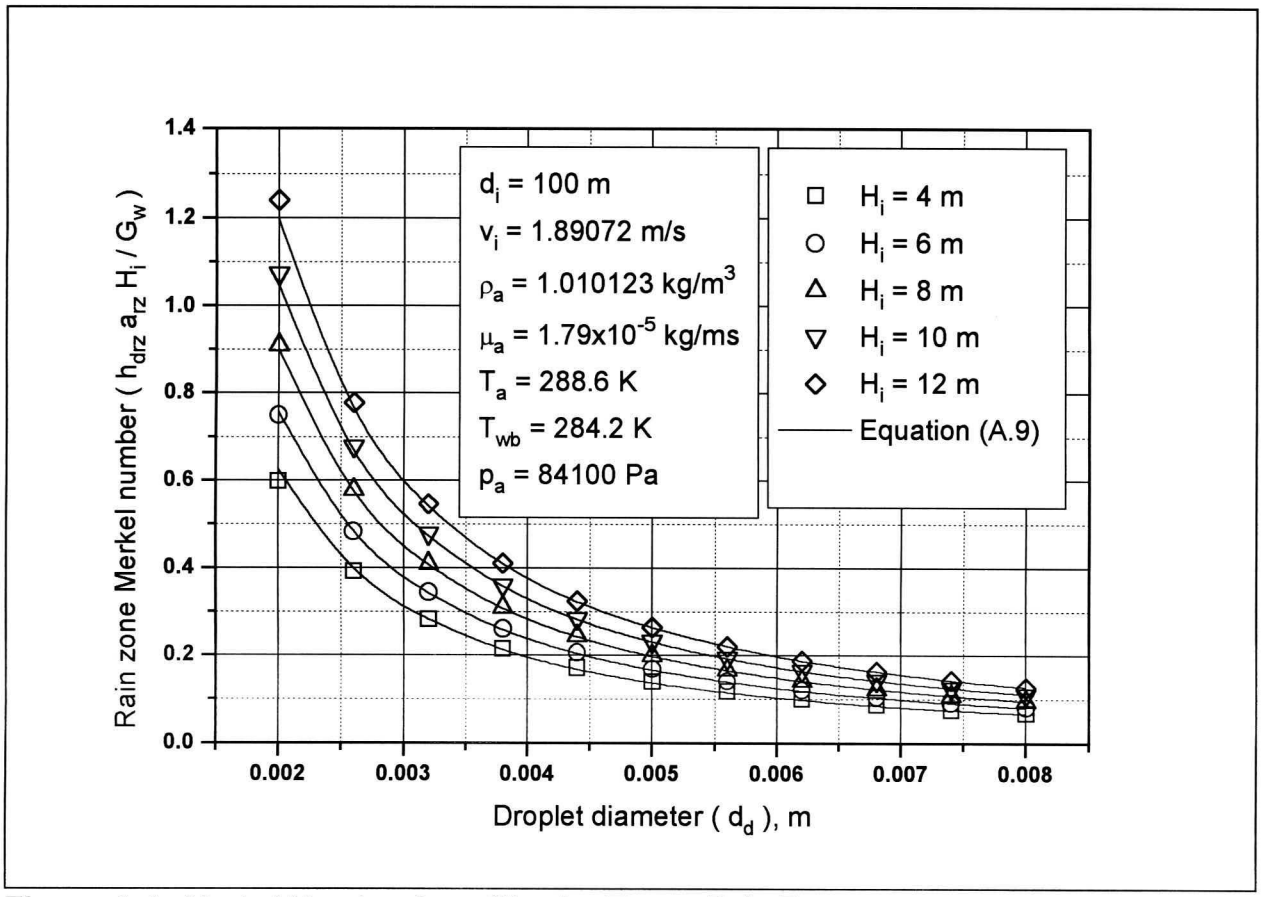

Figure A.1: *Merkel Number for a Circular Tower Rain Zone.*

It is interesting to note that the rain zone Merkel number, is completely independent of the water mass flow rate. This will be true as long as the water is distributed uniformly throughout the rain zone and derives from the definition for the Merkel number.

A similar analysis produces the following equation for the Merkel number of a rectangular tower rain zone,

$$\begin{aligned}\frac{h_{drz}a_{rz}H_i}{G_w} = 3.6&\left(\frac{p_a}{R_vT_a}/\rho_w\right)\left(\frac{D}{v_i d_d}\right)\left(\frac{H_i}{d_d}\right)Sc^{0.33}\times\ln\left[\frac{w_s+0.622}{w+0.622}\right]/\left[w_s-w\right]\\ &\times\left[4.6885a_\rho\rho_a-187128.7a_\mu\mu_a-2.2932+22.412\times\left[0.3504(a_v v_i)^{1.3805}+0.09\right]\right.\\ &\times\left[1.6093(a_L H_i)^{-1.1208}+0.66\right]\times\left[34.6765(a_L d_d)^{0.73245}+0.45\right]\\ &\left.\times e^{\left[7.739e^{-0.3998a_L H_i}\times\ln\left[0.0875e^{0.02662a_L W_i}+0.85\right]\right]}\right]\end{aligned} \tag{A.10}$$

Equation (A.10) is valid over the same range and utilises the same "a-" coefficients as the rectangular rain zone loss equation [eq. (2.74)].

The mass transfer coefficient for a one-dimensional counterflow rain zone (derived in the same manner) is,

$$\begin{aligned}\frac{h_{drz}a_{rz}H_i}{G_w} = 3.6&\left(\frac{p_a}{R_vT_a}/\rho_w\right)\left(\frac{D}{v_i d_d}\right)\left(\frac{H_i}{d_d}\right)Sc^{0.33}\times\ln\left[\frac{w_s+0.622}{w+0.622}\right]/\left[w_s-w\right]\\ &\times\left\{5.011a_\rho\rho_a-192121.7a_\mu\mu_a-2.577+23.618\times\left[0.254(a_v v_i)^{1.670}+0.18\right]\right.\\ &\left.\times\left[0.8367(a_L H_i)^{-0.53}+0.42\right]\times\left[43.07(a_L d_d)^{0.7947}+0.52\right]\right\}\end{aligned} \tag{A.11}$$

Again, restrictions are the same as for the pressure drop equation [eq. (2.76)] and global "a-" coefficients apply.

APPENDIX B

COOLING TOWER PERFORMANCE PREDICTION

All of the preceding chapters in this thesis deal with the acquisition of coefficients and correlations to describe the processes present within cooling towers. These correlations are for use in a one-dimensional point model of counterflow wet-cooling towers. In this section, a sample solution of the point model for a circular cooling tower will be undertaken. In addition, the influence of various factors (that were highlighted during this study) on the performance of the tower will be investigated.

B.1 Sample Calculations for Natural Draft Counterflow Wet-cooling Tower

For the sample solution, one of the hyperbolic natural draft counterflow wet-cooling towers, operated at ESKOM's Duhva power plant (Fig. B.1), was simulated.

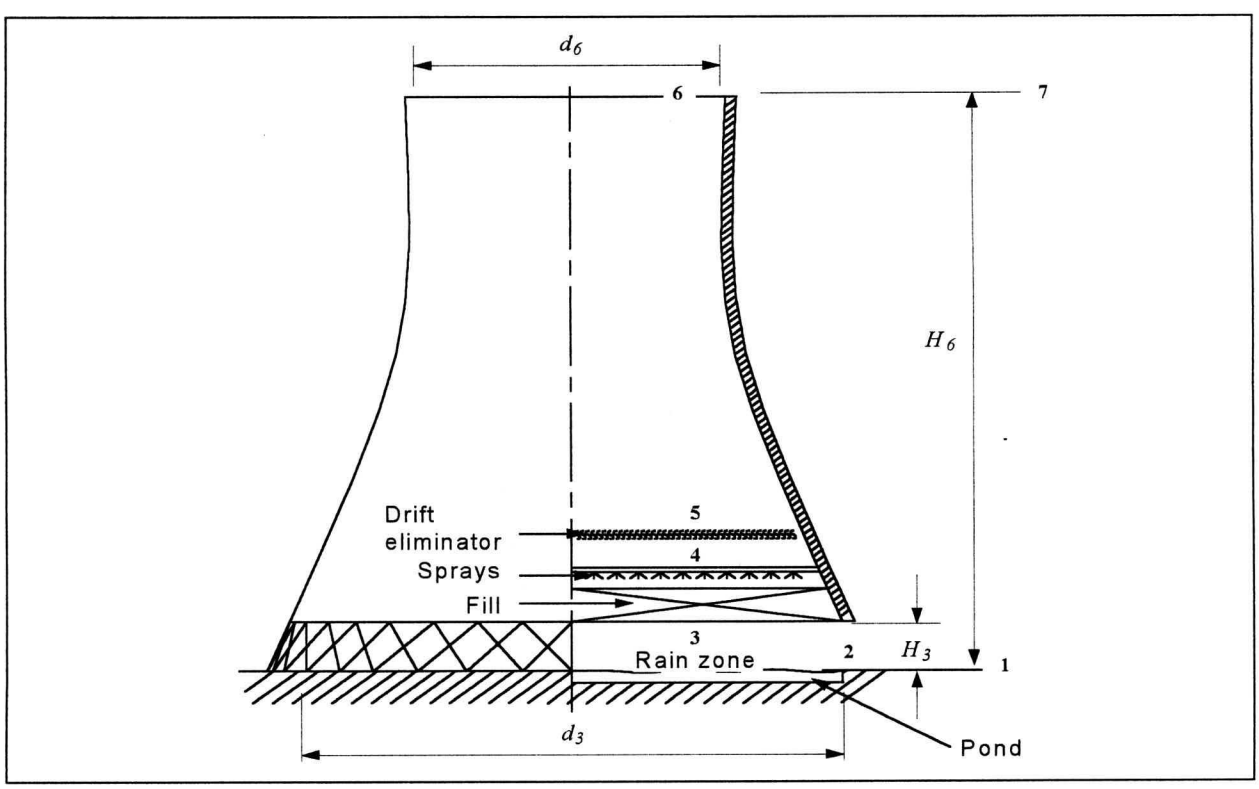

Figure B.1: *Geometry of Sample Tower.*

The problem requires an iterative procedure to satisfy both the energy and draft equations. Consequently, a program, NDCFWCT (Natural Draft CounterFlow Wet-Cooling Tower), was written to solve the point model tower, the last iteration of which is presented in this section.The analysis is based on the cooling tower performance evaluation approach proposed by Kröger [98KR1].

B.1.1 Tower Geometry and Operating Conditions

The water and air flow distribution through the fill is assumed to be uniform .The inside diameter of the upper section of the tower is constant, the tower has a sharp inlet and the following geometry and operational conditions apply,

Ambient conditions:

Air temperature at ground level	T_{a1}	=	15.45 °C (288.6K)
Wetbulb temperature at ground level	T_{wb}	=	11.05 °C (284.2K)
Atmospheric pressure	p_{a1}	=	84100 N/m^2
Ambient temperature gradient from ground level	dT_a / dz	=	-0.00975 K / m

Water characteristics:

Water mass flow rate	m_w	=	12500 kg / s
Water inlet temperature	$T_{wi} = T_{w5}$	=	40 °C (313.15K)

Cooling tower specifications:

Tower height	H_6	=	126.45 m
Tower inlet height	H_3	=	7.25 m
Tower inlet diameter	d_3	=	90.95 m
Tower outlet diameter	d_6	=	55.2 m
Number of tower supports	n_{ts}	=	62
Length of tower supports	L_{ts}	=	7.25 m
Diameter of supports	d_{ts}	=	0.7 m
Tower support drag coefficient	C_{Dts}	=	1.0

Inlet shell thickness	t_s	=	0.86 m

Fill specifications:

The cooling tower is fitted with an asbestos film type (orthotropic) fill (L_{fi} = 2.4 m) for which the characteristics are:

Length of the fill	L_{fi}	=	2.4 m

Fill Merkel number

$$\frac{h_{dfi} a_{fi} L_{fi}}{G_w} = L_{fi} \times 0.5037 \left(\frac{G_w}{G_a} \right)^{-0.71}$$

Fill static loss coefficient

$$K_{fi}^{*} = L_{fi} \times \left(0.9725 \left(\frac{G_w}{G_a} \right) + 1.70 \right)$$

Other specifications:

Depth of the spray zone above the fill	L_{sp}	=	0.925 m
Mean droplet diameter in rain zone	d_d	=	0.005 m
Pressure drop coefficient for contraction and fill supports	$K_{fs} + K_{ctc}$	=	0.5
Loss coefficient for water distribution system	K_{wd}	=	0.5
Kinetic energy coefficient at the tower outlet	α_{e6}	=	1.01

The pressure drop coefficient for the type C drift eliminator is given by [98KR1]

$$K_{de} = 27.4892\, Ry^{-0.14247}$$

B.1.2 Performance Evaluation

The converged solution of the problem, obtained with the program NDCFWCT, gives the following values for the unknown tower properties. These values satisfy both the energy and draft equations and will be used in further calculations.

Mean air-vapour mass flow rate through the fill	m_{av15}	=	12456.431 kg / s
Static pressure above the drift eliminator	p_{a5}	=	83955.287 N / m^2
Air temperature above the drift eliminator	T_{a5}	=	29.6539 °C (302.8039 K)
Mean recooled water temperature in the pond	$T_{wo} = T_{w1}$	=	21.9852 °C (295.1352 K)
Static pressure at the tower outlet	p_{a6}	=	82851.225 N / m^2

Fluid properties

At the specified air inlet drybulb temperature of T_{a1} = 288.6 K and wetbulb temperature of T_{wb} = 284.2 K, find the thermophysical properties employing the equations given in Appendix C.

Humidity ratio of air at inlet	w_1	=	8.127×10^{-3} kg / kg	(C.10)
Density of air vapour mixture	ρ_{av1}	=	1.0101 kg / m^3	(C.8)
Viscosity of the air vapour mixture	μ_{av1}	=	1.7857×10^{-5} kg / ms	(C.12)

The enthalpy of the inlet air is found according to equation (C.9) with c_{pa1} = 1006.44 J / kgK and c_{pv1} = 1869.2 J / kgK being evaluated at (T_{a1} + 273.15)/2 = 280.875 K according to equations (C.2) and (C.5) respectively. The latent heat is found to be $i_{fgw0} = 2.5016 \times 10^6$ J / kgK according to equation (C.18) at 273.15 K. With these values find i_{ma1} = 36114.71 J / kg dry air.

If the air is assumed to be saturated immediately after the drift or droplet eliminator , the wetbulb temperature at 5 will be equal to the given drybulb temperature T_{a5} = 302.8039 K at this elevation. The corresponding thermophysical properties at 5, can be determined according to the equations given in Appendix C.

Saturated vapour pressure	p_{v5}	=	4159.037 N/m^2	(C.4)
Humidity ratio	w_5	=	0.03259 kg/kg	(C.10)
Density of air-vapour	ρ_{av5}	=	0.94761 kg/m^3	(C.8)
Dynamic viscosity of air	μ_{a5}	=	1.86×10^{-5} kg/ms	(C.3)
Dynamic viscosity of vapour	μ_{v5}	=	1.0132×10^{-5} kg/ms	(C.7)
Dynamic viscosity of air-vapour	μ_{av5}	=	1.82616×10^{-5} kg/ms	(C.12)

The enthalpy of the saturated air at 5 is found according to equation (C.9) with c_{pa5} = 1006.5899 J/kgK and c_{pv5} = 1875.187 J/kgK being evaluated at (T_{a5} + 273.15)/2 = 287.9770 K according to equations (C.2) and (C.5) respectively. With these values and i_{fgw0} = 2.5016×10^6 J/kgK find i_{ma5} = 113185.1733 J/kg dry air.

The approximate harmonic mean density of the air vapour in the fill is given by,

$$\rho_{av15} = 2/\left(\frac{1}{\rho_{av1}}+\frac{1}{\rho_{av5}}\right) \qquad (B.1)$$

$$= 2/\left(\frac{1}{1.0101}+\frac{1}{0.94762}\right) = 0.97787 \text{ kg/m}^3$$

The dry air mass flow rate can be determined from the following relation:

$$m_{av15} = \left(m_a(1+w_1)+m_a(1+w_5)\right)/2 \qquad (B.2)$$

or

$$m_a = 2m_{av15}/(2+w_1+w_5) \qquad (B.3)$$

$$= 2\times12456.43/(2+0.008127+0.032589) = 12207.90 \text{ kg/s}$$

The respective air-vapour mass flow rates upstream and down stream of the fill are thus:

$$m_{av1} = m_a(1+w_1) = 12207.90\ (1 + 0.008127) = 12307.12 \text{ kg/s} \quad \text{(B.4)}$$

and

$$m_{av5} = m_a(1+w_5) = 12207.90\ (1 + 0.032589\ ) = 12605.74 \text{ kg/s} \quad \text{(B.5)}$$

The corresponding mass fluxes are

$$G_{av15} = m_{av15} / A_{fr} = 12456.43 / 6496.737 = 1.91734 \text{ kg/m}^2\text{s} \quad \text{(B.6a)}$$

$$G_a = m_a / A_{fr} = 12207.90 / 6496.737 = 1.87908 \text{ kg/m}^2\text{s} \quad \text{(B.6b)}$$

$$G_{av1} = m_{av1} / A_{fr} = 12307.12 / 6496.737 = 1.89435 \text{ kg/m}^2\text{s} \quad \text{(B.6c)}$$

$$G_{av5} = m_{av5} / A_{fr} = 12605.74 / 6496.737 = 1.94032 \text{ kg/m}^2\text{s} \quad \text{(B.6d)}$$

where $A_{fr} = \pi(d_3/2)^2 = \pi(90.95/2)^2 = 6496.737 \text{ m}^2$.

According to equation (C.16) the specific heat of water is c_{pwm} = 4178.21 J/kg evaluated at the mean water temperature of $(T_{wi} + T_{wo})/2$ = (313.15 + 295.1352)/2 = 304.1426 K.

At the mean outlet temperature of the water T_{wo} = 295.1352 K find,

Density of water	ρ_{wo}	=	997.73951 kg/m^3	(C.15)
Surface tension	σ_{wo}	=	0.07247 N/m	(C.19)

The mass velocity for the water based on the frontal area of the fill is

$$G_w = \frac{m_w}{A_{fr}} = 12500 / 6496.737 = 1.92404 \text{ kg/m}^2\text{s} \tag{B.7}$$

Heat and mass transfer

Heat and mass transfer in a counterflow wet-cooling tower occurs mainly in the rain zone, the fill and the area between the sprays and the packing. The Merkel number for the spray zone can be found from an equation that correlates the data of Lowe and Christie [61LO1]

$$\frac{h_{dsp} a_{sp} L_{sp}}{G_w} = 0.2 L_{sp} \left(\frac{G_w}{G_a} \right)^{-0.5} \tag{B.8}$$

$$= 0.2 \cdot 0.925 \cdot \left(\frac{1.92404}{1.87908} \right)^{-0.5} = 0.182826$$

The Merkel number applicable to the fill is specified, i.e.

$$\frac{h_{dfi} a_{fi} L_{fi}}{G_w} = 0.5037 L_{fi} \left(\frac{G_w}{G_a} \right)^{-0.71}$$

$$= 0.5037 \cdot 2.4 \left(\frac{1.92404}{1.87908} \right)^{-0.71} = 1.18876$$

The transfer coefficient in the rain zone can be calculated with the use of equation (A.9). The "a" coefficients used in the correlations for the rain zone Merkel number and loss coefficient are found from the following equations.

$$a_\mu = 3.061 \times 10^{-6} \left[\frac{\rho_{wo}^4 g^9}{\sigma_w} \right]^{0.25} \tag{2.66a}$$

$$= 3.061 \times 10^{-6} \left[\frac{997.7395^4 \times 9.8^9}{0.07247} \right]^{0.25} = 1.00022$$

$$a_\rho = \frac{998.0}{\rho_{wo}} \tag{2.66b}$$

$$= \frac{998.0}{997.7395} = 1.00026$$

$$a_v = 73.298\left[\frac{g^5\sigma_{wo}^3}{\rho_{wo}^3}\right]^{0.25} \tag{2.66c}$$

$$= 73.298\left[\frac{9.8^5 \times 0.07247^3}{997.7395^3}\right]^{0.25} = 0.99999$$

and

$$a_L = 6.122\left[\frac{g\sigma_{wo}}{\rho_{wo}}\right]^{0.25} \tag{2.66d}$$

$$= 6.122\left[\frac{9.8 \times 0.07247}{997.7395}\right]^{0.25} = 0.99998$$

Further quantities needed to evaluate the rain zone transfer coefficient are,

The humidity ratio of saturated air at T_{wo} $w_{s1} = 0.020264$ kg/kg (C.10)

Diffusion coefficient at inlet conditions $D_1 = 2.2997 \times 10^{-5}$ m^2 / s (C.14)

the Schmidt number, $Sc = \frac{\mu_{av1}}{\rho_{av1} D_1} = = \frac{1.7857 \times 10^{-5}}{1.0101 \times 2.997 \times 10^{-5}} = 0.7687$

and the air-vapour velocity before the fill

$$v_{av3} = \frac{m_{av1}}{\rho_{av1} A_{fr}} = 1.875370 \text{ m/s} \tag{B.9}$$

With these values find

$$\frac{h_{drz}a_{rz}H_3}{G_w} = 12\left(\frac{D_1}{v_{av3}d_d}\right)\left(\frac{H_3}{d_d}\right)\left(\frac{p_{a1}}{R_{wv}T_{a1}}/\rho_{wo}\right)Sc^{0.33}\ln\left[\frac{w_{s1}+0.622}{w_1+0.622}\right]/\left[w_{s1}-w_1\right]$$
$$\times\Big[.90757a_\rho\rho_{av1} - 30341.04a_\mu\mu_{av1} - 0.37564$$
$$+ 4.04016\times\Big[\left(0.55+41.7215(a_Ld_d)^{0.80043}\right)\times\left(0.713+3.741(a_LH_3)^{-1.23456}\right)$$
$$\times\left(3.11e^{0.15a_vv_{av3}} - 3.13\right)$$
$$\times e^{\left[\left(5.3759e^{-0.2092a_LH_3}\right)\times\ln\left(0.3719e^{0.00191a_Ld_3}+0.55\right)\right]}\Big]\Big] \qquad \text{(A.9)}$$

$$= 12\left(\frac{2.2997\times10^{-5}}{1.8754\times0.005}\right)\left(\frac{7.25}{0.005}\right)\left(\frac{84100}{461.52\times288.6}/997.7395\right)0.7687^{0.33}$$
$$\times\ln\left[\frac{0.020264+0.622}{0.008127+0.622}\right]/\left[0.020264-0.008127\right]$$
$$\times\Big[.90757\times1.00026\times1.0101 - 30341.04\times1.00022\times1.7857\times10^{-5} - 0.37564$$
$$+ 4.04016\times\Big[\left(0.55+41.7215(0.99998\times0.005)^{0.80043}\right)$$
$$\times\left(0.713+3.741(0.99998\times7.25)^{-1.23456}\right)\times\left(3.11\exp(0.15\times0.99999\times1.8754)-3.13\right)$$
$$\times\exp\Big[\left(5.3759\exp(-0.2092\times0.99998\times7.25)\right)$$
$$\times\ln\left(0.3719\exp(0.00191\times0.99998\times90.95)+0.55\right)\Big]\Big] = 0.184118$$

The Merkel relation will now be applied to the entire wet region, between the inlet of the rain zone and the outlet of the spray zone, over the frontal area of the fill. Since most of the heat and mass transfer occurs in the fill, it is important that the same procedure that was used to determine the fill transfer characteristics be followed to evaluate its performance in the cooling tower.

By adding the transfer coefficients find

$$\frac{h_{drz}a_{rz}H_3}{G_w}+\frac{h_{dfi}a_{fi}L_{fi}}{G_w}+\frac{h_{dsp}a_{sp}L_{sp}}{G_w} = 0.182826 + 1.188755 + 0.184118 = 1.555699$$

$$= \int_{Two}^{Twi} \frac{c_{pw} dT_w}{(i_{masw} - i_{ma})} \tag{B.10}$$

If the four point form of the Chebyshev integral is applied to this relation, the integral on the right hand side can be expressed as

$$\int_{Two}^{Twi} \frac{c_{pw} dT_w}{(i_{masw} - i_{ma})} = \frac{c_{pwm}(T_{wi} - T_{wo})}{4} \left(\frac{1}{\Delta i_{(1)}} + \frac{1}{\Delta i_{(2)}} + \frac{1}{\Delta i_{(3)}} + \frac{1}{\Delta i_{(4)}} \right) \tag{B.11}$$

The enthalpy differentials are dependent on the following intermediate temperatures:

$T_{w(1)} = T_{wo} + 0.1\ (313.15 - T_{wo}) = 295.1352 + 0.1(313.15 - 295.1352) = 296.9367$ K (B.12a)

$T_{w(2)} = T_{wo} + 0.4\ (313.15 - T_{wo}) = 295.1352 + 0.4(313.15 - 295.1352) = 302.3411$ K (B.12a)

$T_{w(3)} = T_{wo} + 0.6\ (313.15 - T_{wo}) = 295.1352 + 0.6(313.15 - 295.1352) = 305.9441$ K (B.12a)

$T_{w(4)} = T_{wo} + 0.9\ (313.15 - T_{wo}) = 295.1352 + 0.9(313.15 - 295.1352) = 311.3485$ K (B.12a)

The bracketed subscript numbers refer to the intervals in the Chebyshev integral and should not be confused with the numbers indicating various positions in the cooling tower.

To find the corresponding increments in enthalpy, determine the enthalpy of saturated air at $T_{w(1)}$ = 296.9367 K. The relevant specific heat of air and water vapour respectively are evaluated at $(T_{w(1)} + 273.15)/2 = (296.9367 + 273.15)/2 + 285.0434$ K.

Specific heat of air $c_{pa(1)} = 1006.522$ J / kgK (C.2)

Specific heat of water vapour $c_{pv(1)} = 1872.698$ J / kgK (C.5)

The pressure of saturated water vapour at $T_{w(1)}$ follows from equation (C.4) and the corresponding humidity ratio from equation (C.10) evaluated at p_{a15}.

Pressure of the water vapour $p_{vs(1)} = 2944.784 \text{ N/m}^2$ (C.4)

Humidity ratio $w_{s(1)} = 0.022706 \text{ kg/kg}$ (C.10)

With these values determine the enthalpy of saturated air at $T_{w(1)}$ according to equation (C.9)

$$i_{masw(1)} = c_{pa(1)} (T_{w(1)} - 273.15) + w_{s(1)} [i_{fgw0} + c_{pv(1)} (T_{w(1)} - 273.15)] \quad \text{(C.9)}$$

$$= 1006.522(296.9367-273.15)+0.0227 [2.5106\times10^{6}+1872.698(296.9367-273.15)]$$

$$= 81755.32 \text{ J/kg dry air}$$

The enthalpy of the air at $T_{w(1)}$ can be determined by applying an energy balance over the frontal area.

$$i_{ma(1)} = m_w c_{pwm} (T_{w(1)} - T_{wo}) / m_a + i_{ma1} \quad \text{(B.13)}$$

$$= 12500\times4178.213(296.9367-295.1352)/12207.90+36114.729$$

$$= 43821.774 \text{ J/kg dry air}$$

With these values find the difference in enthalpy

$$\Delta i_{(1)} = i_{masw(1)} - i_{ma(1)} = 81755.32 - 43821.774 = 37933.5503 \text{ J/kg dry air} \quad \text{(B.14)}$$

Repeat the above procedure in the case of the other three intermediate temperatures and find

$\Delta i_{(2)} = 43369.67$ J/kg dry air

$\Delta i_{(3)} = 51459.63$ J/kg dry air

$\Delta i_{(4)} = 72351.87$ J/kg dry air

Substitute these values into the approximate expression for the integral and find

$$\int_{Two}^{Twi} \frac{c_{pw}dT_w}{(i_{masw} - i_{ma})} = \frac{c_{pwm}(T_{wi} - T_{wo})}{4}\left(\frac{1}{\Delta i_{(1)}} + \frac{1}{\Delta i_{(2)}} + \frac{1}{\Delta i_{(3)}} + \frac{1}{\Delta i_{(4)}}\right) \qquad \text{(B.11)}$$

$$= \frac{4178.213(313.15 - 295.135)}{4}\left(\frac{1}{37933.55} + \frac{1}{43369.67} + \frac{1}{51459.63} + \frac{1}{72351.87}\right)$$

$$= 1.555698$$

This value is, for all practical purposes, identical to the value obtained by adding the transfer coefficients in the three wet zones, which means that the water outlet temperature, T_{wo} = 295.135 K, is correct.

Previous researchers [95OO1] have shown, with the aid of scale model experiments, that recirculating air in the fill forms 'dead' regions, where little or no effective heat transfer occurs. The CFD simulations have shown, however, that these regions shrink to negligible size when a rain zone is added to the cooling tower and can, therefore, be ignored for wet-cooling towers. If it is assumed that the water and air flow through the fill is uniform, the heat rejected by the cooling tower is thus

$$Q_w = m_w c_{pwm} (T_{wi} - T_{wo}) \qquad \text{(B.15)}$$

$$= 12500 \times 4178.213 \ (313.15 - 295.135) = 940.8686 \text{ MW}$$

The correctness of the temperature of the saturated air leaving the spray zone T_{a5} can be confirmed with the aid of the energy equation, i.e.

$$Q_a = m_a (i_{ma5} - i_{ma1}) \qquad \text{(B.16)}$$

$$= 12207.90 \ (113185.17 - 36114.729) = 940.8686 \text{ MW}$$

The heat transfer rates for the water and air side, Q, are in agreement, which implies that the value for T_{a5} is correct and the energy balance is satisfied.

Loss coefficients

All flow resistances must be calculated in terms of average fill conditions for the purpose of solving the draft equation. The specified loss coefficient due to the fill support structure and contraction losses in the fill entrance, referred to the mean density and mass flow rate through the fill, is found from

$$K_{fsfi} + K_{ctcfi} = 0.5\left(\frac{\rho_{av15}}{\rho_{av1}}\right)\left(\frac{m_{av1}}{m_{av15}}\right)^2 \qquad \text{(B.17)}$$

$$= 0.5\left(\frac{0.97787}{1.0101}\right)\left(\frac{12307.12}{12456.43}\right)^2 = 0.47250$$

According to the specified static fill loss coefficient

$$K^*_{fi} = L_{fi} \times \left(0.9725\left(\frac{G_w}{G_a}\right) + 1.70\right)$$

$$= 2.4 \times \left(0.9725\left(\frac{1.9240}{1.8791}\right) + 1.70\right) = 6.469845$$

If dynamic effects are taken into account, the actual fill loss coefficient applicable to the cooling tower is given by

$$K_{fi} = K^*_{fi} + \frac{G^2_{av5}/\rho_{av5} - G^2_{av1}/\rho_{av1}}{G^2_{av15}/\rho_{av15}} \qquad \text{(B.18)}$$

$$= K^*_{fi} + \frac{1.94032^2/0.94762 - 1.89435^2/1.0101}{1.91734^2/0.97787} = 6.581658$$

The loss through the spray zone above the fill (referred to fill conditions) is given by Cale [82CA1] as

$$K_{spfi} = L_{sp}\left[0.4\left(\frac{G_w}{G_a}\right) + 1\right]\left(\frac{\rho_{av15}}{\rho_{av5}}\right)\left(\frac{m_{av5}}{m_{av15}}\right)^2 \qquad \text{(B.19)}$$

$$= 0.925\left[0.4\left(\frac{1.9240}{1.8791}\right)+1\right]\left(\frac{0.97787}{0.94762}\right)\left(\frac{12605.74}{12456.43}\right)^2 = 1.377932$$

For the water distribution system

$$K_{wdfi} = 0.5\left(\frac{\rho_{av15}}{\rho_{av5}}\right)\left(\frac{m_{av5}}{m_{av15}}\right)^2 \qquad \text{(B.20)}$$

$$= 0.5\left(\frac{0.97787}{0.94762}\right)\left(\frac{12605.74}{12456.43}\right)^2 = 0.528408$$

The loss coefficient for the specified type-c drift eliminator based on fill conditions is

$$K_{defi} = 27.4892\, Ry^{-0.14247}\left(\frac{\rho_{av15}}{\rho_{av5}}\right)\left(\frac{m_{av5}}{m_{av15}}\right)^2 \qquad \text{(B.21)}$$

$$= 27.4892\left(\frac{m_{av5}}{\rho_{av5}\, Afr}\right)^{-0.14247}\left(\frac{\rho_{av15}}{\rho_{av5}}\right)\left(\frac{m_{av5}}{m_{av15}}\right)^2$$

$$= 27.4892\left(\frac{12605.74}{0.94762\times 6496.737}\right)^{-0.14247}\left(\frac{0.97787}{0.94762}\right)\left(\frac{12605.74}{12456.43}\right)^2 = 5.585464$$

The total loss in the vicinity of the fill, is found by summing all of the previously calculated loss coefficients

$$K_{he} = \left[K_{fs}+K_{ctc}+K_{fi}+K_{sp}+K_{wd}+K_{de}\right]_{fi} \qquad \text{(B.22)}$$

$$= 0.4725+6.5817+1.3780+0.5284+5.5855$$

$$= 14.5460$$

The loss coefficient due to the tower supports, referred to the fill, is given by

$$K_{tsfi} = \left[C_{dts}L_{ts}d_{ts}n_{ts}\frac{A_{fr}^2}{(\pi d_3 H_3)^3}\right]\left(\frac{\rho_{av15}}{\rho_{av1}}\right)\left(\frac{m_{av1}}{m_{av15}}\right)^2 \qquad \text{(B.23)}$$

$$= \left[1 \times 7.25 \times 0.7 \times 62 \times \frac{6496.737^2}{(\pi \times 90.95 \times 7.25)^3} \right] \left(\frac{0.97787}{1.0101} \right) \left(\frac{12307.12}{12456.43} \right)^2 = 1.411821$$

The inlet loss coefficient for a circular dry-cooling tower with orthotropic resistance (film type) packing and no inlet rounding can be determined according to equation (3.1) [94TE2]. The equation is valid if $10 \leq d_i / H_i \leq 15$ and $5 \leq K_{he} \leq 25$ and is therefore applicable to the current scenario where $d_3 / H_3 = 12.545$ and $K_{he} = 14.54596$. With the loss coefficient in the vicinity of the fill previously evaluated, find

$$K_{ctfi(dry)} = \left[100 - 18\left(\frac{d_3}{H_3} \right) + 0.94\left(\frac{d_3}{H_3} \right)^2 \right] \times K_{he}^{\left[-1.28 + 0.183\left(\frac{d_3}{H_3} \right) - 7.769E-3\left(\frac{d_3}{H_3} \right)^2 \right]} \times \left(\frac{\rho_{av15}}{\rho_{av1}} \right) \left(\frac{m_{av1}}{m_{av15}} \right)^2 \tag{3.1}$$

$$= \left[100 - 18\left(\frac{90.95}{7.25} \right) + 0.94\left(\frac{90.95}{7.25} \right)^2 \right] \times 14.546^{\left[-1.28 + 0.183\left(\frac{90.95}{7.25} \right) - 7.769E-3\left(\frac{90.95}{7.25} \right)^2 \right]} \times \left(\frac{0.97787}{1.0101} \right) \left(\frac{12307.12}{12456.43} \right)^2 = 12.01393$$

To find the inlet loss for an equivalent wet-cooling tower, the above result must be multiplied by the inlet loss correction factor that is given by equation (4.44)

$$dK_{ctrz} = \left[0.2394 + 80.1\left(\frac{0.0954}{d_3 / H_3} + d_d \right) e^{\left(0.395 \frac{G_w}{G_a} \right)} - 966\left(\frac{d_d}{d_3 / H_3} \right) e^{\left(0.686 \frac{G_w}{G_a} \right)} - 0.3195\left(\frac{G_w}{G_a} \right) \right] \times \left(1 - 0.06825 G_w \right) K_{he}^{0.09667} e^{8.7434(1/d_i - 0.01)} \tag{4.44}$$

$$= \left[0.2394 + 80.1\left(\frac{0.0954}{90.95/7.25} + 0.005 \right) e^{\left(0.395 \frac{1.9240}{1.8791} \right)} - 966\left(\frac{0.005}{90.95/7.25} \right) e^{\left(0.686 \frac{1.9240}{1.8791} \right)} \right]$$

$$-0.3195\left(\frac{1.9240}{1.8791}\right)\Big]\times(1-0.06825\times 1.9240)14.546^{0.09667}\,e^{8.7434(1/90.95-0.01)}$$

$$= 0.73791$$

Equation (4.44) is valid as long as $7.5 \le d_i / H_i \le 20$, $3 \le d_d \le 6\,\text{mm}$, $1 \le G_w \le 3\ \text{kg/m}^2\text{s}$, $1.2 \le G_a \le 3.6\ \text{kg/m}^2\text{s}$, $80 \le d_i \le 120\ \text{m}$ and $5 \le K_{fi} \le 25$, all of which are satisfied for the present case. The true value of the inlet loss coefficient can now be found from

$$K_{ctfi} = K_{ctfi(dry)} \times dK_{ctrz} \tag{B.24}$$

$$= 12.01393 \times 0.73791 = 8.865218$$

With equation (2.67), find the loss coefficient for the rain zone referred to fill conditions.

$$K_{rzfi} = 3a_v v_{w3}\left(\frac{H_3}{d_d}\right)\left(\frac{\rho_{av15}}{\rho_{av1}}\right)\left(\frac{m_{av1}}{m_{av15}}\right)^2\Big[0.22460 - 0.31467a_\rho\rho_{av1} + 5263.04a_\mu\mu_{av1}$$
$$+0.775526\times\Big[1.4824163e^{71.52a_L d_d} - 0.91\Big]\times\Big[0.39064e^{0.021824a_L d_3/2} - 0.17\Big]$$
$$\times\Big[2.0892(a_v v_{av3})^{-1.3944} + 0.14\Big]\times\exp\Big[(0.8449\ln(a_L\frac{d_3}{2}) - 2.312)$$
$$\times(0.3724\ln(a_v v_{av3}) + 0.7263)\times\ln\Big[206.757(a_L H_3)^{-2.8344} + 0.43\Big]\Big]\Big] \tag{2.67}$$

With the values of the "a-" coefficients identical to those employed in the mass transfer coefficient equation the value of the loss coefficient is found to be

$$K_{rzfi} = 3\times 0.99998\times 0.001928\left(\frac{7.25}{0.005}\right)\Big[0.22460 - 0.31467\times 1.00026\times 1.0101$$
$$+1.00022\times 5263.0\times 1.7857\times 10^{-5} + 0.775526\times\Big[1.4824e^{(71.52\times 0.99998\times 0.005)} - 0.91\Big]$$
$$\times\Big[0.39064e^{(0.010912\times 0.99998\times 90.95)} - 0.17\Big]\times\Big[2.0892(0.99999\times 1.8754)^{-1.3944} + 0.14\Big]$$
$$\times\exp\Big[(0.8449\ln(0.99998\times 90.95/2) - 2.312)\times(0.3724\ln(0.99999\times 1.8754) + 0.7263)$$
$$\times\ln\Big[206.757(0.99998\times 7.25)^{-2.8344} + 0.43\Big]\Big]\Big]\times\left(\frac{0.97787}{1.0101}\right)\left(\frac{12307.12}{12456.43}\right)^2$$
$$= 7.694738$$

where $v_w = G_w / A_{fr} = 1.92404 / 6496.737 = 0.0019284\,\text{m/s}$. The total loss referred to average fill conditions is

$$K_{tfi} = \left(K_{fs} + K_{ctc} + K_{fi} + K_{sp} + K_{wd} + K_{de} + K_{rz} + K_{ts} + K_{ct}\right)_{fi} \tag{B.25}$$

$$= 0.4725+6.5817+1.3780+0.5284+5.5855+7.694738+1.411821+8.865218$$

$$= 32.51774$$

Static pressures in the tower

At this stage it is possible to confirm the value of p_{a5} by using an abbreviated version of the draft equation [98KR1].

$$p_{a5} = p_{a1}\left[1-0.00975(H_3 + L_{fi}/2)/T_{a1}\right]^{3.5\times(1+w_1)\left[1-w_1/(w_1+0.62198)\right]} - K_{tfi}\times\left(\frac{m_{av15}}{A_{fr}}\right)^2 / (2\rho_{av15}) \tag{B.26}$$

$$= 84100\left[1-0.00975(7.25+2.4/2)/288.6\right]^{3.5\times(1+0.008127)\left[1-.008127/(.008127+0.62198)\right]} - 32.51774\times\left(\frac{12456.43}{6496.737}\right)^2 / (2\times 0.97787) = 83955.287\ \text{N/m}^2$$

This value is in agreement that used previously in calculations in this example.

To find the temperature lapse rate in the tower, the specific heat of water is evaluated at (T_{a5} + 273.15)/2 = (302.804 + 273.15)/2 = 287.977 K. According to equation (C.16) find c_{pw} = 4190.587 J/kgK. Using the previously obtained values for the specific heat of dry air and water vapour at this temperature, the lapse rate is found from an equation by Kröger [98KR1]

$$\xi_{T_{a5}} = \frac{-g(1+w_5)}{\left\{c_{pma} + \frac{7.966\times10^{14}}{p_{a5}T_{a5}^2}\left[i_{fgwo} - \left(c_{pw}-c_{pv}\right)(T_{a5}-273.15)\right]e^{(-5406.1915/T_{a5})}\right\}} \tag{B.27}$$

$$= -9.8(1+0.03259)/\left\{1067.70+\frac{7.966\times10^{14}}{83955.29\times302.804^2}\left[2.5016\times10^6-(4190.587-1875.187)\times(302.804-273.15)\right]e^{\left(\frac{-5406.1915}{302.804}\right)}\right\}$$

$$= -0.00183791\,\text{K/m}$$

To find the pressure difference (p_{a6} - p_{a7}) the air properties and corresponding Froude number must be determined at the tower outlet. Using the lapse rate obtained in equation (B.27) the air temperature at 6 may be determined.

$$T_{a6} = T_{a5}+\xi_{Ta5}\left(H_6-H_3-L_{fi}-L_{sp}\right) \tag{B.28}$$

$$= 302.804\text{-}0.00183791(126.45\text{-}7.25\text{-}2.4\text{-}0.925) = 302.591\ \text{K}$$

Assuming that the humidity remains constant, the corresponding density of the air-vapour mixture at this temperature is

$$\rho_{av6} = (1+w_5)\left[1-w_5/(w_5+0.62198)\right]p_{a6}/(RT_{a6}) \tag{C.8}$$

$$= (1+0.03259)\left[1-0.03259/(0.03259+0.62198)\right]82851.22/(287.08\times302.591)$$

$$= 0.93581\ \text{kg/m}^3$$

The ambient temperature at elevation 7 can be found from the ambient temperature gradient, with $H_7 = H_6$.

$$T_{a7} = T_{a1}+dT_a/dz\times H_6 = 288.6 - 0.00975\times126.45 = 287.367\ \text{K} \tag{B.29}$$

The pressure at 7 may be determined from an equation derived by Kröger [98KR1].

$$p_{a7} = p_{a1}\left[1-0.00975\,H_6/T_{a1}\right]^{3.5(1+w_1)\{1-w_1/(w_1+0.62198)\}} \tag{B.30}$$

$$= 84100\left[1 - 0.00975 \times \frac{126.45}{288.6}\right]^{3.5(1+0.008127)\{1 - 0.008127/(0.008127 + 0.62198)\}}$$

$$= 82855.302 \text{ N/m}^2$$

The corresponding density of the ambient air at elevation 7, assuming a uniform ambient humidity ratio w_1, is according to equation (C.8)

$$\rho_{av7} = (1+w_1)\left[1 - w_1/(w_1 + 0.62198)\right] p_{a7}/(RT_{a7}) \qquad \text{(C.8)}$$

$$= (1+0.008127)\left[1 - 0.008127/(0.008127 + 0.62198)\right] 82851.22/(287.08 \times 287.367)$$

$$= 0.99944 \text{ kg/m}^3$$

With no cold inflow these values yield

$$Fr_D = \left(\frac{m_{av5}}{A_6}\right)^2 / \left[\rho_{av6}(\rho_{av7} - \rho_{av6}) g d_6\right] \qquad \text{(B.31)}$$

$$= \left(\frac{12605.74}{\pi \times 0.25 \times 55.2^2}\right)^2 / \left[0.93581(0.99944 - 0.93581) 9.8 \times 55.2\right] = 0.861360$$

According to Du Preez and Kröger [94DU1] the difference in the mean pressure at the tower outlet (6) and the ambient pressure at the same elevation (7) is given by

$$p_{a6} = p_{a7} + \left[0.02 Fr_D^{-1.5} - 0.14/Fr_D\right] \times (m_{av5}/A_6)^2 / \rho_{av6} \qquad \text{(B.32)}$$

$$= 82855.30 + \left[0.02 \times 0.8614^{-1.5} - 0.14/0.8614\right] \times \left(\frac{12605.74}{0.25 \times \pi \times 55.2^2}\right)^2 / 0.93581$$

$$= 82851.2248 \text{ N/m}^2$$

which is in agreement with the value given initially.

Draft equation

The draft equation [98KR1] may now be solved using the above values. Upon substitution, the left hand side of the equation yields,

$$
\begin{aligned}
LH = p_{a1}\Bigg[& \left\{1-0.00975\left(H_3+L_{fi}/2\right)/T_{a1}\right\}^{3.5(1+w_1)\{1-w_1/(w_1+0.62198)\}} \\
& \times\left\{1+\xi_{Ta5}\left(H_6-H_3-L_{fi}/2\right)/T_{a5}\right\}^{-(1+w_5)\{1-w_5/(w_5+0.62198)\}g/(R\xi_{Ta5})} \\
& -\left\{1-0.00975H_6/T_{a1}\right\}^{3.5(1+w_1)\{1-w_1/(w_1+0.62198)\}} \\
& -\left(0.02Fr_D^{-1.5}-0.14/Fr_D\right)(m_{av5}/A_6)^2/\rho_{av6} \qquad \text{(B.33a)} \\
= 84100\Bigg[& \left\{1-0.00975(7.25+2.4/2)/288.6\right\}^{3.5(1+.008127)\{1-.008127/(.008127+0.62198)\}} \\
& \times\Bigg\{1-0.00183791(126.45-7.25-2.4/2) \\
& /\ 302.804\Bigg\}^{-(1+0.03259)\{1-0.03259/(0.03259+0.62198)\}\times 9.8/(287.08\times.00183791)} \\
& -\left\{1-0.00975\times 126.45/288.6\right\}^{3.5(1+.008127)\{1-.008127/(.008127+0.62198)\}}\Bigg] \\
& -\left(0.02\times 0.8614^{-1.5}-0.14/0.8614\right)\left(\frac{12605.74}{2393.14}\right)^2/0.93581 \\
= & \ 75.303054
\end{aligned}
$$

The value on the right hand side of the equation is

$$
\begin{aligned}
RH = & K_{tfi}\times(m_{av15}/A_{fr})^2/(2\rho_{av15}) \\
& \times\left\{1+\xi_{Ta5}\left(H_6-H_3-L_{fi}/2\right)/T_{a5}\right\}^{-(1+w_5)\{1-w_5/(w_5+0.62198)\}g/(R\xi_{Ta5})} \\
& +\alpha_{e6}(m_{av5}/A_6)^2/(2\rho_{av6}) \qquad \text{(B.33b)}
\end{aligned}
$$

$$= 32.51774 \times \left(\frac{12456.43}{6496.737}\right)^2 / (2 \times 0.97787)$$

$$\times \left\{1 - 0.00183791 \ (126.45 - 7.25 - 2.4/2) \right.$$

$$\left. / \ 302.804 \right\}^{-(1+0.03259)\{1-0.03259/(0.03259+0.62198)\} \times 9.8/(287.08 \times .00183791)}$$

$$+ 1.01\left(\frac{12605.74}{2393.14}\right)^2 / (2 \times 0.93581)$$

$$= 75.303011$$

The fact that the right and left hand sides of equation (B.33) are practically equal, signifies that the original air-vapour mass flow rate was chosen correctly and the solution has converged.

Finally, the amount of water lost due to evaporation is given by,

$$m_{w(evap)} = m_a \ (w_5 - w_1) = 12207.90 \ (0.03259 - .008127) = 298.625 \text{ kg/s} \qquad \text{(B.34)}$$

The dampening effect of the rain zone on the inlet loss is evident in this example. If the inlet loss correction factor is ignored, a heat rejection rate of Q = 927.051 MW is predicted by the tower point model program (NDCFWCT). This value is 1.469 percent lower than that obtained previously, a significant amount considering the large capacity of the cooling tower. The addition of the inlet loss correction factor, therefore, allows a less conservative approach to cooling tower design, with associated cost benefits. In the next section, additional measures, to improve the performance of existing cooling towers, will be explored.

B.2 Cooling Tower Performance Enhancement

It was shown in Appendix A that decreasing the rain zone droplet size improves a cooling tower's heat rejection rate. Smaller droplets can be generated, in cooling towers with film type packing, by adding a layer of splash pack to the bottom of the fill [97CR1]. In Chapter 3, a well rounded inlet was found to decrease a cooling towers inlet loss considerably. The air mass flux through the tower will increase, because of this reduced resistance and the tower cooling capacity will, therefore increase as well. Since both of these modifications are reasonably easy to implement on existing cooling towers, the consequences of applying these changes to the Duhva tower, simulated in the previous section, was investigated. The cooling tower simulation program, NDCFWCT, was used for this purpose.

The additional splash pack, simulated at the bottom of the fill, is of the expanded metal type developed by T.W. Baard [99BA1] shown in figure B.2 and similar in configuration to the isotropic fill material depicted in Chapter 3.

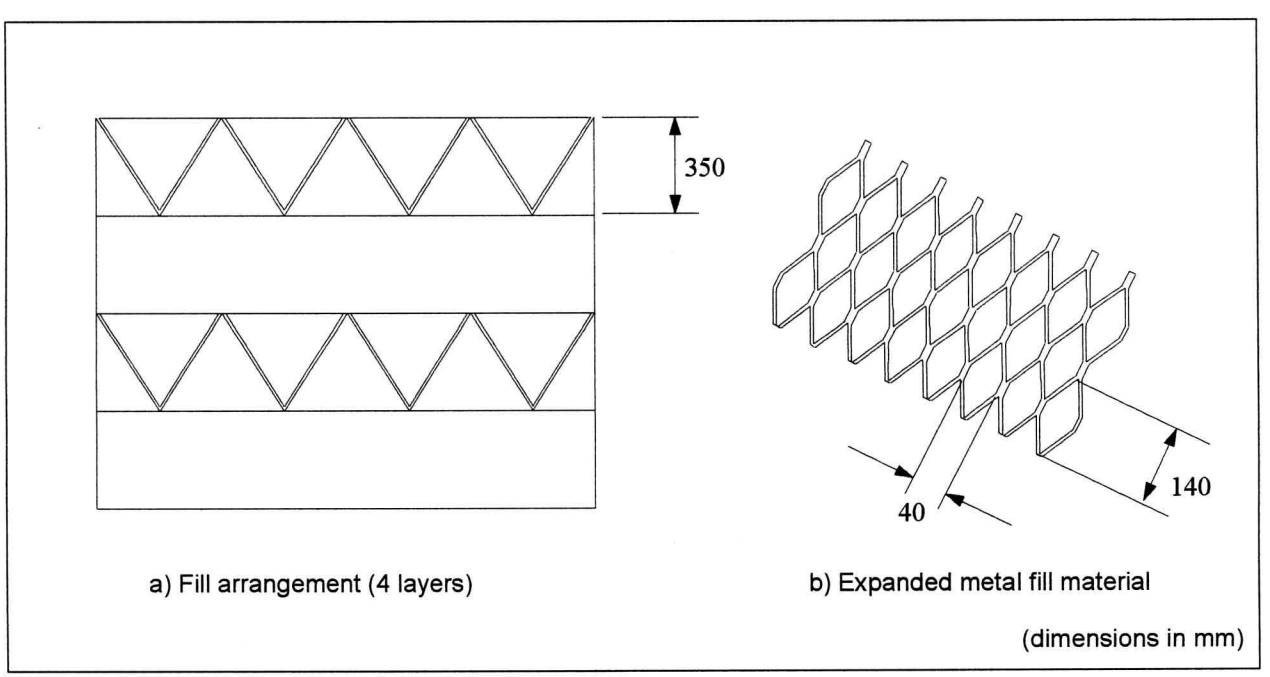

Figure B.2: *Expanded Metal Splash Type Fill.*

The fill mass transfer coefficient is given by [99BA1]

$$\frac{h_{dfi}a_{fi}L_{fi}}{G_w} = 0.4L_{fi}G_w^{-1.276}G_a^{0.615}$$

and the fill static loss coefficient by [99BA1]

$$K_{fi}^{*} = 4.357 L_{fi} G_w^{0.880} G_a^{-0.808}$$

When simulating the additional fill material, its transfer and loss characteristics are simply added to that of the existing fill. This approach is not strictly correct, since the splash pack experiences some crossflow, but serves in place of a more appropriate model. A droplet diameter of $d_d = 0.0035\text{m}$ is used in the rain zone when the splash type fill is present (on the basis of the experimental results at the end of Chapter 2) and the rain zone height is decreased by an amount equal to the additional fill length. The smallest unit of expanded metal fill is 0.35 m in length and it was, therefore simulated in corresponding increments.

The presence of a well rounded inlet is taken into account by substituting equation (3.3), which is valid for circular towers with orthotropic resistance fills and $r_{ir} / d_i \geq 0.01$, for the existing equation (eq. 3.1) for the inlet loss coefficient. The correlation for the inlet loss correction factor remains unchanged, except for the reduced droplet size and higher fill resistance.

Figures B.2 - B4 show the influence of these modifications on the cooling tower's performance. The improvement in tower output with the addition of only a thin layer of splash packing and a well rounded inlet is considerable.

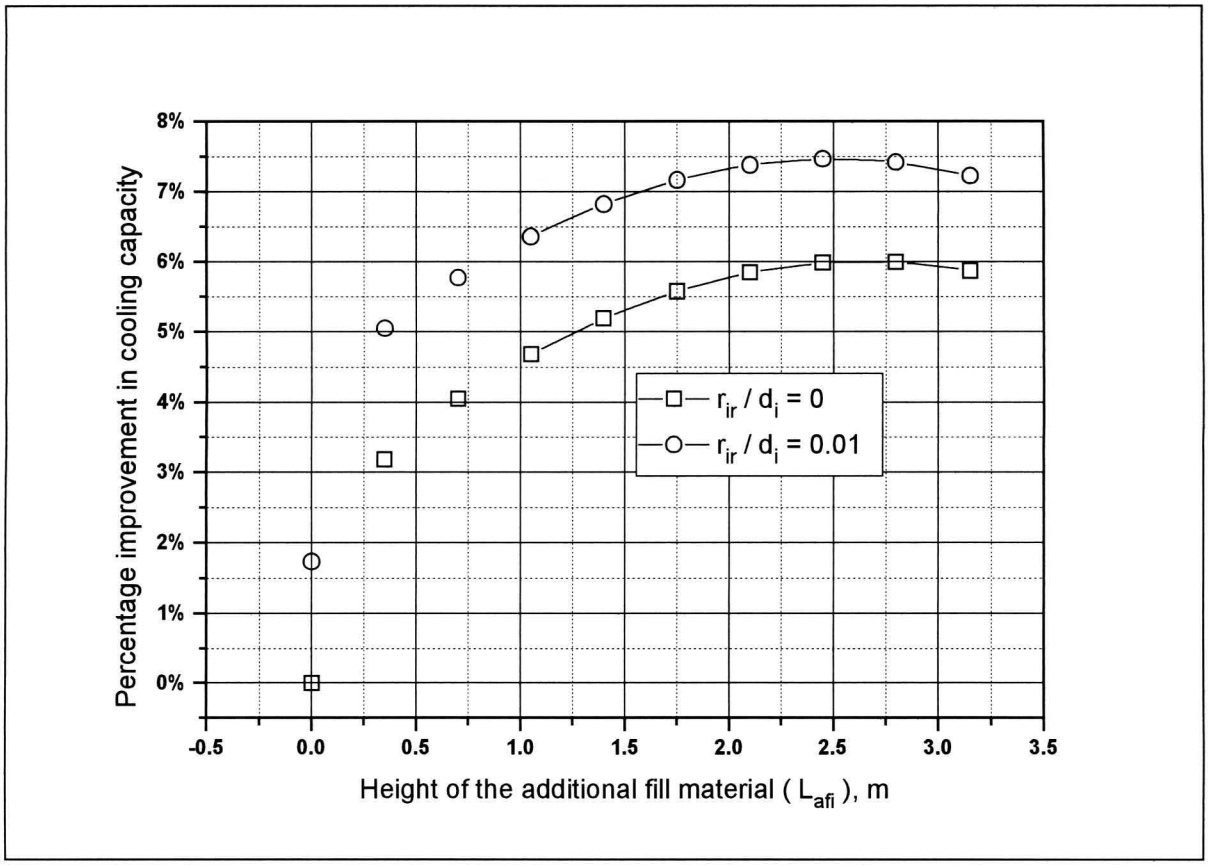

Figure B.3: *Influence of Added Fill Material and Inlet Rounding on Tower Performance.*

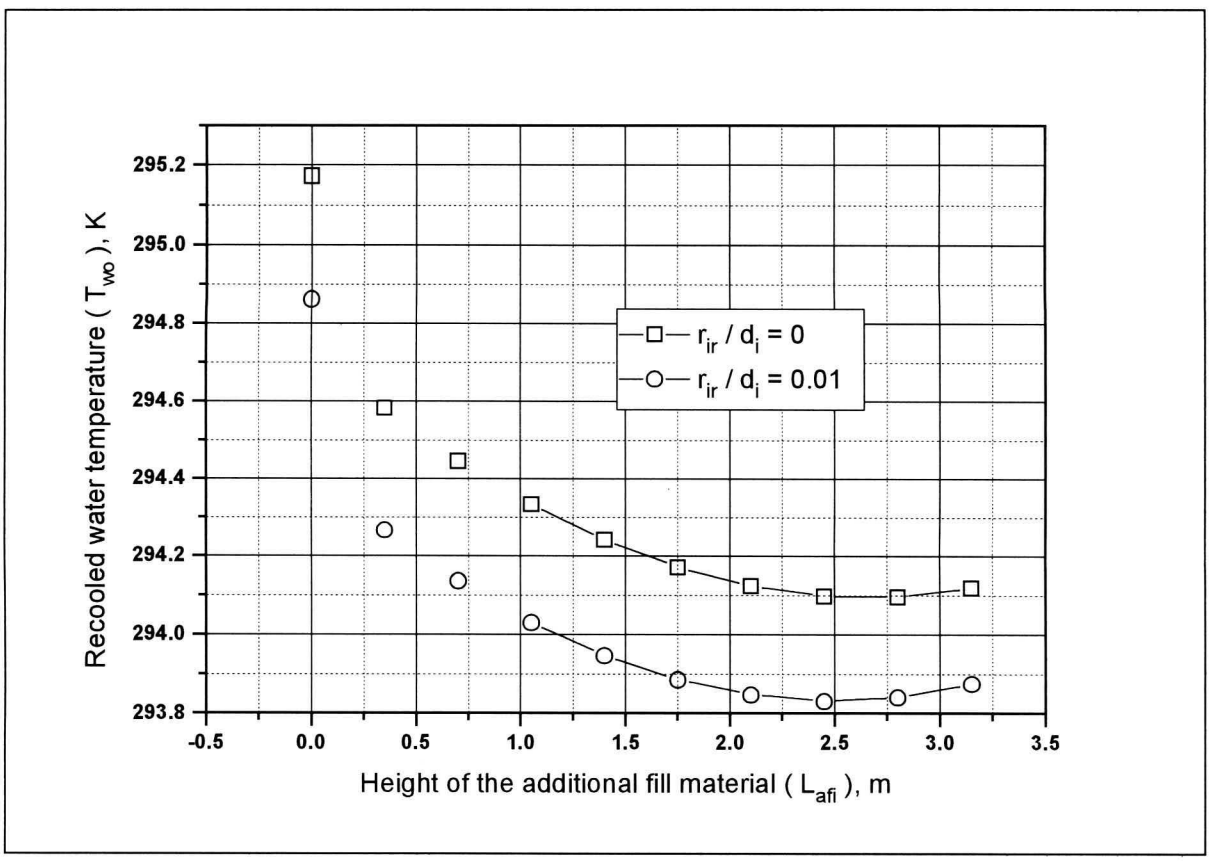

Figure B.4: *The influence of Tower Enhancement on the Water Outlet Temperature.*

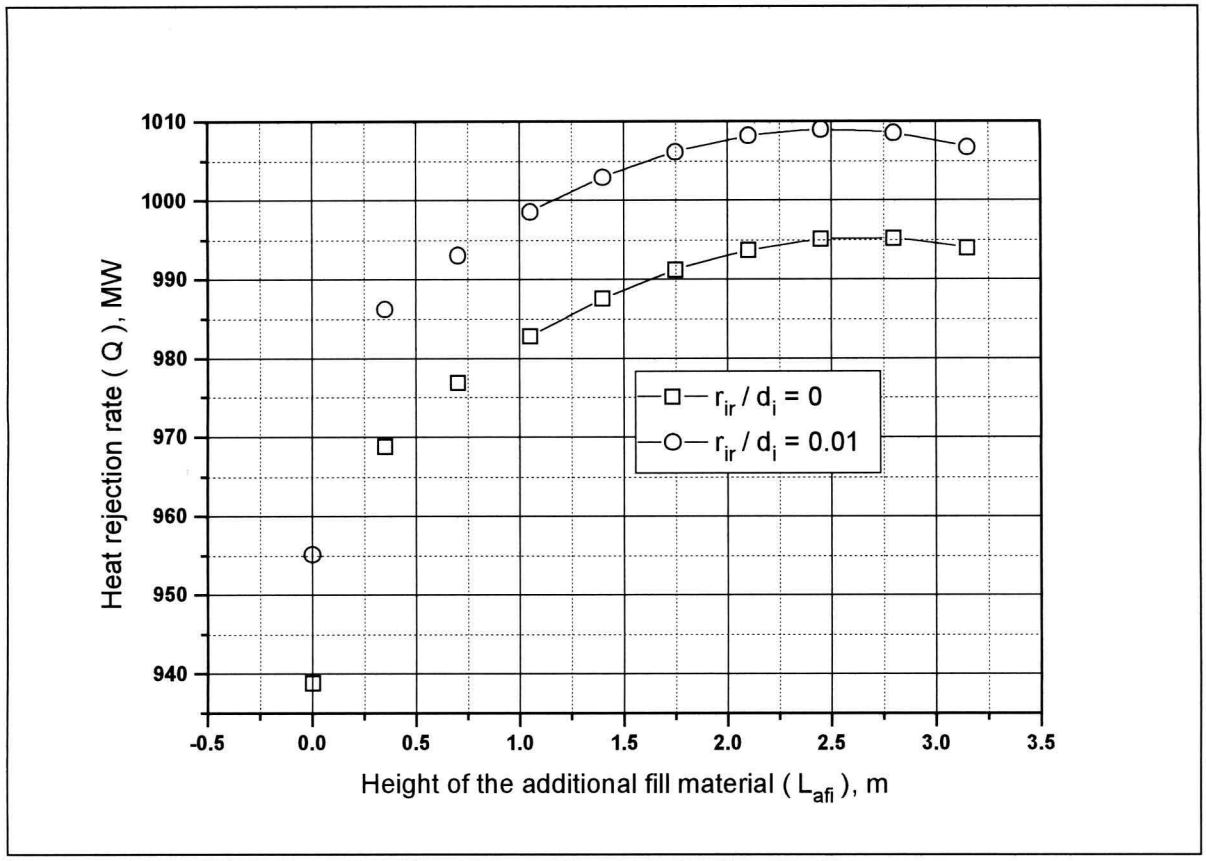

Figure B.5: *Enhanced Cooling Tower Heat Rejection Rate.*

APPENDIX C

THERMOPHYSICAL PROPERTIES OF FLUIDS

(from Kröger [98KR1])

C.1 The thermophysical properties of dry air from 220K to 380K at standard atmospheric pressure (101325 Pa)

Density:

$$\rho_a = \frac{p_a}{287.08T} \ [\mathrm{kg/m^3}] \tag{C.1}$$

Specific heat:

$$c_{pa} = 1.045356\times10^{3} - 3.161783\times10^{-1}T + 7.083814\times10^{-4}T^{2} - 2.705209\times10^{-7}T^{3} \ [\mathrm{J/kgK}] \tag{C.2}$$

Dynamic viscosity:

$$\mu_a = 2.287973\times10^{-6} + 6.259793\times10^{-8}T - 3.131956\times10^{-11}T^{2} + 8.15038\times10^{-15}T^{3} \ [\mathrm{kg/ms}] \tag{C.3}$$

C.2 The thermophysical properties of saturated water vapour from 273.15K to 380K

Vapour pressure:

$$p_v = 10^{z} \ [\mathrm{Pa}] \tag{C.4}$$

$$z = 10.79586(1-x) + 5.02808\log_{10}(x) + 1.50474\times10^{-4}\left[1-10^{-8.29692(1/x-1)}\right] + 4.2873\times10^{-4}\left[10^{4.76955(1-x)}-1\right] + 2.786118312$$

$$x = \frac{273.16}{T}$$

Specific heat:

$$c_{pv} = 1.3605\times10^{3} + 2.31334T - 2.46784\times10^{-10}T^{5} + 5.91332\times10^{-13}T^{6}\ [\mathrm{J/kgK}] \quad (C.5)$$

Density:

$$\rho_v = -4.062329056 + 0.10277044T - 9.76300388\times10^{-4}T^{2} + 4.475240795\times10^{-6}T^{3} - 1.004596894\times10^{-8}T^{4} + 8.9154895\times10^{-12}T^{5}\ [\mathrm{kg/m^3}] \quad (C.6)$$

Dynamic viscosity:

$$\mu_v = 2.562435\times10^{-6} + 1.816683\times10^{-8}T + 2.579066\times10^{-11}T^{2} - 1.067299\times10^{-14}T^{3}\ [\mathrm{kg/ms}] \quad (C.7)$$

C.3 The thermophysical properties of mixtures of air and water vapour

Density:

$$\rho_{av} = (1+w)\left[1-\frac{w}{w+0.62198}\right]\left[\frac{p_a}{287.08T}\right]\ [\mathrm{kg/m^3}] \quad (C.8)$$

Specific heat of the air-vapour mixture per unit mass of dry air:

$$c_{pma} = c_{pa} + wc_{pv} \ [\text{J / kgK}] \tag{C.9}$$

Humidity ratio:

$$w = \left[\frac{2501.6 - 2.3263(T_{wb} - 273.15)}{2501.6 + 1.8577(T - 273.15) - 4.184(T_{wb} - 273.15)}\right]\left[\frac{0.62509 p_{vwb}}{p_{abs} - 1.005 p_{vwb}}\right]$$
$$- \left[\frac{1.00416(T - T_{wb})}{2501.6 + 1.8577(T - 273.15) - 4.184(T_{wb} - 273.15)}\right] \ [\text{kg / kg dry air}] \tag{C.10}$$

Enthalpy of the air-vapour mixture per unit mass of dry air:

$$i_{ma} = c_{pa}(T - 273.15) + w\left[i_{fgwo} + c_{pv}(T - 273.15)\right] \ [\text{J / kg dry air}] \tag{C.11}$$

where the specific heats are evaluated at (T + 273.15)/2 and the latent heat i_{fgwo}, is evaluated at 273.15 K. According to equation (C.18): $i_{fgwo} = 2.5016 \times 10^6$ J/kg.

Dynamic viscosity:

$$\mu_{av} = \frac{\left(X_a \mu_a M_a^{0.5} + X_v \mu_v M_v^{0.5}\right)}{\left(X_a M_a^{0.5} + X_v M_v^{0.5}\right)} \ [\text{kg / ms}] \tag{C.12}$$

where $M_a = 28.97$ kg / mole, $M_v = 18.016$ kg / mole, $X_a = 1/(1 + 1.608w)$ and $X_v = w/(w + 0.622)$

Diffusivity of water vapour in air: [34GI1]

$$D = 435.7 \times 10^{-4} \frac{T_a^{1.5}}{p_a\left(V_a^{1/3} + V_v^{1/3}\right)^2} \sqrt{\frac{1}{M_a} + \frac{1}{M_v}} \ [\mathrm{m}^2/\mathrm{s}] \tag{C.13}$$

where $V_a = 29.9$ and $V_v = 18.8$ are the molecular volumes for air and water vapour respectively and $M_a = 28.97$ and $M_v = 18.016$ are the corresponding molecular masses. Substituting these values into the above equation, reduces it to,

$$D = 0.0003939 \frac{T_a^{1.5}}{p_a} \ [\mathrm{m}^2/\mathrm{s}] \tag{C.14}$$

C.4 The thermophysical properties of saturated water liquid from 273.15K to 380K.

Density:

$$\rho_w = \left[1.49343 \times 10^{-3} - 3.7164 \times 10^{-6} T + 7.09782 \times 10^{-9} T^2 - 1.90321 \times 10^{-20} T^6\right] \ [\mathrm{kg}/\mathrm{m}^3] \tag{C.15}$$

Specific heat:

$$c_{pw} = 8.15599 \times 10^3 - 2.80627 \times 10T + 5.11283 \times 10^{-2} T^2 - 2.17582 \times 10^{-13} T^6 \ [\mathrm{J}/\mathrm{kgK}] \tag{C.16}$$

Dynamic viscosity:

$$\mu_w = 2.414 \times 10^{-5} \times 10^{[247.8/(T-140)]} \ [\mathrm{kg/ms}] \tag{C.17}$$

Latent heat of evaporation:

$$i_{fgw} = 3.4831814 \times 10^{6} - 5.8627703 \times 10^{3} T + 12.139568 T^{2} - 1.40290431 \times 10^{-2} T^{3} \ [\mathrm{J/kg}] \qquad (C.18)$$

Surface tension:

$$\sigma_{w} = 5.148103 \times 10^{-2} + 3.998714 \times 10^{-4} T - 1.4721869 \times 10^{-6} T^{2} + 1.21405335 \times 10^{-9} T^{3} \ [\mathrm{N/m}] \qquad (C.19)$$

APPENDIX D

EXPERIMENTAL RESULTS FOR COOLING TOWER INLET LOSS COEFFICIENT

The data used to generate the correlations, in Chapter 3, for the inlet loss coefficient in isotropic fill resistance counterflow cooling towers, is presented in this section. The calculations employed to determine the inlet loss coefficients from experimental data, are identical to those used by Terblanche [94TE1] and Kröger [98KR1] and will not be repeated. All the relevant dimensions and measurements, needed to reproduce the results, will be given however.

D.1 Circular Tower

For the test section, used to determine the inlet loss coefficient of isotropic fill resistance circular cooling towers (Fig. 3.4), the following dimensions and conditions apply

Diameter of the inlet	d_i	=	4.9 m
Frontal area of the wedge shaped test section	A_{fr}	=	0.2695 m^2
Nozzle diameter	d_n	=	0.2 m
Wind tunnel cross-sectional area	A_{wt}	=	1.44 m^2

The experimental data is grouped according to the fill loss coefficients and atmospheric conditions for each group is included. In the experimental data; Δp_i refers to the pressure difference between ambient conditions and a point just upstream of the fill; Δp_n is the pressure drop across the nozzle used to measure the air flow rate and Δp_u is the difference between atmospheric pressure and the pressure upstream of the nozzle, which is also used in mass flow calculations.

D.1.1 K_{fi} = 24.506

Length of the fill	L_{fi}	=	0.57 m
Atmospheric pressure	p_a	=	101100 Pa
Ambient drybulb temperature	T_a	=	23.0 °C
Wetbulb temperature	T_{wb}	=	17.3 °C

Table D.1: *Tabulated inlet loss coefficient experimental data for* $K_{fi} = 24.506$.

r_{ir} / d_i	d_i / H_i	Δp_i [Pa]	Δp_n [Pa]	Δp_u [Pa]	K_{ct}
0	5	171.9481	452.3688	407.025	5.44242101
0	7.5	182.687	447.9261	414.2672	7.88720276
0	10	198.0117	445.2314	427.4297	11.1816677
0	12.5	222.5662	447.0833	450.3317	16.017901
0	15	256.2771	443.8829	481.2812	23.4146418
0.00510204	5	168.879	452.9544	404.4618	4.80461105
0.00510204	7.5	179.6349	448.7056	411.6299	7.22212713
0.00510204	10	193.4371	444.8772	423.4729	10.2879033
0.00510204	12.5	217.2197	448.3685	446.1559	14.7987089
0.00510204	15	247.0613	448.2679	474.0429	20.9716259
0.00765306	5	168.8272	452.5627	402.9195	4.82174007
0.00765306	7.5	178.1026	449.4472	410.3032	6.86310236
0.00765306	10	188.8374	445.8597	418.2147	9.28005428
0.00765306	12.5	207.1752	450.846	437.1176	12.5351598
0.00765306	15	230.2029	451.503	459.251	17.144869
0.01020408	5	167.3831	451.5644	402.5409	4.6120779
0.01020408	7.5	176.544	449.1106	409.2367	6.58174614
0.01020408	10	187.2763	447.4213	418.1238	8.84063139
0.01020408	12.5	204.1147	451.0553	435.0876	11.902256
0.01020408	15	226.343	452.4273	457.6634	16.2663926
0.01530612	5	167.3437	451.908	402.4367	4.58027044
0.01530612	7.5	176.5176	450.9328	409.8627	6.43998732
0.01530612	10	185.7409	448.3033	416.9355	8.46386616
0.01530612	12.5	202.5301	452.5644	434.4201	11.4540575
0.01530612	15	220.7634	452.9519	451.6278	15.0830603

D.1.2 K_{fi} = 19.692

Length of the fill L_{fi} = 0.42 m

Atmospheric pressure p_a = 100600 Pa

Ambient drybulb temperature T_a = 24.0 °C

Wetbulb temperature T_{wb} = 19.8 °C

Table D.2: *Tabulated inlet loss coefficient experimental data for* K_{fi} = 19.692.

r_{ir} / d_i	d_i / H_i	Δp_i [Pa]	Δp_n [Pa]	Δp_u [Pa]	K_{ct}
0	5	136.62854	451.22087	372.73967	3.57934865
0	7.5	150.41661	450.97172	386.5171	6.21939278
0	10	165.82067	446.02439	397.56685	9.53341833
0	12.5	193.36912	450.64417	427.34296	14.6312811
0	15	225.47969	443.60315	453.6041	21.8009169
0.00510204	5	135.10211	451.7678	371.18576	3.26087075
0.00510204	7.5	147.36946	451.16229	381.89135	5.62433006
0.00510204	10	162.68092	447.78936	394.89659	8.79652427
0.00510204	12.5	188.75247	452.86311	423.73596	13.5392483
0.00510204	15	217.91476	445.92341	447.96109	20.0108262
0.00765306	5	134.90985	452.97118	371.35412	3.15933128
0.00765306	7.5	144.30616	451.94404	380.47017	4.99449107
0.00765306	10	156.02483	448.77265	389.75382	7.43785513
0.00765306	12.5	176.69433	455.36265	412.74065	10.9926386
0.00765306	15	199.48273	451.1968	432.58748	15.8038332
0.01020408	5	133.63445	451.41317	369.97213	3.00329435
0.01020408	7.5	144.28814	451.83918	379.94864	4.99707326
0.01020408	10	155.07032	449.10254	388.61951	7.23188875
0.01020408	12.5	174.95296	456.30737	411.55981	10.5878737
0.01020408	15	193.55586	452.56035	428.70679	14.5128053
0.01530612	5	133.58265	451.84467	370.56594	2.97042461
0.01530612	7.5	142.77272	451.6315	378.03911	4.72094771
0.01530612	10	153.53158	449.11877	387.07237	6.93366841
0.01530612	12.5	171.96665	457.29689	409.75215	9.94285466
0.01530612	15	188.77297	454.1535	423.83853	13.4420347

D.1.3 K_{fi} = 15.651

Length of the fill	L_{fi}	=	0.32 m
Atmospheric pressure	p_a	=	100120 Pa
Ambient drybulb temperature	T_a	=	23.7 °C
Wetbulb temperature	T_{wb}	=	21.2 °C

Table D.3: *Tabulated inlet loss coefficient experimental data for* $K_{fi} = 15.651$.

r_{ir} / d_i	d_i / H_i	Δp_i [Pa]	Δp_n [Pa]	Δp_u [Pa]	K_{ct}
0	5	113.62341	448.63186	353.40743	3.43746818
0	7.5	127.42	443.9047	363.45672	6.2743453
0	10	144.28684	449.19174	382.3948	9.20363974
0	12.5	165.73938	444.19158	399.79471	13.6997182
0	15	200.70062	444.31357	431.92449	20.6976258
0.00510204	5	110.57177	448.00571	349.04882	2.89668821
0.00510204	7.5	124.35825	444.50613	360.70993	5.65940453
0.00510204	10	139.68821	449.1393	376.94573	8.32755631
0.00510204	12.5	159.58254	444.26904	393.94503	12.4818769
0.00510204	15	193.62257	446.10011	427.04091	19.112863
0.00765306	5	110.57379	448.0994	348.59304	2.89279046
0.00765306	7.5	120.98796	444.24161	356.83001	5.03247695
0.00765306	10	135.19981	450.44641	375.35653	7.40185241
0.00765306	12.5	153.61131	446.81538	390.06935	11.1481727
0.00765306	15	185.66132	448.64226	420.73136	17.3143878
0.01020408	5	110.57348	449.40096	350.09196	2.83514491
0.01020408	7.5	119.75125	445.29996	357.11901	4.74604325
0.01020408	10	132.18622	450.9063	371.94876	6.80712281
0.01020408	12.5	147.32993	447.89095	385.12244	9.86632808
0.01020408	15	169.79277	452.8127	407.8762	13.8880665
0.01530612	5	110.56575	448.57331	348.46218	2.87015065
0.01530612	7.5	119.77634	444.79748	356.57678	4.77544662
0.01530612	10	130.5113	450.68549	369.37968	6.50275815
0.01530612	12.5	144.3815	448.84165	382.30886	9.24252495
0.01530612	15	165.7	454.8	404.5	12.9604564

D.1.4 K_{fi} = 11.661

Length of the fill L_{fi} = 0.225 m

Atmospheric pressure p_a = 100120 Pa

Ambient drybulb temperature T_a = 24.3 °C

Wetbulb temperature T_{wb} = 21.6 °C

Table D.4: *Tabulated inlet loss coefficient experimental data for* $K_{fi} = 11.661$.

r_{ir} / d_i	d_i / H_i	Δp_i [Pa]	Δp_n [Pa]	Δp_u [Pa]	K_{ct}
0	5	93.67275	450.88554	336.12532	3.65966805
0	7.5	108.35621	451.81421	350.5137	6.31338682
0	10	127.38801	447.30475	365.77301	10.08386
0	12.5	156.53512	450.56083	391.92566	15.4679251
0	15	197.91774	449.78575	429.70401	23.6630642
0.00510204	5	89.63627	451.78604	333.2476	2.89416833
0.00510204	7.5	104.40708	453.60451	346.96021	5.51340742
0.00510204	10	122.04778	447.4663	360.76585	9.06628553
0.00510204	12.5	150.38216	451.02464	386.23194	14.2551165
0.00510204	15	189.46561	451.20237	422.66859	21.8630682
0.00765306	5	89.05902	451.76183	334.12882	2.7907083
0.00765306	7.5	100.0425	451.25079	343.06373	4.80937925
0.00765306	10	118.23987	448.71825	356.81515	8.28954624
0.00765306	12.5	143.90781	452.10308	381.54619	12.9545406
0.00765306	15	179.77313	454.07679	416.3919	19.7361802
0.01020408	5	89.05368	452.01445	333.25267	2.78081652
0.01020408	7.5	99.7992	451.88307	343.03101	4.73999571
0.01020408	10	113.6156	449.0348	353.53505	7.41094651
0.01020408	12.5	133.19315	453.44168	371.77871	10.8551792
0.01020408	15	156.48115	452.84302	392.09496	15.3111075
0.01530612	5	89.07077	451.65462	332.77773	2.79634902
0.01530612	7.5	99.78916	452.45094	343.35045	4.71594575
0.01530612	10	112.06671	448.60279	352.21272	7.14198784
0.01530612	12.5	130.56566	454.31403	369.54456	10.3170366
0.01530612	15	149.3248	453.33573	386.6243	13.912344

D.1.5 K_{fi} = 5.975

Length of the fill L_{fi} = 0.12 m

Atmospheric pressure p_a = 100700 Pa

Ambient drybulb temperature T_a = 24.2 °C

Wetbulb temperature T_{wb} = 22.0°C

Table D.5: *Tabulated inlet loss coefficient experimental data for* K_{fi} = 5.975.

r_{ir} / d_i	d_i / H_i	Δp_i [Pa]	Δp_n [Pa]	Δp_u [Pa]	K_{ct}
0	5	67.61914	445.94731	309.81085	4.78671928
0	7.5	84.95937	445.92427	325.18808	7.93051626
0	10	112.06481	448.26602	348.55783	12.840878
0	12.5	144.25954	445.57312	375.80783	19.0910135
0	15	191.62718	446.08364	418.34377	28.3873096
0.00510204	5	64.53167	447.50184	306.83038	4.19312629
0.00510204	7.5	81.40342	446.41934	322.0851	7.26567665
0.00510204	10	107.47401	449.31914	346.1834	11.9419033
0.00510204	12.5	139.67402	446.14256	370.73203	18.1739887
0.00510204	15	184.12615	447.24563	411.66289	26.7933789
0.00765306	5	62.99586	448.09266	306.30316	3.90461828
0.00765306	7.5	78.34352	448.17338	320.24976	6.65554772
0.00765306	10	102.84892	450.38359	343.03607	11.0439556
0.00765306	12.5	128.9229	446.84282	363.69275	16.0825404
0.00765306	15	173.37562	449.81845	402.58848	24.4751511
0.01020408	5	63.00486	448.20052	305.55653	3.90348952
0.01020408	7.5	76.79837	448.9789	317.85411	6.35213707
0.01020408	10	95.52507	451.12795	336.41534	9.67344631
0.01020408	12.5	118.18392	448.16476	353.54335	13.9893834
0.01020408	15	147.80375	456.68659	383.56716	19.106564
0.01530612	5	62.99058	448.01374	306.19386	3.90560365
0.01530612	7.5	75.27296	448.54284	317.64554	6.09066142
0.01530612	10	92.2881	451.66592	334.29764	9.06467651
0.01530612	12.5	112.19176	450.38521	351.48661	12.7696351
0.01530612	15	139.66799	458.35001	377.60998	17.4854043

D.2 Rectangular Tower

For the test section, used to determine the inlet loss coefficient of isotropic fill resistance rectangular cooling towers (Fig. 3.13), the following dimensions differ from those of the circular tower. All other parameters stay identical, unless specified otherwise.

Width of the inlet W_i = 3.58 m

Frontal area of the test section A_{fr} = 0.27745 m^2

Nozzle diameter d_n = 0.25 m

D.2.1 K_{fi} = 24.392

Length of the fill L_{fi} = 0.66 m

Atmospheric pressure p_a = 100720 Pa

Ambient drybulb temperature T_a = 27.5 °C

Wetbulb temperature T_{wb} = 24.0°C

Table D.6: *Tabulated inlet loss coefficient experimental data for* $K_{fi} = 24.392$.

r_{ir} / W_i	W_i / H_i	Δp_i [Pa]	Δp_n [Pa]	Δp_u [Pa]	K_{ct}
0	3	488.41752	522.70603	1144.16849	8.11152034
0	5	530.90737	509.665	1166.93327	12.3411214
0	7.5	641.47447	471.98541	1224.10374	25.2414338
0	10	796.23901	439.87423	1274.23982	44.7133801
0.01047486	3	475.24965	524.29383	1134.55074	7.01582625
0.01047486	5	519.67767	511.63162	1160.64043	11.3076789
0.01047486	7.5	616.46301	480.14888	1209.99866	22.1305757
0.01047486	10	739.92087	439.87423	1274.23982	38.9685689
0.01396648	3	473.69363	524.55551	1131.00041	6.88148604
0.01396648	5	513.92166	512.18558	1154.23177	10.8155432
0.01396648	7.5	596.30992	486.35664	1198.4166	19.7592525
0.01396648	10	700.9659	452.38308	1254.51143	33.2599245
0.02094972	3	472.13581	527.4956	1134.0262	6.57682509
0.02094972	5	506.1525	514.87189	1151.50667	10.0151636
0.02094972	7.5	575.92276	492.068	1187.65426	17.493748
0.02094972	10	671.75301	462.43555	1239.56436	29.1575578

D.2.2 K_{fi} = 15.271

Length of the fill	L_{fi}	=	0.38 m
Atmospheric pressure	p_a	=	100780 Pa
Ambient drybulb temperature	T_a	=	28.2 °C
Wetbulb temperature	T_{wb}	=	24.0°C

Table D. 7: *Tabulated inlet loss coefficient experimental data for* $K_{fi} = 15.271$.

r_{ir} / W_i	W_i / H_i	Δp_i [Pa]	Δp_n [Pa]	Δp_u [Pa]	K_{ct}
0	3	331.079	502.0171	964.4467	6.70944224
0	5	389.2865	487.8932	1000.856	11.8917781
0	7.5	512.3133	453.394	1071.495	24.7823354
0	10	699.9413	400.118	1178.709	50.5107018
0.01047486	3	320.2893	506.9259	961.4037	5.69100712
0.01047486	5	379.5297	490.4762	996.4637	10.9819164
0.01047486	7.5	488.968	460.0051	1058.358	22.1301033
0.01047486	10	640.5	418.2	1144.2	41.2283412
0.01396648	3	318.4303	506.4316	958.4497	5.57699965
0.01396648	5	368.4737	492.3629	987.7159	10.0230499
0.01396648	7.5	460.1741	467.714	1039.481	19.0303092
0.01396648	10	591.6629	432.7409	1118.674	34.3961109
0.02094972	3	312.3431	508.2147	956.0529	5.05586239
0.02094972	5	364.0938	493.4806	987.1294	9.62699284
0.02094972	7.5	438.34	474.3444	1028.561	16.714897
0.02094972	10	543.2965	444.7467	1088.307	28.4524671

D.2.3 K_{fi} = 9.531

Length of the fill	L_{fi} =	0.25 m
Atmospheric pressure	p_a =	100680 Pa
Ambient drybulb temperature	T_a =	26.6 °C
Wetbulb temperature	T_{wb} =	22.0°C

Table D.8: *Tabulated inlet loss coefficient experimental data for* $K_{fi} = 9.531$.

r_{ir} / W_i	W_i / H_i	Δp_i [Pa]	Δp_n [Pa]	Δp_u [Pa]	K_{ct}
0	3	263.36763	521.55835	920.80567	6.8238554
0	5	335.89695	515.15022	980.37712	12.2105622
0	7.5	540.96762	511.71747	1166.15791	27.9066029
0	10	849.75949	497.7071	1436.50836	55.7813035
0.01047486	3	250.9506	523.91182	912.7979	5.88964869
0.01047486	5	320.77562	520.29058	970.49462	10.9020369
0.01047486	7.5	504.44284	525.56634	1148.85962	24.072514
0.01047486	10	778.2	523.8	1400.33	46.1082674
0.01396648	3	248.44767	523.24525	909.76841	5.73887564
0.01396648	5	308.27267	522.91492	963.76687	9.91050046
0.01396648	7.5	452.7853	516.53152	1089.50441	20.765181
0.01396648	10	696.3	534.5	1340.3	38.250127
0.02094972	3	245.8	524.2	909.5	5.52741896
0.02094972	5	299.24351	524.69904	957.97909	9.20759645
0.02094972	7.5	427.8	524.5	1075.6	18.4287772
0.02094972	10	613.1065	531.76644	1258.23144	31.9335034

D.2.4 K_{fi} = 5.810

Length of the fill L_{fi} = 0.14 m

Atmospheric pressure p_a = 100680 Pa

Ambient drybulb temperature T_a = 26.6 °C

Wetbulb temperature T_{wb} = 22.0°C

Table D.9: *Tabulated inlet loss coefficient experimental data for* K_{fi} = 5.810.

r_{ir} / W_i	W_i / H_i	Δp_i [Pa]	Δp_n [Pa]	Δp_u [Pa]	K_{ct}
0	3	167.24114	405.35747	680.85108	7.13913108
0	5	232.00673	400.1066	732.37711	13.0766082
0	7.5	411.36881	398.69238	898.88738	30.0292784
0	10	671.97466	395.47865	1140.03487	57.6426778
0.01047486	3	156.43268	406.45509	673.12211	6.17204975
0.01047486	5	222.03137	402.40364	726.19717	12.0701428
0.01047486	7.5	386.74391	403.20089	881.05126	27.2345495
0.01047486	10	632.12396	406.41728	1115.86374	51.5452077
0.01396648	3	154.9786	406.60087	671.6113	6.04268307
0.01396648	5	210.18364	404.93327	719.83337	10.9040925
0.01396648	7.5	346.99376	412.43969	855.76945	22.7693798
0.01396648	10	531.50463	408.06292	1023.66106	40.9359752
0.02094972	3	152	409.3	670.5	5.70415471
0.02094972	5	200.98954	406.58086	713.79063	10.0262417
0.02094972	7.5	313.36437	409.29611	820.22939	19.9132709
0.02094972	10	479.96569	412.91859	978.77977	35.2831074